Chemical Strategies for the Diversification of Landomycins and DEL Target Scaffolds toward the Discovery of New Therapeutics

A dissertation submitted by

Kathleen Grace Maiello

In partial fulfillment of the requirement for the degree of

Doctor of Philosophy

In

Chemistry

Tufts University

February 2026

Advisor: Dr. Clay S. Bennett

Abstract

Deoxy sugar-containing bacterial natural products represent a unique class of bioactive compounds with diverse therapeutic potential. Chapter 1 explores the significance of deoxy oligosaccharides in bacterial natural products, with the focus on the Landomycins. The Landomycins are a class of glycosylated polyketide natural products that exhibit potent anticancer properties. This chapter provides an in-depth overview of the landomycins, with a particular emphasis on Landomycin A (LaA), whose complex structure features a landomycinone aglycone core adorned with an oligosaccharide chain of rare deoxy sugars. Despite their promising therapeutic potential, access to landomycins and their analogs has been limited due to the synthetic challenges associated with both their aromatic core and their stereochemically complex glycan moieties. The chapter first outlines the role of deoxy sugars in bacterial natural products and highlights the importance of glycosylation in mediating biological activity and selectivity. It then focuses on the discovery and biological relevance of LaA and its analogs. Synthetic approaches to access landomycinone and strategies for its functionalization are reviewed, including efforts toward partial and total synthesis of the molecule. Special attention is given to innovative glycosylation techniques used in LaA assembly.

Chapter 2 focuses on improving access to Landomycin A through biological cultures. A rapid, high-throughput spectrophotometric assay was developed to monitor landomycin production in *Streptomyces cyanogenus* S136, enabling optimization of fermentation conditions and reliable, gram-scale isolation. This advancement provided the foundational material needed for late-stage chemical modification and further biological study.

Chapter 3 details a semi-synthetic workflow to investigate the role of LaA's oligosaccharide chain in modulating anticancer activity. Novel landomycin derivatives were

generated through lipidation techniques, in pursuit of enabling structure–activity relationship studies that probed cellular uptake, membrane interactions, and cytotoxic potency. These findings could potentially offer mechanistic insight into the contribution of the glycan moiety to landomycin's mode of action and support further analog development.

Chapter 4 extends this synthetic expertise into small-molecule drug discovery. Solid-phase synthesis (SPS) techniques were applied to resynthesize and diversify common scaffolds identified in DNA-encoded library (DEL) screening campaigns. Using automation methods, key heterocyclic cores such as pyrimidines, oxadiazoles, triazoles, and thiadiazoles were efficiently accessed and modified. These workflows enable high-throughput structure–activity relationship exploration and facilitate rapid progression from DEL hits to validated drug-like candidates.

Together, this thesis demonstrates the power of integrating biosynthesis, semi-synthesis, and solid-phase methodologies to expand the chemical and therapeutic scope of both natural products and small-molecule libraries. These efforts contribute to the broader pursuit of new medicines through strategic scaffold modulation and synthetic innovation.

Acknowledgements

I would like to start off by thanking my advisor, Dr. Clay S. Bennett, for all of his knowledge, expertise, and guidance throughout my program. He always allowed me to explore my literature-founded curiosities and encouraged my scientific development through exploration of new and challenging synthetic problems. I cannot thank him enough for all he has taught me through helpful discussions, his connections within the larger scientific community and all of his amazing chemistry textbooks on synthesis. I am so proud of what I have learned throughout my program, and I would have never been able to do that without him. Thank you for giving me the synthetic tools both in my mind and through my hands that I will use throughout the rest of my career. Additionally, I would like to thank my dedicated committee members, Dr. Luke Davis, Dr. Krishna Kumar, and Dr. Charlie Mace, for all of their hours of help, both scientifically and emotionally throughout my program. Your feedback has been invaluable and it has been a pleasure to work with you all. I would also like to thank Dr. Alexei Demchenko for his support and encouragement. I am so thankful to have met him at the 2022 ACS meeting and I thank him for his continued support as my external committee member.

I would like to thank all my lab mates, past and present for making my experience enjoyable. Particularly, I would like to thank Dr. J. Colin Mizia for training me when I first arrived. Your guidance and expertise in synthetic chemistry inspired me to complete this program and try to learn as much as I could every day. I would like to thank Dr. Joe Romeo for always keeping me company late at night. To Dr. Vanessa Jones, thank you for being my rock and giving me a lifelong friend out of this program. To Jack Florek, thank you so much for doing this program with me. I would be lost without our Friday beers and “middle school boy” jokes. To Theo Dadagian, thank you for picking me up on my slow days and always giving me something to giggle at. Additionally,

I would like to thank Dr. Todd Chappel and Dr. Allison Tierney for their collaboration and contributions to Chapter 2. Todd performed optimization of the expression system and antimicrobial testing. Allison carried out screening against cancer cells. A special thank you to Bohdan Ostash for the genetically engineered line of *Streptomyces* for expression of LaA.

Lastly, I would like to thank my friends and family for all your support. To my Mom and Dad, you are the most amazing human beings I know and I could never have done this without your loving support and guidance throughout my entire life. You always told me to dream big and look where it took us! To my brother, my boys, I love you more than I can express with words and could not imagine this life without you. To my grandmothers for which I am named, Kathleen and Grace, thank you for giving me a reason to do my best every single day for all the women out there that did not have the same opportunities as me. To my best friend (sister actually) Megan, all the memories we have made together, all the laughs and hugs, lived in the front of my head on all my darkest days. I love you. To my partner Alexus, thank you for holding me down when no one else could. You are the foundation to my success, and I cannot wait to see what we build in our lives together.

Table of Contents

List of Figures and Schemes

Chapter 1

Chapter 2

Chapter 3

Chapter 4

Reproduced in part with permissions from:[1]

Chappell, T. C.; Maiello, K. G.; Tierney, A. J.; Yanagi, K.; Lee, J. A.; Lee, K.; Mace, C. R.; Bennett, C. S.; Nair, N. U. Rapid Spectrophotometric Detection for Optimized Production of Landomycins and Characterization of Their Therapeutic Potential. *Biotechnol. Bioeng.* **2024**, *121* (9), 2648–2661. https://doi.org/10.1002/bit.28725.

Chapter 1: The Significance of Deoxy Sugars in the Assembly of Bacterial Natural Products with Medicinal Properties

Abbreviations

ROS: reactive oxygen species

AIF: apoptosis-inducing factor

GSH: glutathione

SAR: Structure-activity relationship

LaA: Landomycin A

LaE: Landomycin E

KHMDS: potassium hexamethyldisilazide

DMF: *N,N*-dimethylformamide

THF: tetrahydrofuran

TsCl: Tosyl chloride (4-methylbenzenesulfonyl chloride)

TTBP: 2,4,6-tri-tert-butylpyrimidine

1.1 The Significance of Deoxy Oligosaccharides in Bacterial Natural Products

Carbohydrates, commonly referred to as sugars, are biologically significant motifs that perform a wide range of functions.[1] It is estimated that approximately 20% of bacterial natural products contain carbohydrate-based scaffolds within their molecular structures.[2] Many of these glycans are deoxy sugar containing oligosaccharides, characterized by the absence of at least one hydroxyl group around the sugar ring, like compounds **1.01-1.09** (**Fig. 1.1**). These carbohydrate-containing natural products have attracted considerable interest from the medicinal chemistry community due to their therapeutic potential against a variety of diseases, including cancer and infectious pathogens.[3–6] In some cases, the structure-activity relationship (SAR) of the sugar motif is well understood, like the off target toxicity effects due to binding differences between Doxorubicin and Epirubicin,

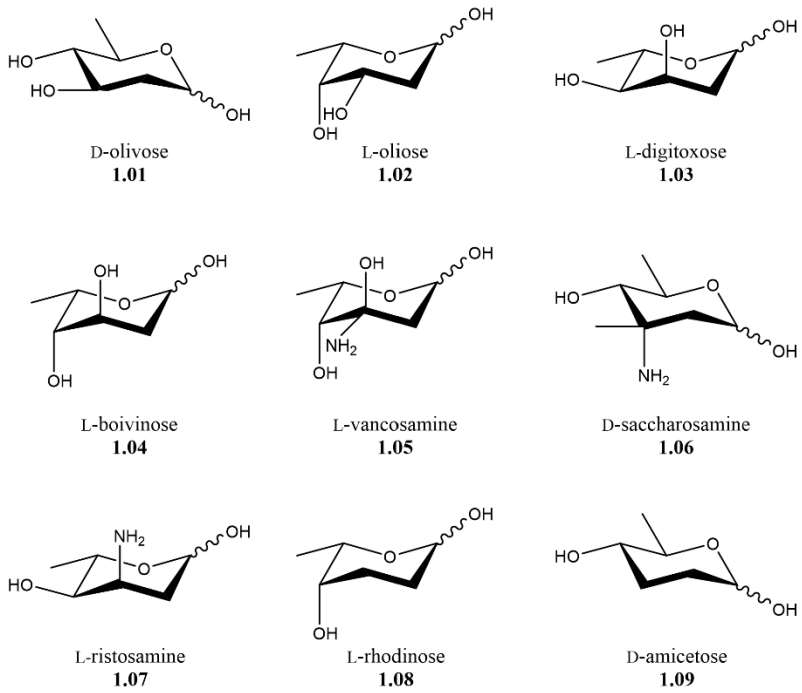

Figure 1.1: Relevant bacterial derived deoxy monosaccharides and their corresponding structure

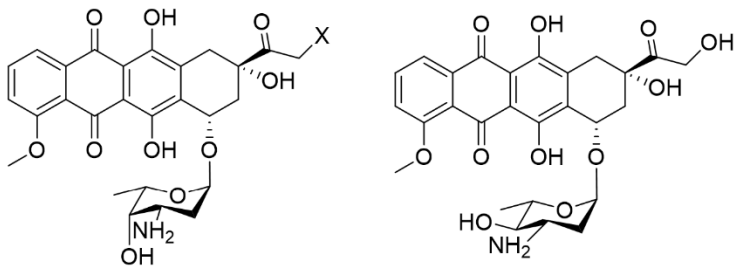

Figure 1.2: Structures of the anti-cancer agents Doxorubicin, Daunorubicin and Epirubicin, all currently used in the clinic

attributed to the epimerization at the C4 position (**Fig. 1.2**).[7] In other cases, the SAR is unknown, attracting researchers to explore these motifs in detailed structure-function experiments. Due to their structural intricacy, many of these carbohydrates are difficult to access. Making the situation more complex, the sensitivity of selective glycosylation reactions poses a significant synthetic challenge, especially with monosaccharides lacking functionality. Glycosylation is a process whereby a nucleophilic glycosyl acceptor and electrophilic glycosyl donor are bonded through the anomeric position, the most reactive position on a monosaccharide. Synthetically, this reaction poses challenges stereochemically because the formation of the glycosidic linkage can create the α and β anomers. Forming anomeric bonds selectively is imperative when synthesizing oligosaccharide containing bacterial natural products so that they can be studied in both native and altered structures. The reaction normally begins with the activation of a donor, followed by the loss of the leaving group at the anomeric position and concluded with attack of the

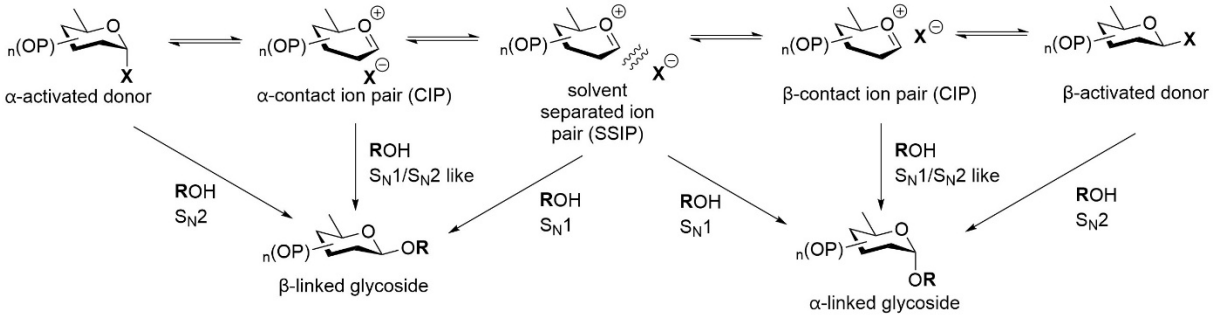

Figure 1.3: Potential mechanistic outcomes and intermediates in glycosylation reactions

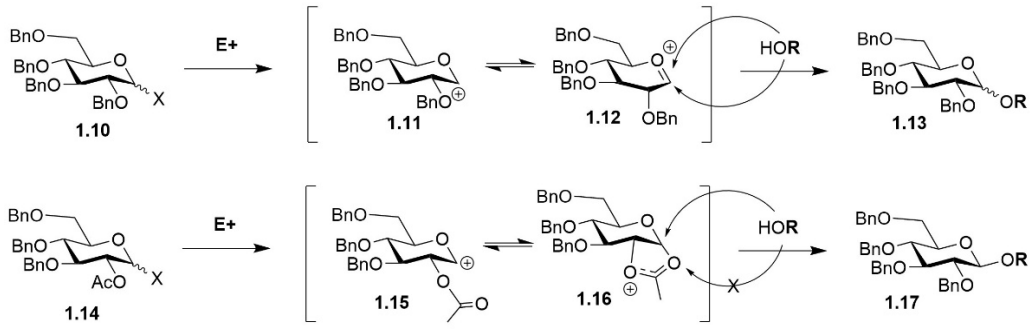

Figure 1.4: The implications of anchimeric assistance in chemical glycosylation

nucleophilic acceptor. Controlling the stereochemical outcomes of glycosylation is challenging because the reaction proceeds somewhere along the S_N1/S_N2 mechanistic continuum (**Fig. 1.3**).[8,9] Depending on the conditions, the reaction could result in the direct S_N2-like displacement of the anomeric leaving group by the glycosyl acceptor, forming the linkage on the opposite side of the molecule from where the leaving group originated. More towards the S_N1 side of the spectrum, the loss of the leaving group from an activated donor results in a closely associated ion pair (CIP) forming an oxocarbenium cation,[10,11] priming the acceptor for a more S_N1 like approach, potentially resulting in multiple stereochemical outcomes (**Fig. 1.3**).[8] To influence the stereochemical outcome on fully substituted sugars, synthetic chemists often make use of protection group participation through the C2 position of the donor, blocking a face of the molecule (**Fig. 1.4**).[12] However, when it comes it 2-Deoxy glycosides, the ability to use anchimeric assistance is lost.[13] Studies by Woerpol on super-reactive oxocarbenium cation species suggest that

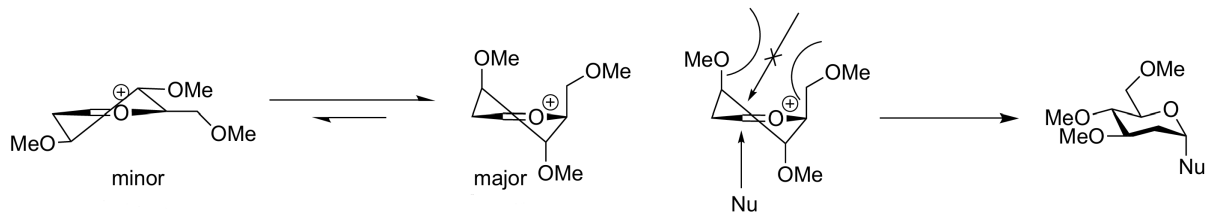

Figure 1.5 Woerpol model for transition state conformation of oxocarbenium carbocations during nucleophilic attack

in this state, alkoxy substituents form axial configurations, lowered in energy by both the dipole moment and counterion present. The nucleophile can attack most freely from the bottom face of the ring, giving an axial anomeric outcome (**Fig. 1.5**).[14] The vast majority of glycosylation reactions are kinetically controlled processes, resulting in α and/or β outcomes depending on the structure and electronics of the donor/acceptor pair and the lowest energy transition state of that corresponding pair.[15] Other factors that influence selectivity include protecting groups, solvents,

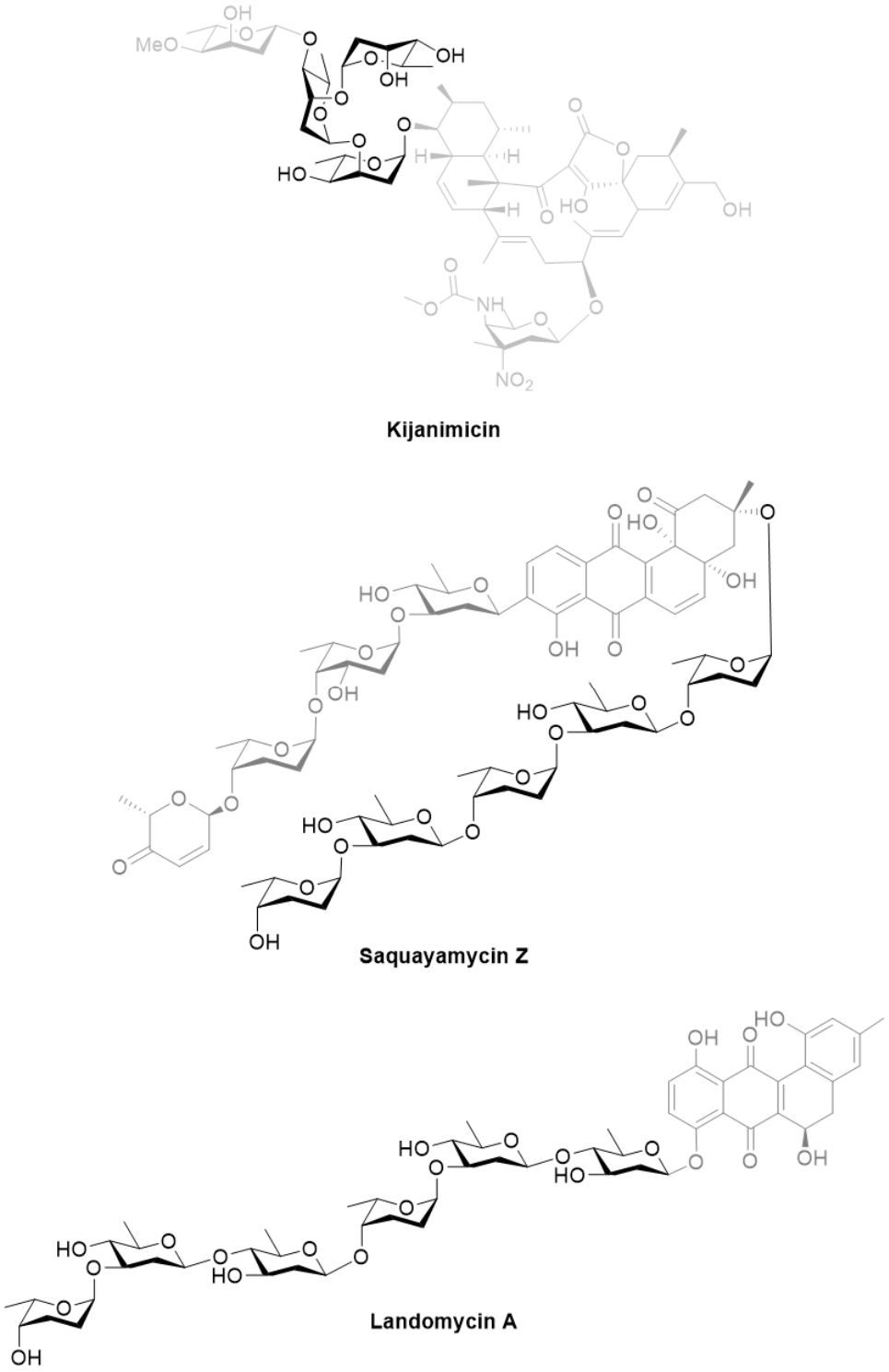

Figure 1.6: The corresponding structures of Kijanimicin, Saquayamycin Z and Landomycin A with their deoxy oligosaccharide chains highlighted

activation/promoter systems and temperatures used during the reaction.[16,17] The implication of these factors will be explained in the synthetic approaches to the glycan of LaA, outlined extensively in Section 1.5 and 1.6.

1.2 Bacterial Secondary Metabolites Containing Deoxy Monosaccharides

In select cases, bacterial secondary metabolites contain exclusively deoxy sugars in their structure.[6] For example, the kijanimicins,[18] saquayamycins,[19,20] and landomycins[21,22] all contain a deoxy sugar chain within their molecular scaffolding. All three of these structures are of interest due to their therapeutic potential (**Fig. 1.6**). First isolated from *actinomadura kijaniata*, Kijanimicin is a scaffold that also possesses broad spectrum activity against gram-positive strains along with moderate antineoplastic properties.[23] Another bacterial secondary metabolite of interest, isolated from actinomycete *micromonospora*, Saquayamycin Z, is a bacterial natural product possessing both anticancer (HM02, MCF7, and HepG2, $GI_{50} < 650$ nM) and antibiotic (*P. aurenscens, B. subtilis, S. aureus*, MIC = 0.1−1 μM) properties.[20] MIC values against gram positive bacteria occur in the sub micromolar range, making this molecule a drug candidate as an antibiotic.[24]

Together, these examples highlight the functional importance of deoxy sugar-containing metabolites in the development of both anticancer and antibacterial agents. Building on these examples, the landomycins represent a unique class of deoxy sugar-containing natural products that are central to the work presented in this thesis. Landomycin A includes an aglycone, landomycinone, a polyketide-derived benz[*a*]anthracene backbone linked to a hexasaccharide composed of a repeated trisaccharide unit of two D-olivoses and a single L-rhodinose. Landomycins B and D are composed of a single oligosaccharide chain comprised of 2 D-olivoses or 5 sugars, 4 D-olivoses and an L-rhodinose. Previous work has shown that both the

landomycinone core alone and derivatives possessing long sugars (5-6 units long) show potent anticancer activity, however, derivatives possessing sugars of intermediate length (1-4 units long) are less active (**Fig. 1.7**).[25,26] This target is attractive for synthesis because altering the structure of oligosaccharide chain results directly in changes to its biological activity.[27]

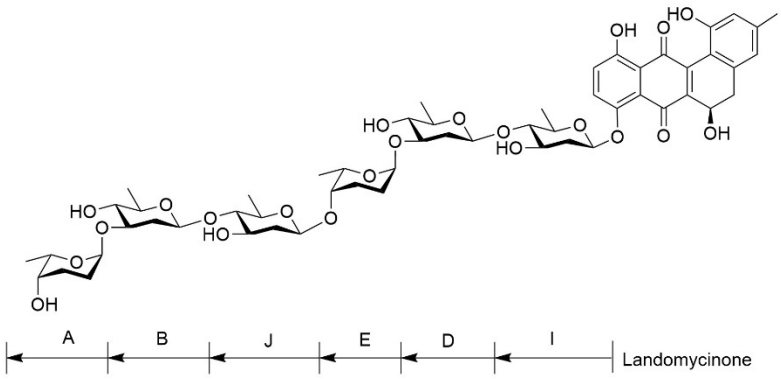

Landomycin	GI_{50} (μM) NCI-H460	MCF7	LL/2
A	2.1	1.8	0.7
B	6.6	2.1	1.5
J	10.2	4.5	1.4
E	5.4	13.0	0.7
D	10.2	4.2	2.1
I	13.9	3.7	3.5
Landomycinone	5.9	2.9	2.9

Figure 1.7 The landomycins and their corresponding biological activity

1.3 Landomycins – Discovery and Isolation

Bacterial natural products have begun to reemerge as promising new drug leads to treat several current health threats such as multidrug resistant cancer and antibiotic resistance in pathogens.[28,29] Among the most prolific producers of these bioactive secondary metabolites are bacteria from the *Streptomyces* genus. These organisms, which colonize diverse ecological habitats, are well known for generating an array of therapeutically relevant compounds, such as the antibiotic streptomycin.[30] The landomycins, first isolated from a soil sample by Rohr and coworkers, are a therapeutically relevant chemical scaffold produced by *Streptomyces cyanogenus* S136.[31] This motif falls into the angucycline family, the largest group of polycyclic aromatic polyketides, denoted by their angled benz[*a*]anthracene backbone (**Fig. 1.8**).[32] Two

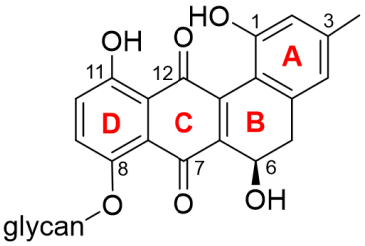

Figure 1.8: Numbering and Naming Scheme for Landomcyinone

distinct structural features of the landomycins include the O-glycosyl linkage at C8 on landomycinone and the chiral hydroxyl at C6.

1.4 The Landomycins – Biological Activity and Proposed Mechanism of Action

LaA, the major bioactive metabolite of *S. cyanogenus* S136 with a repeating trisaccharide unit, has been shown to possess the widest variety of anticancer activity, having been tested against sixty different human cancers at the NCI, the most promising hits against lung (LL/2) and breast cancer (MCF7), highlighted in **Figure 1.7**. There is a direct relationship between potency and the length of the deoxy oligosaccharide chain, however, the trisaccharide version, Landomycin E is a potent anti-cancer agent as well. Furthermore, it has been suggested that landomycin A-D may possess antimicrobial activity because they are part of the greater angucycline family,[33] although detailed studies are lacking. Although these chemical scaffolds possess promising biological activity, none of these compounds have been applied in the clinic due to toxicity and/or solubility issues.[34]

The mode of action of the landomycins is not fully established but has been researched.[35–37] Many of the MOA studies have been conducted on LaE, the simpler trisaccharide conjugate of LaA, which also possesses potent antineoplastic properties. Stoika and coworkers were the first to establish baseline biological values for LaE against a colon cancer model in modern biochemical assays.[38] In 2007, Berger and colleagues discovered that following treatment of LaE to cancer cell line KB-3-1, the carcinoma cells underwent programed cell death. Signs they observed to come to this conclusion included cell shrinkage and formation of apoptotic bodies followed by apoptosis. In addition, the treatment with LaE caused intense intracellular oxidative stress, leading to the breakdown of the mitochondrial membrane visible by staining, accompanied by a drastic reduction in the concentration of ATP. Perhaps most interestingly, they found that LaE did not inhibit DNA

topoisomerase I or II, meaning that LaE did not cause DNA intercalation, a classic hallmark MOA of the biosynthetically related anthracycline group. They continued their investigations and in 2011, they published additional findings concluding that LaE interfered with the initiator caspase-10, which plays a pivotal role in the end stages of cell apoptosis. Related to mitochondrial degradation, LaE caused the release of apoptosis-inducing factor (AIF) after 12 hours of incubation, leading to the generation of reactive oxygen species (ROS) in the cytosol. Both factors directly contribute to programed cell death. In 2017, Berger and collegues expanded on this work, finding that LaE induced apoptosis occurred through the early generation of hydrogen peroxide which caused immediate capsase-7 activation. This is another potential pathway through which LaE acts to elicit cell death. They also found that unlike anthracyclines, LaE did not cause superoxide formation (O_2•−), making the toxicity profile of LaE different from anthracyclines like doxo- and daunorubicin.[39] Most recently, work done by their group in 2021 showed that the quinone motif in landomycinone will spontaneously form Michael-adducts with biothiols, such as cystine and glutathione (GSH). In combination, the depletion of GSH combined with the ROS induction previously mentioned leads to a complex, multi-faceted cell death that is difficult to study due to the lack of probes that resemble the landomcyins.[40] Detailed studies on the structure activity relationships (SAR) of the landomycin sugar chain and its activity have yet to be conducted. In part, the lack of studies done on this promising scaffold can be attributed to the difficulty in obtaining the molecule(s) of interest through both synthetic and biosynthetic methods.

1.5: Landomycins – Synthetic Approaches to the Glycan

Synthetic approaches have been established toward the related core and oligosaccharides; however, these methods are arduous and low yielding, with some approaches only featuring certain

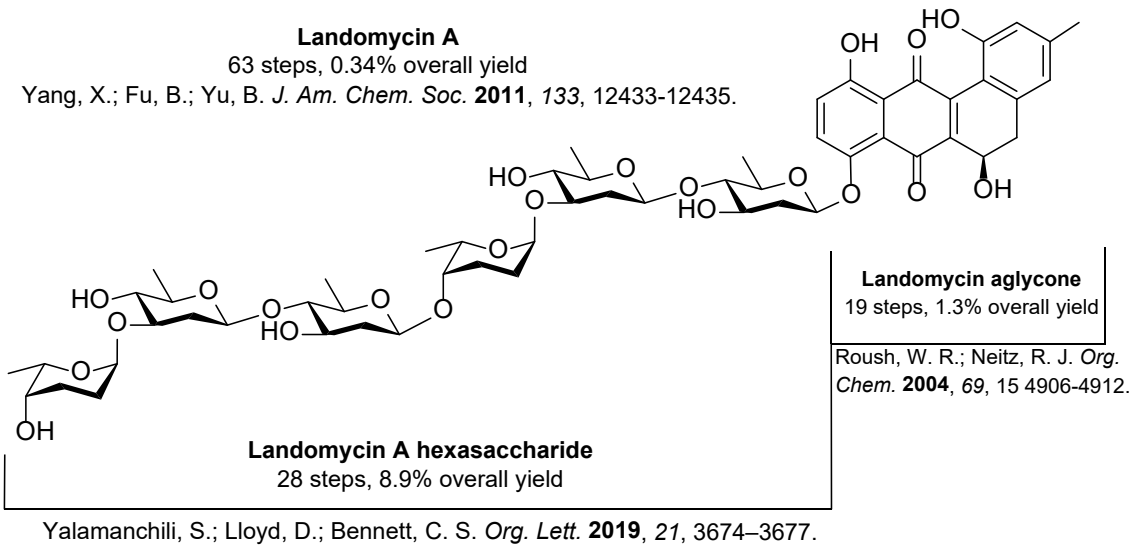

Figure 1.9: Overview of the best synthetic approaches to accessing landomycins

portions of the molecule (**Fig. 1.9**).[22,41–50] To expand, the primary difficulties in the synthesis of the landomycins are as follows:

(i) Landomycinone can easily go through the process of dehydrative aromatization through loss of the chiral hydroxyl on the B ring (**Fig. 1.9**).

(ii) Assembly of the deoxy oligosaccharide chain requires stereoselective reaction conditions to control each anomeric linkage in the hexasaccharide, composed of four 2,6-dideoxy-β-glycosidic linkages and two 2,3,6-trideoxy-α-glycosidic linkages. Additionally, the glycan needs to be coupled with landomycinone at the C8 hydroxyl with β-selectivity through the first D-olivose residue.

(iii) Once selective linkages are formed, later synthetic manipulations must be mild enough to preserve the selective anomeric bonds in the glycan.

(iv) Attaching the deoxy sugars to the poorly nucleophilic, hydrogen-bonded C8 phenolic hydroxyl of landomycinone is difficult synthetically (**Fig. 1.9**).

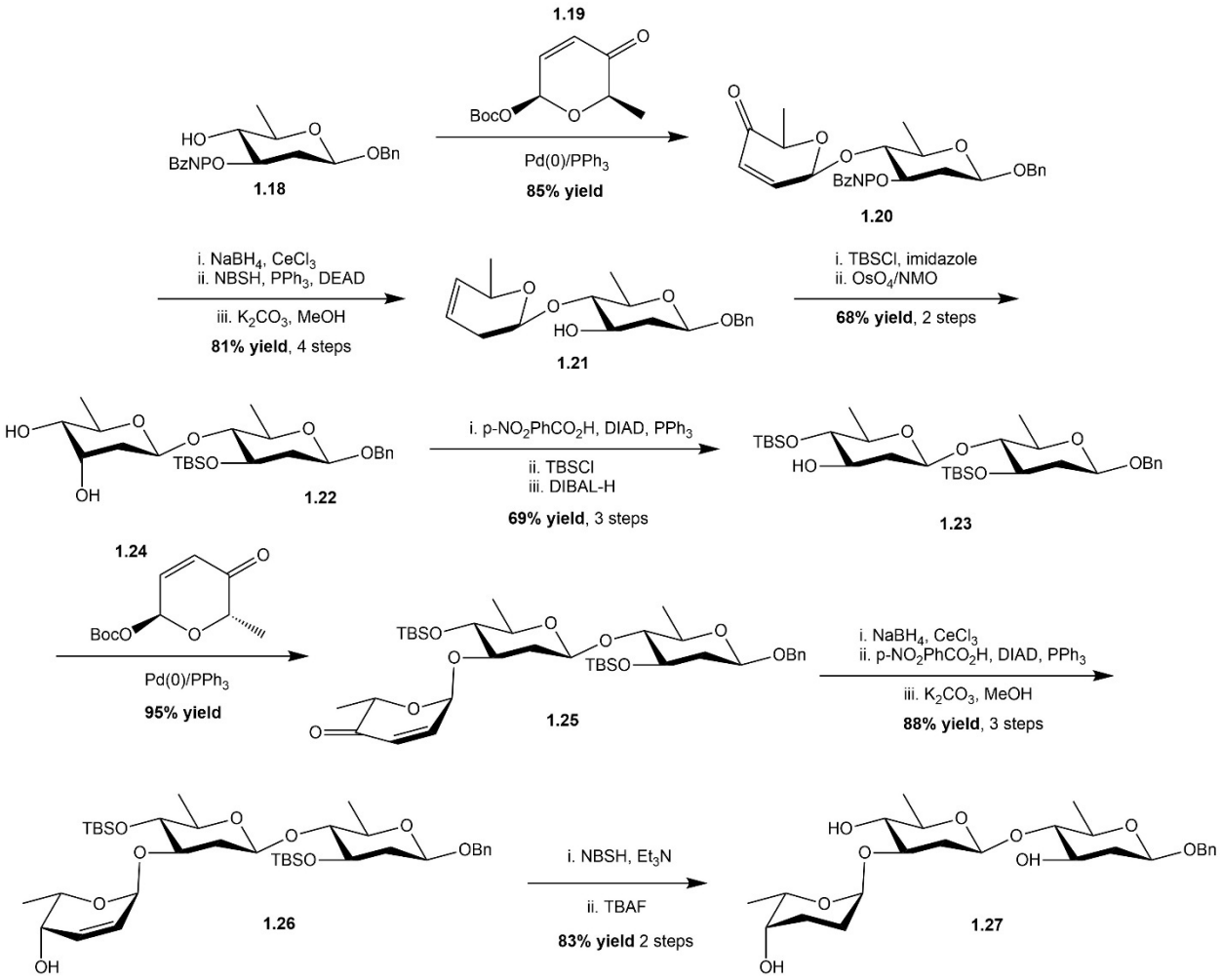

Scheme 1.1: O'Dougherty's method to the trisaccharide fragment. Compound 1.27, of LaA

Some groups have synthesized the trisaccharide unit of LaA. O'Dougherty was able to use a convergent synthesis of the trisaccharide unit beginning with a palladium catalyzed glycosylation between an α-D-pyranone donor **1.19** and a C4-D-olivose acceptor **1.18**. Then, disaccharide **1.20** underwent a Luche reduction of the ketone group, giving a mixture of allylic olefins. Using Myers' reductive 1,3-allylic transposition conditions, they were able to solely isolate the desired pseudo-glycal, with the double bond situated between C3 and C4 of the residue. Upon exposure to basic conditions to hydrolyze the p-nitrobenzoyl group on the C3 alcohol of the D-olivose residue, they isolated disaccharide **1.21** in 81% yield over three steps. Compound **1.21** was then TBS protected

at the C3 alcohol of the D-olivose, followed by a dihydroxylation of the alkene to form compound **1.22** in 68% yield over two steps. They then used a Mitsunobu inversion with an intermediary TBS protection to form compound **1.23** in 69% yield over three steps. With the C3-disacharide acceptor **1.23** in hand, they used α-L-pyranone donor **1.24** in a palladium catalyzed glycosylation to form trisaccharide **1.25** in 95% yield. Leveraging previously performed transformations, trisaccharide **1.25** underwent a Luche reduction, followed by a subsequent Mitsunobu inversion to form trisaccharide **1.26** in 88% yield over three steps. Finally, the removal of the TBS groups and saturation of the alkene gave the final trisaccharide unit **1.27** in 22 steps in 4.5% overall yield.[48] This synthesis heavily relied on post-glycosylation modifications to the glycan.

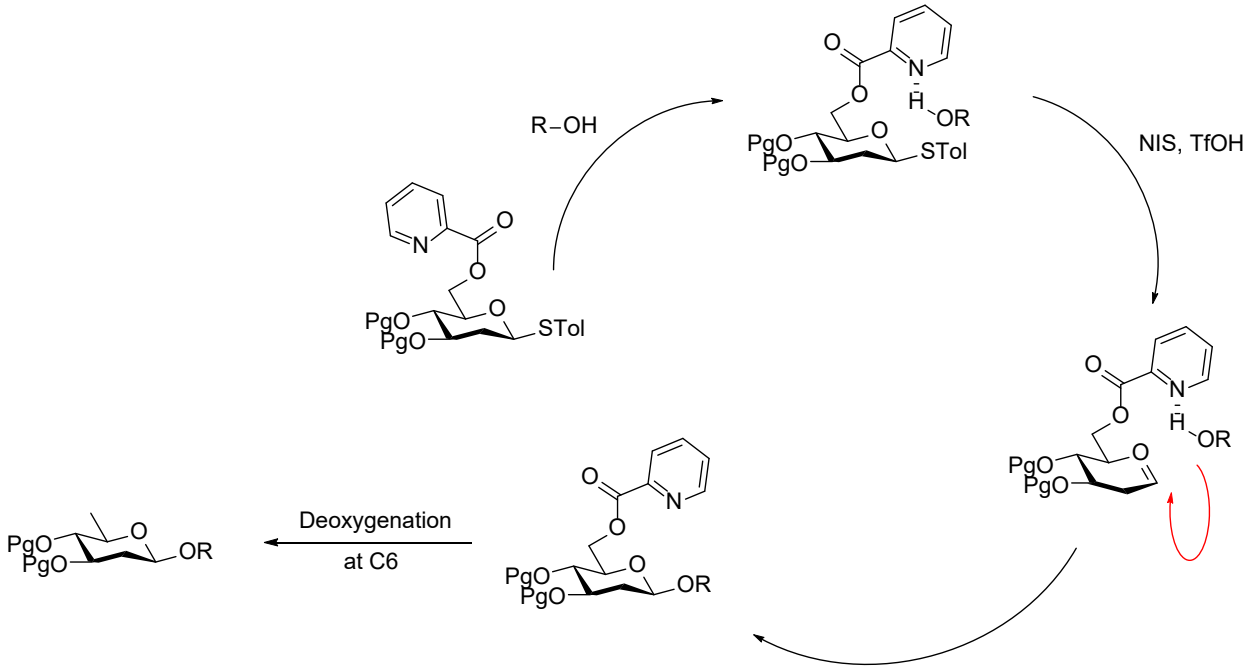

Scheme 1.2: Mechanistic insights into β-selectivity guided by a 6-O-Pico-2-Deoxythioglucoside

Another example of the synthesis of the trisaccharide unit came from Mong and coworkers. Their glycosylation approach for β-selectivity used a 6-*O*-Pico-2-Deoxythioglucoside **1.28** and 2,6-dideoxyolivoside **1.29** under catalytic acidic conditions where the C6 pinacol donor guided the

formation of the β-linkage formed in disaccharide **1.30** in 75% yield (**Sch. 1.2, Sch.1.3**).[51] Since it is known that remote C4 electron donating protecting groups can be leveraged in the presence of a counter ion to yield high α-selectivity in glycosylations,[52] the disaccharide acceptor **1.30** was deprotected at C3 then added with L-rhodinosyl acetate donor **1.31** under acidic conditions with $BF_3 \cdot Et_2O$ to yield trisaccharide **1.32** in 78% yield over two steps. Removal of the C6-pinicol group followed by Barton McCommbie deoxygenation on the C6 of the middle olivose sugar lead them to the final trisaccharide **1.33** in 79% yield over three steps.[53]

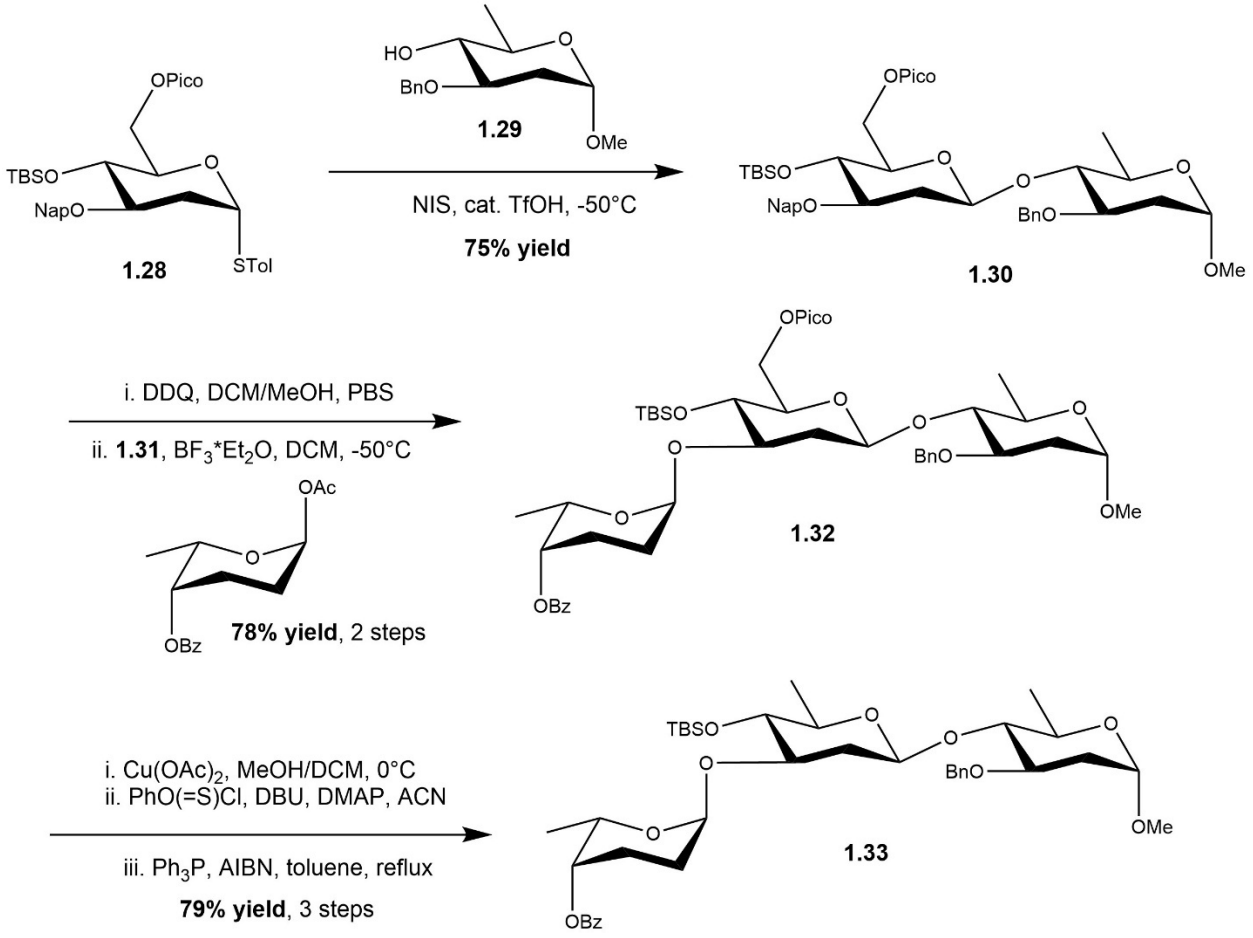

Scheme 1.3: Mong's method to the trisaccharide fragment of LaA

For the preparation of the entire hexasaccharide fragment, Guo and Sulikowski approached the selective synthesis oligosaccharides using glycosyl tetrazoles to guide alpha linkages with Me_3OBF_4 as an activating agent between 2,3,6-trideoxy rhodinose donor and D-rhamnal acceptor (**Sch. 1.4**).[54] Disaccharide **1.36** was acetylated at the C3 alcohol on the rhamnal residue followed by the formation of phenyl selenyl acetates **1.37** and **1.38** in 62% and 21% yield respectively, determined by NMR analysis. Those compounds were inseparable, so the mixture

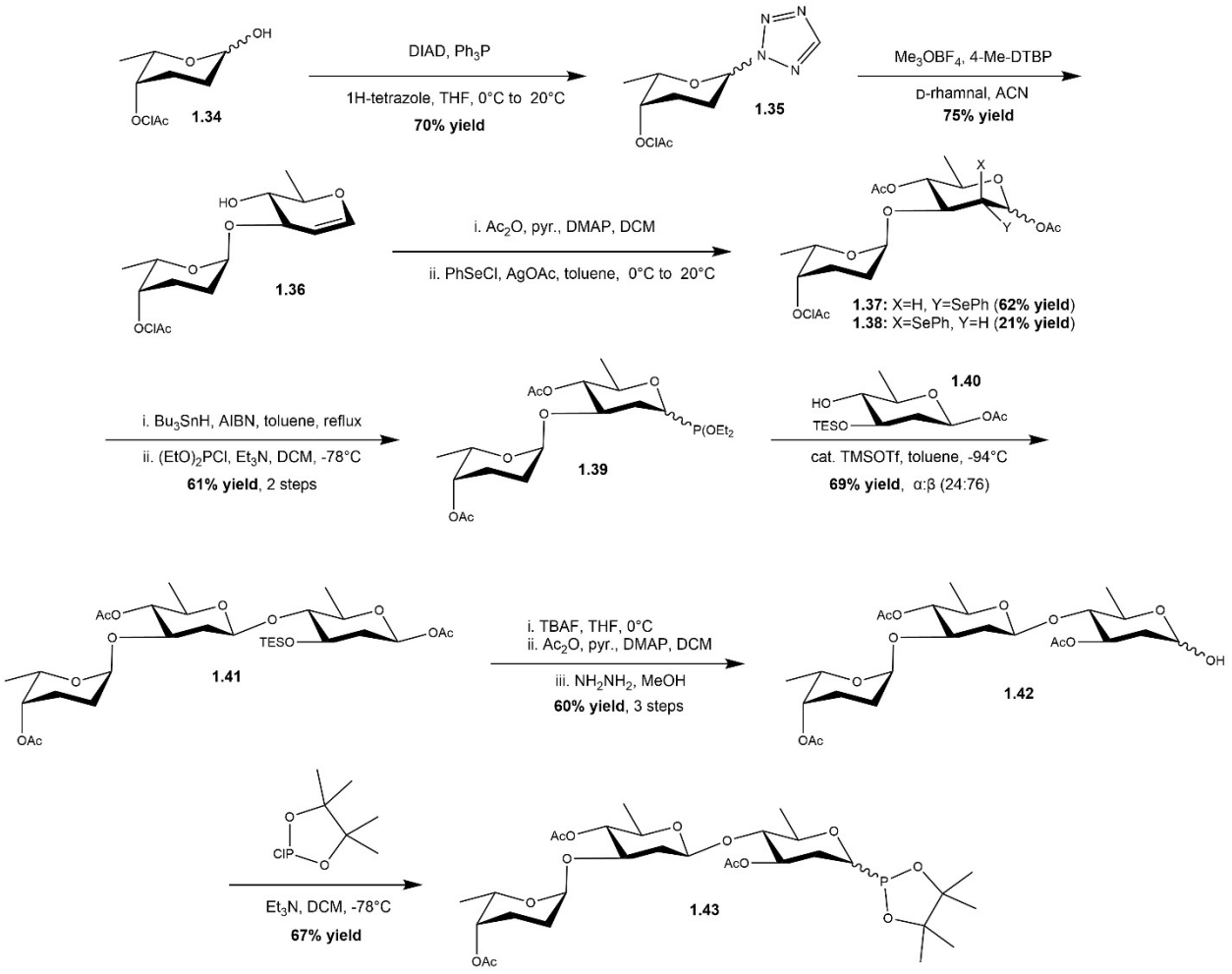

Scheme 1.4: Guo and Sulikowski's method to the trisaccharide donor 1.43, a fragment of LaA

was reduced using organo-tin and AIBN followed by a phosphinite installation at the anomeric position to give compound **1.39** in 61% yield over 2 steps. Disaccharide donor **1.39** was then added with C4 olivose acceptor **1.40** under catalytic acidic conditions to form trisaccharide **1.41** in 69%

yield α:β (24:76). The TES protecting group was then removed using TBAF and replaced with an acetyl protecting group, followed by the hydrolysis of the anomeric acetate selectively to give trisaccharide **1.42** in 60% yield over three steps. To guide beta linkages, they used glycosyl phosphite donors and protected acceptors.[55] Compound **1.42** was glycosylated to a pinacol phosphinite giving the final trisaccharide donor, compound **1.43** in 67% yield. To form the trisaccharide acceptor **1.48**, the group started with D-rhamnal **1.44**, which was selinated at the C2 position to give hemi-acetal product **1.45** in 63% yield over 2 steps. Selenide **1.45** underwent a Mitsunobu reaction with high selectivity (α:β (1:10)). Reduction of the C2 phenyl selenide afforded C4 acceptor **1.46** in 59% yield over those two steps. That acceptor was mixed with disaccharide phosphinite donor **1.47** under catalytic acidic conditions to form trisaccharide **1.48** in 72% yield with good beta selectivity (α:β (26:74)). Following the removal of the silyl group, installation of an acetyl group and hydrolysis of the protecting group on the C4 rhodinose residue, trisaccharide acceptor **1.49** was prepared in 55% yield over three steps. Finally, they linked trisaccharide donor **1.** and trisaccharide acceptor **1.49** together in a [3+3] fashion using catalytic acidic conditions to form the octo-aceyl-LaA hexasaccharide in 42% yield and 52:48 α:β selectivity.

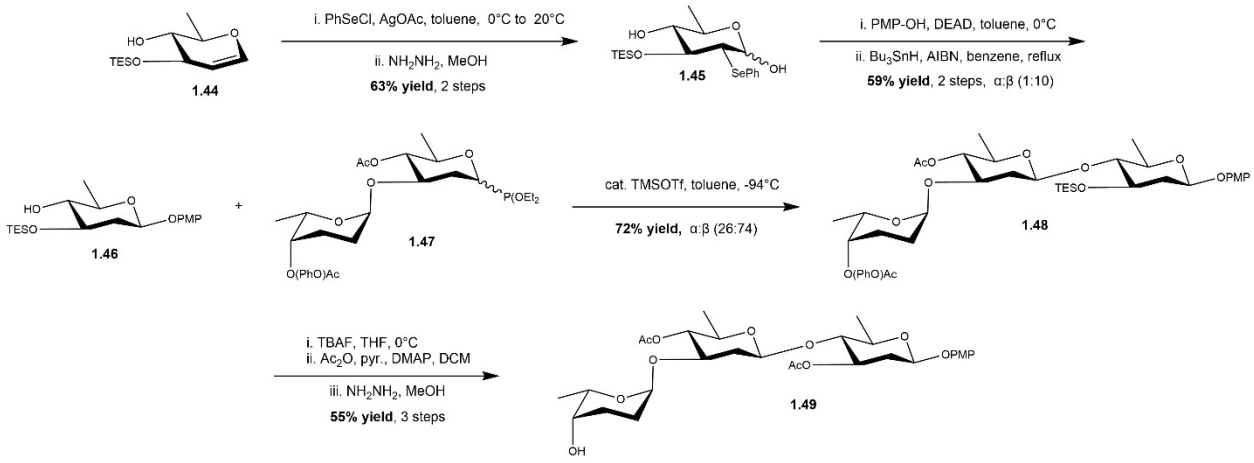

Scheme 1.5: Guo and Sulikowski's method to the trisaccharide acceptor, 1.49, a fragment of LaA

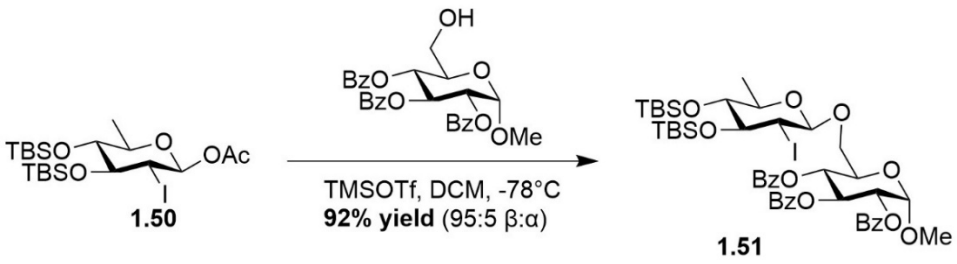

Scheme 1.6: Precedent for the indirect glycosylation approach used by Bennet and Roush in the synthesis of the LaA Hexasaccharide

A prominent approach to glycosylation includes indirect methods, which make use of a temporary prosthetic group at the C2 position. The temporary group helps to modulate the reactivity of the system and to influence the approach of the nucleophile. However, the removal of that group does add steps when applied to total syntheses, needing a reduction to reach the final 2-deoxy sugar product. Common functionalities in these reactions include halides,[56] selenides,[57] and thioacetates.[58] An example of indirect techniques can be found by Roush and Bennet in the synthesis of hexasaccharide of LaA, where the group used a C2 equatorial iodide to guide the formation of the beta linkages featured in that natural product.[46] Beginning with protected C4 acceptor **1.52** and glycosyl trichloroacetimidate donor **1.53**, the monosaccharides were glycosylated under catalytic acidic conditions giving disaccharide **1.54** in 93% yield with >1:19 α:β selectivity. Acetolysis of the 1,6-anhydro linkage followed by deprotection of the C3 silyl ether afforded disaccharide acceptor **1.55** in 91% yield over two steps. Using L-rhodinosyl acetate donor **1.56** under catalytic acidic conditions, the disaccharide acceptor **1.55** and donor were coupled together in 91% yield, favoring the β-acetate trisaccharide **1.57** (α:β, 1:3). That trisaccharide was then converted to trichloroacetimidate trisaccharide donor **1.58** in 78% yield over two steps. Compound **1.58** was glycosylated with an DMPM-alcohol acceptor followed by TBS deprotection

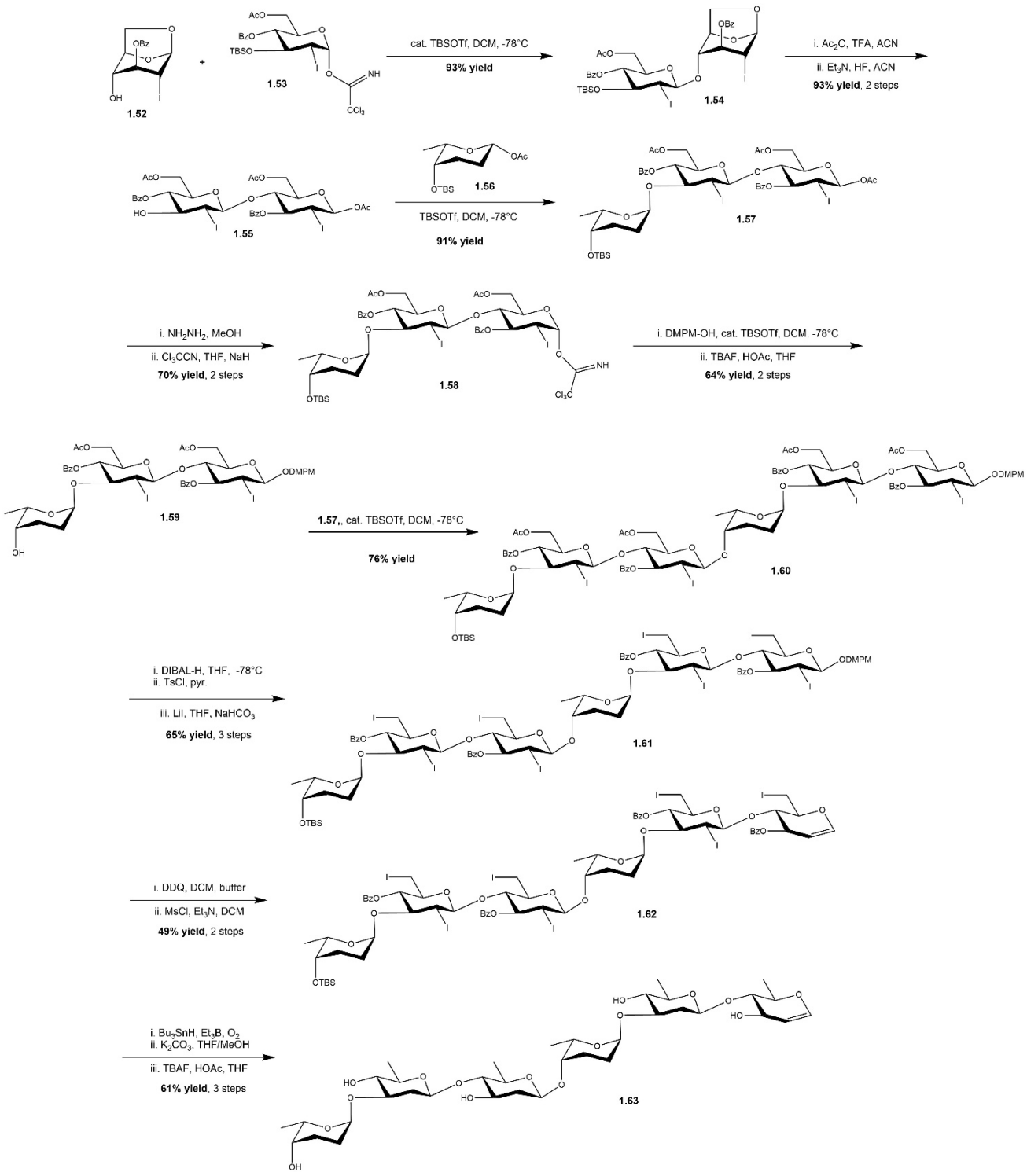

Scheme 1.7: Roush and Bennet's approach to the synthesis of the hexasaccharide 1.63, belonging to LaA

on the rhodinose residue to afford trisaccharide acceptor **1.59** in 64% yield over 2 steps. That acceptor **1.59** was then added to an acid catalyzed glycosylation with trisaccharide donor **1.57** to

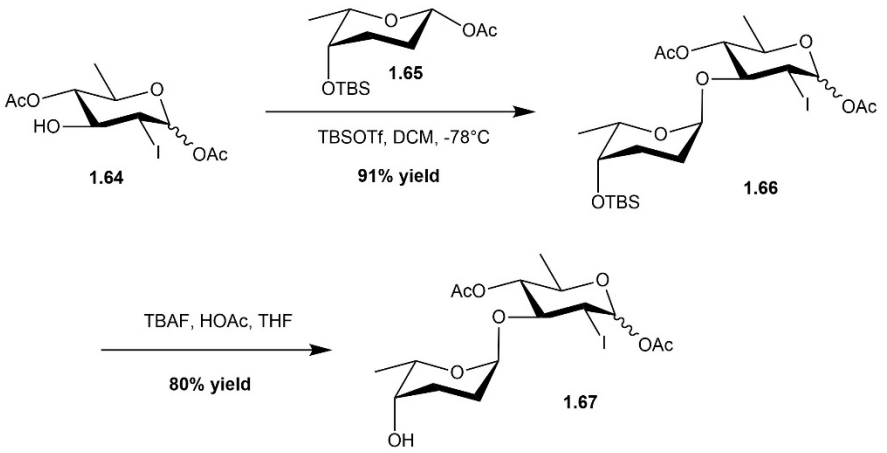

Scheme 1.8: Yu's approach to the synthesis of the disaccharide 1.67 in route to the total compound, LaA

furnish a hexasaccharide, compound **1.60** in 76% yield, with β-selectivity. The four acetate groups were cleaved with DIBAL-H, tosylated, and then replaced with an iodide group using LiI in the presence of base, giving hexasaccharide **1.61** in 65% yield over three steps. The glycosyl DMPM group was removed under basic conditions with DDQ, followed by the addition of methane sulfonyl chloride which promoted the reductive elimination to glycal

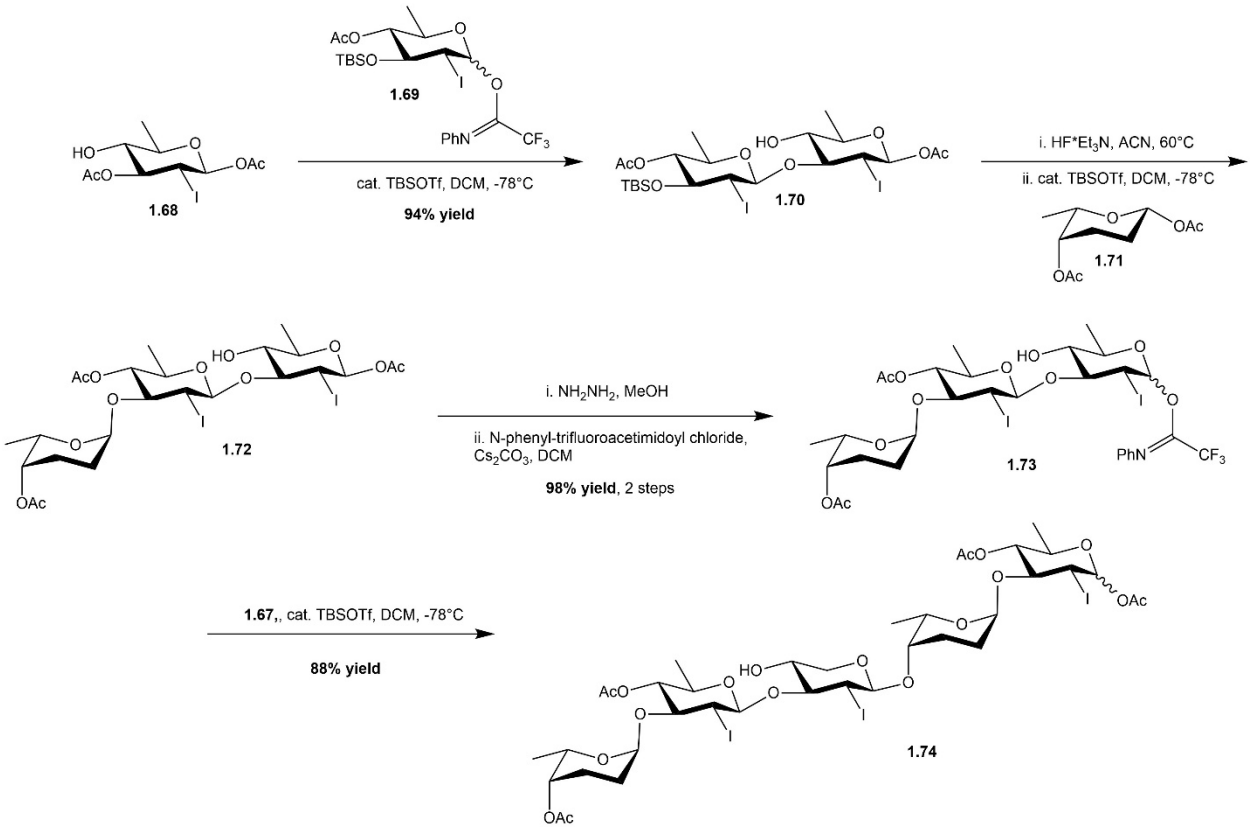

Scheme 1.9: Yu's approach to the synthesis of the pentasaccharide 1.74 in route to the total compound, LaA

hexasaccharide **1.62** in 41% yield over two steps. Finally, reduction of the remaining iodide groups and removal of the TBS ether furnished the final hexasaccharide glycal, compound **1.63** in 63% yield over three steps. A similar approach was used by Yu in his work to synthesize the total compound, LaA.[45] Starting with acceptor **1.64** and donor **1.65**, an acid catalyzed glycosylation gave disaccharide **1.66** in 91% yield. A subsequent TBS removal from the C4 on the rhodinose residue gave disachharide acceptor **1.67** in 80% yield. Following assembly of the disaccharide **1.67**, the group used acceptor **1.68** and phenyltrichloroacetimidate donor **1.69** in an acid catalyzed glycosylation to reach disaccharide **1.70** in 94% yield with β-selectivity. They removed the anomeric acetyl group selectively and formed another phenyltrichloroacetimidate donor, trisaccharide **1.73** in 98% yield over two steps. In a [2+3] fashion, they glycosylated trisaccharide **1.73** and disaccharide **1.67** to get pentasaccharide **1.74** in 88% yield with β-selectivity. The remaining steps of this synthesis will be explained in Section 1.6 of this chapter.

Because deoxy sugars lack functionality at the C2 position and are more reactive than their substituted equivalents,[59] the Bennett lab developed a reagent-controlled dehydrative glycosylation, where the anomeric linkage formed depends on the tosylate promoter system used in the reaction.[60] At cryogenic temperatures, a 2-deoxy hemi-acetal donor is deprotonated at the anomeric position by a strong base. Then, the promoter is added to the reaction at cryogenic temperatures. Low temperature NMR showed the formation of an α-sulfonate intermediate, leading to the S_N2-like conversion to the final β-glycoside after attack by the acceptor. Because the electronic properties and size of the of the promoter system have a direct effect on the stereochemical outcome, the Bennett lab has been able to synthesize a variety of α- and β- linked

deoxy sugar natural products selectively using different tosylate promoters (**Sch. 1.10**).[61]

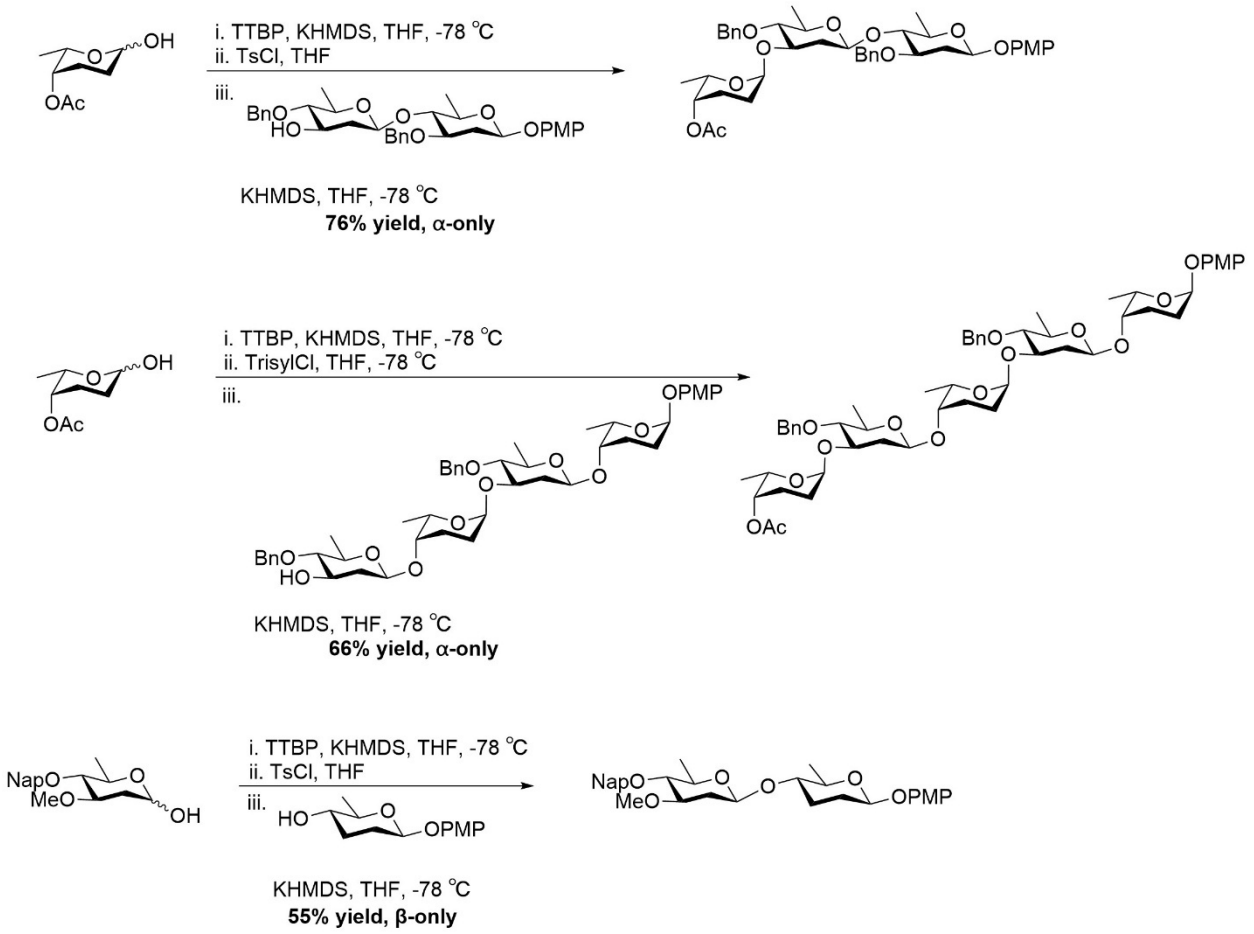

Scheme 1.10: Examples of deoxy oligosaccharide chains assembled using different tosylate promoters under the Bennett lab's reagent controlled dehydrative glycosylation conditions[62]

Using donor **1.75** and PMP-acceptor **1.76** in dehydrative conditions with TsCl as a promoter, they accessed disaccharide **1.77** in 81% yield with high β-selectivity. Following denapthalation of disaccharide **1.77**, that compound was used as a C3 acceptor in a dehydrative glycosylation with rhodinose donor **1.78** to give trisaccharide **1.80** in high α-selectivity. Interestingly, using TsCl instead of TrisylCl gave a higher yield and α-selectivity remained with either, so TsCl was the promoter of choice for this donor/acceptor pair. Trisaccharide **1.80** was converted into both the donor **1.81** and acceptor **1.82** in high yields, setting the group up for the [3+3] glycosylation to a hexasaccharide fragment (**Sch. 1.11, Sch. 1.12**). When the hexasaccharide fragment from the

dehydrative glycosylation was purified, issues with degradation were identified. Due to this, the group opted to remove the benzyl ethers and install acetates. Thankfully, removal of the benzyl ethers with Raney nickel, followed by global acetyl protection gave hexasaccharide **1.83**, which was more easily purified. This three-step sequence gave a 55% yield in three steps to hexasaccharide **1.83**. Finally, the removal of the acetates under mildly basic conditions furnished the final hexasaccharide, compound **1.84**, in 91% yield. Using this method, the Bennett lab was able to successfully synthesize the LaA hexasaccharide **1.84** in 25 steps and 8.9% overall yield, starkly outperforming other methods.

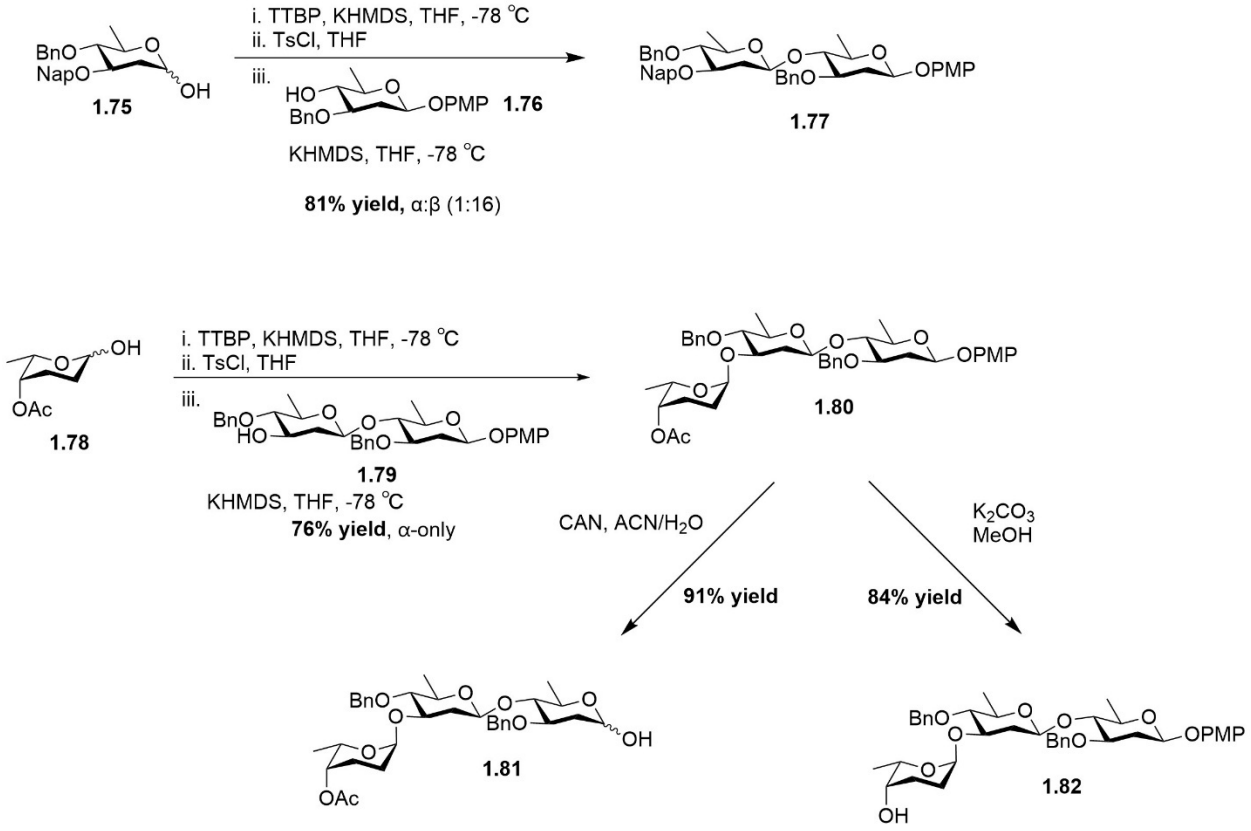

Scheme 1.11: Bennett's approach to the synthesis of trisaccharide donor 1.81 and trisaccharide acceptor 1.82 in route to the hexasaccharide portion of LaA

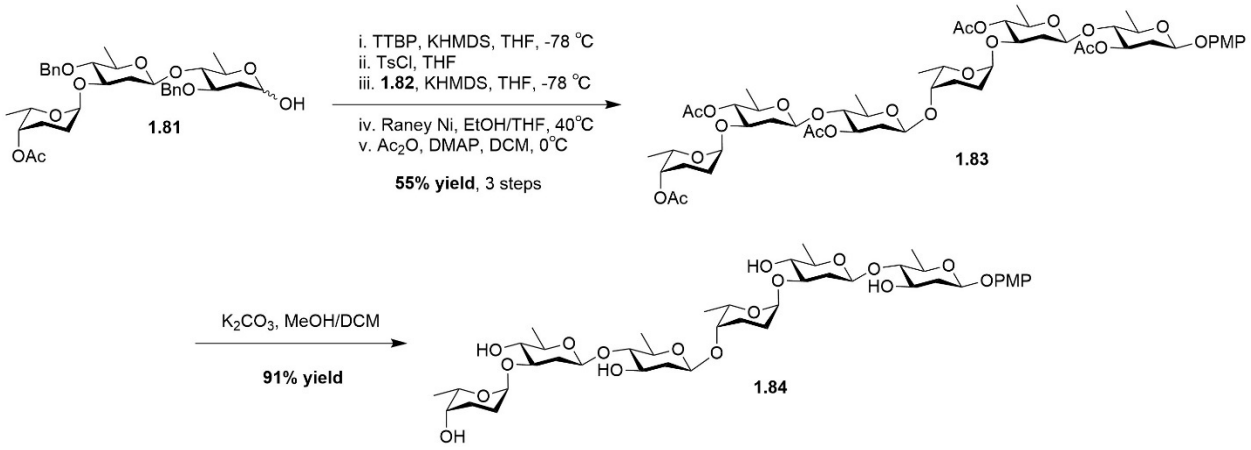

Scheme 1.12: Bennett's approach to the synthesis of the hexasaccharide portion of LaA, compound 1.84

1.6: Landomycins – Synthetic Approaches to the Aglycone and Total Synthesis

The Roush group has synthesized the aglycone of this molecule, with syntheses proceeding it based off their findings. Key steps in this synthesis featured a Dötz Bezanulation of a chromium carbene **1.86** with an alkyne **1.87** to form the D/C ring system. An intramolecular Michael-type

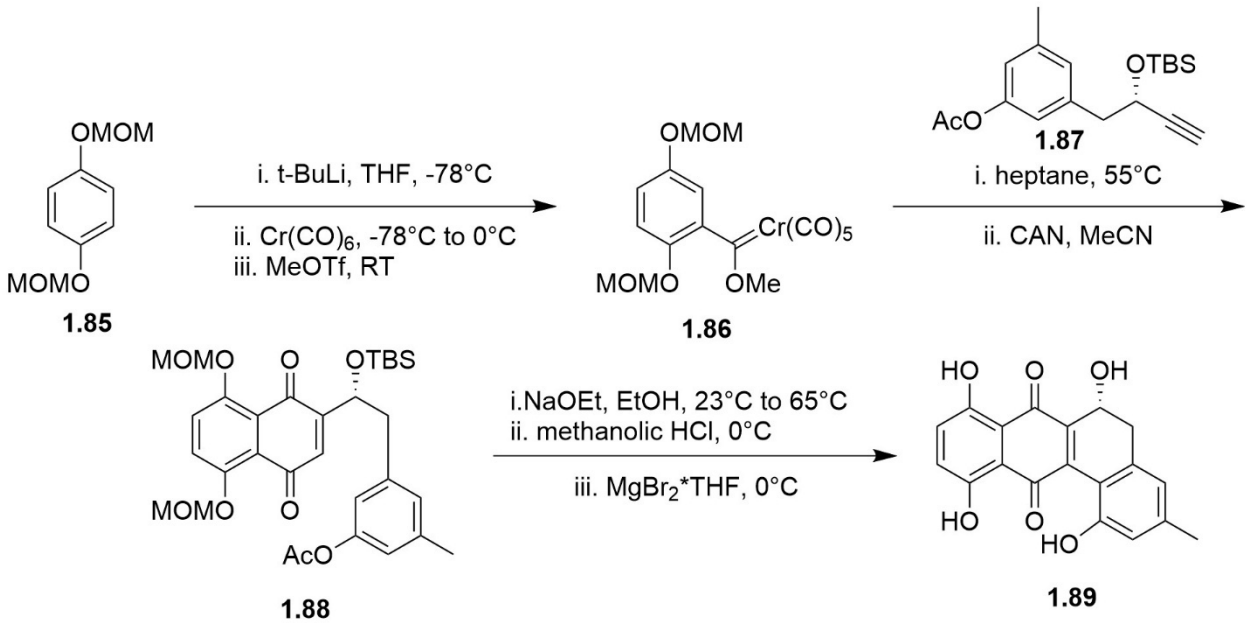

Scheme 1.13: Roush and Neitz's synthesis of landomycinone, compound 1.89

cyclization was used in the formation of the B ring (**Sch. 1.13**). Subsequently, deprotection steps lead to the formation of the aglycone, compound **1.89**, in 19 steps in 1.3% overall yield. The

stability of the aglycone in basic conditions was low, affecting yield negatively. This was due in part to the dehydrative aromatization process that the chiral TBS group underwent, forming an unwanted side product throughout multiple steps, therefore effecting overall yield negatively. To date, the Yu group is the only to complete the total synthesis of LaA and their approach to

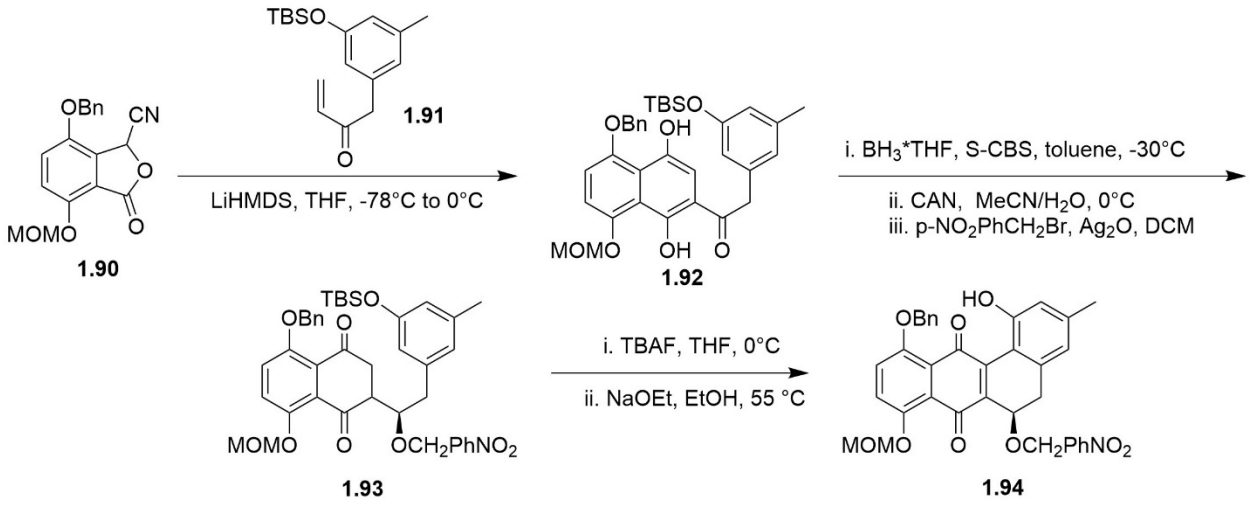

Scheme 1.14: Yu's synthesis of landomycinone, compound 1.94

landomycinone relied on using the Hauser annulation to form the B ring followed by a Michael-type addition to form the C ring (**Sch. 1.14**). Sugar synthesis was performed by acid catalyzed glycosylation techniques, employing indirect methods leveraging C2 glycosyl iodides, explained in the previous section. Because the phenolic C8 -OH is so poorly nucleophilic and because of the propensity for aromatization of the B ring, selecting glycosylation conditions to the final product proved challenging. Thankfully, methods developed by Gervay-Hague using glycosyl iodides under cryogenic, anionic conditions successfully formed the sugar linked aglycone, compound **1.98**.[63] This technique was employed to form the selective β-linkage between the aglycone **1.77** and a 6-bromo-D-olivose monosacharide **1.95** (**Sch. 1.15**). Then, the corresponding

pentasaccharide trifluoroacetimidate was coupled to the landomycinone monoglycoside **1.99**

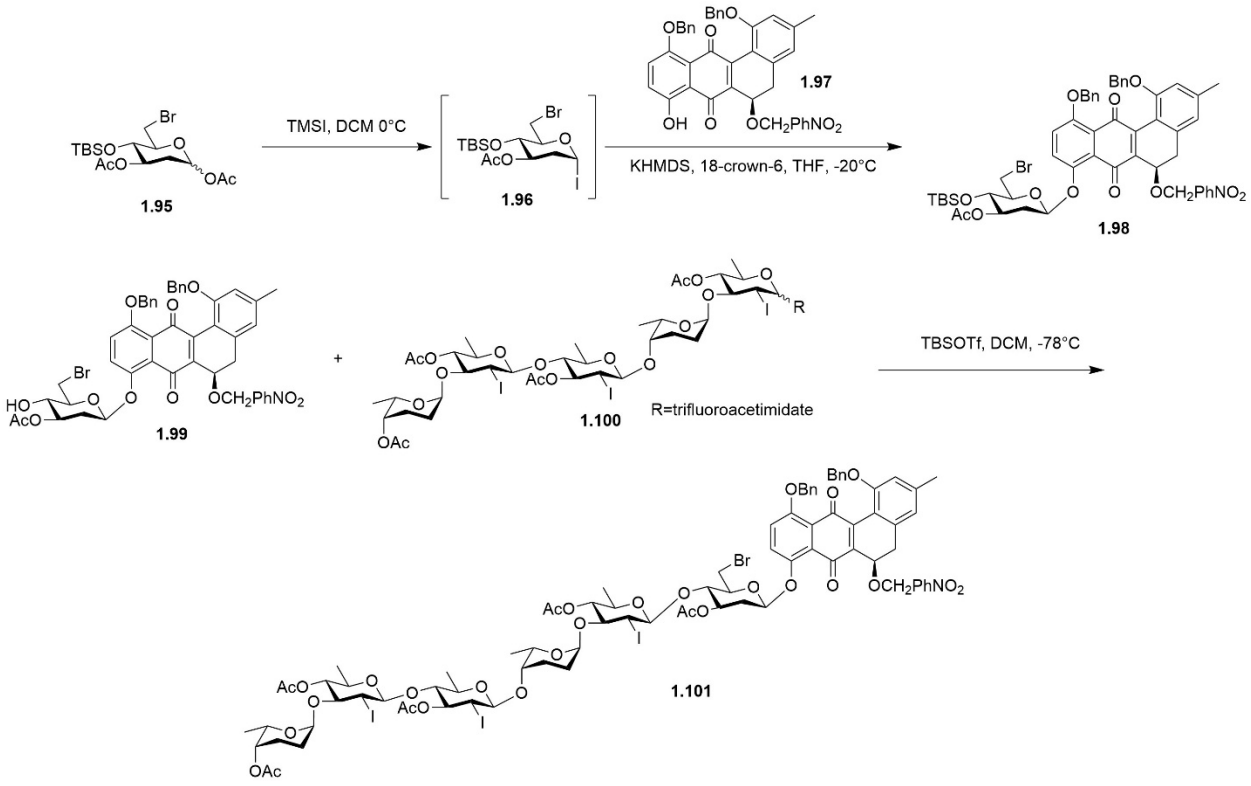

Scheme 1.15: The final steps of Yu's synthesis of LaA, compound 1.101, the only total synthesis of this compound to date

using catalytic TBSOTf (**Sch. 1.15**). By reduction of the remaining C2 iodides with Raney nickel and removing the acetyl protecting groups with sodium methoxide, they afforded the total compound, LaA, in 63 steps and 0.34% overall yield.

1.7: Landomycins – Synthetic Biology Approaches

There are also approaches to isolate the target molecule(s) from bacterial cultures. Advances in higher throughput and more sensitive technologies for the identification of natural products and biosynthetic gene clusters (BGCs) – genes that encode enzymatic pathways responsible for natural product biosynthesis – have revealed a vast landscape of natural biochemical diversity.[64,65] In particular, genome mining has revealed the vast number of cryptic or

low yield biosynthetic gene clusters in the genus *Streptomyces*. Though biosynthesis is a catalytically efficient method to produce natural products, BGC expression is often poor and pathway activation mechanisms remain indeterminant. Of the thousands of identified microbial BGCs, the genus *Streptomyces* encodes the greatest number and highest density, producing numerous bioactive compounds and relevant chemical scaffolds.[66–68] Among these, landomycins – polyketides that belong to the angucycline family – exhibit bioactivity via diverse and potentially novel mechanism(s) of action, explained previously, making them promising therapeutics to target drug-resistant phenotypes.[21,36,40] Landomycin BGCs have only been directly identified in three genomic samples, though a fourth is presumed due to landomycin detection in culture extracts.[69–72] *Streptomyces cyanogenus* 136 (S136) is the only known natural source of LaA.[25,73] Control over the biosynthetic regulon via genetic interventions and optimization of culture conditions have proven quite successful at improving yield or altering dominant products.[74–77] In particular, modifications to the major pathway regulators *adpA* and *bldA* have improved landomycin titers – though modifications to pathway gene expression can alter the composition of landomycin products compared to wildtype S136.[78–80] Of particular note is recent work that showed that complementation of S136 with a functional copy of the transcription factor *adpA* from *S. ghanaensis* (*adpA*$_{gh}$) improved LaA yields by more than 5-fold and rendered S136 capable of synthesizing LaA in a variety of media. Still, additional improvements to increase the yield, as well as methods that facilitate the purification of landomycins, will aid in their potential for future clinical testing and modification into next-generation, semi-synthetic analogs unavailable via biosynthesis. Additionally, while efforts to develop chemical synthesis methods have met with significant success, they are often expensive, time-consuming, and low-yielding, and thus are better suited for semi-synthetic methods that start with biologically derived chemical scaffolds.[81]

Thus, production of sufficient bioactive natural products remains a major hurdle that limits their eventual translation to clinical applications. If equipped with the proper bacterial strain of S. *cyanogenus* to access these molecule(s) through fermentation, purification can be grueling, requiring up to four different chromatographic techniques, which is not conducive to the scale up in production needed for extensive biological studies. Rohr and Shabaan both isolated low recovery percentages of pure LaA from bacterial cultures using multiple purification methods including normal-phase column chromatography, reverse phase column chromatography, PREP-HPLC purification, and size exclusion chromatography.[21,42] Some of these methods are quite expensive and not available to all academic research labs, like PREP-HPLC, with costs for the system ranging from $50,000 to $200,000. Size exclusion chromatography is useful but has several limitations including low sample loading, extended elution times, and costly resins. Given these factors, we have initiated research directed at optimizing the production of landomycin A in a novel bacterial strain, S136-9a, and simplifying the necessary purification strategies to the target to employ semi-synthetic methods for compound derivatization. Further expansion on this work can be found in Chapter 2 and Chapter 3.

1.8 Concluding Remarks

Deoxy oligosaccharide-containing bacterial natural products represent a chemically diverse and biologically significant class of molecules with broad therapeutic potential. However, the challenges associated with their synthesis—especially glycosylation reactions involving deoxy sugars—and their limited natural abundance have hindered detailed structure–activity relationship studies. The landomycins exemplify these challenges and opportunities. With a complex benz[a]anthracene-derived aglycone and varied deoxy sugar chains that modulate biological activity, landomycins offer a compelling platform for therapeutic development. Their unique,

ROS-mediated mechanism of action further differentiates them from other polyketide-derived anticancer agents, despite similar structural features. Yet, poor synthetic accessibility and the need for improved biosynthetic yields continue to limit translational progress. This thesis aims to address these limitations through the development of improved production and purification strategies in *Streptomyces cyanogenus* S136-9a and the synthesis of semi-synthetic derivatives. The following chapters will explore these approaches in detail and evaluate their implications for future therapeutic development.

1.9: Works Cited

(1) Bertozzi, C. R.; Kiessling, and L. L. Chemical Glycobiology. *Science (80-.).* **2001**, *291* (5512), 2357–2364. https://doi.org/10.1126/science.1059820.

(2) Elshahawi, S. I.; Shaaban, K. A.; Kharel, M. K.; Thorson, J. S. A Comprehensive Review of Glycosylated Bacterial Natural Products. *Chem. Soc. Rev.* **2015**, *44* (21), 7591–7697. https://doi.org/10.1039/c4cs00426d.

(3) Zong, A.; Cao, H.; Wang, F. Anticancer Polysaccharides from Natural Resources: A Review of Recent Research. *Carbohydr. Polym.* **2012**, *90* (4), 1395–1410. https://doi.org/10.1016/j.carbpol.2012.07.026.

(4) Khan, T.; Date, A.; Chawda, H.; Patel, K. Polysaccharides as Potential Anticancer Agents—A Review of Their Progress. *Carbohydr. Polym.* **2019**, *210* (January), 412–428. https://doi.org/10.1016/j.carbpol.2019.01.064.

(5) Friedman, M. Mushroom Polysaccharides: Chemistry and Antiobesity, Antidiabetes, Anticancer, and Antibiotic Properties in Cells, Rodents, and Humans. *Foods* **2016**, *5* (4), 1–40. https://doi.org/10.3390/foods5040080.

(6) Chevrette, M. G.; Handelsman, J. Needles in Haystacks: Reevaluating Old Paradigms for the Discovery of Bacterial Secondary Metabolites. *Nat. Prod. Rep.* **2021**, *38* (11), 2083–2099. https://doi.org/10.1039/d1np00044f.

(7) Kaklamani, V. G.; Gradishar, W. J. Epirubicin versus Doxorubicin: Which Is the Anthracycline of Choice for the Treatment of Breast Cancer? *Clin. Breast Cancer* **2003**, *4* (SUPPL. 1), S26–S33. https://doi.org/10.3816/CBC.2003.s.012.

(8) Krumper, J. R.; Salamant, W. A.; Woerpel, K. A. Continuum of Mechanisms for Nucleophilic Substitutions of Cyclic Acetals. *Org. Lett.* **2008**, *10* (21), 4907–4910. https://doi.org/10.1021/ol8019956.

(9) Hansen, T.; Lebedel, L.; Remmerswaal, W. A.; Van Der Vorm, S.; Wander, D. P. A.; Somers, M.; Overkleeft, H. S.; Filippov, D. V.; Désiré, J.; Mingot, A.; Bleriot, Y.; Van Der Marel, G. A.; Thibaudeau, S.; Codée, J. D. C. Defining the SN1 Side of Glycosylation Reactions: Stereoselectivity of Glycopyranosyl Cations. *ACS Cent. Sci.* **2019**, *5* (5), 781–788. https://doi.org/10.1021/acscentsci.9b00042.

(10) Romero, J. A. C.; Tabacco, S. A.; Woerpel, K. A. Stereochemical Reversal of Nucleophilic Substitution Reactions Depending upon Substituent: Reactions of Heteroatom-Substituted Six-Membered-Ring Oxocarbenium Ions through Pseudoaxial Conformers. *J. Am. Chem. Soc.* **2000**, *122* (1), 168–169. https://doi.org/10.1021/ja993366o.

(11) Ayala, L.; Lucero, C. G.; Antoinette, J.; Romero, C.; Tabacco, S. A.; Woerpel, K. A. Stereochemistry of Nucleophilic Substitution Reactions Depending upon Substituent: Evidence for Electrostatic Stabilization of Pseudoaxial Conformers of Oxocarbenium Ions by Heteroatom Substituents. *J. Am. Chem. Soc.* **2003**, *125* (50), 15521–15528. https://doi.org/10.1021/ja037935a.

(12) Zhu, D.; Adhikari, S.; Baryal, K. N.; Abdullah, B. N.; Zhu, J. Stereoselective Synthesis of α-Digitoxosides and α-Boivinosides via Chelation-Controlled Anomeric O-Alkylation. *J. Carbohydr. Chem.* **2014**, *33* (7–8), 438–451. https://doi.org/10.1080/07328303.2014.931965.

(13) Chen, J. H.; Ruei, J. H.; Mong, K. K. T. Iterative α-Glycosylation Strategy for 2-Deoxy- and 2,6-Dideoxysugars: Application to the One-Pot Synthesis of Deoxysugar-Containing Oligosaccharides. *European J. Org. Chem.* **2014**, *2014* (9), 1827–1831. https://doi.org/10.1002/ejoc.201400006.

(14) Chamberland, S.; Ziller, J. W.; Woerpel, K. A. Structural Evidence That Alkoxy Substituents Adopt Electronically Preferred Pseudoaxial Orientations in Six-Membered Ring Dioxocarbenium Ions. *J. Am. Chem. Soc.* **2005**, *127* (15), 5322–5323. https://doi.org/10.1021/ja050830i.

(15) Cumpstey, I. On a So-Called "Kinetic Anomeric Effect" in Chemical Glycosylation. *Org. Biomol. Chem.* **2012**, *10* (13), 2503–2508. https://doi.org/10.1039/c2ob06696c.

(16) Chatterjee, S.; Moon, S.; Hentschel, F.; Gilmore, K.; Seeberger, P. H. An Empirical Understanding of the Glycosylation Reaction. *J. Am. Chem. Soc.* **2018**, *140* (38), 11942–11953. https://doi.org/10.1021/jacs.8b04525.

(17) Zhu, X.; Schmidt, R. R. New Principles for Glycoside-Bond Formation. *Angew. Chemie - Int. Ed.* **2009**, *48* (11), 1900–1934. https://doi.org/10.1002/anie.200802036.

(18) Zhang, H.; White-Phillip, J. A.; Melançon, C. E.; Kwon, H. J.; Yu, W. L.; Liu, H. W. Elucidation of the Kijanimicin Gene Cluster: Insights into the Biosynthesis of Spirotetronate Antibiotics and Nitrosugars. *J. Am. Chem. Soc.* **2007**, *129* (47), 14670–14683. https://doi.org/10.1021/ja0744854.

(19) Shaaban, K. A.; Ahmed, T. A.; Leggas, M.; Rohr, J. Saquayamycins G-K, Cytotoxic Angucyclines from Streptomyces Sp. Including Two Analogues Bearing the Aminosugar Rednose. *J. Nat. Prod.* **2012**, *75* (7), 1383–1392. https://doi.org/10.1021/np300316b.

(20) Secondary, N.; Ströch, K.; Zeeck, A.; Antal, N.; Fiedler, H. [_ ANTIBIOTICS J Retymicin , Galtamycin B , Saquayamycin Z and Ribofuranosyllumichrome ,. **2005**, *58* (2), 103–110.

(21) Henkel, T.; Rohr, J.; Beale, J. M.; Schwenen, L. Landomycins, New Angucycline Antibiotics from Streptomyces Sp. I. Structural Studies on Landomycins A~D. *J. Antibiot. (Tokyo).* **1990**, *43* (5), 492–503. https://doi.org/10.7164/antibiotics.43.492.

(22) Shaaban, K. A.; Stamatkin, C.; Damodaran, C.; Rohr, J. 11-Deoxylandomycinone and Landomycins X-Z, New Cytotoxic Angucyclin(on)Es from a Streptomyces Cyanogenus K62 Mutant Strain. *J. Antibiot. (Tokyo).* **2011**, *64* (1), 141–150. https://doi.org/10.1038/ja.2010.121.

(23) Bradner, W. T.; Claridge, C. A.; Huftalen, J. B. Antitumor Activity of Kijanimicin. *J. Antibiot. (Tokyo).* **1983**, *36* (8), 1078–1079. https://doi.org/10.7164/antibiotics.36.1078.

(24) Mizia, J. C.; Syed, M. U.; Bennett, C. S. Synthesis of the α-Linked Digitoxose Trisaccharide Fragment of Kijanimicin: An Unexpected Application of Glycosyl Sulfonates. *Org. Lett.* **2022**, *24* (2), 731–735. https://doi.org/10.1021/acs.orglett.1c04190.

(25) Weber, S.; Zolke, C.; Rohr, J.; Beale, J. M. Investigations of the Biosynthesis and Structural Revision of Landomycin A. *J. Org. Chem.* **1994**, *59* (15), 4211–4214. https://doi.org/10.1021/jo00094a037.

(26) Ostash, B.; Rix, U.; Rix, L. L. R.; Liu, T.; Lombo, F.; Luzhetskyy, A.; Gromyko, O.; Wang, C.; Brañ, A. F.; Mé Ndez, C.; Salas, J. A.; Fedorenko, V. Generation of New Landomycins by Combinatorial Biosynthetic Manipulation of the LndGT4 Gene of the Landomycin E Cluster in S. Globisporus. *Chem. Biol.* **2004**, *11*, 547–555.

https://doi.org/10.1016/j.

(27) Seeberger, P. H. Chemical Glycobiology: Why Now? *Nat. Chem. Biol.* **2009**, *5* (6), 368–372. https://doi.org/10.1038/nchembio0609-368.

(28) Harvey, A. L.; Edrada-Ebel, R.; Quinn, R. J. The Re-Emergence of Natural Products for Drug Discovery in the Genomics Era. *Nature Reviews Drug Discovery*. Nature Publishing Group January 1, 2015, pp 111–129. https://doi.org/10.1038/nrd4510.

(29) Pham, J. V.; Yilma, M. A.; Feliz, A.; Majid, M. T.; Maffetone, N.; Walker, J. R.; Kim, E.; Cho, H. J.; Reynolds, J. M.; Song, M. C.; Park, S. R.; Yoon, Y. J. A Review of the Microbial Production of Bioactive Natural Products and Biologics. *Front. Microbiol.* **2019**, *10* (JUN). https://doi.org/10.3389/fmicb.2019.01404.

(30) Otani, H.; Udwary, D. W.; Mouncey, N. J. Comparative and Pangenomic Analysis of the Genus Streptomyces. *Sci. Rep.* **2022**, *12* (1), 18909. https://doi.org/10.1038/s41598-022-21731-1.

(31) Henkel, T.; Rohr, J.; Beale, J. M.; Schwenen, L. Landomycins, New Angucycline Antibiotics from Streptomyces Sp. I. Structural Studies on Landomycins A-D. *J. Antibiot. (Tokyo).* **1990**, *43* (5), 492–503. https://doi.org/10.7164/antibiotics.43.492.

(32) Rohr, J.; Thiericke, R. Angucycline Group Antibiotics. *Nat. Prod. Rep.* **1992**, *9* (2), 103–137. https://doi.org/10.1039/np9920900103.

(33) Rohr, J.; Thiericke, R. Angucycline Group Antibiotics. *Nat. Prod. Rep.* **1992**, *9* (2), 103–137. https://doi.org/10.1039/np9920900103.

(34) Kharel, M. K.; Pahari, P.; Shepherd, M. D.; Tibrewal, N.; Nybo, S. E.; Shaaban, K. A.;

Rohr, J. Angucyclines: Biosynthesis, Mode-of-Action, New Natural Products, and Synthesis. *Nat. Prod. Rep.* **2012**, *29* (2), 264–325. https://doi.org/10.1039/c1np00068c.

(35) Korynevska, A.; Heffeter, P.; Matselyukh, B.; Elbling, L.; Micksche, M.; Stoika, R.; Berger, W. Mechanisms Underlying the Anticancer Activities of the Angucycline Landomycin E. *Biochem. Pharmacol.* **2007**, *74* (12), 1713–1726. https://doi.org/https://doi.org/10.1016/j.bcp.2007.08.026.

(36) Panchuk, R. R. Signaling Pathways Involved in Apoptosis Induced by Novel Angucycline Antibiotic Landomycin E in Jurkat T-Leukemia Cells. **2011**, *27* (2), 124–131. https://doi.org/10.7124/bc.00008B.

(37) Lushchak, V. I. Glutathione Homeostasis and Functions: Potential Targets for Medical Interventions. *J. Amino Acids* **2012**, *2012*, 1–26. https://doi.org/10.1155/2012/736837.

(38) Korynevska, A. V.; Matselyukh, B. P.; Stoika, R. S. In Vitro Study of Landomycin E Antitumor Activity. *Exp. Oncol.* **2003**, *25* (2), 98–104.

(39) Panchuk, R. R.; Lehka, L. V.; Terenzi, A.; Matselyukh, B. P.; Rohr, J.; Jha, A. K.; Downey, T.; Kril, I. J.; Herbacek, I.; van Schoonhoven, S.; Heffeter, P.; Stoika, R. S.; Berger, W. Rapid Generation of Hydrogen Peroxide Contributes to the Complex Cell Death Induction by the Angucycline Antibiotic Landomycin E. *Free Radic. Biol. Med.* **2017**, *106*, 134–147. https://doi.org/10.1016/j.freeradbiomed.2017.02.024.

(40) Terenzi, A.; La Franca, M.; van Schoonhoven, S.; Panchuk, R.; Martínez, Á.; Heffeter, P.; Gober, R.; Pirker, C.; Vician, P.; Kowol, C. R.; Stoika, R.; Salassa, L.; Rohr, J.; Berger, W. Landomycins as Glutathione-Depleting Agents and Natural Fluorescent Probes for Cellular Michael Adduct-Dependent Quinone Metabolism. *Commun. Chem.* **2021**, *4* (1),

1–13. https://doi.org/10.1038/s42004-021-00600-4.

(41) Bugaut, X.; Guinchard, X.; Roulland, E. Synthesis of the Landomycinone Skeleton. *J. Org. Chem.* **2010**, *75* (23), 8190–8198. https://doi.org/10.1021/jo1018377.

(42) Shaaban, K. A.; Srinivasan, S.; Kumar, R.; Damodaran, C.; Rohr, J. Landomycins P-W, Cytotoxic Angucyclines from Streptomyces Cyanogenus S-136. *J. Nat. Prod.* **2011**, *74* (1), 2–11. https://doi.org/10.1021/np100469y.

(43) Roush, W. R.; Neitz, R. J. Studies on the Synthesis of Landomycin A. Synthesis of the Originally Assigned Structure of the Aglycone, Landomycinone, and Revision of Structure. *J. Org. Chem.* **2004**, *69* (15), 4906–4912. https://doi.org/10.1021/jo049426c.

(44) Guo, Y.; Sulikowski, G. A. Synthesis of the Hexasaccharide Fragment of Landomycin A: Application of Glycosyl Tetrazoles and Phosphites in the Synthesis of a Deoxyoligosaccharide. *J. Am. Chem. Soc.* **1998**, *120* (7), 1392–1397. https://doi.org/10.1021/ja973348b.

(45) Yang, X.; Fu, B.; Yu, B. Total Synthesis of Landomycin A, a Potent Antitumor Angucycline Antibiotic. *J. Am. Chem. Soc.* **2011**, *133* (32), 12433–12435. https://doi.org/10.1021/ja205339p.

(46) Roush, W. R.; Bennett, C. E. A Highly Stereoselective Synthesis of the Landomycin a Hexasaccharide Unit [10]. *J. Am. Chem. Soc.* **2000**, *122* (25), 6124–6125. https://doi.org/10.1021/ja000743k.

(47) Yalamanchili, S.; Lloyd, Di.; Bennett, C. S. Synthesis of the Hexasaccharide Fragment of Landomycin A Using a Mild, Reagent-Controlled Approach. *Org. Lett.* **2019**, *21* (10),

3674–3677. https://doi.org/10.1021/acs.orglett.9b01118.

(48) Zhou, M.; O'Doherty, G. A. De Novo Synthesis of the Trisaccharide Subunit of Landomycins A and E. *Org. Lett.* **2008**, *10* (11), 2283–2286. https://doi.org/10.1021/ol800697k.

(49) Lai, Y. H.; Mondal, S.; Su, H. T.; Huang, S. C.; Wu, M. H.; Huang, I.; Yang Lauderdale, T. L.; Song, J. S.; Shia, K. S.; Mong, K. K. T. Total Synthesis of Landomycins Q and R and Related Core Structures for Exploration of the Cytotoxicity and Antibacterial Properties. *RSC Adv.* **2021**, *11* (16), 9426–9432. https://doi.org/10.1039/d1ra01088c.

(50) Li, X.; Woodward, J.; Hourani, A.; Zhu, D.; Ayoub, S.; Zhu, J. Synthesis of the 2-Deoxy Trisaccharide Glycal of Antitumor Antibiotics Landomycins A and E. *Carbohydr. Res.* **2016**, *430*, 54–58. https://doi.org/https://doi.org/10.1016/j.carres.2016.04.031.

(51) Yasomanee, J. P.; Demchenko, A. V. Effect of Remote Picolinyl and Picoloyl Substituents on the Stereoselectivity of Chemical Glycosylation. *J. Am. Chem. Soc.* **2012**, *134* (49), 20097–20102. https://doi.org/10.1021/ja307355n.

(52) Demchenko, A. V; Rousson, E.; Boons, G.-J. Stereoselective 1,2-Cis-Galactosylation Assisted by Remote Neighboring Group Participation and Solvent Effects. *Tetrahedron Lett.* **1999**, *40* (36), 6523–6526. https://doi.org/https://doi.org/10.1016/S0040-4039(99)01203-4.

(53) Ruei, J.-H.; Venukumar, P.; Ingle, A. B.; Mong, K.-K. T. C6 Picoloyl Protection: A Remote Stereodirecting Group for 2-Deoxy-β-Glycoside Formation. *Chem. Commun.* **2015**, *51* (25), 5394–5397. https://doi.org/10.1039/C4CC08465A.

(54) Sobti, A.; Kim, K.; Sulikowski, G. A. Application of Glycosyltetrazoles in Oligosaccharide Synthesis: Assembly of the C3 Trisaccharide Component of the Antibiotic PI-080. *J. Org. Chem.* **1996**, *61*, 6–7.

(55) Hashimoto, S.; Umeo, K.; Sano, A.; Watanabe, N.; Nakajima, M.; Ikegami, S. An Extremely Mild and Stereocontrolled Construction of 1,2-Trans-β-Glycosidic Linkages Capitalizing on Benzyl-Protected Glycopyranosyl Diethyl Phosphites as Glycosyl Donors. *Tetrahedron Lett.* **1995**, *36* (13), 2251–2254. https://doi.org/https://doi.org/10.1016/0040-4039(95)00263-C.

(56) Bock, K.; Lundt, I.; Pedersen, C. 2-Bromo-2-Deoxy Sugars as Starting Materials for the Synthesis of α- or β-Glycosides of 2-Deoxy Sugars. *Carbohydr. Res.* **1984**, *130*, 125–134. https://doi.org/https://doi.org/10.1016/0008-6215(84)85275-1.

(57) Rodríguez, M. Á.; Boutureira, O.; Arnés, X.; Matheu, M. I.; Díaz, Y.; Castillón, S. Stereoselective Synthesis of 2-Deoxy-2-Iodo-Glycosides from Furanoses. A New Route to 2-Deoxy-Glycosides and 2-Deoxy-Oligosaccharides of Ribo and Xylo Configuration. *J. Org. Chem.* **2005**, *70* (25), 10297–10310. https://doi.org/10.1021/jo051461b.

(58) Knapp, S.; Kirk, B. A. Glycosylation with 2′-Thio-S-Acetyl Participation. *Tetrahedron Lett.* **2003**, *44* (41), 7601–7605. https://doi.org/10.1016/j.tetlet.2003.08.063.

(59) Overend, W. G.; Rees, C. . W.; Sequeira, J. S. Overend, Rees, and Sequeira. 3429 675. Reactions at Position 1. *J. Chem. Soc.* **1962**, 3429–3440.

(60) Issa, J. P.; Bennett, C. S. A Reagent-Controlled SN2-Glycosylation for the Direct Synthesis of β-Linked 2-Deoxy-Sugars. *J. Am. Chem. Soc.* **2014**, *136* (15), 5740–5744. https://doi.org/10.1021/ja500410c.

(61) Zhuo, M.-H.; Wilbur, D. J.; Kwan, E. E.; Bennett, C. S. Matching Glycosyl Donor Reactivity to Sulfonate Leaving Group Ability Permits SN2 Glycosylations. *J. Am. Chem. Soc.* **2019**, *141* (42), 16743–16754. https://doi.org/10.1021/jacs.9b07022.

(62) Lloyd, D.; Bennett, C. S. An Improved Approach to the Direct Construction of 2-Deoxy-β-Linked Sugars: Applications to Oligosaccharide Synthesis. *Chem. - A Eur. J.* **2018**, *24* (30), 7610–7614. https://doi.org/10.1002/chem.201800736.

(63) Lam, S. N.; Gervay-Hague, J. Efficient Route to 2-Deoxy Beta-O-Aryl-d-Glycosides via Direct Displacement of Glycosyl Iodides. *Org. Lett.* **2003**, *5* (22), 4219–4222. https://doi.org/10.1021/ol035705v.

(64) Lee, N.; Hwang, S.; Kim, J.; Cho, S.; Palsson, B.; Cho, B.-K. Mini Review: Genome Mining Approaches for the Identification of Secondary Metabolite Biosynthetic Gene Clusters in Streptomyces. *Comput. Struct. Biotechnol. J.* **2020**, *18*, 1548–1556. https://doi.org/https://doi.org/10.1016/j.csbj.2020.06.024.

(65) Liu, R.; Yu, D.; Deng, Z.; Liu, T. Harnessing in Vitro Platforms for Natural Product Research: In Vitro Driven Rational Engineering and Mining (IDREAM). *Curr. Opin. Biotechnol.* **2021**, *69*, 1–9. https://doi.org/https://doi.org/10.1016/j.copbio.2020.08.006.

(66) Yoon-Hee, C.; Hiyoung, K.; Chang-Hun, J.; Hyun-Woo, J.; Dongho, L.; Hee, S. S.; Hwang-Soo, J.; Hahk-Soo, K. Comparative Genomics Reveals a Remarkable Biosynthetic Potential of the Streptomyces Phylogenetic Lineage Associated with Rugose-Ornamented Spores. *mSystems* **2021**, *6* (4), 10.1128/msystems.00489-21. https://doi.org/10.1128/msystems.00489-21.

(67) Belknap, K. C.; Park, C. J.; Barth, B. M.; Andam, C. P. Genome Mining of Biosynthetic

and Chemotherapeutic Gene Clusters in Streptomyces Bacteria. *Sci. Rep.* **2020**, *10* (1), 2003. https://doi.org/10.1038/s41598-020-58904-9.

(68) Ward, A. C.; Allenby, N. E. Genome Mining for the Search and Discovery of Bioactive Compounds: The Streptomyces Paradigm. *FEMS Microbiol. Lett.* **2018**, *365* (24). https://doi.org/10.1093/femsle/fny240.

(69) Westrich, L.; Domann, S.; Faust, B.; Bedford, D.; Hopwood, D. A.; Bechthold, A. Cloning and Characterization of a Gene Cluster from Streptomyces Cyanogenus S136 Probably Involved in Landomycin Biosynthesis. *FEMS Microbiol. Lett.* **1999**, *170* (2), 381–387. https://doi.org/https://doi.org/10.1016/S0378-1097(98)00561-8.

(70) Matselyukh, B. P.; Polishchuk, L. V; Lukyanchuk, V. V; Golembiovska, S. L.; Lavrenchuk, V. Y. Sequences of Landomycin E and Carotenoid Biosynthetic Gene Clusters, and Molecular Structure of Transcriptional Regulator of Streptomyces Globisporus 1912. *Mikrobiol. Z.* **2016**, *78* (6), 60–70.

(71) Feng, Z.; Kallifidas, D.; Brady, S. F. Functional Analysis of Environmental DNA-Derived Type II Polyketide Synthases Reveals Structurally Diverse Secondary Metabolites. *Proc. Natl. Acad. Sci.* **2011**, *108* (31), 12629–12634. https://doi.org/10.1073/pnas.1103921108.

(72) Peng, A.; Qu, X.; Liu, F.; Li, X.; Li, E.; Xie, W. Angucycline Glycosides from an Intertidal Sediments Strain Streptomyces Sp. and Their Cytotoxic Activity against Hepatoma Carcinoma Cells. *Marine Drugs*. 2018. https://doi.org/10.3390/md16120470.

(73) Pavlo Hrab, Christian Rückert , Tobias Busche, Iryna Ostash, Jörn Kalinowski, Victor Fedorenko, O. Y. & B. O. Complete Genome Sequence of Streptomyces Cyanogenus S136, Producer of Anticancer Angucycline Landomycin A. *3Biotech* **2021**, No. 11, 228.

(74) von Mulert, U.; Luzhetskyy, A.; Hofmann, C.; Mayer, A.; Bechthold, A. Expression of the Landomycin Biosynthetic Gene Cluster in a PKS Mutant of Streptomyces Fradiae Is Dependent on the Coexpression of a Putative Transcriptional Activator Gene. *FEMS Microbiol. Lett.* **2004**, *230* (1), 91–97. https://doi.org/https://doi.org/10.1016/S0378-1097(03)00861-9.

(75) Shaaban, K. A.; Stamatkin, C.; Damodaran, C.; Rohr, J. 11-Deoxylandomycinone and Landomycins X-Z, New Cytotoxic Angucyclin(on)Es from a Streptomyces Cyanogenus K62 Mutant Strain. *J. Antibiot. (Tokyo).* **2011**, *64* (1), 141–150. https://doi.org/10.1038/ja.2010.121.

(76) Luzhetskyy, A.; Zhu, L.; Gibson, M.; Fedoryshyn, M.; Dürr, C.; Hofmann, C.; Hoffmeister, D.; Ostash, B.; Mattingly, C.; Adams, V.; Fedorenko, V.; Rohr, J.; Bechthold, A. Generation of Novel Landomycins M and O through Targeted Gene Disruption. *Chembiochem* **2005**, *6* (4), 675–678. https://doi.org/10.1002/cbic.200400316.

(77) Shaaban, K. A.; Srinivasan, S.; Kumar, R.; Damodaran, C.; Rohr, J. Landomycins P-W, Cytotoxic Angucyclines from Streptomyces Cyanogenus S-136. *J. Nat. Prod.* **2011**, *74* (1), 2–11. https://doi.org/10.1021/np100469y.

(78) Myronovskyi, M.; Brötz, E.; Rosenkränzer, B.; Manderscheid, N.; Tokovenko, B.; Rebets, Y.; Luzhetskyy, A. Generation of New Compounds through Unbalanced Transcription of Landomycin A Cluster. *Appl. Microbiol. Biotechnol.* **2016**, *100* (21), 9175–9186. https://doi.org/10.1007/s00253-016-7721-3.

(79) Yushchuk, O.; Ostash, I.; Vlasiuk, I.; Gren, T.; Luzhetskyy, A.; Kalinowski, J.; Fedorenko, V.; Ostash, B. Heterologous AdpA Transcription Factors Enhance

Landomycin Production in Streptomyces Cyanogenus S136 under a Broad Range of Growth Conditions. *Appl. Microbiol. Biotechnol.* **2018**, *102* (19), 8419–8428. https://doi.org/10.1007/s00253-018-9249-1.

(80) Gessner, A.; Heitzler, T.; Zhang, S.; Klaus, C.; Murillo, R.; Zhao, H.; Vanner, S.; Zechel, D. L.; Bechthold, A. Changing Biosynthetic Profiles by Expressing BldA in Streptomyces Strains. *Chembiochem* **2015**, *16* (15), 2244–2252. https://doi.org/10.1002/cbic.201500297.

(81) Li, C.-J.; Trost, B. M. Green Chemistry for Chemical Synthesis. *Proc. Natl. Acad. Sci.* **2008**, *105* (36), 13197–13202. https://doi.org/10.1073/pnas.0804348105.

Chapter 2: Rapid Spectrophotometric Detection for Optimized Production of Landomycins and Characterization of their Therapeutic Potential

Todd C. Chappell[1], Kathleen G. Maiello[2], Allison J. Tierney[2], Karin Yanagi[1], Jessica A. Lee[1], Kyongbum Lee[1], Charles R. Mace[2], Clay S. Bennett[2], and Nikhil U. Nair[1,*]

[1] Department of Chemical & Biological Engineering, Tufts University, Medford, MA

[2] Department of Chemistry, Tufts University, Medford, MA

Abbreviations

BGC – biosynthetic gene cluster

LaA – landomycin A

LaB – landomycin B

LaD – landomycin D

LaE – landomycin E

LaR – landomycin R

Lan – landomycinone

A-Lan – anhydrolandomycinone

Sc136 – *S. cyanogenus* 136

Sc92a – *S. cyanogenus* 136 +pOOB92a

SG – soytone glucose medium

Co30 – soytone glucose medium + 30 μM $CoCl_2$

Trace – soytone glucose medium + 1× Trace metals solution

2.1 Introduction

Microbial derived natural products remain a major source of structurally diverse bioactive compounds and chemical scaffolds that have the potential as new therapeutics to target drug resistant pathogens and cancers, as outlined in detail in Chapter 1. Genome mining has revealed the vast number of cryptic or low yield biosynthetic gene clusters in the genus Streptomyces. However, low natural product yields, improvements to which have been hindered by the lack of high throughput methods, have slowed the discovery and development of many potential therapeutics, as outlined in Chapter 1. Here, we describe our efforts to improve yields of landomycins by a genetically modified Streptomyces cyanogenus-136. After simplifying the extraction process from S. cyanogenus cultures, we identified a wavelength at which the major landomycin products are absorbed in culture extracts, which we used to systematically explore culture medium compositions to improve total landomycin titers. Through correlational analysis, we simplified the culture optimization process by identifying an alternative wavelength at which culture supernatants absorb yet is representative of total landomycin titers. Using the subsequently improved sample throughput, we explored landomycin production during the culturing process to further increase landomycin yield and reduce culture time. Testing the antimicrobial activity of the isolated landomycins, we report broad inhibition of Gram-positive bacteria, inhibition of fungi by landomycinone, and broad landomycin resistance by Gram-negative bacteria that is likely mediated by the exclusion of landomycins by the bacterial membrane. Finally, the anticancer activity of the isolated landomycins against A549 lung carcinoma cells agrees with previous reports on other cell lines that glycan chain length correlates with activity. Given the prevalence of natural products produced by Streptomyces, as well as the light‐absorbing moieties common to bioactive natural products and their metabolic precursors, our method is relevant to improve the

yields of other natural products of interest in pursuit of further synthetic modification to the parent scaffold.

2.2: Materials and Methods

Culture conditions

Strains used in this study are listed in **Table S1**. *S. cyanogenus* was grown in TSB for general propagation. *Bacillus subtilis*, *Listeria seeligeri*, *Lactococcus cremoris*, *Enterococcus faecium*, *Staphylococcus aureus*, *E. coli*, *Pseudomonas aeruginosa*, and *Salmonella enterica* ser. Typhimurium were cultured in Brain Heart Infusion (BHI) broth. *Saccharomyces cerevisiae*, and *Candida albicans* were cultured in 2×YPD (40 g/L casein peptone, 20 g/L yeast extract, 20 g/L glucose, 100 mg/L adenine). For solid media growth, 15 g/L agar was added to BHI or 2×YPD. All cultures were grown at 250 rpm shaking and 37 °C, except for *S. cyanogenus*, *L. cremoris*, *S. cerevisiae*, and *C. albicans*, which were grown at 30 °C.

Landomycin production and mycelia fractionation

Initial *S. cyanogenus* propagation and landomycin production conditions were kindly provided by personal communication from Prof. Bohdan Ostash (Ivan Franko Lviv National University, Lviv, Ukraine). *S. cyanogenus* 136 +pOOB92a (a.k.a. Sc92a) frozen stock was streaked on soy mannitol agar (SMA; 20 g/L soy flour, 20 g/L mannitol, 15 g/L agar, pH to 8.0) and grown for 48 h. Colonies with a red-brown halo were used for preculture. A 1–2 cm^2 piece of agar with visibly grown colonies was cut from the plate and added to 30 mL of SG medium (20 g/L glucose, 10 g/L phytone peptone, 2 g/L $CaCO_3$, pH to 7.0; autoclave; add 1.9 mg/L $CoCl_2{\cdot}6H_2O$) in a 250 mL flask and grown for 48 h as preculture. 2.5 mL of preculture was used to inoculate each of 10 × 500 mL flask with 100 mL SG and grown for 48 h as the production culture. SG was modified as required

for medium optimization by adding or replacing components prior to autoclaving (nitrogen sources), or adding concentrated stocks after autoclaving (glucose, metal ions). The culture solids were pelleted by centrifugation (4500 ×g for 10 min) and the supernatant decanted, buffered to pH 7.0, and set aside for extraction. The cell-mycelium and culture solids pellet were then resuspended in PBS, vortexed vigorously to homogenize, and centrifuged (4500 ×g for 5 min) again. The supernatant was decanted and set aside for extraction. The pellets were again resuspended to 35 mL total volume in PBS and vortexed vigorously. The homogenized samples were then centrifuged for 1–1.5 min at 4500 ×g to selectively pellet the cell-mycelium fraction, while retaining the culture solids in suspension to decant for extraction. Resuspension, vortexing, and centrifugation steps were repeated until the pellet was composed only of a beige-grey cell-mycelium pellet, and the supernatant was clear.

Isolation of pure landomycins

Initial isolation methods were determined from previous works and adapted as needed.[10,19] The supernatant fraction (~1 L) from the *S. cyanogenus* 136 +pOOB92a was extracted once with 1 L and twice with 500 mL ethyl acetate. The 500 mL culture solids suspension was extracted with three 1 L, followed by two 500 mL volumes of ethyl acetate. The combined extract was evaporated down to solid crude material and put under high vacuum to ensure dryness.

The crude red solid (904.2 mg) was dissolved in about 5 mL of 7% MeOH/$CHCl_3$ solution and loaded on to a Yamazen column (180 g of silica) equilibrated for two minutes at 3% MeOH/$CHCl_3$. The system used was an Automated flash column chromatography (normal phase) Smart Flash EPCLC W-Prep 2XY Dual Channel Automated Flash Chromatography System with an additional ELSD detector, provided by Yamazen Corporation. The column was run at 4% MeOH/$CHCl_3$ for twenty minutes then increased over two minutes to 10% MeOH/$CHCl_3$ to run for an additional

fifteen minutes. This column yielded fractions I (pink/purple solid), II (red solid), and III (orange/red solid). Fraction I was evaporated to dryness, then separated further by size exclusion chromatography with 40 g LH-20 Sephadex (Sigma Aldrich), in 50% MeOH/$CHCl_3$ (2 × 50 cm) to yield pure landomycinone (6.7 mg) and 5,6-anhydrolandomycinone (0.3 mg). Fraction II was evaporated to dryness, then precipitated from a concentrated chloroform solution into pentane, giving pure landomycin A (423.1 mg). Fraction III was evaporated to dryness, then separated further with 40 g LH-20 Sephadex in MeOH (2 × 50 cm) to yield landomycin B and landomycin D. After rotary evaporation, landomycin B (39.2 mg) was precipitated from a concentrated chloroform solution into pentane. Landomycin D (9.6 mg) was precipitated from a concentrated ethyl acetate solution into pentane. Products were visualized on TLC using UV and by staining with a 5% aqueous sulfuric acid solution. The purity of all landomycin species was confirmed by a normal phase Elite LaChrom Hitachi HPLC (90% EtOAc in Hexanes). NMR spectra were recorded on a Bruker Avance III NMR spectrometer at 500 MHz for ^{1}H NMR and 125 MHz for ^{13}C-NMR. Mass spectrometry data was collected on a low resolution Finnigan LTQ ESI-MS (ThermoFisher). See Supplementary Information for more details. All solvents used were HPLC grade (ThermoFisher Scientific).

Landomycin standard curves

All standard curves were generated by diluting landomycin stocks (10 mg/mL in DMSO) 10× into Dulbecco's PBS (DPBS, pH 7.0; Corning), followed by 3-fold serial dilutions into DPBS 10% DMSO, and performing an absorbance spectral scan (200–1000 nm; 5 nm increments) using a Spectramax M3 (Molecular Devices).

Spectrophotometric detection of landomycins from culture extracts and supernatants

Absorbance of culture supernatants was determined by pelleting culture solids from the landomycin production cultures and diluting the resulting supernatant 2× into DPBS or 10× into HEPES buffer (100 mM, pH 7.0). Extraction of landomycin fractions for spectrophotometric determination of relative concentrations was performed by adding 300–500 µL aliquots of landomycin culture (supernatant, cells, and mycelia) to an equal volume of chloroform. Samples were then vortexed for 30 s and centrifuged to separate fractions. Samples were vortexed and centrifuged for a second time and a 100 µL aliquot of the chloroform extract was removed from the lower fraction. Samples were dried at room temperature under vacuum for approximately 30 min using an Eppendorf Vacufuge and stored at –80 °C. Immediately before recording absorbance readings, samples were resuspended in 100 µL DMSO and diluted 10× into DPBS. Spectrophotometric scans from 200–800 nm at 5 nm intervals were performed for all supernatant and extract samples.

General A549 cell culture

Human non-small cell lung cancer (NSCLC) cells (A549; CCL-185) from ATCC were cultured in F-12K medium (ATCC) with 10 % (v/v) fetal bovine serum (Neuromics). Cultures of A549 cells were incubated at 37 °C, 95 % humidity, and 5 % CO_2 atmosphere. Cells were passaged every three to four population doubling times, when their concentration was approximately 4×10^6 cells mL^{-1} (approximately 3 days between each passage). All experiments were performed using cultures that had been passaged less than twenty times.

A549 viability assay

A549 cells were seeded at 10,000 cells per well (200 µL) in 96-well tissue culture treated plates (CellTreat) (t = 0 h). 20 mM concentrated stocks of landomycins and doxorubicin hydrochloride

(Tocris Biosciences) were made in DMSO immediately prior to addition to cells. Concentrated stocks to 20 mM were diluted to make working stocks that were diluted to 0–100 μM in cell culture medium with a final DMSO concentration of 0.5 % (v/v). At 24 h, the medium was aspirated from each well, washed with 100 μL PBS, and 0–100 μM of product of interest was added to each well in complete media (supplemented with a final concentration 0.5% v/v DMSO), and incubated cells for 24 h. This concentration of DMSO afforded no change in viability when assessed without drug present and compared to the 0 μM sample (> 95% cell viability with 0.05% DMSO). Then, the medium was aspirated, washed cells with PBS, and trypsinized cells using 100 μL of 0.25% trypsin/EDTA (Gibco) to release the cells from the surface of the plate. Trypsin/EDTA was neutralized with an equal amount (100 μL) of complete media. Cells were pelleted (300 × g, 8 minutes), and washed with 100 μL PBS. Three stains were used to classify the viability of cells: Hoechst 33342 to identify nuclei, and Annexin V-FITC, and Ethidium homodimer I to label viable, apoptotic, and necrotic cells, respectively. 100 μM concentrated stocks of Ethidium homodimer I and Hoechst 33342 were prepared in PBS. Then, 5 μM working solutions of Annexin V-FITC (BioLegend), Ethidium homodimer I (Biotium), and Hoechst 33342 (Thermo Scientific) were prepared in 1× Annexin V Binding Buffer (100 mM HEPES, 25 mM $CaCl_2$, 1.4 M NaCl; BioLegend). To analyze cells, 50 μL of Annexin V-FITC, Ethidium homodimer I, and Hoechst 33342 working solutions was added to each well containing a washed cell pellet. An additional three wells received each of the single dyes for compensation controls. Samples were incubated in the well plate for 10 minutes (37 °C, 5% CO_2). Prior to plate analysis via flow cytometry, 200 μL of 1× Binding Buffer was added to each well. All wells were analyzed using a Guava easyCyte 12HT flow cytometer (Cytek). Different laser/filter combinations were used for each dye (**Table S2**). Gain controls were adjusted for GRN-B, RED-B, and BLU-V channels to 1.00 to

accommodate dyes used (**Table S3**), and YEL-B (emission filter 575/25) was also adjusted to 1.00 to accommodate the natural fluorescence of doxorubicin hydrochloride (ex/em: 470/560).

Agar well diffusion assay

Landomycin stock solutions were made by resuspending purified landomycin solid fractions at 10 mg/mL (LaD, LaB, LaA, Lan, and A-Lan) in DMSO. Stock solutions were stored at –20 °C. Overnight cultures of each strain were diluted 50× into fresh medium and 100 µL was spread-plated on the appropriate solid agar medium. Agar plates were allowed to dry and circular wells were excised. Working solutions of landomycin were made by diluting concentrated stocks to 250 ppm (µg/mL) into PBS pH 7.0, and 100 µL of a working solution was added to an agar well. Plates were imaged after overnight incubation at the appropriate temperature.

Microbial MIC assay

Overnight cultures were sub-cultured 1:1000 (bacteria) or 1:500 (fungi) into fresh media containing 250 µg/mL landomycin (diluted from 10 mg/mL stocks), or 2.5% (v/v) DMSO (control) and aliquoted into 96-well plates. Subcultures were serially diluted 2-fold into fresh medium with 2.5% DMSO to ensure consistent vehicle concentration. Plates were sealed with parafilm to prevent culture evaporation and grown in a Biotek Epoch 2 microplate reader (37 °C, continuous linear shaking at 731 cpm) for 24–48 h, with an absorbance reading at 600 nm taken every 5 min. Due to the change in absorbance caused by the likely breakdown of the landomycins, cultures were blanked at each time point using BHI media with an equivalent concentration of each landomycin.

Statistics

Standard linear regression was performed using GraphPad Prism and Microsoft Excel. Ordinary one-way ANOVA and correlational analysis (Pearson's r) were performed using GraphPad Prism. See SI for description of non-linear regression used for MIC calculation.

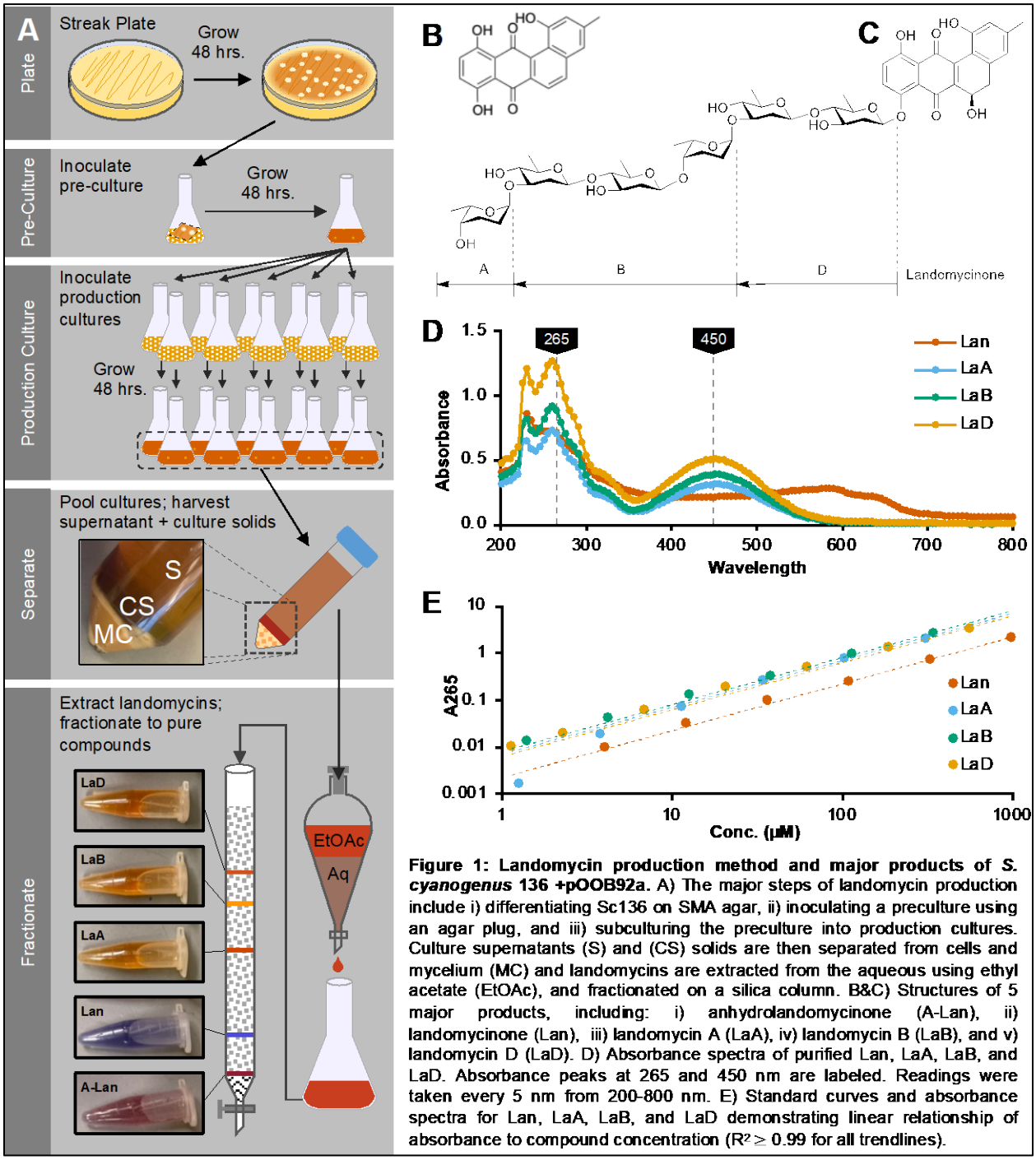

Figure 1: Landomycin production method and major products of *S. cyanogenus* 136 +pOOB92a. A) The major steps of landomycin production include i) differentiating Sc136 on SMA agar, ii) inoculating a preculture using an agar plug, and iii) subculturing the preculture into production cultures. Culture supernatants (S) and (CS) solids are then separated from cells and mycelium (MC) and landomycins are extracted from the aqueous using ethyl acetate (EtOAc), and fractionated on a silica column. B&C) Structures of 5 major products, including: i) anhydrolandomycinone (A-Lan), ii) landomycinone (Lan), iii) landomycin A (LaA), iv) landomycin B (LaB), and v) landomycin D (LaD). D) Absorbance spectra of purified Lan, LaA, LaB, and LaD. Absorbance peaks at 265 and 450 nm are labeled. Readings were taken every 5 nm from 200-800 nm. E) Standard curves and absorbance spectra for Lan, LaA, LaB, and LaD demonstrating linear relationship of absorbance to compound concentration ($R^2 \geq 0.99$ for all trendlines).

2.3: Results

An improved extraction and isolation protocol for landomycin products

Landomycin production by *Streptomyces* is commonly performed in a three-step process: i) differentiation on agar plates, ii) preculturing, and iii) production culturing (**Fig. 1A**).[19] Landomycins are then extracted from production cultures using a biphasic extraction, and then individual compounds are isolated using traditional separation methods. Though landomycins can be extracted quite simply from the supernatant, this approach sacrifices much of the landomycin produced (>80%), which remains trapped in culture solids. Previous reports of extraction from total cultures (cells+mycelia+solids+supernatant) have been reported to produce higher yields, however, our initial efforts produced greasy, poorly crystalized solids that retained a considerable amount of contaminant.[19,34] To improve product quality and reduce the complexity of separations, we developed a simple method to fractionate the colored culture solids, likely densely packed with secondary metabolites such as landomycins, from the remaining cells and/or mycelia. We found that the size and/or density difference between cells/mycelia and culture solids were sufficient to fractionate samples by differential centrifugation. Successive rounds of vortexing and pelleting generated two distinct layers of well separated solids: i) a white-tan layer (cells+mycelium) on the bottom and ii) a red-brown layer (culture solids) on the top (**Fig. 1A, Fig. S1**). Using the extracts from the supernatant and culture solids fractions, we simplified the previously reported fractionation process to a single normal phase silica column and a precipitation step to obtain 390–430 mg/L LaA at high purity (>97%). In total, we identified 5 major products in Sc92a cultures: anhydrolandomycinone (A-Lan), landomycinone (Lan), landomycin A (LaA), landomycin B (LaB), and landomycin D (LaD) (**Fig. 1A–C**).

Optimized media formulations enhance landomycin production

The electron orbitals of polyketides are frequently oriented such that electrons can absorb light in the near UV (>200 nm) to near infra-red (< 800 nm) range, which is detectable by standard UV-vis spectroscopy. More specifically, LaA production by Sc136 has been estimated by measuring the absorbance of culture extracts at 445 nm.[36] We therefore explored the applicability of a similar spectrophotometric approach to detect the other soluble landomycin products that we identified in culture extracts (Lan, LaA, LaB and LaD). To validate this approach, we acquired absorbance spectra of the purified compounds from 200–800 nm (**Fig. 1D**). We found a wide absorbance peak from approximately 350–550 nm, with a maximum at 450 nm, which was specific to the glycosylated forms of landomycin (LaA, LaB, and LaD). Conversely, Lan absorbed well from 575–650 nm, while the glycosylated forms had negligible absorbance in this range. All compounds absorbed well in the UV range, with peak maxima at 230 and 260 nm, suggesting absorbances near these wavelengths could be effective determinants of total Lan and LaA/B/D production. We generated standard curves using linear regression for Lan, LaA, LaB, and LaD at 265 nm and found a strong goodness of fit for all compounds ($R^2 \geq 0.99$) (A265; **Fig. 1E**).

Integration of *adpA* in Sc136 alters the conditional expression of the landomycin biosynthetic pathway in diverse media. This alleviates the dependence on the standard soytone-glucose (SG) production medium for landomycin production and presents an opportunity to improve production by optimizing the medium composition. SG is composed of a soybean derived peptone (soytone or phytone peptone), glucose, calcium carbonate and cobalt, though the causal components of SG essential to landomycin production are unknown.[19] Accordingly, we utilized our newly identified

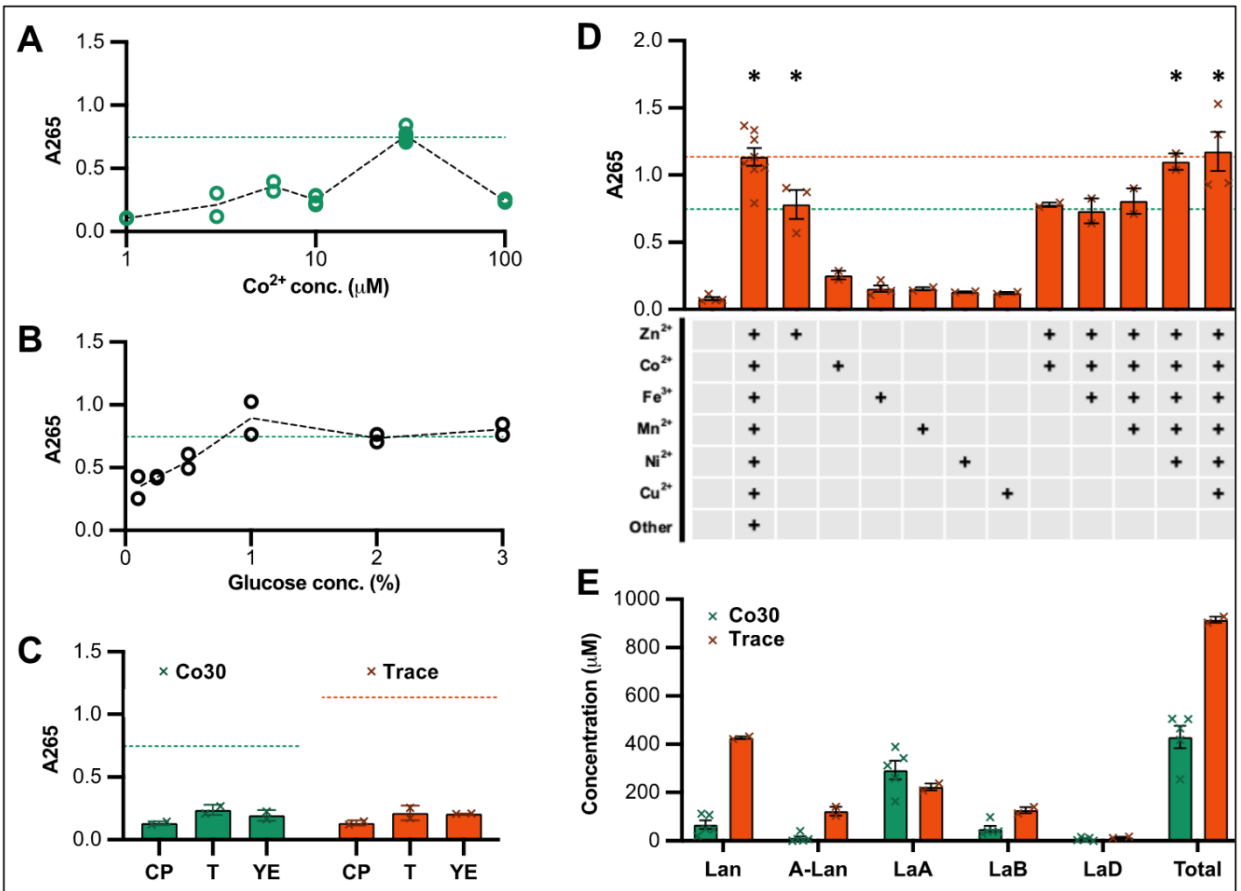

Figure 2: Optimization of landomycin production medium. Chloroform extractions of cultures with modified media compositions were tested to determine the impact on landomycin production A) Effect of cobalt concentration on landomycin production in SG medium. Concentrations tested include 1, 3, 6, 10, 30 and 100 μM. B) Effect of glucose concentration on landomycin production in SG medium with 30 μM Co. Concentrations tested include 0.1, 0.25, 0.5, 1, 2, and 3% (w/v) glucose C) Effect of replacing phytone peptone with casein peptone (CP), tryptone (T), or yeast extract (YE) in the presence of 30 μM Co (green) or trace metals solution (orange). D) Impact of trace metal composition in SG medium on landomycin production. Metal ions were added as the following salts from 1000x stocks (final concentrations given): 10 μM $ZnCl_2$, 2 μM $CoCl_2$, 50 μM $FeCl_3$, 10 μM $MnCl_2$, 2 μM $NiCl_2$, 2 μM $CuSO_4$. Other indicates the use of a commercial trace metals solution which additionally contains 2 μM Na_2MoO_4, 2 μM Na_2SeO_3, 20 μM $CaCl_2$, and 2 μM $B(OH)_3$. ✱ denotes samples with means significantly different from all other unlabeled means and not significantly different from one another, as determined by ordinary one-way ANOVA and Tukey multiple comparison test ($p<0.05$). E) Landomycin yield from 1 L production cultures of Co30 (green) or Trace (orange) media. Error bars represent SEM.

correlation between A265 and the concentration of the major landomycin products to identify modified SG compositions that improve landomycin yield from Sc92a cultures.

We first investigated the effect of cobalt concentration on landomycin production (**Fig. 2A**). SG medium contains 0.001 g/L (7.7 μM) cobalt, yet we found that increasing cobalt to 30 μM increased total landomycins by ~2-fold. Increasing cobalt concentration further to 100 μM resulted in a drop in landomycin production, and cultures turned a dark brown-black, which is frequently

associated with poor yields that are thought to be due to degradation of landomycins. Using the improved 30 μM cobalt concentration in the SG base medium (Co30), we next investigated the effect of glucose concentration on landomycin production (**Fig. 2B**). Relatively high glucose concentrations (2.0 %) are stipulated as necessary for good landomycin production. However, glucose is also known to frequently repress secondary metabolism while nutrients are abundant. We found that glucose is required at a minimum concentration of 1.0 % (w/v) to obtain maximum landomycin titers and there was no detriment to further increasing its concentration, indicating that production is not glucose inhibited or limited (**Fig. 2C**). Maintaining 2.0 % glucose, we then investigated different complex nitrogen sources but found that they all resulted in a drastic reduction in landomycin titer. This result suggests that specific components of the phytone peptone are necessary to achieve maximum landomycin yields. Finally, since previous studies have had success in replacing cobalt with other divalent metal ions, we tested the suitability of a commercially available trace metals mixture (Trace) as well as a previously reported minimal trace metals solution (T2) (**Fig. 2D, Fig. S2A**).[36] While we found that T2 decreased landomycin production, Trace increased it by ~50 % when compared to the Co30 base medium.

To determine the ions responsible for inducing landomycin production in Trace, we evaluated the impact of six of the dominant ions in Trace (Zn^{2+}, Co^{2+}, Fe^{3+}, Mn^{2+}, Ni^{2+}, and Cu^{2+}) on landomycin titers (**Fig. 2D**). We found that Zn^{2+} was the major inducer of landomycin production in the trace mixture, achieving equivalent landomycin production at 10 μM as Co^{2+} did at 30 μM. Though the other individual ions yielded more modest landomycin titers, addition of any one of the metals was an improvement over the base medium, suggesting all six cations can activate the landomycin biosynthetic pathway. We then explored the additive effect of the metal ions by successively adding metal ions to the medium in an order based upon their individual effect. Addition of (i)

Co^{2+}, (ii) Co^{2+} and Fe^{3+}, or (iii) Co^{2+}, Fe^{3+}, and Mn^{2+} to Zn^{2+} had no additional benefit relative to Zn^{2+} alone, while addition of Co^{2+}, Fe^{3+}, Mn^{2+}, and Ni^{2+} yielded landomycins equivalent to the trace mixture. These observations suggest that a minimal solution of Zn^{2+}, Co^{2+}, Fe^{3+}, Mn^{2+} and Ni^{2+} is sufficient to achieve landomycin yields equivalent to that of the complete Trace mix. Growth in 30 μM Zn^{2+}, Mn^{2+}, Ni^{2+}, or Cu^{2+}, did not improve yield further, nor did the addition of 30 μM Co^{2+}, 20 μM Zn^{2+} or 30 μM Co^{2+} and 20 μM Zn^{2+} in combination with Trace (**Fig. S2B–C**). To validate that our improved production conditions are relevant at scale, we characterized the relative product yields of 1 L production cultures of Co30 and Trace. Trace produced more than double the total landomycin products compared to Co30 (915 vs. 430 μM). However, Trace produced less total and relative LaA, the pathway end-product, compared to Co30 (223 vs 293 μM; 24 vs. 68% total products), and far more of the intermediates or byproducts Lan, LaB, and A-Lan (427 vs. 68 μM, 127 vs 49 μM, and 123 vs 12 μM, respectively).

A rapid spectrophotometric approach to quantifying landomycins helps shorten production runs and improve yield

Although the A265 of culture extracts proved to be an effective descriptor of landomycin titer, the requirement of an extraction step limited sample throughput for production optimization. When we plotted the absorbance (200-800 nm) of the supernatants of each of the 55 media compositions for which we had previously evaluated the A265 of culture extracts, we found that the peaks identified in the purified landomycins or culture extracts (265 and 450 nm) were masked (**Fig. 3A**). To identify a more descriptive wavelength of landomycin titer in culture supernatants, we used linear regression to evaluate the correlation of the A265 of culture extracts

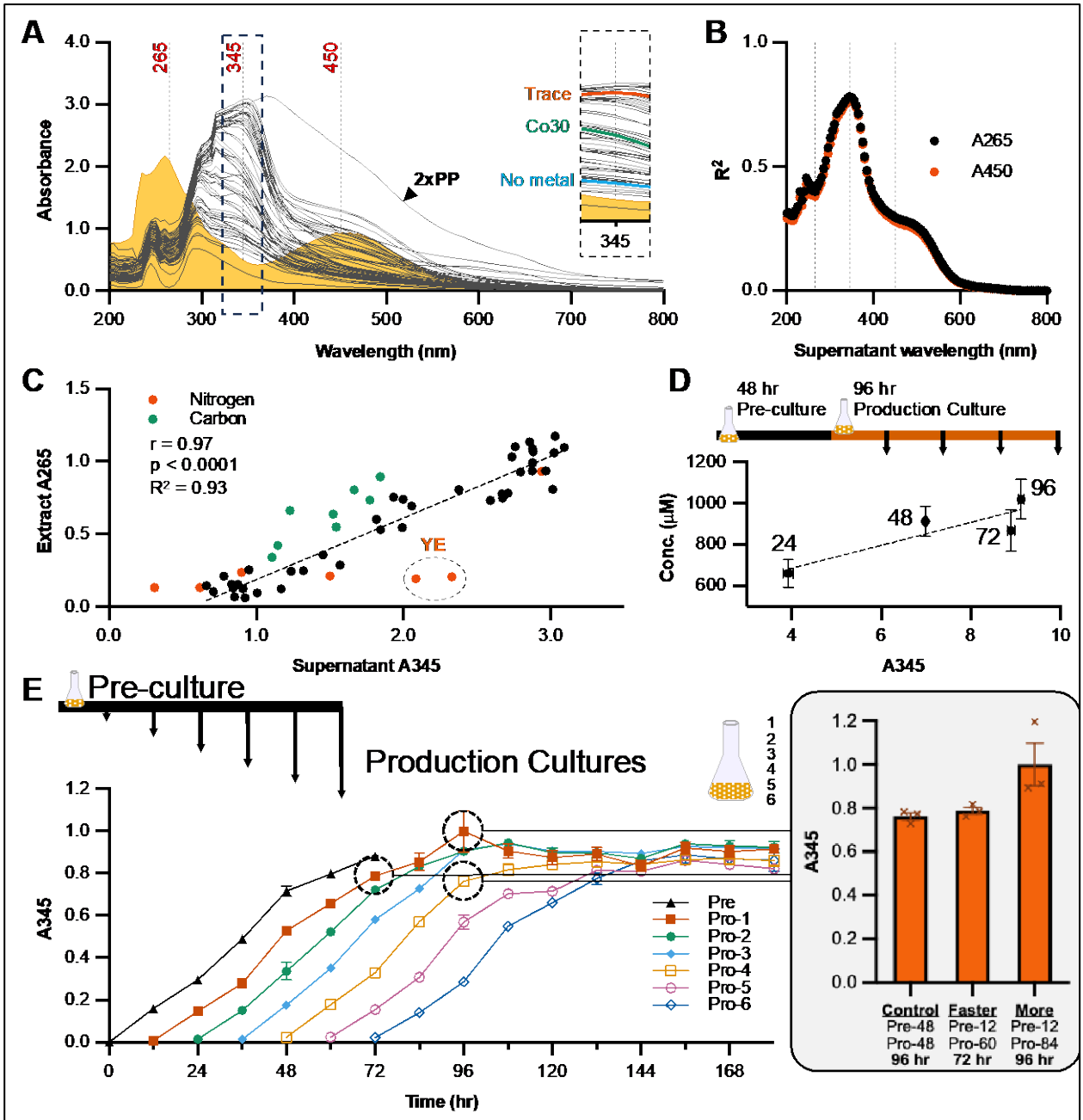

Figure 3: Detection of Relative Landomycin Production in Culture Supernatants. A) Average absorbance spectrum of the supernatant of 55 distinct production conditions tested for method optimization (grey lines). The absorbance spectrum of purified LaA (0.1 mg/mL) is shown in yellow. Vertical dashed lines indicate 265, 345, and 450 nm wavelengths. The spectrum of SG containing 2x phytone peptone (2xPP) is indicated by the label and black arrow. The inset depicts 345 nm with Trace, Co30 and No metal conditions labeled in orange, green, and blue, respectively. B) R^2 values for linear regression analysis of supernatant absorbance at the given wavelength relative to the extract absorbance at 265 nm (black circles) or 450 nm (orange circles). Vertical dashed lines indicate 265 (R^2 approx. 0.4), 345 (the maximum; $R^2 = 0.78$), and 450 nm (R^2 approx. 0.3) wavelengths. C) Plot of extract absorbance at 265 nm versus supernatant absorbance at 345 nm. Samples from media containing different nitrogen and carbon sources are orange and green, respectively. Yeast extract samples are encircled and labeled YE. Nitrogen and carbon samples were removed from correlational and linear regression analysis due to apparent non-correlational clustering thought to result from the different base media absorbance. Pearson correlation coeff. and R^2 of final 42 conditions are 0.965 ($p<0.0001$) and 0.93, respectively. D) Linear regression analysis of total landomycin concentration determined by LC-MS relative to A345 of culture time-course with samples taken every 24 hr from production cultures ($R^2 = 0.78$). Arrows from production culture indicate sampling time points. E) Time-course analysis of pre-culture and production culture landomycin production determined by A345. Production cultures were set every 12 hr from the pre-culture and A345 was measured every 12 hrs (n=3). The bar plot depicts the magnitude of two different improved production methods (Faster and More), compared to the starting condition (Control), which decreased production time by 24 hr or increased yield by 32%.

to the absorbance of culture supernatants at every 5 nm interval (200–800 nm) for the 55 media

compositions tested previously (**Fig. 3B, 3A inset**). When we plotted the R^2 for the resulting trendline at each supernatant wavelength, A265 and A450 of culture supernatants indeed proved to be very poor predictors of landomycin titer (R^2 = 0.4 & 0.3, respectively). The maximum R^2 was identified at 345 nm, with a value of 0.78, suggesting it is a good predictor of the extract A265, and thus total landomycin titer. When we plotted A265 of culture extracts versus A345 of culture supernatants, we were able to identify specific outlier sets within our data that likely resulted from different background media absorbances, including those in which glucose was added post autoclaving (Carbon) and those with different peptone sources (Nitrogen) (**Fig. 3C**). When we excluded these data from our analyses, the remaining 42 conditions retained a Pearson correlation coefficient of 0.97 ($p<0.0001$) and the trendline had a R^2 of 0.93, both indicating A345 is an effective measure of total landomycin titer. We further validated the effectiveness of A345 of culture supernatants as a measure of landomycin production by directly measuring total landomycin production in production cultures by LC-MS at different timepoints during a production run (**Fig. 3D**).

Utilizing the increase in sample throughput provided by supernatant A345, we investigated the optimal subculture timepoint and production culture endpoint (**Fig. 3E**). Starting at the pre-culture step, we subcultured pre-cultures into new production cultures every 12 hours, while monitoring landomycin production. We found that using a protocol that we named Faster, we could reduce the pre-culture from 48 hr to 12 hr, while extending the production culture from 48 hr to 60 hr, thereby reducing total production by 24 hr, without any loss in landomycin production. We also developed a protocol that we named More, where the production culture from a 12 hr pre-culture was extended to 84 hr, resulting in a further 32% increase in landomycin production compared to the starting condition (Control; 48 hr pre-culture, 48 hr production culture).

Landomycins exhibit antibacterial and antifungal activities

Although landomycins are commonly reported to exert antimicrobial activity, the breadth of their activity spectra is poorly described.[38–40] Additionally, the different landomycins, complex and impure mixtures, and/or qualitative metrics used in these studies limit comparison between them. We screened the five major landomycins found in production cultures for their antimicrobial activity against a diverse array of microbes (five Gram-positive, three Gram-negative, and two fungi) using an agar well diffusion assay. We found that LaA was active against all Gram-positive bacteria, while Lan, LaB, and LaD inhibited at least three of the five Gram-positive strains tested (**Fig. 4A**). Lan also inhibited the growth of the fungi *S. cerevisiae* and *C. albicans*. A-Lan was not active against any of the organisms tested, although this may be a result of the compound precipitating out when added to the medium. None of the landomycins inhibited the growth of Gram-negative bacteria. Given the broad antimicrobial activity we found landomycins had against Gram-positive bacteria and fungi, as well as the well-characterized anti-cancer activity of many landomycins, we postulated that the complete absence of growth inhibition seen with any Gram-negative bacterium may be due to the impermeability of the outer membrane. To

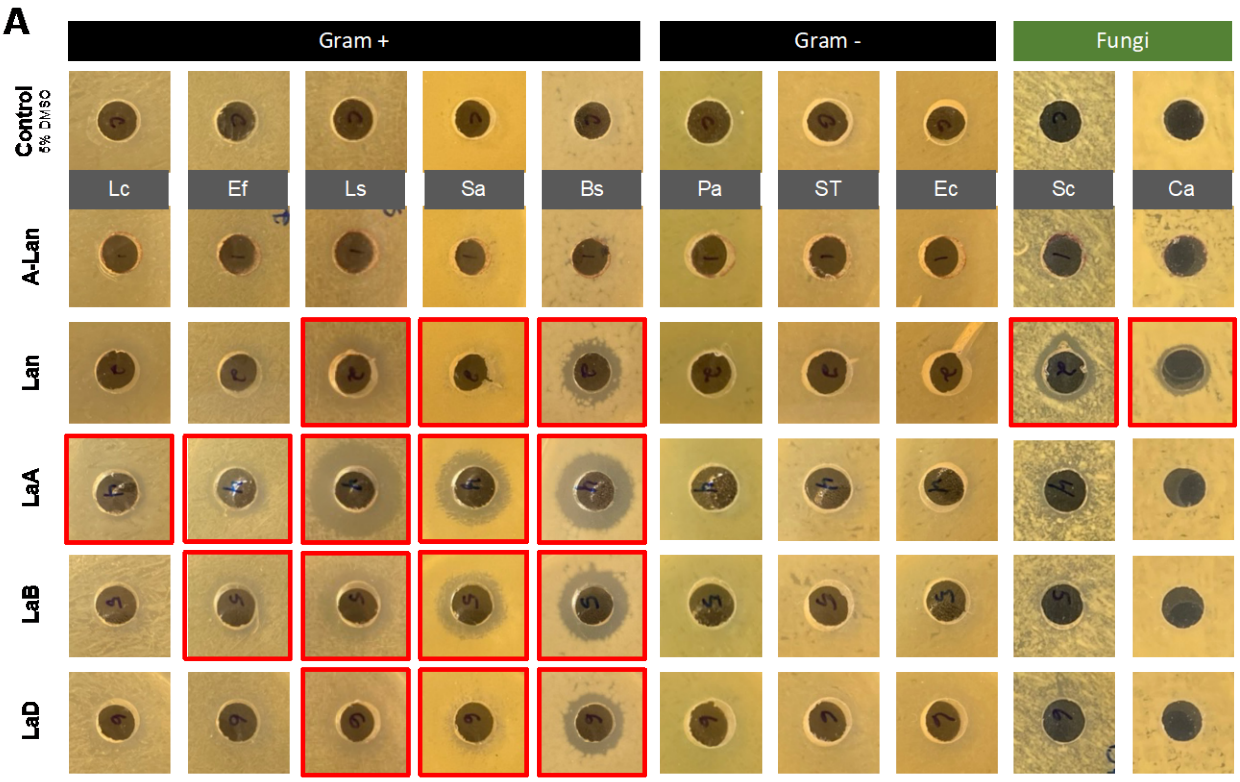

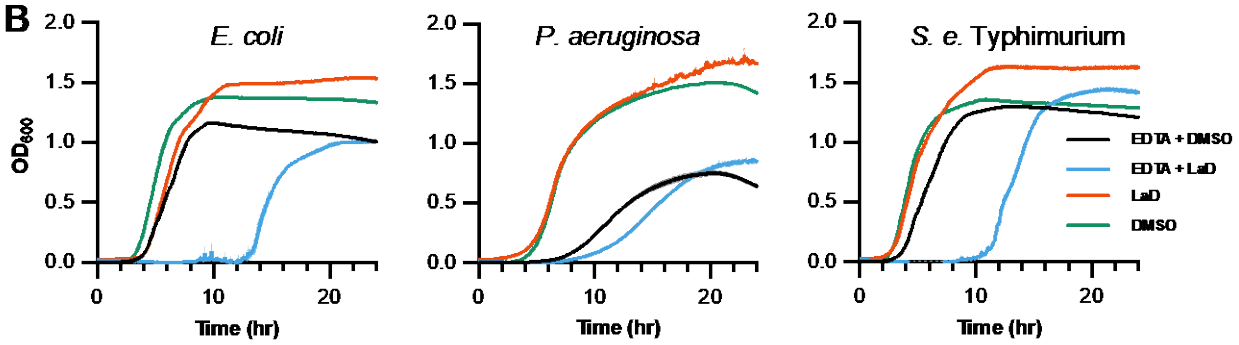

C

Organism	Lan	LaA	LaB	LaD
B. subtilis	172	>230	>257	<6.5
S. aureus	478	152	193	113
E. faecium	>739	>230	>257	418
L. seeligeri	179	>230	>257	78
C. albicans	116	>230	>257	>418
S. cerevisiae	45	107	170	83

Figure 4: Antimicrobial spectrum of landomycin products of *S. cyanogenus* 136 +pOOB92a. A) Inhibitory spectrum of anhydrolandomycinone (A-Lan), landomycinone (Lan), landomycin A (LaA), landomycin B (LaB), and landomycin D (LaD), against: *L. cremoris* (Lc), *E. faecium* (Ef), *L. seeligeri* (Ls), *S. aureus* (Sa), *B. subtilis* (Bs), *P. aeruginosa* (Pa), *S. enterica* ser. Typhimurium (ST), *E. coli* (Ec), *S. cerevisiae* (Sc), *and C. albicans* (Ca) as determined by agar well diffusion assay. 100 µL of 250 µg/mL of each compound was added per agar well; Control contained only DMSO (5% v/v). Wells where inhibition of growth was visible are outlined with a bold red border. **B)** Growth curves of *E. coli*, *P. aeruginosa*, and *S.* Typhimurium in the presence of 250 ug/mL LaD with and without the addition of 1 mM EDTA. DMSO and EDTA+DMSO are provided as controls; growth inhibition by LaD required EDTA in Gram-negative organisms. **C)** Minimum Inhibitory concentration values (µM) calculated from growth inhibition curves (Fig. S5) for organisms sensitive to at least one landomycin.

investigate this hypothesis, we assessed whether permeabilization of the outer membrane using

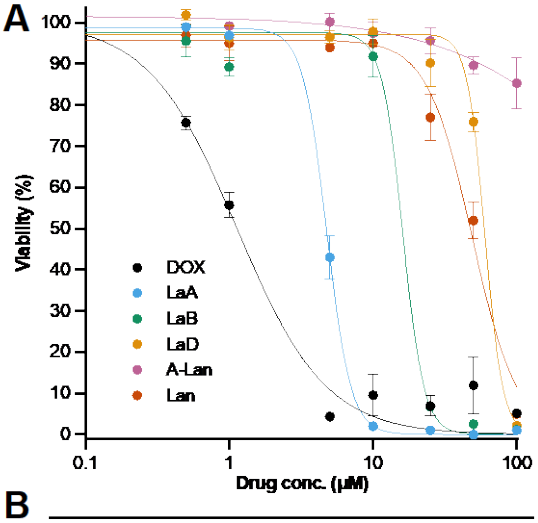

B

Compound	LC_{50} ± SEM (μM)
Doxorubicin	1.1 ± 0.2
Landomycin A	4.8 ± 0.1
Landomycin B	16.1 ± 1.4
Landomycin D	59.9 ± 2.9
Landomycinone	48.9 ± 2.5
Anhydrolandomycinone	>100

Figure 5: Viability of non-small cell lung carcinoma (A549) cells treated with landomycins. A) Dose response curves for A549 cells treated with 0–100 μM DOX, landomycin A, landomycin B, landomycin D, landomycinone, and anhydrolandomycinone for 24 hours prior to analysis via flow cytometry. We report the average percent viability (n=3), normalized to the 0 μM sample. Error bars represent the SEM. We fit each data point to a non-linear [inhibitor] versus response curve. B) tabulated LC_{50} values from dose response curves.

EDTA could sensitize Gram-negative bacteria to LaD.[41] We initially determined non-inhibitory concentrations of EDTA for each Gram-negative strain (**Fig. S6**). The addition of 1 mM EDTA to growth medium was not inhibitory for *S.* Typhimurium or *E. coli*, but it was partially inhibitory to *P. aeruginosa*. As hypothesized, the addition of 1 mM EDTA sensitized both *S.* Typhimurium and *E. coli* to LaD, as evidenced by the delay in initiation of detectable growth from 4 h to 12 h (**Fig. 4B**). The growth delay for *P. aeruginosa* was less drastic due to the partial toxicity of EDTA. To better validate the bioactivity of the active landomycins, we also ran MIC assays on the landomycin-sensitive organisms *E. faecium*, *L. seeligeri*, *S. aureus*, *B. subtilis*, *S. cerevisiae*, and *C. albicans* (**Fig. S4 & S5**). The activity of erythromycin on *B. subtilis* was used as a control to validate our MIC method (MIC = 133 ng/mL). Although we found these compounds frequently delayed growth, similar to our findings for LaD activity in the presence of EDTA for Gram-negative organisms, most compounds eventually permitted some microbial growth at the 24 h time point used to calculate the MIC (**Fig. S5 & Fig. 4C**). Only LaD and Lan completely inhibited *B. subtilis* and *S. cerevisiae* growth, respectively, at sub-50 μM concentrations. Overall, these five landomycins appear to have limited antimicrobial applications but show promise as starting scaffolds to synthesize a

next generation of improved landomycins.

Landomycins exhibit anticancer activity.

We tested the efficacy of each of the landomycin products identified against human non-small cell lung cancer (NSCLC) cell line (A549-CCL-185; A549), using doxorubicin hydrochloride (DOX) as a positive control. After 24 hours of incubation with each compound of interest, we analyzed the A549 cells using flow cytometry. To determine the efficacy of each compound against A549 cells, we normalized to the negative control (0 μM), fit curves to each data set (**Fig. 5A**) and determined LC_{50} values for each drug of interest (**Fig. 5B**). These results indicate that while LaA is not as potent as DOX, it was the most potent member of the products of interest. For landomycins containing deoxy oligosaccharides, LaA was the most active while LaD was the least active. Additionally, we found that Lan was one of the least active landomycins in this assay while A-Lan was inactive up to 100 μM.

2.4: Discussion

Unspecified production/induction conditions and low yield are major obstacles to the translation of natural products into viable therapeutics and chemical goods. Similarly, complicated separations add considerable costs and require the use of large amounts of energy and/or harmful solvents. Landomycins are not unique in this regard, and the lack of studies performed on this promising scaffold can be attributed, in part, to the difficulty in obtaining the molecule(s) of interest. To this end, we developed a spectrophotometric method using culture extracts to screen media compositions that reached LaA concentrations as high as 390 μM and a total polyketide concentration of 915 μM. By simplifying this method through the substitution of culture extracts with culture supernatants, we rapidly increased sample throughput, allowing us to monitor landomycin titers during production and across multiple cultures. Compared to other relatively

high throughput analytical methods such as UPLC and RapidFire, which can accommodate analysis of hundreds of samples, the spectrophotometric method proposed here is faster, low-cost, and offers real-time production information that can be acted upon immediately.[42,43] While the detection of natural products by UV-vis spectroscopy is context dependent and may not be applicable to all products of interest and media conditions, the underlying methodology that we developed—finding a universal absorbance distinct to pure compounds of interest and correlating that to an equally representative wavelength in the culture supernatant—is high throughput, low-cost, and can be easily extended to other natural products that absorb light in the UV-vis range. Furthermore, by developing a differential centrifugation method to isolate landomycin-rich culture solids, we reduced the typically grueling purification method for LaA to a single normal phase silica column and precipitation step to yield >97% pure LaA.[10,34] This application should also serve to simplify the isolation of other natural products expressed in culture solids of *Streptomyces*.

Of the landomycins investigated in this work (LaA, LaB, LaD, and Lan), all compounds generally inhibited the growth of Gram-positive bacteria, Lan inhibited the growth of fungi, and none of the compounds were active against Gram-negative bacteria without the addition of EDTA. LaA and LaB had the broadest spectrum of activity against Gram-positive bacteria in the agar well diffusion assay, but they generally had high MICs. Only LaD and Lan had <50 μM MIC when treating *B. subtilis* and *S. cerevisiae,* respectively. Interestingly, LaA, LaB, and LaD only differ structurally by the length of the glycan chain, yet these subtle differences resulted in vastly different antimicrobial activity. In another study, landomycin R (LaR) – an anhydro-landomycin with a disaccharide glycan – was more inhibitory than landomycin Q, which only differs from LaR by an extra rhodinose on the glycan chain.[38] Similarly, LaR only differs from LaD by the loss of an alcohol group and subsequent formation of a carbon-carbon double bond in the polyketide core,

yet we found LaD to be far less active against *S. aureus* than was previously found for lanR (7 & 14 μM vs. 104 μM, respectively). Together, these findings better elucidate some of the activity-defining moieties of landomycins. In particular, the length and composition of the glycan chain are key to the bioactivity of landomycins and provide targets for future structure-function studies and synthetic modifications intended to improve potency and/or spectrum.

A common feature of many landomycins is their color (**Fig. 1A**), and during the course of the MIC assay, we noticed that the orange (LaA, LaB, LaD) or dark blue (Lan) tinted media changed color to a darker, brown-black (**Fig. S7**). Even the aseptic media underwent this transformation. Given the underlying physical properties determinant of color, we hypothesize that a chemical reaction that alters the bonding in landomycin structures to be the likely cause. This suggests that the landomycins in this study are not particularly stable under the conditions tested, which could account for the transient growth inhibition found for many of the MIC assay samples. In fact, previous mechanistic investigations into the bioactivity of LaE noted both the rapid generation and subsequent decline of reactive oxygen species (ROS) in cancer cells, as well as the rapid generation and subsequent quenching of a fluorescent Michael adduct with biothiols, predicted to be mediated by the oxygen-dependent removal of the glycan.[11,13] Taken with our findings, this suggests stabilization of the landomycin backbone and glycan may be an effective strategy to generally improve the bioactivity of landomycins. Identification of the probable degradation products could further direct chemical modifications that improve landomycin stability and should be considered an important step in engineering a next generation of semi-synthetic landomycin therapeutics.

LaA and LaE are the most studied landomycins for their chemotherapeutic potential, which are reported to be mediated by inhibition of DNA synthesis, and/or oxidative stress to mitochondria

via the rapid generation of ROS.[11–13,44,45] We found the LC_{50} of LaA to be 4.8 μM, which is within the range previously reported by the NCI for A549 cells (LC_{50} = 0.8 μM and ≥10 μM), and near the reported IC_{50}.[46–49] Concerning the broader activity trend of the glycated landomycins tested, we found an inverse relationship between oligosaccharide chain length and LD_{50} (LaA<LaB<LaD). This trend has been identified in other cell lines, which suggests that longer glycan chains generally enhance landomycin anticancer activity, and glycan composition can heavily impact activity.[32,34] Though the aglycone Lan was previously reported to have an IC_{50} below LaA for this cell line, we found Lan to have reduced efficacy, and similar activity to LaD.[49] Interestingly, by substituting the more common, but less informative, binary viability methods with a multiplexed, fluorescent dye assay, we identified that landomycin treated A549 cells undergo late-stage apoptosis, compared to DOX-treated cells that exhibit cellular necrosis (**Table S4**). Indeed, investigations into the mechanism of LaE bioactivity on Jurkat T-cell leukemia cells have noted that while both landomycins and DOX result in ROS generation, they may travel different paths to their common fate.[13,44,50] Taken together, and given our improved production of the polyketide core, landomycins are promising chemotherapeutic candidates. Our results provide further guidance towards the designing and testing of new, semi-synthetic landomycins that better elucidate the relevant structural features by which landomycins mediate their cytotoxic effects, thereby improving candidate efficacy.

2.5 References

(1) Lee, N.; et al. Mini review: Genome mining approaches for the identification of secondary metabolite biosynthetic gene clusters in *Streptomyces*. *Comput. Struct. Biotechnol. J.* **2020**, *18*, 1548–1556.

(2) Liu, R.; Yu, D.; Deng, Z.; Liu, T. Harnessing in vitro platforms for natural product research: in vitro driven rational engineering and mining (iDREAM). *Curr. Opin. Biotechnol.* **2021**, *69*, 1–9.

(3) Pham, J. V.; et al. A review of the microbial production of bioactive natural products and biologics. *Front. Microbiol.* **2019**, *10*, 1–27.

(4) Patridge, E.; Gareiss, P.; Kinch, M. S.; Hoyer, D. An analysis of FDA-approved drugs: Natural products and their derivatives. *Drug Discov. Today* **2016**, *21*, 204–207.

(5) Harvey, A. L.; Edrada-Ebel, R.; Quinn, R. J. The re-emergence of natural products for drug discovery in the genomics era. *Nat. Rev. Drug Discov.* **2015**, *14*, 111–129.

(6) Li, C. J.; Trost, B. M. Green chemistry for chemical synthesis. *Proc. Natl. Acad. Sci. U. S. A.* **2008**, *105*, 13197–13202.

(7) Chung, Y.-H.; et al. Comparative genomics reveals a remarkable biosynthetic potential of the *Streptomyces* phylogenetic lineage associated with rugose-ornamented spores. *mSystems* **2021**, *6*, 1–15.

(8) Belknap, K. C.; Park, C. J.; Barth, B. M.; Andam, C. P. Genome mining of biosynthetic and chemotherapeutic gene clusters in *Streptomyces* bacteria. *Sci. Rep.* **2020**, *10*, 1–9.

(9) Ward, A. C.; Allenby, N. E. Genome mining for the search and discovery of bioactive compounds: The *Streptomyces* paradigm. *FEMS Microbiol. Lett.* **2018**, *365*, 1–20.

(10) Henkel, T.; Rohr, J.; Beale, J. M.; Schwenen, L. Landomycins, new angucycline antibiotics from *Streptomyces* sp. I. Structural studies on landomycins A–D. *J. Antibiot. (Tokyo)* **1990**, *43*, 492–503.

(11) Terenzi, A.; et al. Landomycins as glutathione-depleting agents and natural fluorescent probes for cellular Michael adduct-dependent quinone metabolism. *Commun. Chem.* **2021**, *4*, 1–13.

(12) Crow, R. T.; et al. Landomycin A inhibits DNA synthesis and G1/S cell cycle progression. *Bioorg. Med. Chem. Lett.* **1999**, *9*, 1663–1666.

(13) Panchuk, R. R.; et al. Rapid generation of hydrogen peroxide contributes to the complex cell death induction by the angucycline antibiotic landomycin E. *Free Radic. Biol. Med.* **2017**, *106*, 134–147.

(14) Westrich, L.; et al. Cloning and characterization of a gene cluster from *Streptomyces cyanogenus* S136 probably involved in landomycin biosynthesis. *FEMS Microbiol. Lett.* **1999**, *170*, 381–387.

(15) Matselyukh, B. P.; Polishchuk, L. V.; Lukyanchuk, V. V.; Golembiovska, S. L.; Lavrenchuk, V. Y. Sequences of landomycin E and carotenoid biosynthetic gene clusters, and molecular structure of transcriptional regulator of *Streptomyces globisporus* 1912. *Mikrobiol. Z.* **2016**, *78*, 60–70.

(16) Feng, Z.; Kallifidas, D.; Brady, S. F. Functional analysis of environmental DNA-derived type II polyketide synthases reveals structurally diverse secondary metabolites. *Proc. Natl. Acad. Sci. U. S. A.* **2011**, *108*, 12629–12634.

(17) Peng, A.; et al. Angucycline glycosides from an intertidal sediments strain *Streptomyces* sp. and their cytotoxic activity against hepatoma carcinoma cells. *Mar. Drugs* **2018**, *16*.

(18) Kharel, M. K.; et al. Angucyclines: Biosynthesis, mode-of-action, new natural products, and synthesis. *Nat. Prod. Rep.* **2012**, *29*, 264–325.

(19) Weber, S.; Zolke, C.; Rohr, J.; Beale, J. M. Investigations of the biosynthesis and structural revision of landomycin A. *J. Org. Chem.* **1994**, *59*, 4211–4214.

(20) Hrab, P.; et al. Complete genome sequence of *Streptomyces cyanogenus* S136, producer of anticancer angucycline landomycin A. *3 Biotech* **2021**, *11*, 1–10.

(21) Bugaut, X.; Guinchard, X.; Roulland, E. Synthesis of the landomycinone skeleton. *J. Org. Chem.* **2010**, *75*, 8190–8198.

(22) Roush, W. R.; Neitz, R. J. Studies on the synthesis of landomycin A. Synthesis of the originally assigned structure of the aglycone, landomycinone, and revision of structure. *J. Org. Chem.* **2004**, *69*, 4906–4912.

(23) Guo, Y.; Sulikowski, G. A. Synthesis of the hexasaccharide fragment of landomycin A: Application of glycosyl tetrazoles and phosphites in the synthesis of a deoxyoligosaccharide. *J. Am. Chem. Soc.* **1998**, *120*, 1392–1397.

(24) Yang, X.; Fu, B.; Yu, B. Total synthesis of landomycin A, a potent antitumor angucycline antibiotic. *J. Am. Chem. Soc.* **2011**, *133*, 12433–12435.

(25) Yalamanchili, S.; Lloyd, D.; Bennett, C. S. Synthesis of the hexasaccharide fragment of landomycin A using a mild, reagent-controlled approach. *Org. Lett.* **2019**, *21*, 3674–3677.

(26) Roush, W. R.; Bennett, C. E. A highly stereoselective synthesis of the landomycin A hexasaccharide unit. *J. Am. Chem. Soc.* **2000**, *122*, 6124–6125.

(27) Yu, B.; Wang, P. Efficient synthesis of the hexasaccharide fragment of landomycin A using phenyl 2,3-O-thionocarbonyl-1-thioglycosides as 2-deoxy-β-glycoside precursors. *Org. Lett.* **2002**, *4*, 1919–1922.

(28) Yang, X.; Yu, B. Synthesis of landomycin D: Studies on the saccharide assembly. *Synthesis* **2016**, *48*, 1693–1699.

(29) Tanaka, H.; et al. Combinatorial synthesis of deoxyhexasaccharides related to the landomycin A sugar moiety, based on an orthogonal deprotection strategy. *Chem. Asian J.* **2010**, *5*, 1407–1424.

(30) Lee, J.; Kang, S.; Kim, J.; Moon, D.; Rhee, Y. H. A convergent synthetic strategy towards oligosaccharides containing 2,3,6-trideoxypyranoglycosides. *Angew. Chem. Int. Ed.* **2019**, *58*, 628–631.

(31) von Mulert, U.; Luzhetskyy, A.; Hofmann, C.; Mayer, A.; Bechthold, A. Expression of the landomycin biosynthetic gene cluster in a PKS mutant of *Streptomyces fradiae* is dependent on the coexpression of a putative transcriptional activator gene. *FEMS Microbiol. Lett.* **2004**, *230*, 91–97.

(32) Shaaban, K. A.; Stamatkin, C.; Damodaran, C.; Rohr, J. 11-Deoxylandomycinone and landomycins X–Z, new cytotoxic angucyclin(on)es from *Streptomyces cyanogenus* K62 mutant strain. *J. Antibiot. (Tokyo)* **2011**, *64*, 141–150.

(33) Luzhetskyy, A.; et al. Generation of novel landomycins M and O through targeted gene disruption. *ChemBioChem* **2005**, *6*, 675–678.

(34) Shaaban, K. A.; Srinivasan, S.; Kumar, R.; Damodaran, C.; Rohr, J. Landomycins P–W, cytotoxic angucyclines from *Streptomyces cyanogenus* S-136. *J. Nat. Prod.* **2011**, *74*, 2–11.

(35) Myronovskyi, M.; et al. Generation of new compounds through unbalanced transcription of landomycin A cluster. *Appl. Microbiol. Biotechnol.* **2016**, *100*, 9175–9186.

(36) Yushchuk, O.; et al. Heterologous AdpA transcription factors enhance landomycin production in *Streptomyces cyanogenus* S136 under a broad range of growth conditions. *Appl. Microbiol. Biotechnol.* **2018**, *102*, 8419–8428.

(37) Gessner, A.; et al. Changing biosynthetic profiles by expressing *bldA* in *Streptomyces* strains. *ChemBioChem* **2015**, *16*, 2244–2252.

(38) Lai, Y. H.; et al. Total synthesis of landomycins Q and R and related core structures for exploration of the cytotoxicity and antibacterial properties. *RSC Adv.* **2021**, *11*, 9426–9432.

(39) Matseliukh, B. P.; Konovalova, T. A.; Polishchuk, L. V.; Bambura, O. I. The sensitivity to landomycins A and E of streptomycetes, producers of polyketide antibiotics. *Mikrobiol. Z.* **1998**, *60*, 31–36.

(40) Yushchuk, O.; et al. Eliciting the silent lucensomycin biosynthetic pathway in *Streptomyces cyanogenus* S136 via manipulation of the global regulatory gene *adpA*. *Sci. Rep.* **2021**, *11*, 1–14.

(41) Brown, M. R. W.; Richards, R. M. E. Effect of ethylenediamine tetraacetate on the resistance of *Pseudomonas aeruginosa* to antibacterial agents. *Nature* **1965**, *207*, 1391–1393.

(42) Vervoort, N.; Goossens, K.; Baeten, M.; Chen, Q. Recent advances in analytical techniques for high-throughput experimentation. *Anal. Sci. Adv.* **2021**, *2*, 109–127.

(43) Dueñas, M. E.; et al. Advances in high-throughput mass spectrometry in drug discovery. *EMBO Mol. Med.* **2023**, *15*, 1–15.

(44) A.; K.; et al. Mechanisms underlying the anticancer activities of the angucycline landomycin E. *Biochem. Pharmacol.* **2007**, *74*, 1713–1726.

(45) Lehka, L. V.; Panchuk, R. R.; Berger, W.; Rohr, J.; Stoika, R. S. The role of reactive oxygen species in tumor cell apoptosis induced by landomycin A. *Ukr. Biochem. J.* **2015**, *87*, 72–82.

(46) Shoemaker, R. H. The NCI60 human tumour cell line anticancer drug screen. *Nat. Rev. Cancer* **2006**, *6*, 813–823.

(47) Shankavaram, U. T.; et al. CellMiner: A relational database and query tool for the NCI-60 cancer cell lines. *BMC Genomics* **2009**, *10*, 1–10.

(48) Reinhold, W. C.; et al. CellMiner: A web-based suite of genomic and pharmacologic tools to explore transcript and drug patterns in the NCI-60 cell line set. *Cancer Res.* **2012**, *72*, 3499–3511.

(49) Zhang, Y.; et al. Himalaquinones A–G, angucyclinone-derived metabolites produced by the Himalayan isolate *Streptomyces* sp. PU-MM59. *J. Nat. Prod.* **2021**, *84*, 1930–1940.

(50) Panchuk, R. R. Signaling pathways involved in apoptosis induced by novel angucycline antibiotic landomycin E in Jurkat T-leukemia cells. *Exp. Oncol.* **2011**, *27*, 124–131.

(51) Lambert, R. J. W.; Pearson, J. Susceptibility testing: Accurate and reproducible minimum inhibitory concentration (MIC) and non-inhibitory concentration (NIC) values. *J. Appl. Microbiol.* **2000**, *88*, 784–790.

Chapter 3: A Semi-Synthetic Method for the Structural Derivatization of the Landomycins

Abbreviations

MDR: multi-drug resistant

LaA: Landomcyin A

CPP: Cell penetrant peptide

HIV: Human immunodeficiency viruses

3.1: Introduction

The functional role of the oligosaccharide chain in the landomycin mode of action remains unclear, in part due to limited access to the structurally intact LaA in preparative quantities. To address this limitation, we envisioned a semi-synthetic approach involving isolation of natural LaA, followed by late-stage chemical derivatization. Recent genome sequencing by the Ostash lab[1,2] enabled our group, in collaboration with the Nair and Mace labs, to optimize the fermentation and purification work-flow, yielding gram scale quantities of LaA, described in detail in Chapter 2.[3] With reliable access to LaA, we set out to probe the functional role of its glycan moiety in anticancer activity. Therapeutic molecules and their interaction with cell membranes are essential for biological activity, influencing cellular uptake and accumulation within the cell. We hypothesized that the sugar chain may either mediate a certain molecular interaction and/or serve as a transport handle for cellular uptake. To test this, we developed a strategy for selectively replacing the native glycan with alternative cell penetrant groups via late-stage modification. Cell-penetrating peptides (CPPs), like the HIV-1 TAT protein,[4] are short peptides that have a unique ability to pass through cell membranes while preserving their structural and functional properties.[5] This function is especially useful in the development of therapeutics which otherwise have poor membrane permeability.[6–8] Previous groups have established that appending cell penetrant groups to established drug moieties, such as lipids and peptides can potentiate drug activity in anti-cancer models and across other disease areas.[9–11]

In 2008, the Wender group used taxol-peptide conjugates to study how these motifs behaved in multi-drug-resistant (MDR) ovarian cancer lines (OVCA 429, OVCA 433), impervious to treatment with the native taxol structure. They linked an octo-arginine peptide to taxol via a simple disulfide linker that was cleaved upon entry into the cell by a reducing molecule such as

glutathione, promoting selective administration and biodistribution. They found that the C2' conjugation of an octo-arginine transporter to taxol allowed for the release of the drug in the cytosol, providing an enhanced cytotoxic benefit that increased the life of the infected mice in MDR models.[12] Because of this finding, we decided to try appending TAT, a short, arginine-containing CPP derived from the HIV virus, to landomycinone through a releasable disulfide linker in pursuit of a more efficacious therapeutic effect.

In 2022, the Trauner group studied how different lipid chains appended to natural product effect their therapeutic potential. Using a database to analyze known lipaded natural products, they found a trend that the removal of the lipid chain on these motifs is often associated with a decrease in bioactivity. To test this computational finding, the group conjugated different length short chain lipids to different rhodamine- and nitrobenzoxadizole-based probes to track cellular uptake. They found that the addition of small chain lipids, ranging from eight to fourteen carbons in length, increased cellular uptake and gave favorable membrane partitioning. Interestingly, longer lipid congeners decreased cellular uptake, leading to low concentrations of the probe in the cytosol.[13] Taking note of this finding, we decided to settle on conjugating a lipid containing twelve carbons to landomycinone for our study.

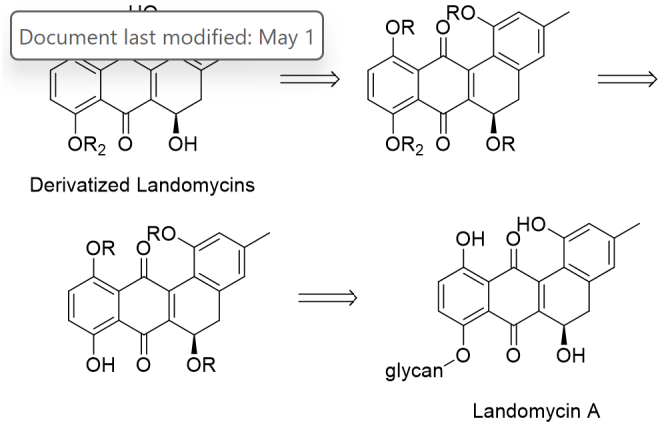

Figure 3.1: Retrosynthetic analysis towards diverse landomycins

3.2: Methods

Our initial synthetic strategy involved the global protection of the native LaA, followed by selective acidic cleavage of the carbohydrate tail (**Fig. 3.1**). We then planned to couple either a lipid or linker moiety to the resulting aglycone followed by the removal of the protecting groups to give the lipated/linker compounds. Further complexation of the linker moiety would be accomplished through disulfide exchange (**Sch. 3.1**). Recognizing the need for protecting groups compatible with lipid and peptide synthetic conditions, we turned to silyl ethers. However, initial attempts to install silyl groups using basic conditions with silyl chlorides and various bases were unsuccessful due to the facile dehydrative aromatization of the chiral C6 hydroxyl. Using a two-step strategy, we successfully installed TBS and TIPS protecting groups

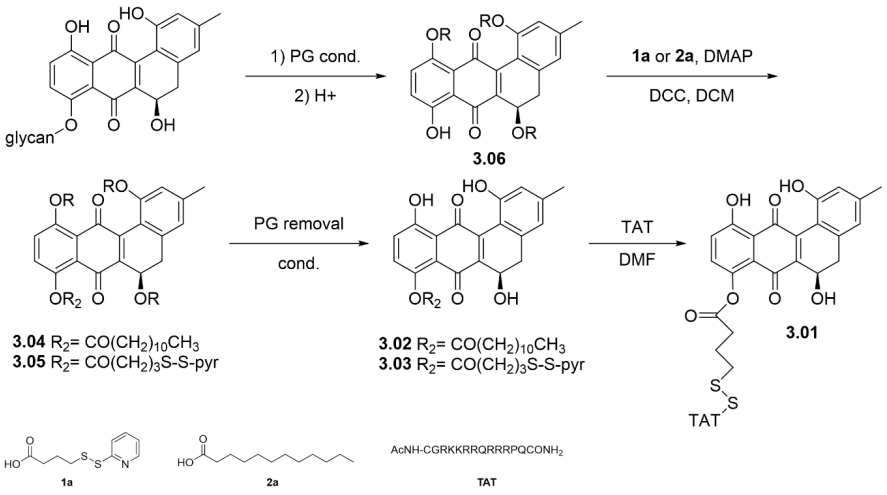

Scheme 3.1: Proposed forward synthesis towards derivatized landomycin compounds

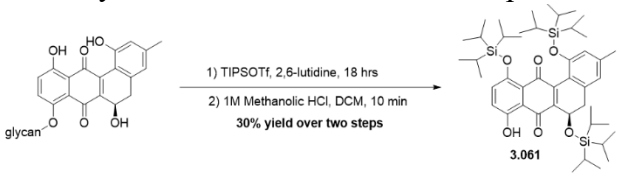

Entry	Scale (mg)	Solvent	Rxn 1 Eq. Base	Rxn 1 Eq. TBSOTf	Rxn 2 HCl Conc.	Rxn. 2 Time (min)	Yield (%)
1	100	DCM	12	9	N/A	N/A	0
2	100	DCM	12	9	2 M	20	20
3	200	DCM	16	12	1 M	20	28
4	100	ACN/DCM	16	12	1 M (cooled)	10	17
5	**230**	**ACN/DCM**	**16**	**12**	**1 M**	**5**	**30**
6	190	ACN/DCM	16	12	0.01 M	20	13
7	100	ACN/DCM	16	12	0.1 M (cooled)	10	17
8	160	ACN/DCM	16	12	0.1 M (cooled)	30	13
9	215	ACN/DCM	16	12	0.1 M	30	20
10	300	ACN/DCM	16	12	0.1 M	10	23

Figure 3.1: Optimization of the two-step process towards the TIPS protected landomycinone, compound 3.061

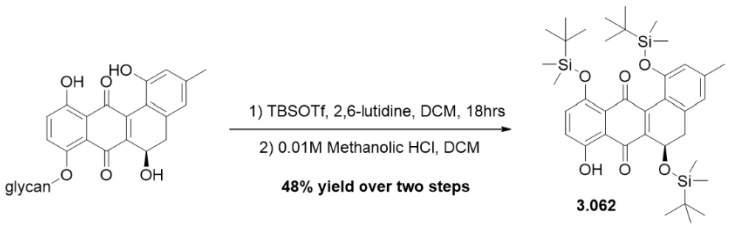

Figure 3.3: Optimized two-step approach to the TBS-protected landomycinone, compound 3.062

using the corresponding silyl triflate and 2,6-lutidine, followed by cleavage of the sugar moiety by methanolic HCl, though overall yields were low for efficient downstream optimization (**Fig. 3.2**, **Fig. 3.3**). In pursuit of a more refined process, we investigated a one-pot strategy, where one equivalent of triflic acid was generated slowly in situ to promote both selective silyl protection and glycan cleavage. This approach was successful with the TIPS group, affording the selectively protected aglycone in 72% yield over a single process (**Fig. 3.4**). Serendipitously, subsequent reaction screening revealed that TBS protected aglycones were unstable in the basic conditions of the coupling step, undergoing aromatization, where the TIPS protected moiety remained stable. Because of this finding, we decided to move forward with the TIPS-protected landomycinone in

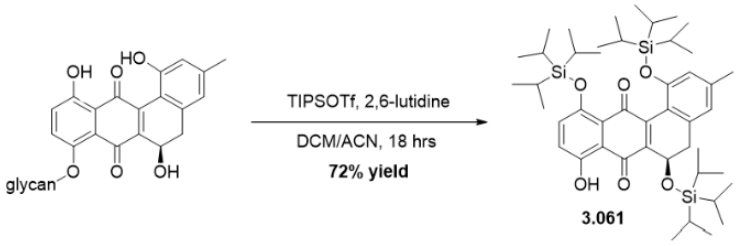

Entry	Scale (mg)	Eq. Base	Eq. TIPSOTf	Yield (%)
1	450	14	16	41
2	**660**	**14**	**15**	**71**
4	50	14	14	0

Figure 3.4: Optimized one-pot process to TIPS-protected landomycinone, compound 3.061

synthetic pursuit of both a lipated and peptidated compound.

3.3: Discussion: Lando-Lipid Synthesis

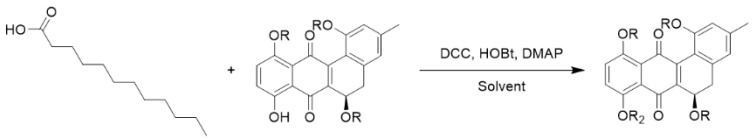

Entry	R	Eq. DCC	Eq. HOBt	Eq. DMAP	Eq. Lipid	Solvent	Yield (%)
1	TIPS	2	2	2	2	DCM	12
2	TBS	2	2	2	2	DCM	0
3	TIPS	2	2	2	2	DMF	0
4	TIPS	2.5	2.5	2.5	2.5	DMF	0
5	TBS	2	2	2	2	DMF	0
6	TIPS	2	2	1	2	DMF	
7	TBS	2	2	1	2	DCM	0
8	TIPS	2	2	0.1	2	DCM	trace
9	TBS	2	2	0.1	2	DCM	0
10	TIPS	10	5	2	10	DCM	10
11	TIPS	10	5	1	10	DCM	13

Figure 3.5: Optimization attempts coupling the carboxylic acid of the lipid to the protected core(s)

With a reliable supply of protected aglycone secured, we moved forward coupling the lipid to the core. Initial attempts focused on coupling the carboxylic acid of the lipid to the core through conventional peptide coupling techniques. After screening various conditions with DCC, DCC/HOBt, only trace amounts of products formed, leaving most of the starting material remaining (**Fig. 3.5**). In addition, other conditions attempted include HATU, HATU/HOAt, EDC, and T3P along with different bases, reaction times, concentrations, solvents and temperatures. None of these conditions gave rise to better outcomes than DCC/HOBt. Given these challenges, we shifted to an acylation approach, leveraging a commercially available lipid-derived acid chloride. Due to the low nucleophilicity of the TIPS protected core, high concentrations of both acid chloride and base were needed to get an optimal conversion to lipated product (**Fig. 3.6)**. The protected lipid compound was identified via high resolution QTOF-MS. Nevertheless, the purified yellow oil rapidly degraded, visibly browning within an hour of isolation. Extensive efforts exploring a wide variety of storage conditions both neat and in solution at different termperatures failed to prevent this decomposition. After that reaction, the components could not be purified without turning to a brown sludge on the

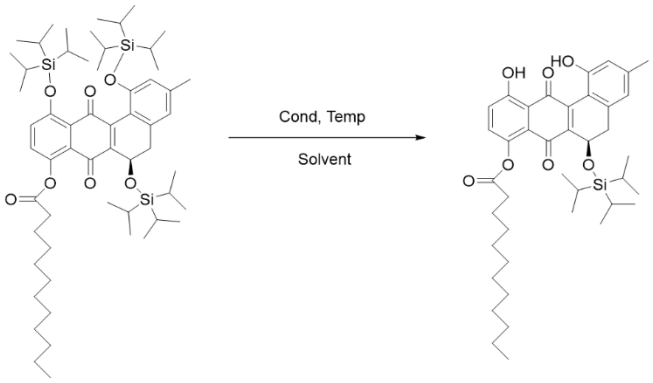

Entry	Cond.	Temp	Solvent	Outcome	Yield %
1	TBAF	RT	-	degradation	0
2	TBAF	0	-	degradation	0
3	TBAF	0	DCM	trace new orange/red spot	<1
4	HF*pyr	0	DCM	tar	0
5	0.05 M methanolic HCl	0	DCM	degradation	0
6	0.1M methanolic HCl	0	DCM	degradation	0
7	**TBAF**	**-5**	**DCM**	**new orange/red spot**	**73**

Figure 3.7: Optimization towards the mono-TIPS protected aglycone towards the final Lando-lipid product

column. To mitigate degradation, we attempted instant fluoride mediated deprotection of the silyl ether to the semi-purified yellow mixture by rapid PREP-TLC. After optimal conditions were identified, we isolated a new compound which we determined to be the mono-TIPS-protected lipid compound in 48% yield over those two steps (**Fig. 3.7**). Deprotection of the last silyl group on the chiral hydroxyl proved more challenging. In our hands, fluoride sources failed to produce the final product. The conditions reported by Roush and colleagues in the total synthesis of landomycinone using 0.01 M methanolic HCl,[14] was

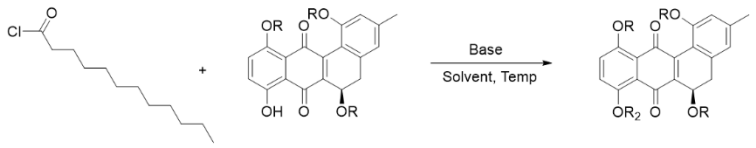

Entry	R	Solvent	Base	Base Eq.	Lipid Eq.	Total Rxn Time (hrs)	Semi-crude Yield (%)	Temp (°C)
1	TBS	DCM	Pyridine	2	1.1	4	0	RT
2	TBS	DCM	Triethylamine	2	1.1	4	0	RT
3	TBS	DCM	Pyridine	2	1.1	18	0	RT
4	TBS	DCM	Triethylamine	2	1.1	18	0	RT
5	TBS	DCM	NaH	1.3	1.1	4	0	RT
6	TBS	DCM	Pyridine	4	2.2	4	0	RT
7	TBS	DCM	Triethylamine	4	2.2	4	0	RT
8	TIPS	-	Pyridine	excess, used as solvent	60	6	trace	(-5) to RT
9	TIPS	-	Pyridine, DMAP	excess, used as solvent	60	6	degradation	(-5) to RT
10	TBS	DCM	Pyridine	30	35	5	degradation	held at 0
11	TIPS	DCM	Pyridine	30	35	24	trace	held at (-5)
12	TIPS	DCM/ACN	Pyridine	30	35	5	9	held at 0
13	TIPS	DCM	Pyridine	60	60	24	25	held at 0
14	TIPS	DCM	Pyridine	60	60	12	0	(-5) to RT
15	**TIPS**	**DCM/ACN**	**Pyridine**	**60**	**60**	**18**	**50**	**held at -5**
16	**TIPS**	**DCM/ACN**	**Pyridine**	**60**	**60**	**20**	**51**	**held at -5**
17	TIPS	DCM/ACN	Pyridine	60	60	16	degradation	0 to RT OV

Figure 3.6: Optimization towards the protected and lipidated landomcyinone

ineffective on the TIPS group. However, slightly more acidic, cooler conditions with an elongated reaction were ultimately successful, furnishing the final lipidated product in 26% yield (**Fig 3.2**). Unfortunately, the compound exhibited insufficient stability for biological evaluation. Though, this is still the first example of an effective semi-synthetic derivatization of the landomycins, creating a lipidated version in 7% overall yield (**Sch. 3.2**).

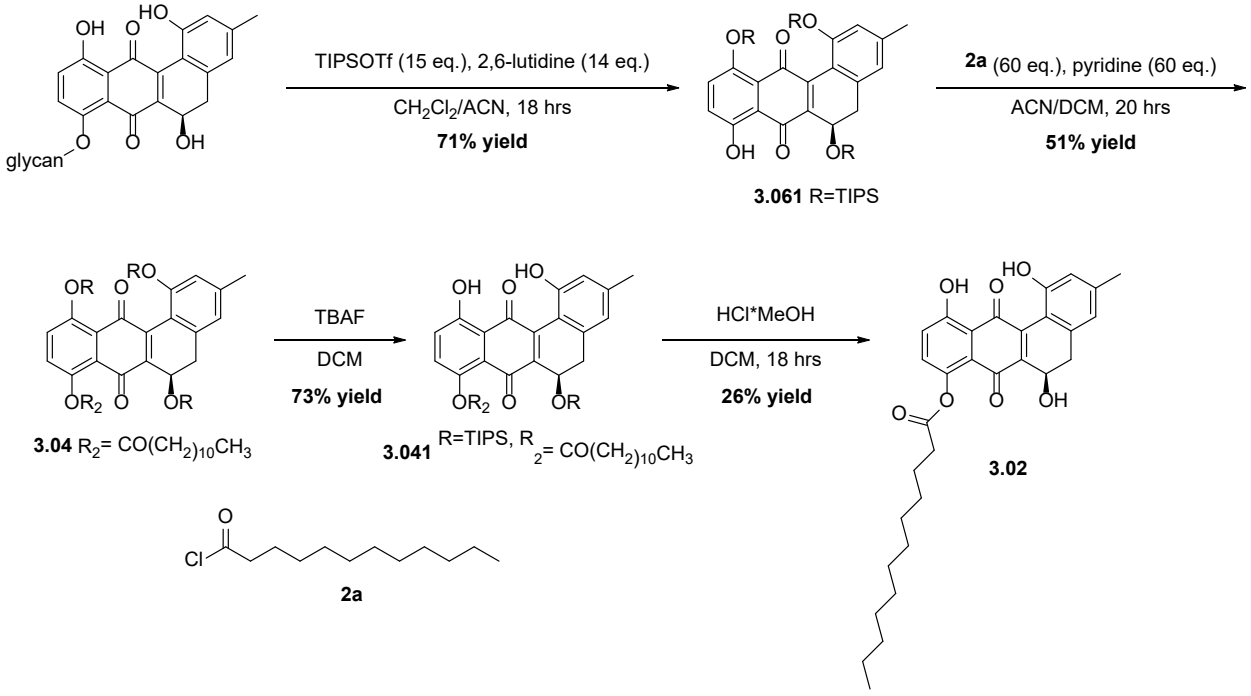

Scheme 3.2: Optimized route to Lando-lipid, compound 3.02

3.4: Discussion: Lando-Peptide Synthesis

Initially, we synthesized the carboxylic acid containing disulfide linker, following the protocol from the Wender group (**Sch. 3.3**). Similarly to the lipid, the acid of the linker did not react in standard peptide coupling conditions including DCC, DCC/HOBt, HATU, HATU/HOAt, EDC, and T3P, which we attributed to the weak nucleophilicity of the TIPS-protected core. Because of this,

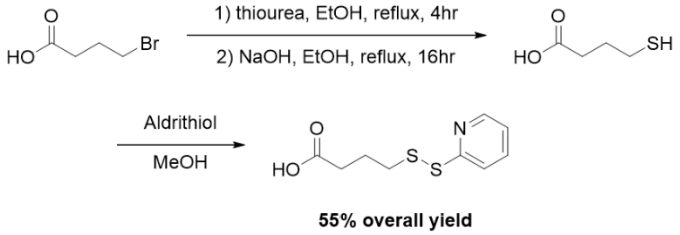

Scheme 3.3: Synthesis of the disulfide linker

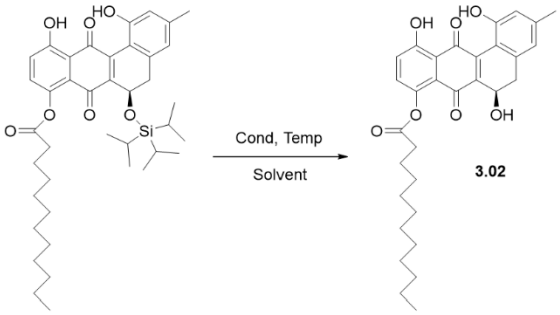

Entry	Conditions	Temp (°C)	Time (hrs)	Solvent	Outcome
1	TBAF	RT	24	DCM	SM recovered
2	TBAF	RT	48	DCM	SM recovered
3	TBAF	35	18	DCM	elimination
4	HF*pyr	RT	3	DCM	elimination
5	HF*pyr	RT	3	Pyr.	elimination
6	HF*pyr	0	18	DCM	elimination
7	HF*pyr	0	18	Pyr.	trace prod
8	3HF[NEt3]	0	18	DCM	elimination
9	0.1M MeOH*HCl	RT	3	DCM	trace new spot
10	**0.2M MeOH*HCl**	**0**	**24**	**DCM**	**7.3mg product, 26% yield**
11	TBAF, AcOH	RT	18	DCM	elimination

Figure 3.8: Final deprotection of the mono-TIPS lipid to get to the final compound 3.02

we generated the acyl chloride of the linker in situ using acetyl chloride, followed by the addition of the core to solution under basic conditions. Similarly to the lipid, the crude reaction material broke down immediately, visible by a color change from red to brown that happened during the concentration of the reaction materials. Immediate fluoride deprotection did not prevent

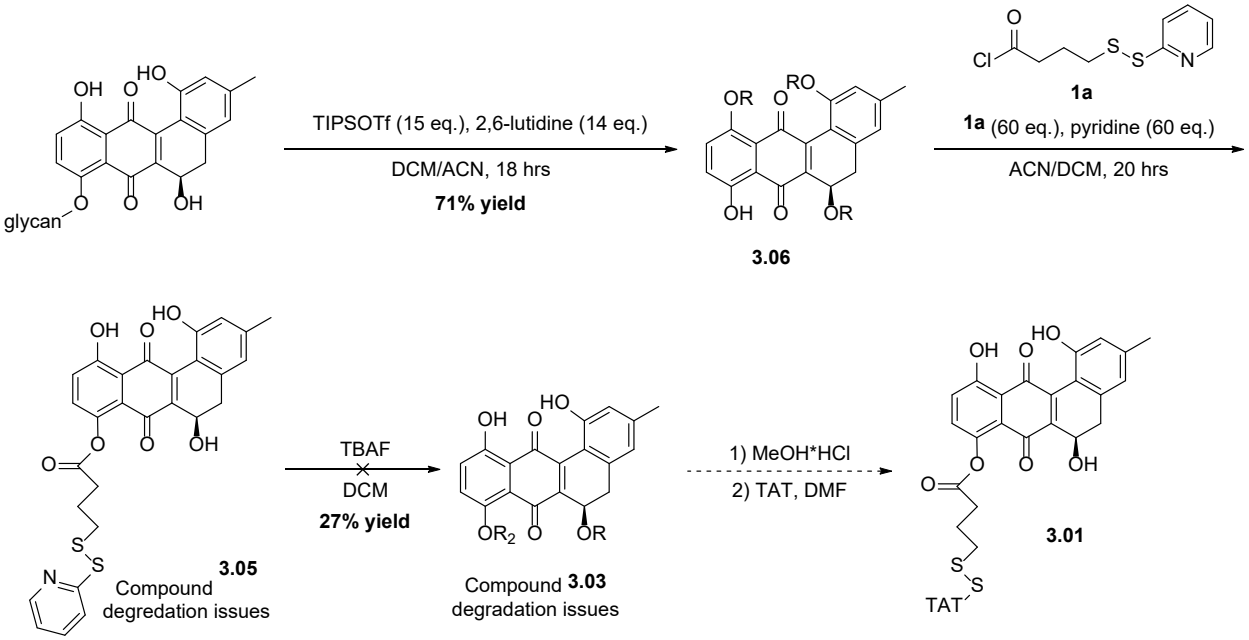

Scheme 3.4: Progress towards peptidated landomycin, compound 3.01

the degradation of the compound, which was too rapid to mitigate. Unfortunately, no product was ever detected for the linked aglycone (**Sch. 3.4**). Further synthetic investigation is needed to determine if a different linker motif would promote a more stable, isolatable structure.

3.5: Concluding Remarks

In this chapter, we explored the first semi-synthetic derivatization of landomycin A to probe the functional role of its oligosaccharide chain in cellular uptake and biological activity. Motivated by evidence that lipids and cell-penetrating peptides (CPPs) can modulate pharmacokinetics and efficacy, we pursued the synthesis of both lipidated and peptidated landomycinone analogs through late-stage chemical derivatization. The inherent complexity of the landomycin scaffold demanded careful protecting group strategy and mild conditions to preserve the sensitive core. We developed a robust one-pot protocol for simultaneous silyl protection and selective glycan removal, ultimately identifying TIPS as compatible protecting groups for downstream acylation chemistry. While conventional coupling techniques failed due to the core's poor nucleophilicity, acyl chloride-based strategies enabled the successful attachment of a dodecanoic acid chain, yielding the first lipidated landomycinone analog. However, rapid degradation of the intermediate and final products posed a major challenge. In parallel, we attempted to introduce a disulfide-based CPP linker, inspired by previous successes in peptide-drug conjugates by the Wender group. Despite replicating reported linker synthesis and employing similar conjugation strategies, the resulting adducts proved highly unstable. These findings suggest that the landomycinone core may require alternative linker moieties to remain viable during conjugation and purification. Ultimately, although limited by stability issues, this work lays the foundation for future efforts in modifying the landomycins via semi-synthetic routes. Our results demonstrate that site-selective modification of LaA is chemically feasible, and that lipid-based

analogs, while synthetically accessible, require different strategies to enhance stability. These findings open the door to further structure-activity studies and the design of next-generation aglycone-modified analogs.

3.6: Works Cited

(1) Hrab, P.; Rückert, C.; Busche, T.; Ostash, I.; Kalinowski, J.; Fedorenko, V.; Yushchuk, O.; Ostash, B. Complete Genome Sequence of Streptomyces Cyanogenus S136, Producer of Anticancer Angucycline Landomycin A. *3 Biotech* **2021**, *11* (6), 282. https://doi.org/10.1007/s13205-021-02834-4.

(2) Deneka, M., Ostash, I., Yalamanchili, S. et al. Insights into the Biological Properties of Ligands and Identity of Operator Site for LanK Protein Involved in Landomycin Production. *Curr Microbiol* **2024**, *81* (5).

(3) Chappell, T. C.; Maiello, K. G.; Tierney, A. J.; Yanagi, K.; Lee, J. A.; Lee, K.; Mace, C. R.; Bennett, C. S.; Nair, N. U. Rapid Spectrophotometric Detection for Optimized Production of Landomycins and Characterization of Their Therapeutic Potential. *Biotechnol. Bioeng.* **2024**, *121* (9), 2648–2661. https://doi.org/10.1002/bit.28725.

(4) Green, M.; Loewenstein, P. M. Autonomous Functional Domains of Chemically Synthesized Human Immunodeficiency Virus Tat Trans-Activator Protein. *Cell* **1988**, *55* (6), 1179–1188. https://doi.org/10.1016/0092-8674(88)90262-0.

(5) Gori, A.; Lodigiani, G.; Colombarolli, S. G.; Bergamaschi, G.; Vitali, A. Cell Penetrating Peptides: Classification, Mechanisms, Methods of Study, and Applications. *ChemMedChem* **2023**, *18* (17), e202300236. https://doi.org/https://doi.org/10.1002/cmdc.202300236.

(6) Rüter, C. Delivery of Antibiotics by Cell-Penetrating Peptides to Kill Intracellular Pathogens BT - Cell Penetrating Peptides: Methods and Protocols; Langel, Ü., Ed.; Springer US: New York, NY, 2022; pp 335–345. https://doi.org/10.1007/978-1-0716-

1752-6_22.

(7) Hasannejad-Asl, B.; Pooresmaeil, F.; Takamoli, S.; Dabiri, M.; Bolhassani, A. Cell Penetrating Peptide: A Potent Delivery System in Vaccine Development. *Front. Pharmacol.* **2022**, *13*, 1072685. https://doi.org/10.3389/fphar.2022.1072685.

(8) Tietz, O.; Cortezon-Tamarit, F.; Chalk, R.; Able, S.; Vallis, K. A. Tricyclic Cell-Penetrating Peptides for Efficient Delivery of Functional Antibodies into Cancer Cells. *Nat. Chem.* **2022**, *14* (3), 284–293. https://doi.org/10.1038/s41557-021-00866-0.

(9) Borrelli, A.; Tornesello, A. L.; Tornesello, M. L.; Buonaguro, F. M. Cell Penetrating Peptides as Molecular Carriers for Anti-Cancer Agents. *Molecules* **2018**, *23* (2). https://doi.org/10.3390/molecules23020295.

(10) Hammond, S. M.; Aartsma-Rus, A.; Alves, S.; Borgos, S. E.; Buijsen, R. A. M.; Collin, R. W. J.; Covello, G.; Denti, M. A.; Desviat, L. R.; Echevarría, L.; Foged, C.; Gaina, G.; Garanto, A.; Goyenvalle, A. T.; Guzowska, M.; Holodnuka, I.; Jones, D. R.; Krause, S.; Lehto, T.; Montolio, M.; Van Roon-Mom, W.; Arechavala-Gomeza, V. Delivery of Oligonucleotide-Based Therapeutics: Challenges and Opportunities. *EMBO Mol. Med.* **2021**, *13* (4), e13243. https://doi.org/10.15252/emmm.202013243.

(11) Sauter, M.; Strieker, M.; Kleist, C.; Wischnjow, A.; Daniel, V.; Altmann, A.; Haberkorn, U.; Mier, W. Improving Antibody-Based Therapies by Chemical Engineering of Antibodies with Multimeric Cell-Penetrating Peptides for Elevated Intracellular Delivery. *J. Control. release Off. J. Control. Release Soc.* **2020**, *322*, 200–208. https://doi.org/10.1016/j.jconrel.2020.03.005.

(12) Dubikovskaya, E. A.; Thorne, S. H.; Pillow, T. H.; Contag, C. H.; Wender, P. A.

Overcoming Multidrug Resistance of Small-Molecule Therapeutics through Conjugation with Releasable Octaarginine Transporters. *Proc. Natl. Acad. Sci. U. S. A.* **2008**, *105* (34), 12128–12133. https://doi.org/10.1073/pnas.0805374105.

(13) Morstein, J.; Capecchi, A.; Hinnah, K.; Park, B.; Petit-jacques, J.; Lehn, R. C. Van; Reymond, J.; Trauner, D. Medium-Chain Lipid Conjugation Facilitates Cell-Permeability and Bioactivity. **2022**. https://doi.org/10.1021/jacs.2c07833.

(14) Roush, W. R.; Bennett, C. E. A Highly Stereoselective Synthesis of the Landomycin a Hexasaccharide Unit [10]. *J. Am. Chem. Soc.* **2000**, *122* (25), 6124–6125. https://doi.org/10.1021/ja000743k.

Chapter 4: Optimized Solid Phase Small Molecule Syntheses Toward Common DEL Hit Cores

Disclaimer:
The work presented in this chapter was conducted during my Co-Op internship at Vertex Pharmaceuticals. This experience contributed to the development of the experimental approaches and scientific perspective reflected in this research. However, all data, analyses, and conclusions described herein are the result of independently conducted work and do not incorporate any proprietary, confidential, or unpublished materials originating from Vertex Pharmaceuticals. This thesis does not disclose any information specific to Vertex projects, compounds, or internal research.

I am sincerely grateful to Vertex Pharmaceuticals for the opportunity to gain industry experience and for the valuable mentorship and training I received during my time there.

Abbreviations

DEL: DNA-encoded libraries

HTE: High-throughput experimentation

SAR: structure–activity relationship

SPS: Solid-phase synthesis

4.1: Introduction

Because drug discovery is a complex and capital-intense process, the pharmaceutical industry has long sought after a high-throughput approach to early-stage target identification. In modern workflows, scientists use synthetic design and medicinal chemistry to identify hits against an array of biological targets. Once a hit is identified, medicinal chemists optimize its properties—such as potency, bioavailability, selectivity, and metabolic stability—through iterative design cycles with the goal of ending with a drug on the market.[1] However, these efforts depend first on identifying promising molecular scaffolds through efficient early-stage screening. Traditionally, lead identification involves running singleton reactions to generate individual compounds—a slow, laborious, and resource-heavy approach. High-throughput experimentation (HTE) has significantly accelerated this process by allowing for the miniaturized, parallel execution of chemical reactions using well-plate formats on automated platforms (**Fig. 4.1**). HTE allows chemists to explore multiple variables concurrently, such as reagent choice, concentration, temperature, and solvent, across hundreds or even thousands of reaction wells. This capability enables the rapid optimization of reaction conditions by reducing time and conserving starting materials.[2,3] In early discovery settings, HTE is also used to generate structurally diverse libraries by varying chemical building blocks or functional groups across a target motif. These libraries are then screened for biological

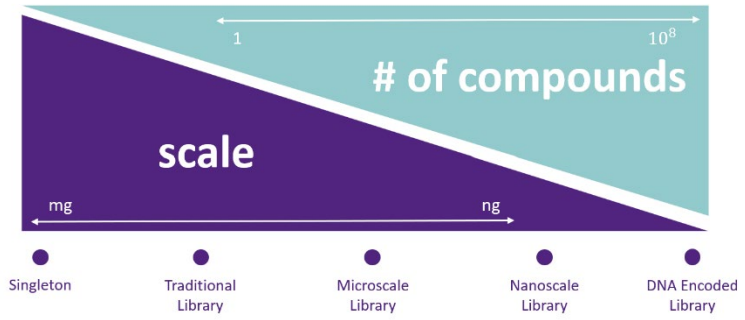

Figure 4.1: Comparing different high throughput approaches in the scale and number of compounds

activity, allowing for super-efficient hit identification and structure–activity relationship (SAR) development.

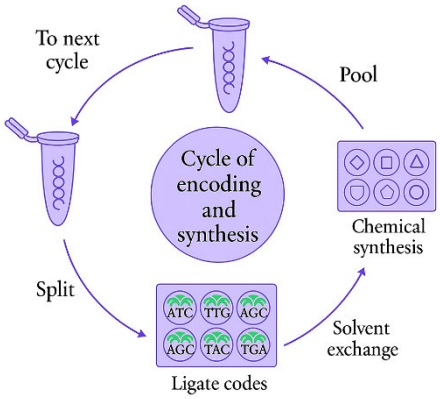

Figure 4.2: The cycle of encoding and synthesis of DEL

An additional tool employed for hit identification in early-stage drug discovery is DNA-encoded libraries, which enable the ultra-high-throughput screening of small molecules against biological targets. DELs combine combinatorial chemistry and molecular biology to generate libraries containing millions to billions of unique compounds, each covalently linked to a DNA barcode that houses its structural information.[4] Library building begins with a DNA "headpiece" bearing a primary amine, which serves as the reactive functional group for synthesis. Then, specific ligation codes are appended to the headpiece DNA and serve as a record of what building blocks will be added. Each unique functionality is incorporated in a stepwise fashion using split-pool synthesis, where the library is divided, modified with specific reagents, and then recombined before the following splitting iteration (**Fig. 4.2**). This process is often repeated multiple times and allows for the generation of expansive molecular outcomes. Once synthesized, the entire DEL is incubated with a biological target. Then, non-binding compounds are washed away while binding molecules remain appended to the target. The DNA tags of the retained molecules are then PCR-amplified and sequenced to identify promising hits. DEL technology offers several key advantages: it drastically reduces reagent consumption, allows for the parallel screening of vast chemical space, and facilitates hit identification through DNA sequencing.[5]

Transitioning from DEL screening to traditional validation efforts presents significant synthetic challenges. DEL-compatible reactions are typically performed under dilute, aqueous

conditions with large excesses of reagents—conditions that are often incompatible with traditional organic synthesis and purification methods.[6] Moreover, many DEL-derived structures feature functional groups or scaffolds that are difficult to reproduce off-DNA using standard solution-phase organic chemistry.[7] These challenges highlight the need for new synthetic platforms that can better replicate on-DNA conditions to streamline the resynthesis and structural derivatization of hit compounds.

To address these limitations, solid-phase synthesis (SPS) offers a promising alternative for the resynthesis and exploration of DEL hits. Originally developed for peptide synthesis, SPS leverages inert, polymer resin beads that serve as the insoluble support for stepwise chemical transformations.[8] The general workflow involves immobilizing a starting molecule onto the solid support, performing iterative chemical reactions on the bead-bound intermediate, and ultimately cleaving the final product from the resin using acidic conditions (**Fig. 4.3**). This method offers several advantages over traditional solution-phase synthesis, particularly in terms of ease of purification, reaction monitoring, and automation. SPS allows for straightforward removal of excess reagents and byproducts through simple filtration and washing, eliminating the need for extensive purification at each step. Furthermore, the spatial confinement of molecules on the bead mimics the constrained environment seen in on-DNA chemistry, making SPS an attractive proxy for recreating most-similar

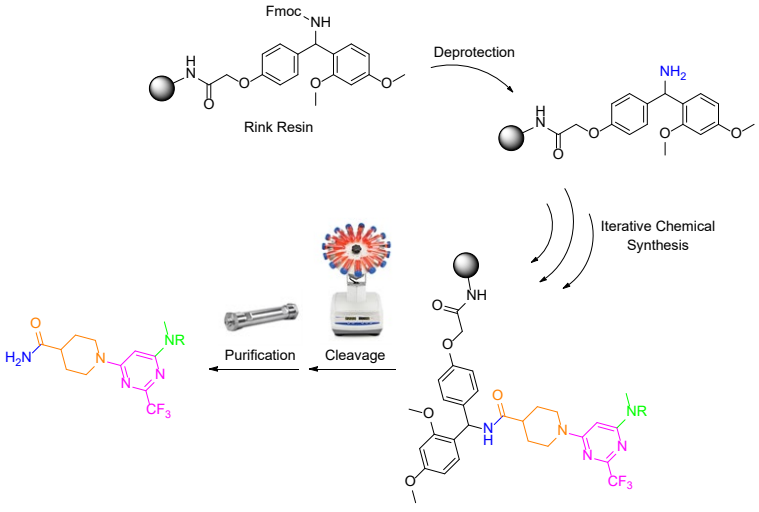

Figure 4.3: Applying solid phase synthesis techniques to small molecule generation

conditions under which DEL hits are originally synthesized.

In this work, we aim to explore the applicability of SPS beyond its conventional use in amide bond formation. Specifically, we evaluate whether typical organic transformations—including S_NAr reactions, heterocycle formation, and C–X bond-forming reactions—can be efficiently conducted on resin to access structurally complex, drug-like small molecules. This approach is intended to bridge the gap between DEL screening and hit validation by providing a more practical route to making and expanding upon hit compounds under conditions that better reflect DEL synthesis. Additionally, by capturing side products and off-pathway intermediates that may arise from bead-associated effects, SPS can also offer mechanistic insights that may be obscured in solution-phase synthesis or overlooked in standard resynthesis workflows.

4.2: Results & Discussion

Interesting structural motifs commonly identified in DEL screens include pyrimidines, 1,3,4-oxadiazoles, 1,2,4-oxadiazoles, and 1,2,4-triazoles. We began our efforts on pyrimidine targets, leveraging a similar double S_NAr pathway previously developed at Vertex Pharmaceuticals (**Fig. 4.4**). This strategy was appealing because the conditions for these transformations were quite mild and mimicked reagents used in traditional SPS reactions. To our satisfaction, this pathway was effectively translated to bead-format. The reaction sequence (**Fig. 5**) was carried out on Rink-Amide resin in a telescoped fashion, with

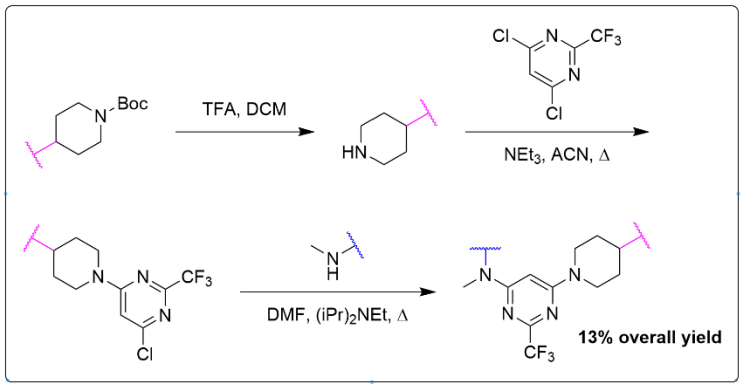

Figure 4.4: Previously developed synthetic route to pyrimidine cores

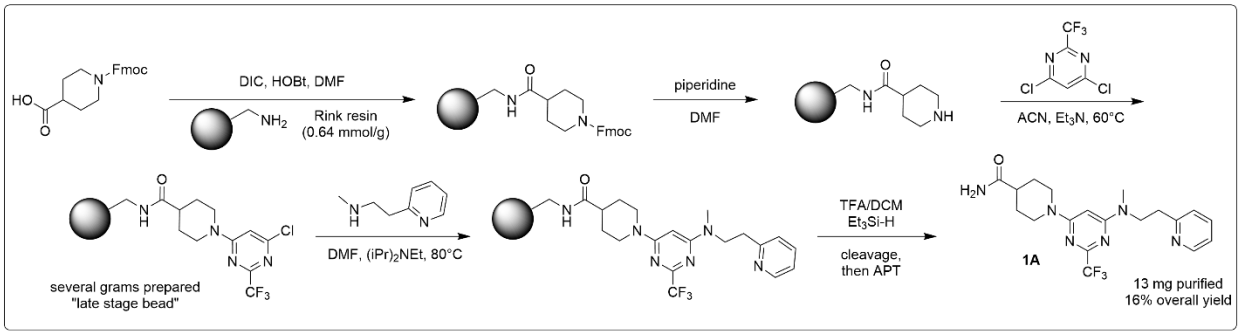

Figure 4.5: SPS pathway to compound 1A, a pyrimidine motif

purification steps limited to simple washes between transformations to remove excess reagents followed by filtrations to isolate functionalized beads. Final purification was performed only after resin cleavage, minimizing the overall number of purification steps required. The final substituted pyrimidine compound 1A (**Fig. 4.5**) was isolated in 16% yield over five steps. Notably, the quantity of compound generated exceeded the material requirements for typical hit-confirmation efforts. For library generation efforts towards SAR studies, we adapted this SPS protocol to the automated platform at Vertex Pharmaceuticals. Late-stage functionalized beads were prepared, and the QS-30 solid doser was used to aliquot both beads and solid reagents into multi-well vials. Liquid reagents and solvents were delivered via multichannel pipette from prepared stock solutions. Reactions were stirred overnight on a heated plate, followed by standard washing, cleavage, and concentration steps. The crude concentrates were purified via HPLC to yield the final compounds. Of the seven intended pyrimidine analogs, six were successfully synthesized, with isolated yields

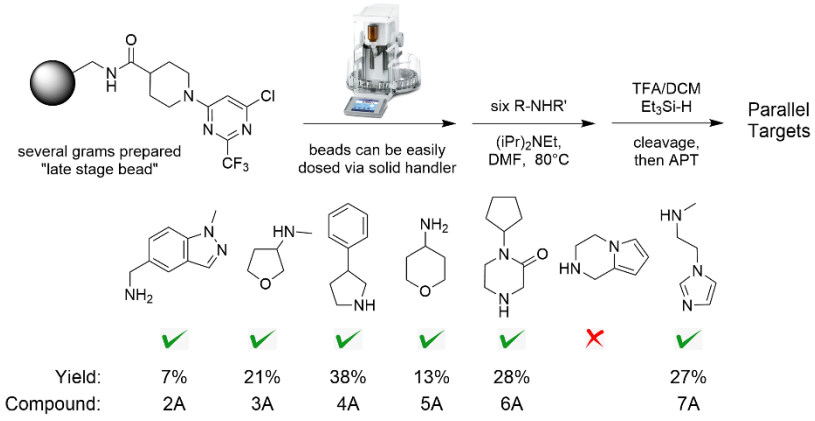

Figure 4.6: Library generation of diversified pyrimidine compounds

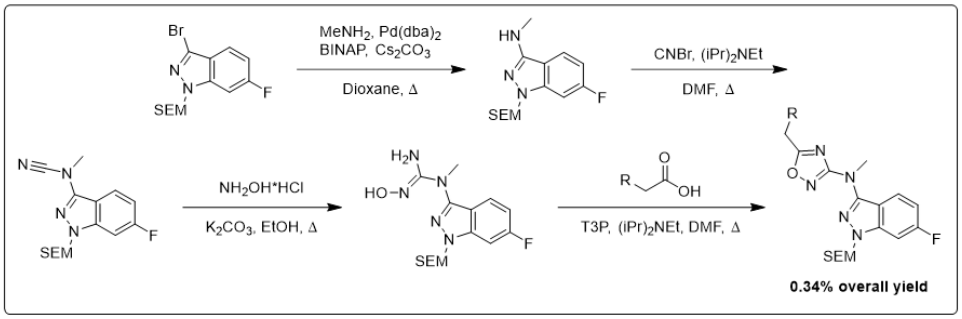

Figure 4.7: Previously developed synthetic route to 1,2,4-oxadiazole core

ranging from 7–38% (**Fig. 4.6**). Overall, this method proved to be a robust and scalable approach to accessing pyrimidine-based targets.

Our next scaffold of interest was the 1,2,4-oxadiazole core, where we leveraged a second in-house synthetic pathway, though overall yields were quite low (**Fig. 4.7**). The largest yield losses occurred during the N-cyanation and final cyclization steps respectively. When adapted to SPS, this route delivered the intended product in 2% isolated yield—outperforming the solution-phase equivalent, though still insufficient for large-scale library synthesis (**Fig. 4.8**). However, this method remains valuable for hit-validation applications involving 1,2,4-oxadiazole-containing compounds.

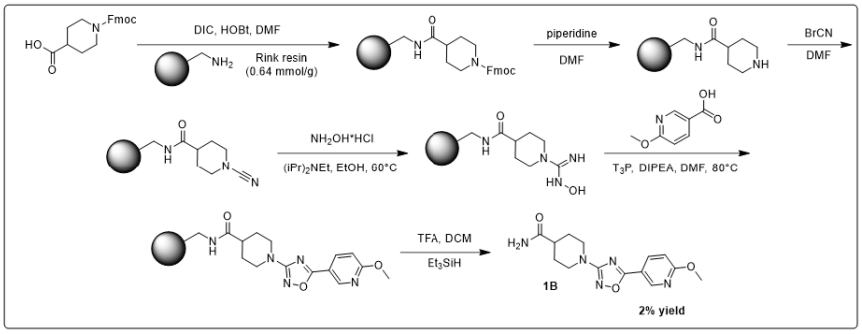

Figure 4.8: SPS pathway to compound 1B, a 1,2,4-oxadizole motif

We then targeted both the 1,3,4-oxadiazole and 1,2,4-triazole motifs, adapting a literature precedent that utilized DNA-conjugated thiosemicarbazide handles to access the target motifs.[9] By installing a thiosemicarbazide functionality on-bead and employing T3P as both a coupling and dehydrating agent, we isolated the intended heterocyclic target in 9% overall yield (**Fig. 4.9**). However, substantial side product formation was observed, with a major impurity differing from the target by 16 mass units. Although the proton NMR spectra were indistinguishable, carbon

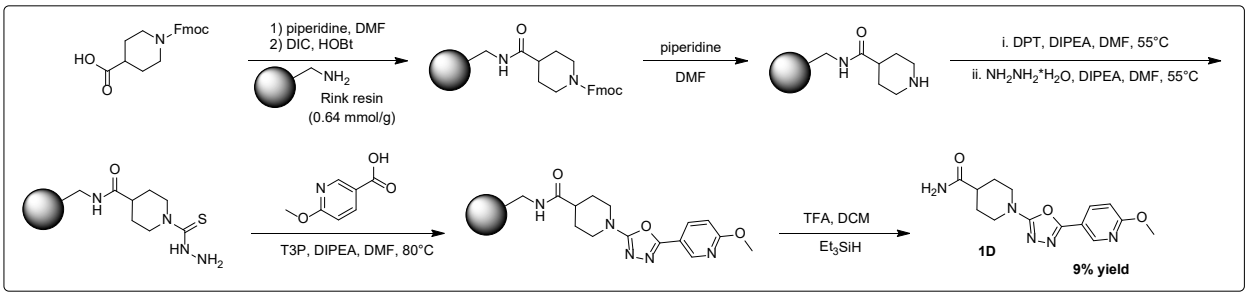

Figure 4.9: SPS pathway to compound 1D, a 1,3,4-oxadizole motif which also produced compound 1C, the 1,3,4-thiadiazole core.

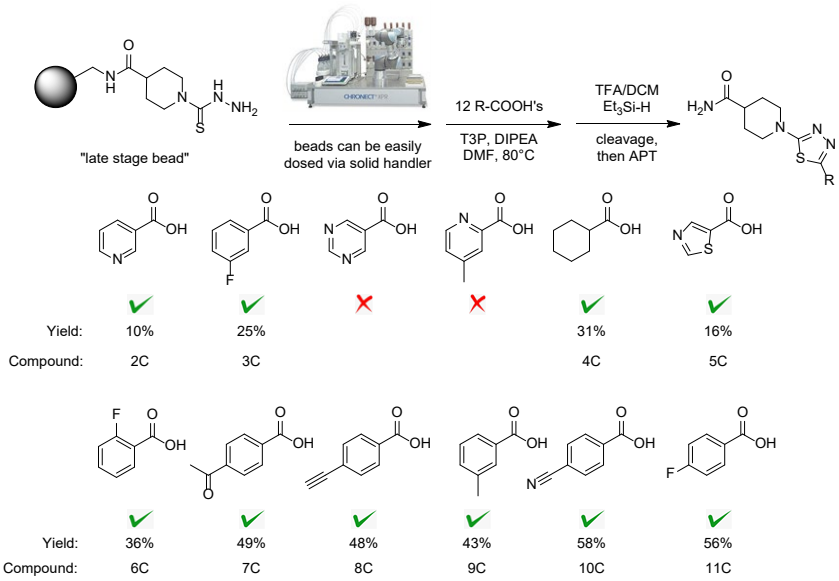

Figure 4.10: Library generation of diversified 1,3,4-thiadiazole targets

NMR revealed an upfield shift consistent with the formation of compound 1C, the 1,3,4-thiadiazole core, which was isolated in 23% yield. Given the relevance of thiadiazoles as privileged scaffolds,[10] we exploited this serendipitous outcome to generate a thiadiazole library. Solid reagents were dispensed using the Cronect solid doser, and liquid reagents and solvents were added via multichannel pipette. Reactions were stirred overnight on a heated plate and processed with standard SPS workflows. Crude products were purified by HPLC. Of the twelve intended thiadiazole analogs, ten were successfully synthesized, with isolated yields ranging from 10–58% (**Fig. 4.10**). The high

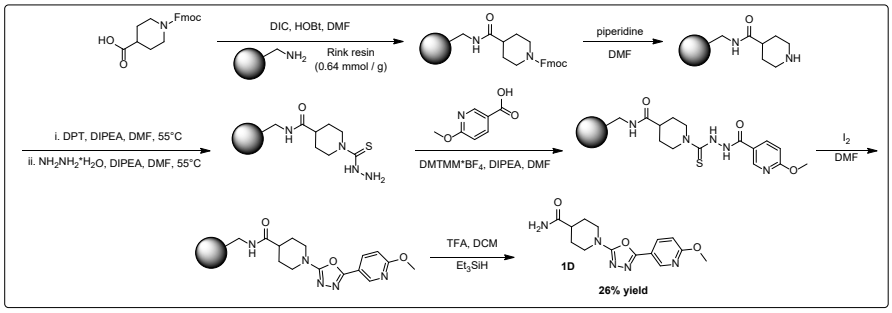

Figure 4.11: Optimized SPS pathway to compound 1D, a 1,3,4-oxadiazole target

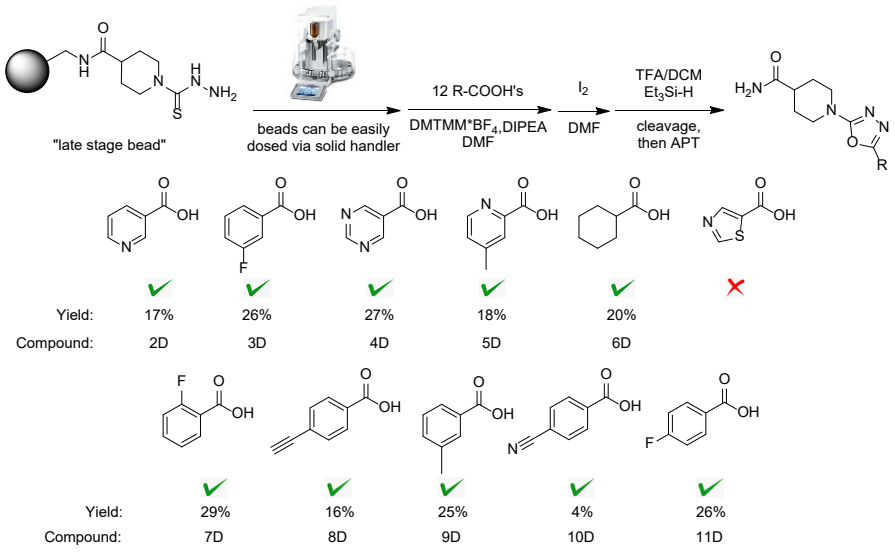

Figure 4.12: Figure 10: Library generation of diversified 1,3,4-oxadiazole targets

yield and success rate made this library particularly impressive. After the generation of the thiadiaole library, different acylation and cyclization techniques were explored to reach the original 1,3,4-oxadiazole core. By mirroring those conditions more closely to the on-DNA literature precedent, we were able to synthesize the intended oxadiazole target in 26% overall yield (**Fig. 4.11**). Those conditions were then adapted to the same library format used for the pyrimidine targets, leveraging the abilities of the QS-30 solid doser. Of the eleven intended 1,3,4-oxadiazole analogs, ten were successfully synthesized, with isolated yields ranging from 4–29% (**Fig. 4.12**). This success

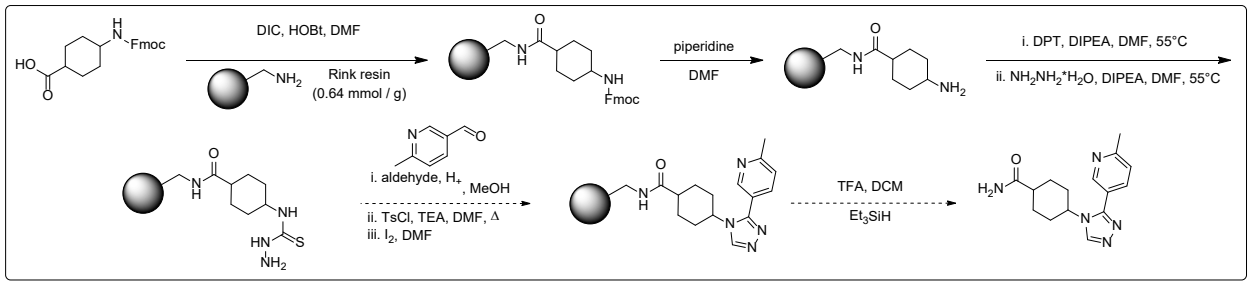

Figure 4.13: Progress towards the SPS of the 1,2,4-triazole core

demonstrated that the methodology was well-suited for generating SAR libraries based on DEL hits containing the 1,3,4-oxadiaz ole motif. Ongoing work SPS towards the 1,2,4-triazole core is currently underway (**Fig. 4.13**) at Vertex.

4.3: Conclusion

In summary, we successfully translated four different synthetic pathways towards relevant small molecule cores to SPS formats. Three of those four pathways were on-boarded to high throughput automated workflows for library generation, enabling efficient access to key heterocyclic motifs commonly resulting from DEL campaigns. The pyrimidine core SPS proved robust, resulting in multiple different compounds for both hit validation and SAR efforts. While the 1,2,4-oxadiazole synthesis was limited by low yield, it still offered an advantage for hit confirmation efforts as compared to its solution phase counterpart. The unexpected formation of the 1,3,4-thiadiazole led to the development of the highest yielding library, demonstrating the flexibility of SPS platform design. Lastly, be refining reaction conditions, we were able to establish an effective SPS route 1,3,4-oxadiazole cores, further expanding the synthetic toolkit available for DEL hit confirmation and rapid structural derivatization. Collectively, these efforts display the power of solid-phase synthesis and automation to rapidly access structurally diverse, pharmaceutically relevant scaffolds to streamline the transition from hit discovery to lead optimization.

4.4: Works Cited

(1) Plowright, A. T.; Johnstone, C.; Kihlberg, J.; Pettersson, J.; Robb, G.; Thompson, R. A. Hypothesis Driven Drug Design: Improving Quality and Effectiveness of the Design-Make-Test-Analyse Cycle. *Drug Discov. Today* **2012**, *17* (1), 56–62. https://doi.org/https://doi.org/10.1016/j.drudis.2011.09.012.

(2) Krska, S. W.; DiRocco, D. A.; Dreher, S. D.; Shevlin, M. The Evolution of Chemical High-Throughput Experimentation To Address Challenging Problems in Pharmaceutical Synthesis. *Acc. Chem. Res.* **2017**, *50* (12), 2976–2985. https://doi.org/10.1021/acs.accounts.7b00428.

(3) Biyani, S. A.; Moriuchi, Y. W.; Thompson, D. H. Advancement in Organic Synthesis Through High Throughput Experimentation. *Chemistry–Methods* **2021**, *1* (7), 323–339. https://doi.org/https://doi.org/10.1002/cmtd.202100023.

(4) Clark, M. A.; Acharya, R. A.; Arico-Muendel, C. C.; Belyanskaya, S. L.; Benjamin, D. R.; Carlson, N. R.; Centrella, P. A.; Chiu, C. H.; Creaser, S. P.; Cuozzo, J. W.; Davie, C. P.; Ding, Y.; Franklin, G. J.; Franzen, K. D.; Gefter, M. L.; Hale, S. P.; Hansen, N. J. V.; Israel, D. I.; Jiang, J.; Kavarana, M. J.; Kelley, M. S.; Kollmann, C. S.; Li, F.; Lind, K.; Mataruse, S.; Medeiros, P. F.; Messer, J. A.; Myers, P.; O'Keefe, H.; Oliff, M. C.; Rise, C. E.; Satz, A. L.; Skinner, S. R.; Svendsen, J. L.; Tang, L.; Van Vloten, K.; Wagner, R. W.; Yao, G.; Zhao, B.; Morgan, B. A. Design, Synthesis and Selection of DNA-Encoded Small-Molecule Libraries. *Nat. Chem. Biol.* **2009**, *5* (9), 647–654. https://doi.org/10.1038/nchembio.211.

(5) Satz, A. L.; Brunschweiger, A.; Flanagan, M. E.; Gloger, A.; Hansen, N. J. V.; Kuai, L.;

Kunig, V. B. K.; Lu, X.; Madsen, D.; Marcaurelle, L. A.; Mulrooney, C.; O'Donovan, G.; Sakata, S.; Scheuermann, J. DNA-Encoded Chemical Libraries. *Nat. Rev. Methods Prim.* **2022**, *2* (1). https://doi.org/10.1038/s43586-021-00084-5.

(6) Fitzgerald, P. R.; Paegel, B. M. DNA-Encoded Chemistry: Drug Discovery from a Few Good Reactions. *Chem. Rev.* **2021**, *121* (12), 7155–7177. https://doi.org/10.1021/acs.chemrev.0c00789.

(7) Sarvary, I.; Vestergaard, M.; Moretti, L.; Andersson, J.; Peiró Cadahía, J.; Cowland, S.; Flagstad, T.; Franch, T.; Gouliaev, A.; Husemoen, G.; Jacso, T.; Kronborg, T.; Kuropatnicka, A.; Nadali, A.; Madsen, M.; Nielsen, S.; Pii, D.; Ryborg, S.; Soede, C.; Allen, J. R.; Bourbeau, M.; Li, K.; Liu, Q.; Lo, M. C.; Madoux, F.; Mardirossian, N.; Moriguchi, J.; Ngo, R.; Peng, C. C.; Pettus, L.; Tamayo, N.; Wang, P.; Kapoor, R.; Belmontes, B.; Caenepeel, S.; Hughes, P.; Liu, S.; Slemmons, K. K.; Yang, Y.; Xie, F.; Ghimire-Rijal, S.; Mukund, S.; Glad, S. From DNA-Encoded Library Screening to AM-9747: An MTA-Cooperative PRMT5 Inhibitor with Potent Oral In Vivo Efficacy. *J. Med. Chem.* **2025**, *68* (6), 6534–6557. https://doi.org/10.1021/acs.jmedchem.4c03101.

(8) Merrifield, R. B. Solid Phase Peptide Synthesis. I. The Synthesis of a Tetrapeptide. *J. Am. Chem. Soc.* **1963**, *85* (14), 2149–2154. https://doi.org/10.1021/ja00897a025.

(9) Wang, G.; Tan, Y.; Zou, H.; Sui, X.; Wang, Z.; Satz, A. L.; Kuai, L.; Su, W.; Zhang, Q. DNA-Compatible Cyclization Reaction to Access 1,3,4-Oxadiazoles and 1,2,4-Triazoles. *Org. Lett.* **2024**, *26* (7), 1353–1357. https://doi.org/10.1021/acs.orglett.3c04240.

(10) Haider, S.; Alam, M. S.; Hamid, H. 1,3,4-Thiadiazoles: A Potent Multi Targeted Pharmacological Scaffold. *Eur. J. Med. Chem.* **2015**, *92*, 156–177.

https://doi.org/https://doi.org/10.1016/j.ejmech.2014.12.035.

Appendix I: Supporting Information for Chapter 2

Rapid spectrophotometric detection for optimized production of landomycins and characterization of their therapeutic potential.

Todd C. Chappell[1], Kathleen G. Maiello[2], Allison J. Tierney[2], Karin Yanagi[1], Jessica A. Lee[1], Kyongbum Lee[1], Charles R. Mace[2], Clay S. Bennett[2], and Nikhil U. Nair[1,*]

[1] Department of Chemical & Biological Engineering, Tufts University, Medford, MA

[2] Department of Chemistry, Tufts University, Medford, MA

S2.1: Materials and Methods

Microbial MIC calculation

The MIC for each compound that exhibited complete inhibition was calculated by plotting the log of the concentration versus the OD_{600} normalized to control condition, and then performing nonlinear regression (curve fit) in GraphPad Prism 9.5.0 using the equations[51]

$$\text{Eq 1: } \mathrm{M} = \mathrm{logMIC} - \frac{1}{\mathrm{B}}$$

$$\text{Eq 2: } Y = \mathrm{A} + \mathrm{C} \times e^{(-e^{(\mathrm{B}(\mathrm{X}-\mathrm{M}))})}$$

Where M is the log concentration of the inflexion point, logMIC is the log value of the MIC, B is the slope, A is the lower asymptote of y (approx. 0), and C is the distance between the lower and upper asymptote (approx. 1). The rules for the initial values for the variables were: logMIC was set to the value of X at YMID, B was selected as the initial value to be fit, A was set to the YMIN (ideally ~0), and C was set to YMAX-YMIN (the range). For negative OD values, OD were changed to 0. For compounds where complete growth inhibition was not reached, the MIC was determined to be greater than the maximum value tested. For compounds where no growth was visible even at the lowest concentrations, MIC was determined to be less than the minimum value tested.

LC-MS

Culture extracts were analyzed for landomycins using targeted LC-MS experiments on a quadrupole-time of flight instrument (AB Sciex, TripleTOF 5600+). Chromatographic separation was performed on a C18 column (Synergi 4 µm Hydro-RP 80 Å, 250 x 2 mm, Phenomenex) as gradient indicated at Table S5. Solvent A was 0.1% formic acid in water (v/v). Solvent B was 0.1%

formic acid in methanol (v/v). Injection volume was 10 μL, and the oven temperature was set to 15℃. The flow rate was kept constant at 0.2ml/min. Product Ion scan experiments were set for each compound of interest as Table S6. Areas under curve (AUC) were interpolated using Skyline (22.2.0.255) and normalized with total ion currents (TIC). Each compound's corresponding product ions used for quantification and retention times were also included in Table S6.

S2.2: Figures

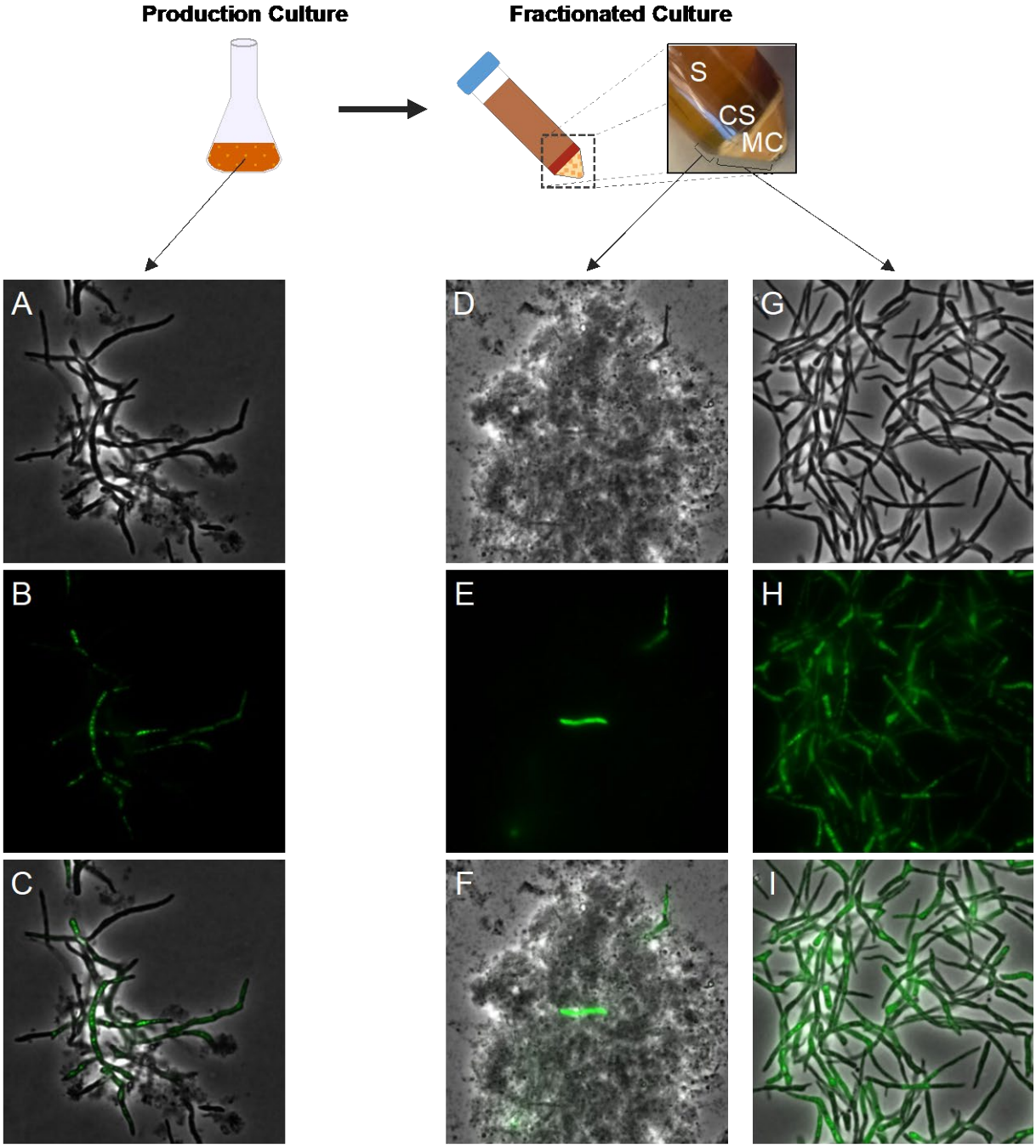

Figure S1: Morphology of production cultures, culture solids, and mycelia/cell fractions. Phase contrast (A,D,G) fluorescence (B,E,H), and overlay (C, F, I) microscopy images of production cultures of Sc92a (A-C) and fractionated Culture solids (CS; D-F) and mycelia/cells (MC; G-I). Samples were stained with SYBRSafe DNA stain prior to imaging to facilitate identification of intact cells and were imaged at 100x magnification.

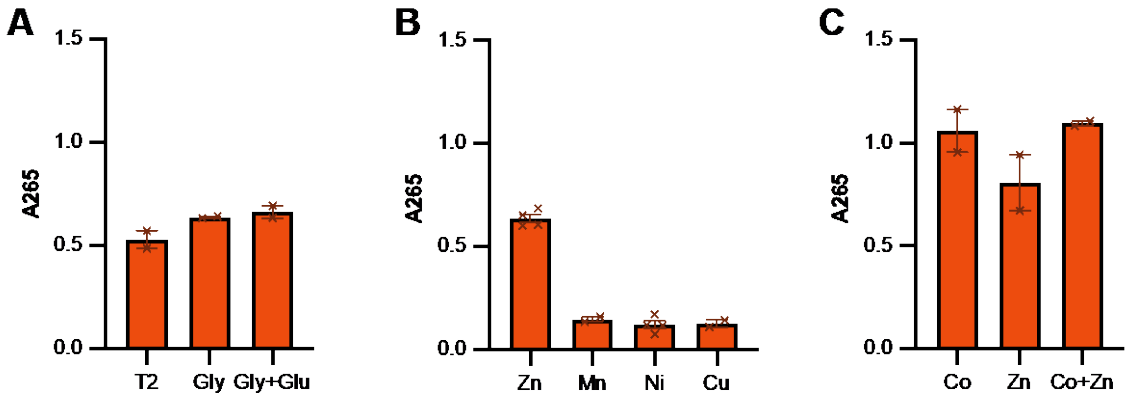

Figure S2: Relative landomycin production in additional production medium compositions. A) Landomycin production in SG with A) Trace 2 metals (T2), 2% glycerol (Gly) or 1% glycerol and 1% glucose (Gly+Glu); B) 30 µM Zn, Mn, Ni, or Cu; C) Trace with 30 µM Co, 20 Zn, or 30 µM Co + 20 µM Zn.

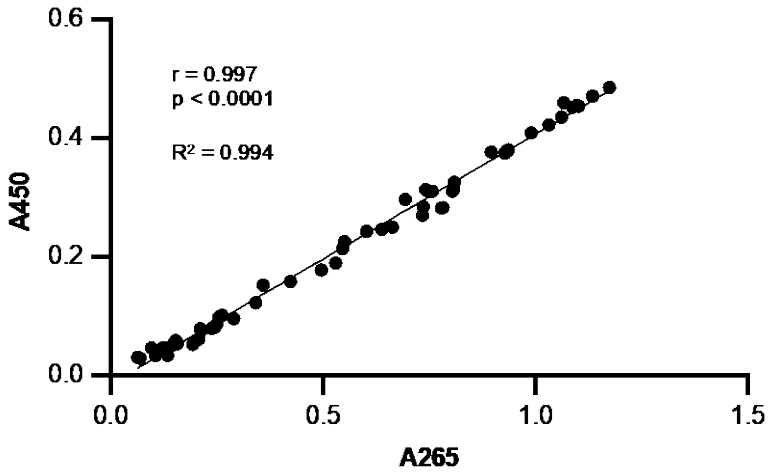

Figure S3: Correlational Analysis of Extract A265 and A450. Extract absorbance at 265 nm plotted vs. extract absorbance at 450 nm. Pearson correlation coefficient is 0.997 ($p<0.0001$), indicating a strong correlation between absorbance measurements at these wavelengths.

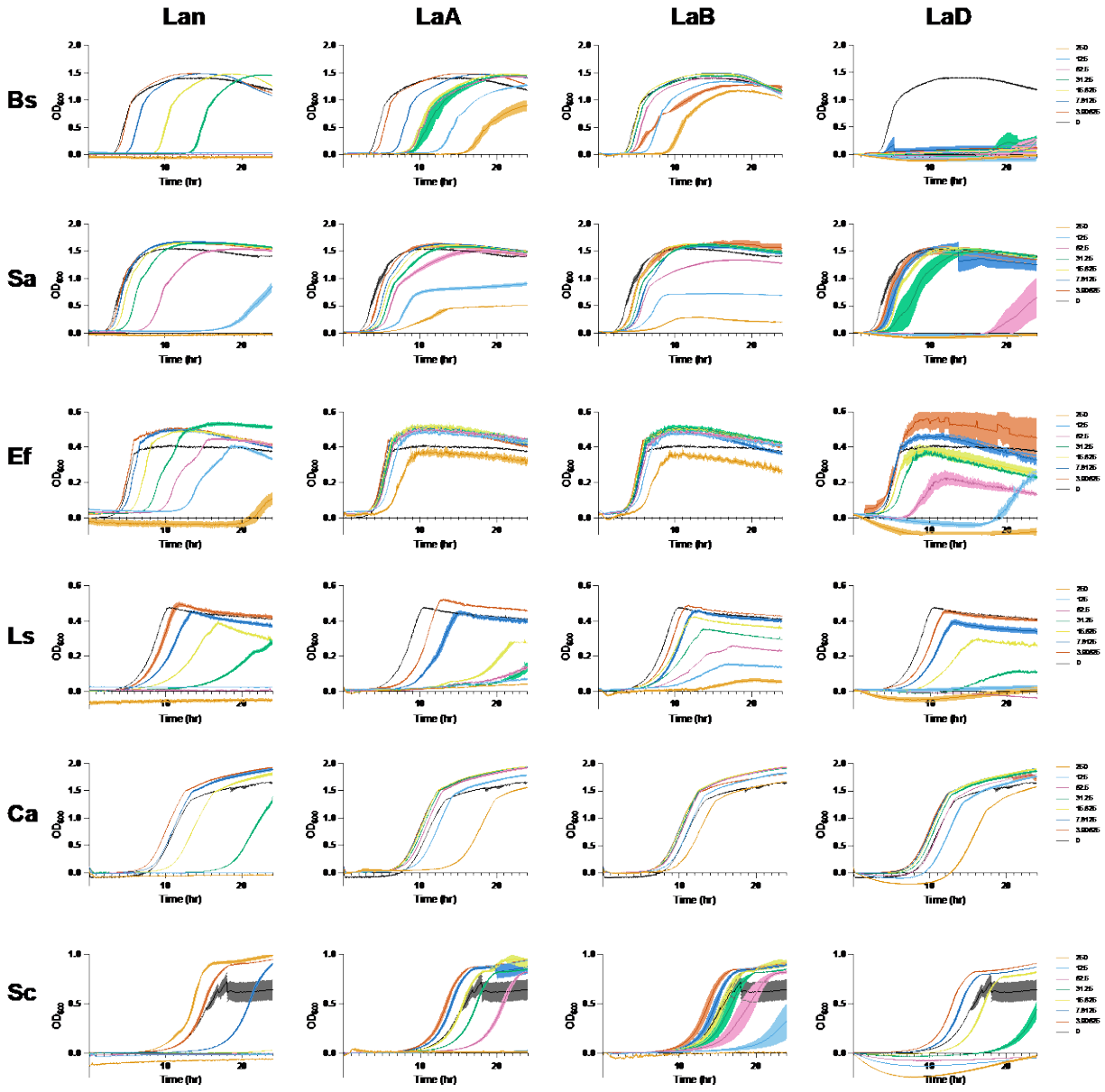

Figure S4: Growth curves used for MIC determination. Growth curves of *B. subtilis* (Bs), *S. aureus* (Sa), *E. faecium* (Ef), *L. seeligeri* (Ls), *C. albicans* (Ca), and *S. cerevisiae* (Sc) in the presence of different concentrations of landomycinone (Lan), landomycin A (LaA), landomycin B (LaB), and landomycin D (LaD).

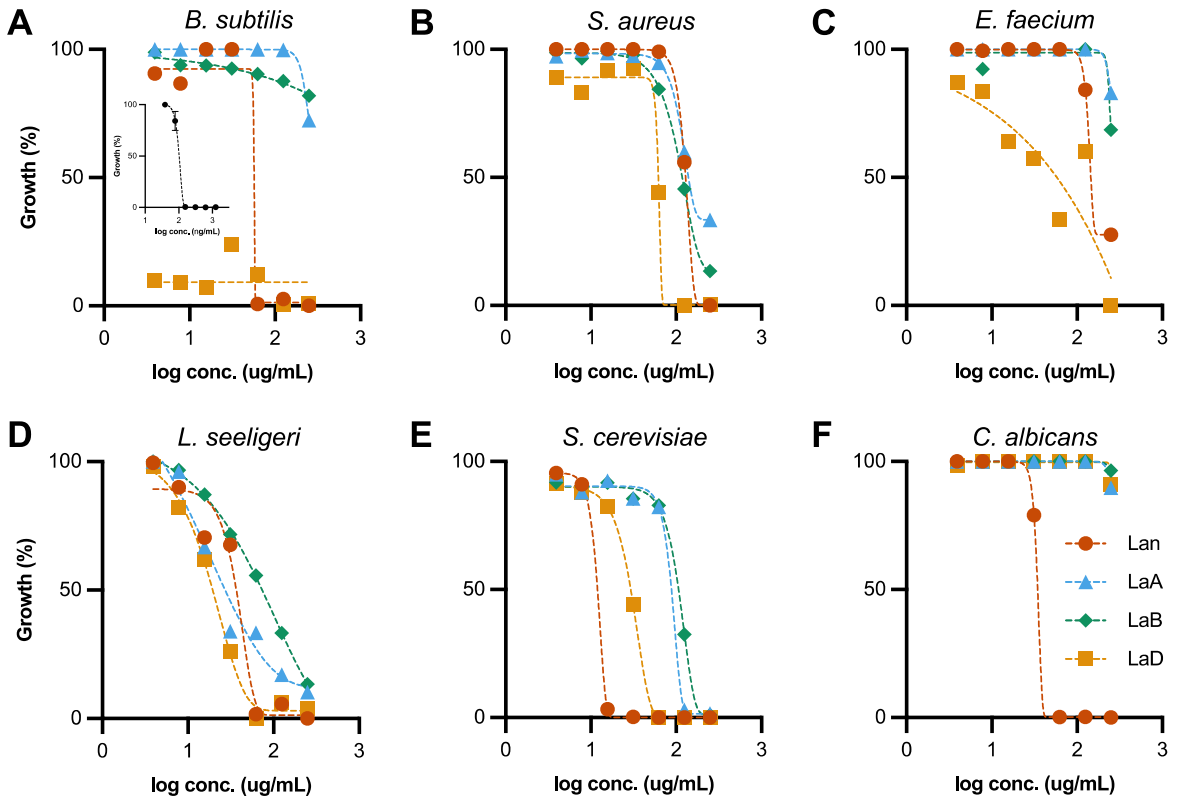

Figure S5: Minimum Inhibitory Concentration of Landomycins. Growth inhibition plots of landomyninone (Lan; orange circles), landomycin A (LaA; blue triangles), landomycin B (LaB; green diamonds), and landomycin D (LaD; yellow squares) calculated at 24 hr for A) *B. subtilis*, B) *S. aureus*, C) *E. faecium*, D) *L. seeligeri*, E) *S. cerevisiae*, and F) *C. albicans*. Inset in A shows erythromycin MIC control for *B. subtilis* (MIC = 133 ng/mL). Non-linear regression was performed to fit curves to growth inhibition data (color matched to symbol color) and calculate MIC values (Fig. 4B).

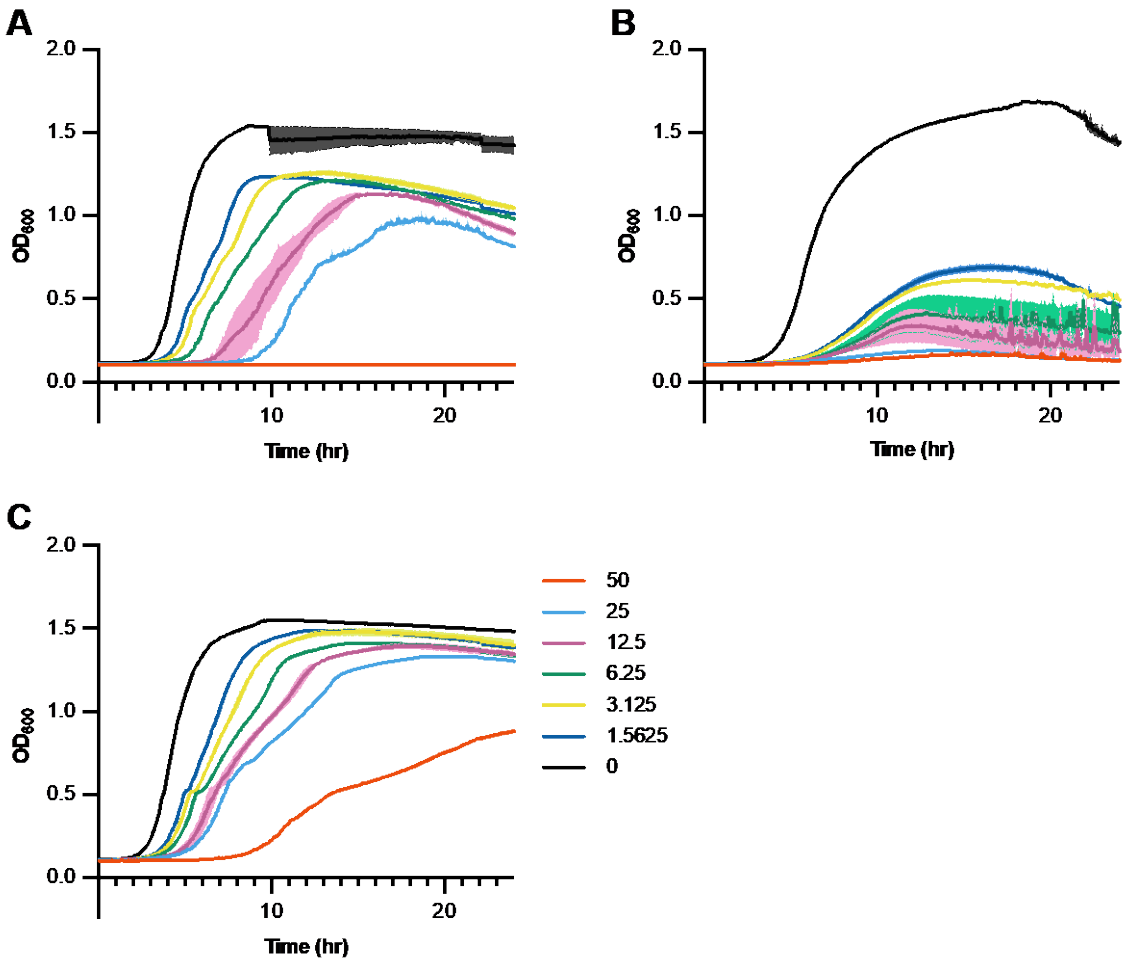

Figure S6: Gram-negative EDTA growth inhibition. Growth curves of A) *E. coli*, B) *P. aeruginosa*, and C) *S. typhimurium* grown in BHI containing different concentrations of EDTA (0-50 mM).

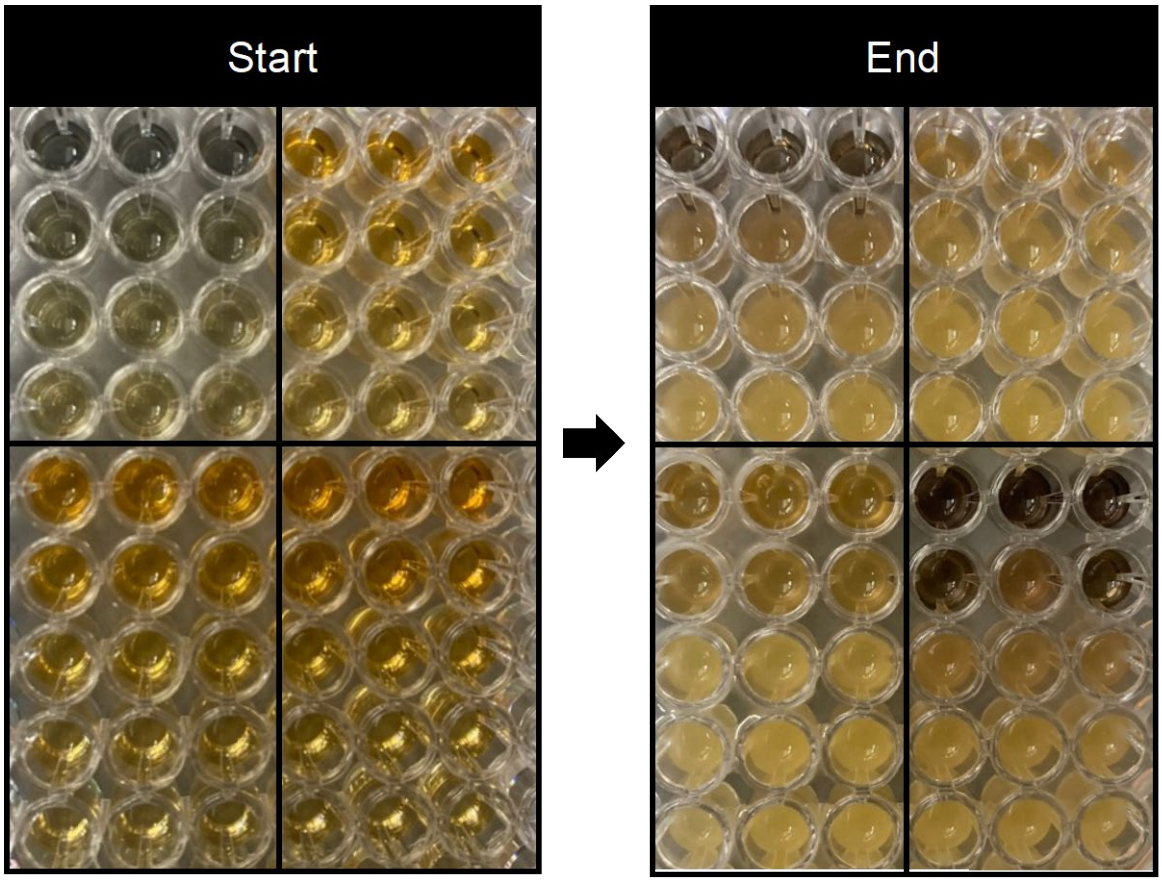

layout	
Lan	LaA
LaB	LaD

Figure S7: Changing color of media containing landomycins. Landomycins changed color during incubation at 37 ºC, shaking, regardless of growth of microbes. The sample layout is depicted to indicate location of Lan, LaA, LaB and LaD containing media. Biological triplicates are shown in adjacent columns and each row going down is a 2-fold dilution of the target compound in growth media.

S2.3: Tables

Table S1: Strains used in this study.

Strain	Genotype/Use/Origin	Source/Origin
Streptomyces cyanogenus 136 +pOOB92a (Sc92a)	*Streptomyces cyanogenus* 136 with plasmid pOOB92a integrated into the genome.	Dr. Bohdan Ostash, Lviv University
Pseudomonas aeruginosa	Strain PA14. Burn wound isolate.	Dr. Roberto Kolter, HMS
Staphylococcus aureus	Strain UAMS-1. Osteomyelitis isolate.	Dr. Abraham L. Sonenshein, TUSM
Escherichia coli Nissle 1917	Probiotic strain. Human fecal isolate.	iGEM team, Tufts University
Salmonella enterica subsp. *enterica* serovar Typhimurium	Strain SL1344. Auxotrophic mutant of S2337 (also known as 4/74 and S2337/65), an isolate from a calf with salmonellosis.	Dr. Dayong Wu, Tufts U.
Lactococcus cremoris	Subsp. c*remoris, s*train MG1363.	Dr. Jan Peter van Pijkeren, UW
Enterococcus faecium	Strain NRRL B-2354.	NRRL
Listeria seeligiri	Strain NRRL B-33019.	NRRL
Bacillus subtilis	Strain 168.	BGSC
Saccharomyces cereviseae	Strain BMA64-1A.	Euroscarf
Candida albicans	Strain SC5314.	Dr. Carol Kumamoto, TUSM

Table S2. Filter/Laser Combinations for Viability Dyes

Cell Stain	Annexin V-FITC	Ethidium homodimer I	Hoechst 33342
Ex/Em	485/535	528/617	350/461
Filter - Laser	Green – B	Red – B	Blue – V
Emission Filter	512/18	695/50	450/45

Table S3. Compensation Control Values to Remove Spectral Overlap

	Compensation Value			
Channel of Interest	**GRN-B**	**RED-B**	**BLU-V**	**YEL-B**
GRN-B	--	--	5.0	--
RED-B	9.5	--	--	11.5
BLU-V	--	--	--	--
YEL-B	--	45.7	--	--

"--" denotes no compensation needed

Table S4. Raw viable, apoptotic, and necrotic A549 cell populations under challenge conditions

Compound	[Compound] (μM)	Average Viable (%)	Viable SEM	Average Early Apoptotic (%)	Early Apoptotic SEM	Average Late Apoptotic (%)	Late Apoptotic SEM	Average Necrotic (%)	Necrotic SEM
DOX	0	89.9	0.8	2.2	0.2	4.6	0.6	3.3	0.2
	0.5	68.1	1.6	3.9	0.3	12.3	1.4	15.7	0.5
	1	50.1	3.0	5.0	0.8	16.1	1.6	28.7	1.1
	5	3.9	0.7	0.3	0.1	25.3	2.1	70.4	1.5
	10	8.5	5.1	0.5	0.1	26.9	4.5	64.1	9.4
	25	6.2	2.4	0.4	0.1	18.8	1.3	74.5	3.3
	50	10.8	7.0	0.6	0.4	17.4	5.6	71.2	12.9
	100	5.2	0.8	0.0	0.0	20.6	4.9	74.2	21.4
LaA	0	92.8	0.7	1.1	0.2	3.7	0.3	2.3	0.3
	0.5	91.0	0.3	1.4	0.2	4.7	0.3	2.9	0.1
	1	88.9	1.1	1.8	0.3	6.5	0.4	2.7	0.6
	5	39.3	5.3	2.8	0.5	41.5	3.5	16.5	1.8
	10	1.9	0.4	0.5	0.1	80.0	1.6	17.6	1.6
	25	1.4	0.8	1.0	0.5	95.9	0.8	1.7	0.6
	50	0.0	0.0	0.6	0.3	98.2	0.5	1.2	0.3
	100	0.5	0.2	1.2	0.2	97.0	0.8	1.4	0.6
LaB	0	82.3	4.7	13.7	3.5	3.0	0.9	1.0	0.4
	0.5	78.7	3.9	16.2	2.8	4.1	1.1	1.0	0.2
	1	73.4	2.2	20.9	1.5	4.3	1.0	1.3	0.3
	5	87.0	1.8	10.0	1.4	2.0	0.3	1.0	0.2
	10	75.6	5.1	14.1	3.4	8.9	1.4	1.4	0.3
	25	5.6	0.8	31.9	4.1	59.9	3.3	2.7	0.7
	50	2.1	0.5	90.1	2.4	5.5	0.9	2.3	0.9
	100	0.9	0.2	82.1	2.7	16.0	2.7	0.9	0.2
LaD	0	86.3	0.9	9.1	0.4	3.0	0.2	1.6	0.3
	0.5	88.0	1.4	6.2	0.3	4.6	0.9	1.2	0.2
	1	83.2	3.1	9.6	1.5	5.0	1.3	2.1	0.4
	5	83.3	1.5	10.0	0.9	4.9	0.6	1.8	0.2
	10	84.5	3.0	8.2	2.0	5.5	1.0	1.8	0.1
	25	77.9	5.7	12.7	2.8	7.6	2.6	1.7	0.4
	50	65.6	2.4	16.9	1.5	15.0	1.0	2.6	0.3
	100	1.8	0.3	46.5	1.9	43.9	2.7	7.8	1.3
Lan	0	88.7	2.0	5.8	0.7	3.9	1.2	1.6	0.2
	0.5	86.0	2.8	6.6	0.8	5.6	1.8	1.7	0.2
	1	84.4	4.1	8.4	2.3	5.1	1.3	2.0	0.6
	5	83.2	0.5	7.9	0.4	6.9	0.6	2.0	0.1
	10	84.6	0.8	8.3	0.5	5.0	0.4	2.2	0.1
	25	68.7	5.7	13.7	1.9	15.1	3.7	2.6	0.3
	50	46.0	4.5	15.4	0.9	34.9	3.1	3.8	0.6
	100	4.3	1.1	35.2	1.2	54.1	1.2	6.4	1.2
A-Lan	0	86.0	0.9	9.7	1.0	3.2	0.2	1.1	0.2
	0.5	89.7	1.1	6.2	1.1	3.0	0.5	1.1	0.2
	1	85.3	0.9	8.9	1.2	4.4	0.4	1.4	0.1
	5	86.2	2.1	6.8	0.9	5.0	1.4	1.9	0.2
	10	83.9	2.8	9.0	1.9	5.4	1.0	1.7	0.1
	25	82.3	3.2	10.6	1.9	5.4	1.5	1.7	0.3
	50	77.1	2.1	11.8	1.2	8.6	1.2	2.5	0.5
	100	73.4	6.3	11.7	1.4	12.3	4.8	2.5	0.3

Table S5: LC-MS Gradient method for landomycins.

Time (min)	Flow Rate (mL/min)	% Solvent A	% Solvent B
0	0.2	97	3
8	0.2	97	3
38	0.2	5	95
45	0.2	5	95
47	0.2	97	3
65	0.2	97	3

Table S6: MS and Quantification parameters for landomycins.

Landomycins	Polarity	Declustering Potential	Collision Energy	Retention Time	Precursor(m/z)	Product (m/z)
Landomycinone	Negative	65	35	42.54	337.07	318.05
Landomycin A	Negative	30	70	42.97	1085.46	925.41
Landomycin B	Negative	30	60	42.05	971.39	811.34
Landomycin D	Negative	30	40	40.9	597.20	437.15

S2.4: Structure Characterization

Landomycin A

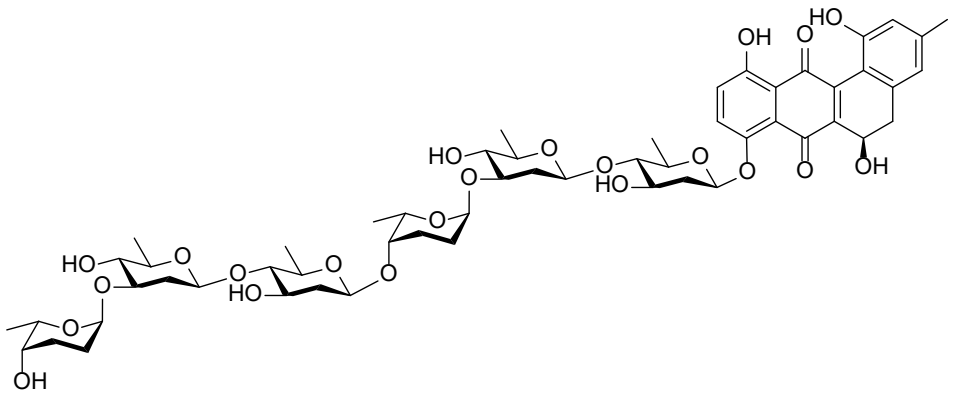

Chemical Formula: $C_{55}H_{74}O_{22}$

^{1}H NMR (500 MHz, $CDCl_3$) δ 12.35 (s, 1H), 8.87 (s, 1H), 7.55 (d, *J* = 9.4 Hz, 1H), 7.28 (s, 1H), 6.80 (s, 1H), 6.76 (s, 1H), 5.08 (dd, *J* = 8.9, 3.0 Hz, 2H), 4.96 (s, 2H), 4.70 (s, 1H), 4.62 (s, 1H), 4.56 – 4.43 (m, 4H), 4.34 (s, 1H), 4.18 – 4.03 (m, 2H), 3.72 (m, 1H), 3.65 (s, 1H), 3.60 (dq, *J* = 13.0, 6.2 Hz, 1H), 3.56 – 3.47 (m, 3H), 3.39 (td, *J* = 8.0, 5.3 Hz, 3H), 3.29 (dt, *J* = 12.4, 6.2 Hz, 1H), 3.15 – 3.02 (m, 4H), 2.98 (t, *J* = 8.8 Hz, 1H), 2.90 (dd, *J* = 15.8, 4.5 Hz, 1H), 2.80 (d, *J* = 4.4 Hz, 1H), 2.73 (m, 1H), 2.32 (m, 4H), 2.28 – 2.19 (m, 2H), 2.14 (m, 1H), 2.07 – 1.87 (m, 5H), 1.77 (d, *J* = 11.2 Hz, 1H), 1.73 – 1.61 (m, 4H), 1.39 (dd, *J* = 8.0, 6.1 Hz, 6H), 1.27 (dd, *J* = 16.5, 6.2 Hz, 6H), 1.22 (dd, *J* = 8.6, 6.5 Hz, 6H).

^{13}C NMR (126 MHz, $CDCl_3$) δ 192.74, 182.95, 159.75, 155.14, 150.71, 146.93, 143.71, 138.76, 136.69, 132.82, 126.75, 123.71, 120.14, 119.25, 114.89, 113.26, 101.48, 100.90, 100.86, 99.69, 97.79, 97.50, 88.52, 87.87, 80.56, 80.37, 75.77, 75.26, 75.23, 72.35, 72.26, 70.86, 70.34, 69.64, 69.24, 67.72, 67.09, 62.38, 38.27, 37.62, 37.13, 37.02, 36.29, 25.48, 25.07, 24.46, 24.09, 21.19, 17.84, 17.82, 17.80, 17.01, 16.94.

ESI-MS: [M+Na]: 1109.45

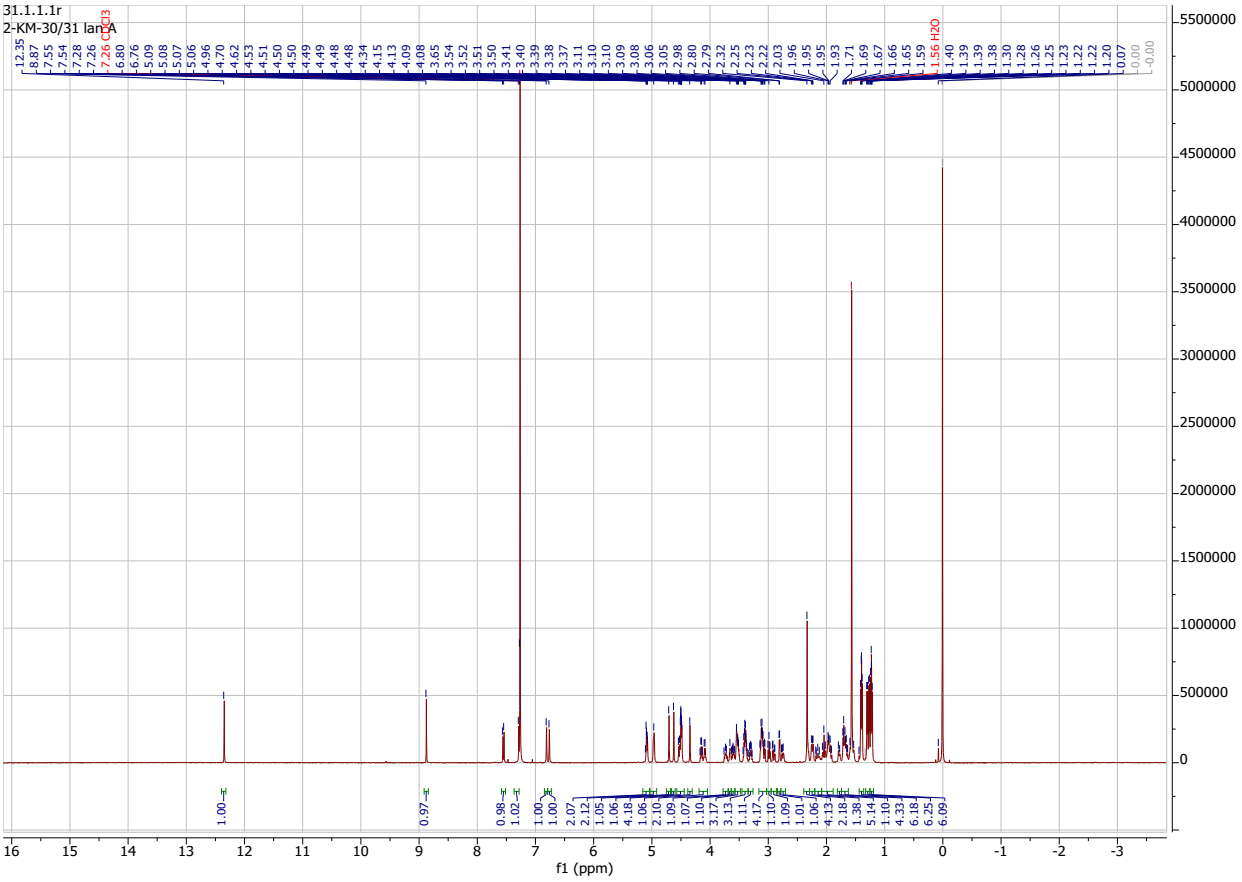
31.1.1.1r
2-KM-30/31 lan-A
f1 (ppm)

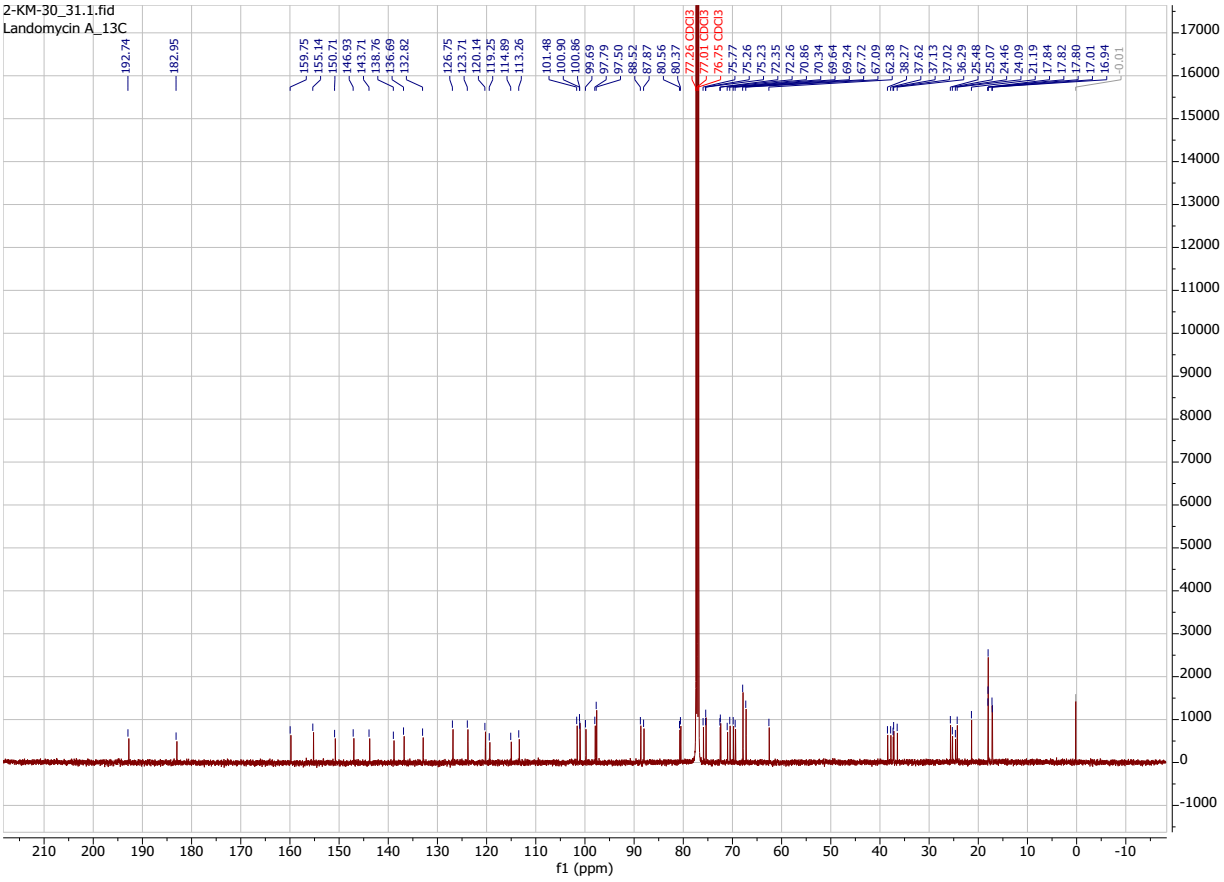
2-KM-30_31.1.fid
Landomycin A_13C
192.74
182.95
159.75
155.14
150.71
146.93
143.71
138.76
136.69
132.82
126.75
123.71
120.14
119.25
114.89
113.26
101.48
100.90
100.86
99.69
97.79
97.50
88.52
87.87
80.56
80.37
77.26 CDCl3
77.01 CDCl3
76.75 CDCl3
75.77
75.26
75.23
72.35
72.26
70.86
70.34
69.64
69.24
67.72
67.09
62.38
38.27
37.62
37.13
37.02
36.29
25.48
25.07
24.46
24.09
21.19
17.84
17.82
17.80
17.01
16.94
0.01
f1 (ppm)

Landomycin B

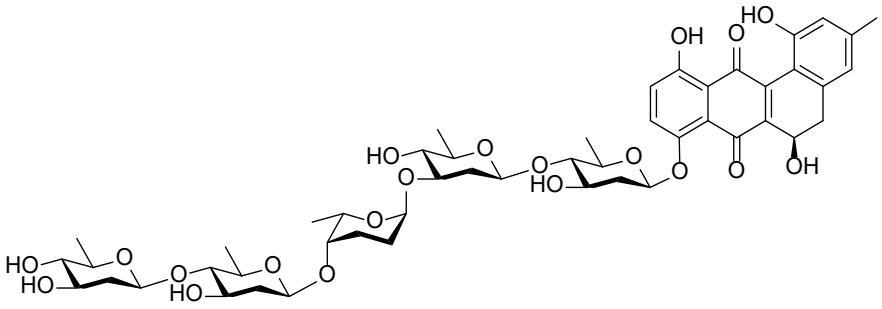

Chemical Formula: $C_{49}H_{64}O_{20}$

^{1}H NMR (500 MHz, DMSO) δ 11.69 (s, 1H), 9.63 (s, 1H), 7.51 (d, *J* = 9.4 Hz, 1H), 7.32 (d, *J* = 9.4 Hz, 1H), 6.63 (s, 1H), 6.57 (s, 1H), 5.25 (d, *J* = 9.4 Hz, 1H), 5.11 (d, *J* = 5.6 Hz, 1H), 5.04 (m, 2H), 4.96 (m, 2H), 4.88 (s, 1H), 4.77 – 4.63 (m, 2H), 4.59 (m, 2H), 4.52 (d, *J* = 9.6 Hz, 1H), 4.13 (q, *J* = 7.0 Hz, 1H), 3.66 – 3.41 (m, 5H), 3.37 (m, 2H), 3.26 (dt, *J* = 9.1, 6.2 Hz, 2H), 3.10 (t, *J* = 8.8 Hz, 1H), 2.94 (m, 2H), 2.86 (d, *J* = 16.1 Hz, 1H), 2.81 – 2.68 (m, 2H), 2.37 (dd, *J* = 38.5, 9.6 Hz, 2H), 2.25 (s, 3H), 2.15 – 2.00 (m, 2H), 1.93 (m, 1H), 1.88 – 1.72 (m, 2H), 1.66 (q, *J* = 11.3 Hz, 1H), 1.40 – 1.26 (m, 4H), 1.19 (dt, *J* = 21.7, 5.6 Hz, 12H), 1.00 (d, *J* = 6.4 Hz, 3H).

^{13}C NMR (126 MHz, DMSO) δ 188.33, 181.48, 155.80, 155.45, 149.76, 142.22, 141.60, 140.77, 138.74, 128.73, 125.14, 121.45, 119.74, 116.34, 115.91, 113.66, 101.24, 100.67, 100.39, 98.17, 92.55, 87.57, 86.90, 76.86, 76.11, 74.33, 73.60, 72.39, 70.62, 70.51, 70.14, 69.14, 68.78, 65.66, 57.81, 39.98, 39.21, 38.65, 37.08, 36.22, 24.47, 21.55, 18.36, 18.23, 18.19, 18.12, 17.41.

ESI-MS: [M+Na]: 995.36

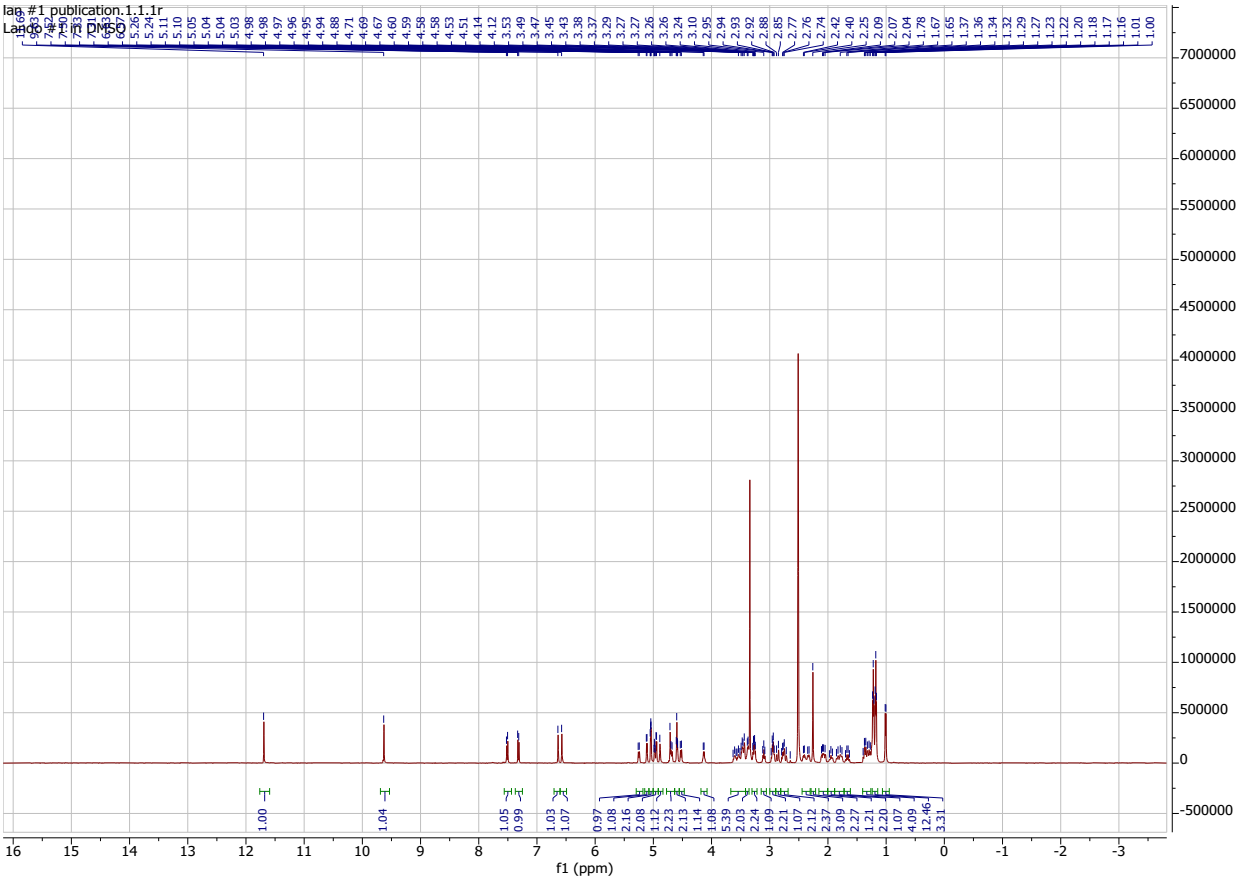
lab #1 publication.1.1.1r
Lando #1 in DMSO
f1 (ppm)

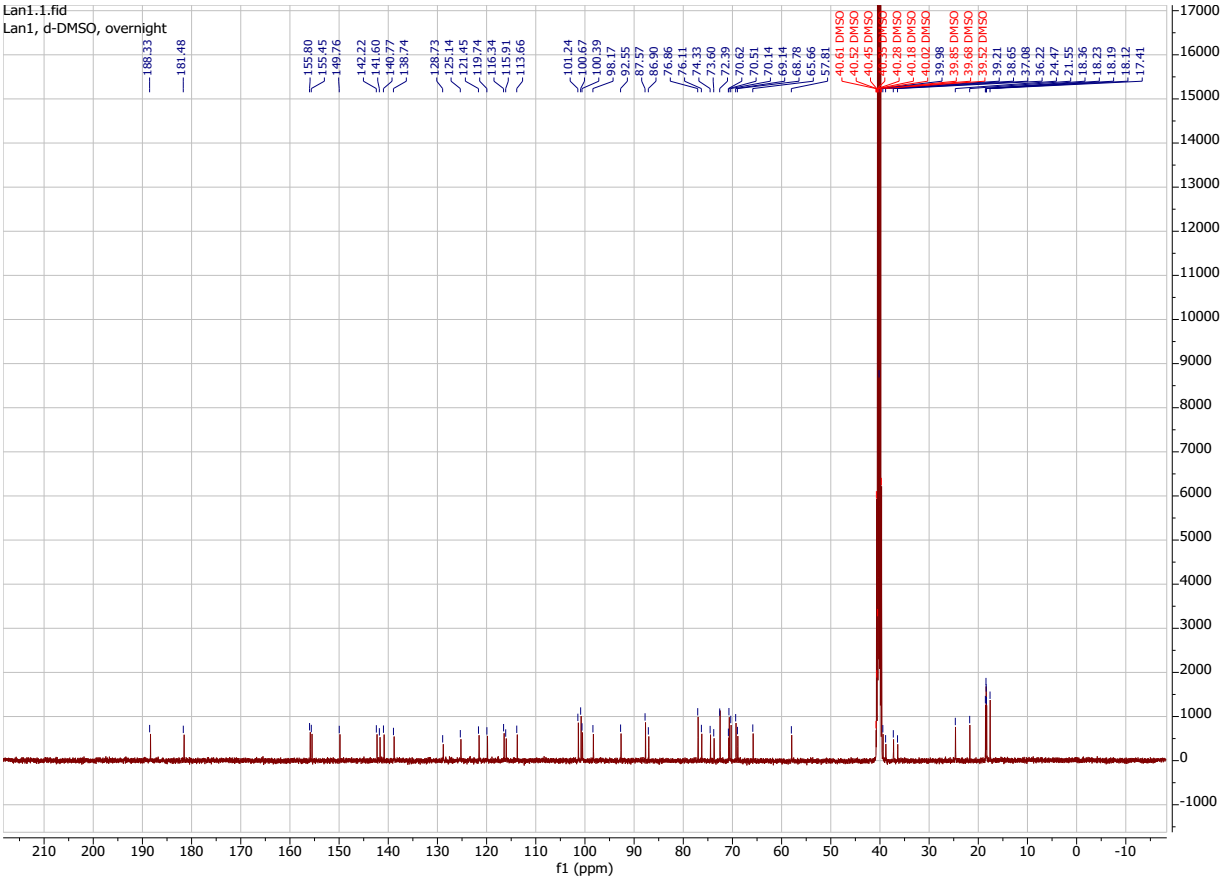
Lan1.1.fid
Lan1, d-DMSO, overnight
188.33
181.48
155.80
155.45
149.76
142.22
141.60
140.77
138.74
128.73
125.14
121.45
119.74
116.34
115.91
113.66
101.24
100.67
100.39
98.17
92.55
87.57
86.90
76.86
76.11
74.33
73.60
72.39
70.62
70.51
70.14
69.14
68.78
65.66
57.81
40.61 DMSO
40.52 DMSO
40.45 DMSO
40.28 DMSO
40.18 DMSO
40.02 DMSO
39.98
39.85 DMSO
39.68 DMSO
39.52 DMSO
39.21
38.65
37.08
36.22
24.47
21.55
18.36
18.23
18.19
18.12
17.41
f1 (ppm)

Landomycin D

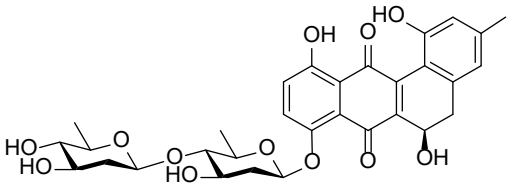

Chemical Formula: $C_{31}H_{34}O_{12}$

^{1}H NMR (500 MHz, DMSO) δ 11.69 (s, 1H), 9.63 (s, 1H), 7.51 (d, *J* = 9.4 Hz, 1H), 7.32 (d, *J* = 9.3 Hz, 1H), 6.64 (s, 1H), 6.57 (s, 1H), 5.35 – 5.17 (m, 1H), 5.10 – 4.88 (m, 4H), 4.71 (s, 1H), 4.63 (d, *J* = 9.6, 1H), 3.59 (m, 1H), 3.47 (dd, *J* = 9.1, 6.0 Hz, 1H), 3.25 (s, 1H), 3.07 (t, *J* = 8.9 Hz, 1H), 2.92 – 2.68 (m, 3H), 2.44 – 2.35 (m, 1H), 2.26 (s, 3H), 2.07 (dd, *J* = 13.3, 5.1 Hz, 1H), 1.66 (d, *J* = 11.5 Hz, 2H), 1.36 (m, 1H), 1.20 (d, *J* = 6.2 Hz, 6H)

ESI-MS: [M+Na]: 621.27

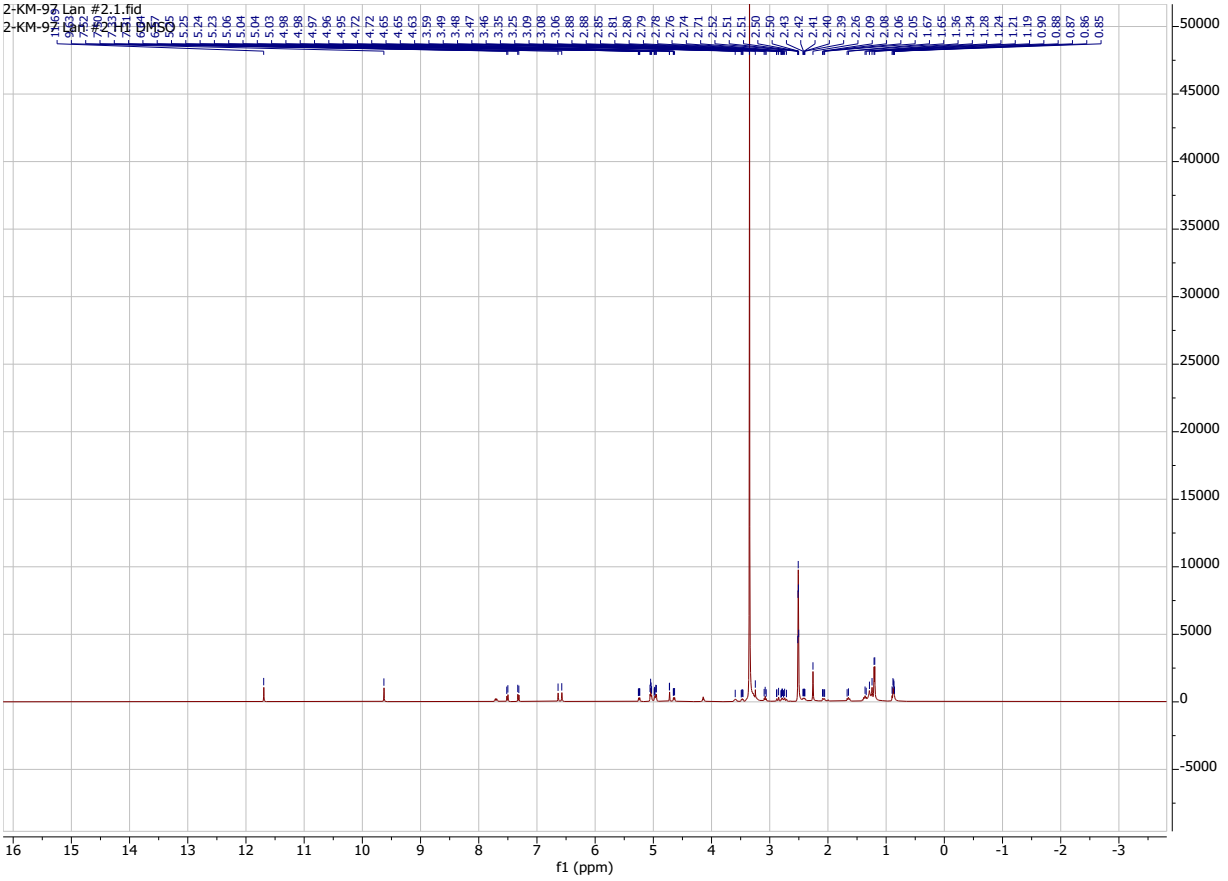

Landomycinone

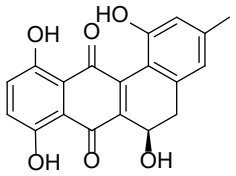

Chemical Formula: $C_{19}H_{14}O_6$

^{1}H NMR (500 MHz, $CDCl_3$) δ 12.90 (s, 1H), 12.80 (s, 1H), 9.04 (s, 1H), 7.42 – 7.31 (m, 2H), 6.85 (s, 1H), 6.80 (s, 1H), 5.26 (m, 1H), 3.14 (dd, *J* = 15.8, 4.8 Hz, 1H), 2.97 (dd, *J* = 15.6, 4.3 Hz, 1H), 2.67 (d, *J* = 5.4 Hz, 1H), 2.36 (s, 3H).

ESI-MS: [M+Na]: 360.19

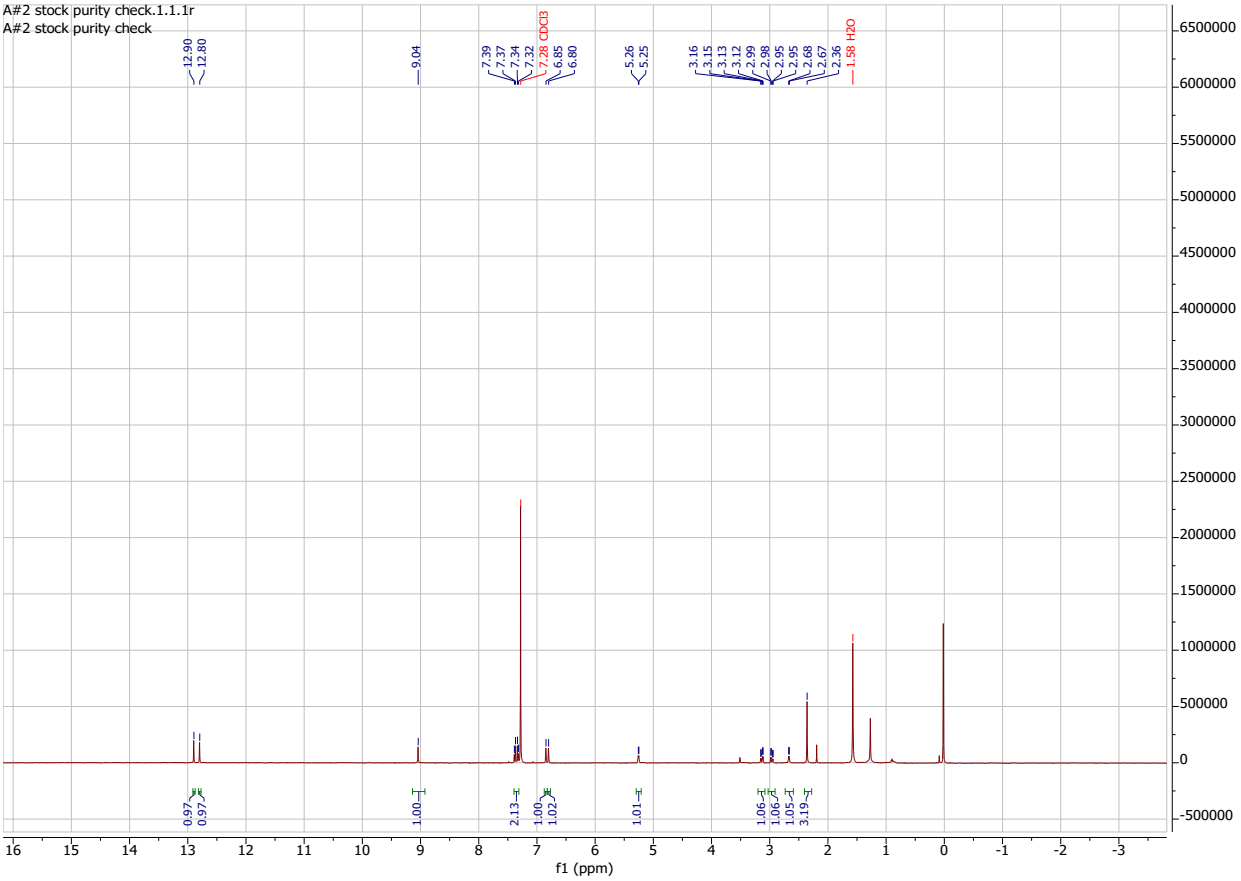

Anhydrolandomycinone

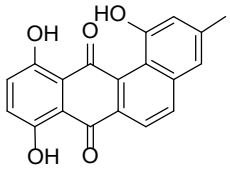

Chemical Formula: $C_{19}H_{12}O_5$

^{1}H NMR (500 MHz, $CDCl_3$) δ 13.04 (s, 1H), 12.55 (s, 1H), 11.15 (s, 1H), 8.39 (d, *J* = 8.6 Hz, 1H), 8.20 (d, *J* = 8.6 Hz, 1H), 7.44 – 7.34 (m, 2H), 7.33 (s, 1H), 7.22 (d, *J* = 1.9 Hz, 1H), 2.54 (s, 3H).

ESI-MS: [M+Na]: 342.01

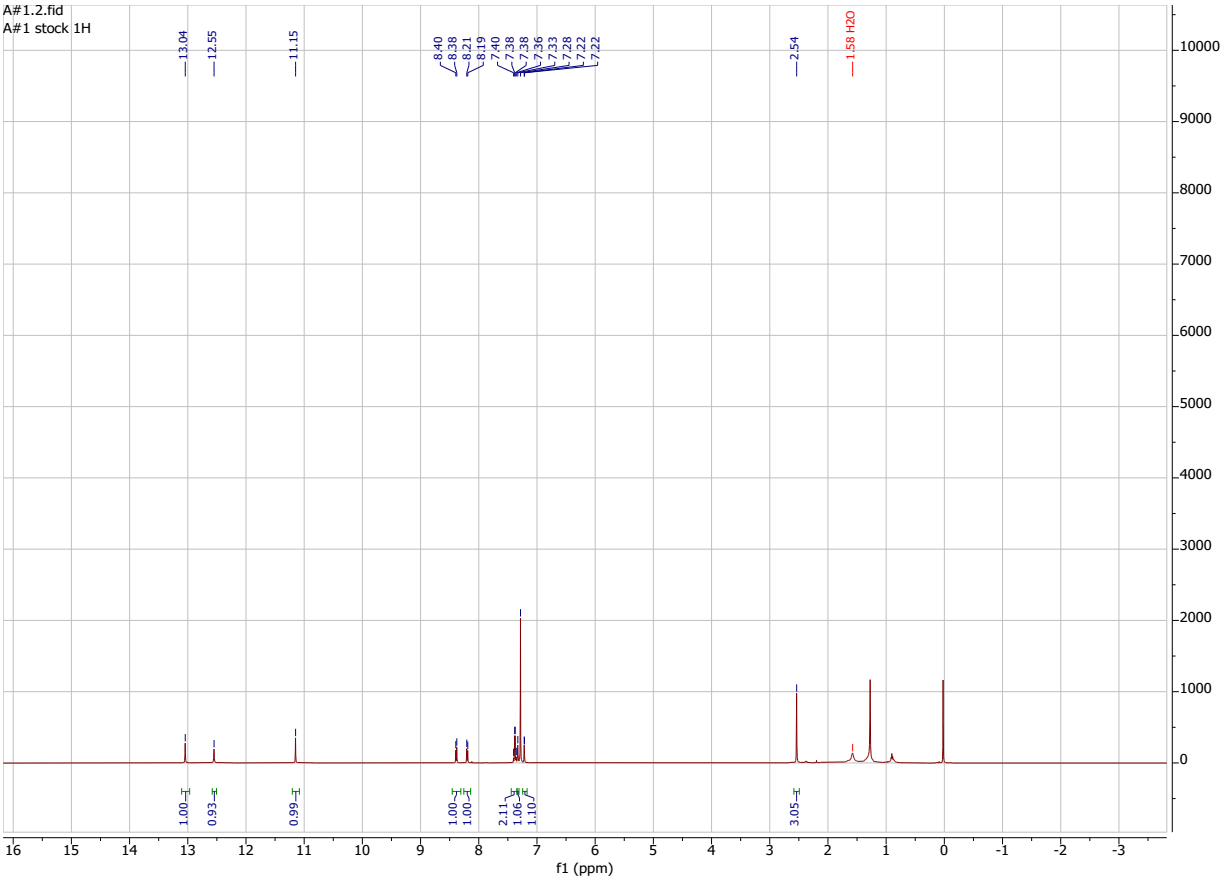

Compound structures were verified with previously reported data.[10,19,22,24,28]

References

(1) Lee, N.; et al. Mini review: Genome mining approaches for the identification of secondary metabolite biosynthetic gene clusters in *Streptomyces*. *Comput. Struct. Biotechnol. J.* **2020**, *18*, 1548–1556.

(2) Liu, R.; Yu, D.; Deng, Z.; Liu, T. Harnessing in vitro platforms for natural product research: in vitro driven rational engineering and mining (iDREAM). *Curr. Opin. Biotechnol.* **2021**, *69*, 1–9.

(3) Pham, J. V.; et al. A review of the microbial production of bioactive natural products and biologics. *Front. Microbiol.* **2019**, *10*, 1–27.

(4) Patridge, E.; Gareiss, P.; Kinch, M. S.; Hoyer, D. An analysis of FDA-approved drugs: Natural products and their derivatives. *Drug Discov. Today* **2016**, *21*, 204–207.

(5) Harvey, A. L.; Edrada-Ebel, R.; Quinn, R. J. The re-emergence of natural products for drug discovery in the genomics era. *Nat. Rev. Drug Discov.* **2015**, *14*, 111–129.

(6) Li, C. J.; Trost, B. M. Green chemistry for chemical synthesis. *Proc. Natl. Acad. Sci. U. S. A.* **2008**, *105*, 13197–13202.

(7) Chung, Y.-H.; et al. Comparative genomics reveals a remarkable biosynthetic potential of the *Streptomyces* phylogenetic lineage associated with rugose-ornamented spores. *mSystems* **2021**, *6*, 1–15.

(8) Belknap, K. C.; Park, C. J.; Barth, B. M.; Andam, C. P. Genome mining of biosynthetic and chemotherapeutic gene clusters in *Streptomyces* bacteria. *Sci. Rep.* **2020**, *10*, 1–9.

(9) Ward, A. C.; Allenby, N. E. Genome mining for the search and discovery of bioactive compounds: The *Streptomyces* paradigm. *FEMS Microbiol. Lett.* **2018**, *365*, 1–20.

(10) Henkel, T.; Rohr, J.; Beale, J. M.; Schwenen, L. Landomycins, new angucycline antibiotics from *Streptomyces* sp. I. Structural studies on landomycins A–D. *J. Antibiot. (Tokyo)* **1990**, *43*, 492–503.

(11) Terenzi, A.; et al. Landomycins as glutathione-depleting agents and natural fluorescent probes for cellular Michael adduct-dependent quinone metabolism. *Commun. Chem.* **2021**, *4*, 1–13.

(12) Crow, R. T.; et al. Landomycin A inhibits DNA synthesis and G1/S cell cycle progression. *Bioorg. Med. Chem. Lett.* **1999**, *9*, 1663–1666.

(13) Panchuk, R. R.; et al. Rapid generation of hydrogen peroxide contributes to the complex cell death induction by the angucycline antibiotic landomycin E. *Free Radic. Biol. Med.* **2017**, *106*, 134–147.

(14) Westrich, L.; et al. Cloning and characterization of a gene cluster from *Streptomyces cyanogenus* S136 probably involved in landomycin biosynthesis. *FEMS Microbiol. Lett.* **1999**, *170*, 381–387.

(15) Matselyukh, B. P.; Polishchuk, L. V.; Lukyanchuk, V. V.; Golembiovska, S. L.; Lavrenchuk, V. Y. Sequences of landomycin E and carotenoid biosynthetic gene clusters, and molecular structure of transcriptional regulator of *Streptomyces globisporus* 1912. *Mikrobiol. Z.* **2016**, *78*, 60–70.

(16) Feng, Z.; Kallifidas, D.; Brady, S. F. Functional analysis of environmental DNA-derived type II polyketide synthases reveals structurally diverse secondary metabolites. *Proc. Natl. Acad. Sci. U. S. A.* **2011**, *108*, 12629–12634.

(17) Peng, A.; et al. Angucycline glycosides from an intertidal sediments strain *Streptomyces* sp. and their cytotoxic activity against hepatoma carcinoma cells. *Mar. Drugs* **2018**, *16*.

(18) Kharel, M. K.; et al. Angucyclines: Biosynthesis, mode-of-action, new natural products, and synthesis. *Nat. Prod. Rep.* **2012**, *29*, 264–325.

(19) Weber, S.; Zolke, C.; Rohr, J.; Beale, J. M. Investigations of the biosynthesis and structural revision of landomycin A. *J. Org. Chem.* **1994**, *59*, 4211–4214.

(20) Hrab, P.; et al. Complete genome sequence of *Streptomyces cyanogenus* S136, producer of anticancer angucycline landomycin A. *3 Biotech* **2021**, *11*, 1–10.

(21) Bugaut, X.; Guinchard, X.; Roulland, E. Synthesis of the landomycinone skeleton. *J. Org. Chem.* **2010**, *75*, 8190–8198.

(22) Roush, W. R.; Neitz, R. J. Studies on the synthesis of landomycin A. Synthesis of the originally assigned structure of the aglycone, landomycinone, and revision of structure. *J. Org. Chem.* **2004**, *69*, 4906–4912.

(23) Guo, Y.; Sulikowski, G. A. Synthesis of the hexasaccharide fragment of landomycin A: Application of glycosyl tetrazoles and phosphites in the synthesis of a deoxyoligosaccharide. *J. Am. Chem. Soc.* **1998**, *120*, 1392–1397.

(24) Yang, X.; Fu, B.; Yu, B. Total synthesis of landomycin A, a potent antitumor angucycline antibiotic. *J. Am. Chem. Soc.* **2011**, *133*, 12433–12435.

(25) Yalamanchili, S.; Lloyd, D.; Bennett, C. S. Synthesis of the hexasaccharide fragment of landomycin A using a mild, reagent-controlled approach. *Org. Lett.* **2019**, *21*, 3674–3677.

(26) Roush, W. R.; Bennett, C. E. A highly stereoselective synthesis of the landomycin A hexasaccharide unit. *J. Am. Chem. Soc.* **2000**, *122*, 6124–6125.

(27) Yu, B.; Wang, P. Efficient synthesis of the hexasaccharide fragment of landomycin A using phenyl 2,3-O-thionocarbonyl-1-thioglycosides as 2-deoxy-β-glycoside precursors. *Org. Lett.* **2002**, *4*, 1919–1922.

(28) Yang, X.; Yu, B. Synthesis of landomycin D: Studies on the saccharide assembly. *Synthesis* **2016**, *48*, 1693–1699.

(29) Tanaka, H.; et al. Combinatorial synthesis of deoxyhexasaccharides related to the landomycin A sugar moiety, based on an orthogonal deprotection strategy. *Chem. Asian J.* **2010**, *5*, 1407–1424.

(30) Lee, J.; Kang, S.; Kim, J.; Moon, D.; Rhee, Y. H. A convergent synthetic strategy towards oligosaccharides containing 2,3,6-trideoxypyranoglycosides. *Angew. Chem. Int. Ed.* **2019**, *58*, 628–631.

(31) von Mulert, U.; Luzhetskyy, A.; Hofmann, C.; Mayer, A.; Bechthold, A. Expression of the landomycin biosynthetic gene cluster in a PKS mutant of *Streptomyces fradiae* is dependent on the coexpression of a putative transcriptional activator gene. *FEMS Microbiol. Lett.* **2004**, *230*, 91–97.

(32) Shaaban, K. A.; Stamatkin, C.; Damodaran, C.; Rohr, J. 11-Deoxylandomycinone and landomycins X–Z, new cytotoxic angucyclin(on)es from *Streptomyces cyanogenus* K62 mutant strain. *J. Antibiot. (Tokyo)* **2011**, *64*, 141–150.

(33) Luzhetskyy, A.; et al. Generation of novel landomycins M and O through targeted gene disruption. *ChemBioChem* **2005**, *6*, 675–678.

(34) Shaaban, K. A.; Srinivasan, S.; Kumar, R.; Damodaran, C.; Rohr, J. Landomycins P–W, cytotoxic angucyclines from *Streptomyces cyanogenus* S-136. *J. Nat. Prod.* **2011**, *74*, 2–11.

(35) Myronovskyi, M.; et al. Generation of new compounds through unbalanced transcription of landomycin A cluster. *Appl. Microbiol. Biotechnol.* **2016**, *100*, 9175–9186.

(36) Yushchuk, O.; et al. Heterologous AdpA transcription factors enhance landomycin production in *Streptomyces cyanogenus* S136 under a broad range of growth conditions. *Appl. Microbiol. Biotechnol.* **2018**, *102*, 8419–8428.

(37) Gessner, A.; et al. Changing biosynthetic profiles by expressing *bldA* in *Streptomyces* strains. *ChemBioChem* **2015**, *16*, 2244–2252.

(38) Lai, Y. H.; et al. Total synthesis of landomycins Q and R and related core structures for exploration of the cytotoxicity and antibacterial properties. *RSC Adv.* **2021**, *11*, 9426–9432.

(39) Matseliukh, B. P.; Konovalova, T. A.; Polishchuk, L. V.; Bambura, O. I. The sensitivity to landomycins A and E of streptomycetes, producers of polyketide antibiotics. *Mikrobiol. Z.* **1998**, *60*, 31–36.

(40) Yushchuk, O.; et al. Eliciting the silent lucensomycin biosynthetic pathway in *Streptomyces cyanogenus* S136 via manipulation of the global regulatory gene *adpA*. *Sci. Rep.* **2021**, *11*, 1–14.

(41) Brown, M. R. W.; Richards, R. M. E. Effect of ethylenediamine tetraacetate on the resistance of *Pseudomonas aeruginosa* to antibacterial agents. *Nature* **1965**, *207*, 1391–1393.

(42) Vervoort, N.; Goossens, K.; Baeten, M.; Chen, Q. Recent advances in analytical techniques for high-throughput experimentation. *Anal. Sci. Adv.* **2021**, *2*, 109–127.

(43) Dueñas, M. E.; et al. Advances in high-throughput mass spectrometry in drug discovery. *EMBO Mol. Med.* **2023**, *15*, 1–15.

(44) A.; K.; et al. Mechanisms underlying the anticancer activities of the angucycline landomycin E. *Biochem. Pharmacol.* **2007**, *74*, 1713–1726.

(45) Lehka, L. V.; Panchuk, R. R.; Berger, W.; Rohr, J.; Stoika, R. S. The role of reactive oxygen species in tumor cell apoptosis induced by landomycin A. *Ukr. Biochem. J.* **2015**, *87*, 72–82.

(46) Shoemaker, R. H. The NCI60 human tumour cell line anticancer drug screen. *Nat. Rev. Cancer* **2006**, *6*, 813–823.

(47) Shankavaram, U. T.; et al. CellMiner: A relational database and query tool for the NCI-60 cancer cell lines. *BMC Genomics* **2009**, *10*, 1–10.

(48) Reinhold, W. C.; et al. CellMiner: A web-based suite of genomic and pharmacologic tools to explore transcript and drug patterns in the NCI-60 cell line set. *Cancer Res.* **2012**, *72*, 3499–3511.

(49) Zhang, Y.; et al. Himalaquinones A–G, angucyclinone-derived metabolites produced by the Himalayan isolate *Streptomyces* sp. PU-MM59. *J. Nat. Prod.* **2021**, *84*, 1930–1940.

(50) Panchuk, R. R. Signaling pathways involved in apoptosis induced by novel angucycline antibiotic landomycin E in Jurkat T-leukemia cells. *Exp. Oncol.* **2011**, *27*, 124–131.

(51) Lambert, R. J. W.; Pearson, J. Susceptibility testing: Accurate and reproducible minimum inhibitory concentration (MIC) and non-inhibitory concentration (NIC) values. *J. Appl. Microbiol.* **2000**, *88*, 784–790.

Appendix II: Supporting Information for Chapter 3

S3.1: General Details and Experimental Protocols

Each reaction was run in a flame dried vessel under an inert argon atmosphere. All anhydrous solvents for reactions were dried using a commercial solvent purification system prior to reactions. Any silyl triflate used during synthesis was distilled via a short path distillation apparatus directly prior to use. Methanolic HCl was generated in situ using the proper equivalents of acetyl chloride and stirring it in methanol. All other solvents and chemicals were purchased at the highest quality and used as received. Flash column chromatography was performed on 230−400 mesh silica gel. Analytical and preparative thin layer chromatography was done on silica gel 60 F-254 plates. NMR spectra were recorded on a Bruker 500 MHz NMR spectrometer for ^{1}H NMR and 125 MHz for ^{13}C NMR. Chemical shifts are reported in ppm relative to TMS in deuterated solvent (C_6D_6 or $CDCl_3$) purchased from Cambridge Isotope Labs. For 1H NMR spectra, data are reported as follows: δ shift, multiplicity (s = singlet, m = multiplet, t = triplet, d = doublet, q = quartet, dd = doublet of doublets, td = triplet of doublets, dt = doublet of triplets, dq = doublet of quartets). Coupling constants are reported in Hertz. High-resolution mass spectra (HRMS) were obtained on Electrospray Ionization (ESI) on a Agilent QTOF instrument in positive mode.

S3.2 Two-step synthesis of tri-TIPS/TBS- landomycinone

To a flame dried flask charged with a stir bar and backfilled with argon was added landomycin A (215 mg, 0.2 mmol). Anhydrous solvents [DCM (4.5mL) and ACN (2.2 mL), 3:1, 0.03M] were added and the reaction flask was set to stir for 15 minutes on an ice bath to cool to 0°C. After the cooling period, 2,6-lutidine (0.37 mL, 3.2 mmol) was added to the reaction flask over 1 minute. After stirring for 25 minutes, freshly distilled TIPSOTf (0.65 mL, 2.4 mmol) was added to the

reaction flask dropwise over 4 minutes. Some more ice was added to the bath and the reaction was allowed to stir overnight (18 hrs). The reaction was quenched slowly using 4 mL of sat. sodium bicarbonate solution. The mixture was poured over DCM/H_2O and extracted three times. The organic layer was washed with a sat. sodium bicarbonate solution followed by a sat. brine solution. The organic layer was dried on sodium sulfate then rotovaped down and dried on high vacuum for an hour. The crude solution was dissolved in 15 mL of dry DCM (~0.013M). Then, 5 mL of 1M MeOH*HCl was added to the reaction flask to stir. Small aloquots of acid were added until the visible darkening of the solution to a bright/deep orange color. After that time, the reaction was quenched with a sat. sodium bicarbonate solution. The mixture was poured over DCM/H_2O and extracted three times. The organic layer was washed with a sat. sodium bicarbonate solution followed by a sat. brine solution. The organic layer was dried on sodium sulfate then rotovaped down. Using a normal phase medium injection column, the sample was loaded in 30% toluene/DCM and run onto a large silica column at 30% toluene/DCM for 16 minutes, then ramped up to 50% toluene/hexanes for 15 minutes. After concentrating down and drying on high vacuum, the tri-TIPS landomycinone product was isolated (48.4 mg, 30% yield) as an orangy red, sticky amorphous solid.

S3.3 One-pot Synthesis of tri-TIPS landomycinone

To a flame dried flask charged with a stir bar and backfilled with argon was added landomycin A (635 mg, 0.584 mmol). Anhydrous solvents [DCM (13mL) and ACN (6.5 mL), 3:1, 0.03M] were added and the reaction flask was set to stir for 15 minutes on an ice bath to cool to 0°C. After the cooling period, 2,6-lutidine (0.95 mL, 8.18 mmol) was added to the reaction flask over 2 minutes. After stirring for 25 minutes, freshly distilled TIPSOTf (2.4 mL, 8.94 mmol) was added to the reaction flask dropwise over 6 minutes. Some more ice was added to the bath and the reaction was

allowed to stir overnight (18 hrs). The reaction was quenched slowly using 12 mL of sat. sodium bicarbonate solution. The mixture was poured over DCM/H_2O and extracted three times. The organic layer was washed with a sat. sodium bicarbonate solution followed by a sat. brine solution. The organic layer was dried on sodium sulfate then rotovaped down and dried on high vacuum. For purification, the system used was an Automated flash column chromatography Smart Flash EPCLC W-Prep 2XY Dual Channel Automated Flash Chromatography System provided by Yamazen Corporation. Using a normal phase medium injection column, the sample was loaded in 30% toluene/DCM and run onto a large silica column at 30% toluene/DCM for 16 minutes, then ramped up to 50% toluene/hexanes for 15 minutes. After concentrating down and drying on high vacuum, the tri-TIPS landomycinone product was isolated (339.3 mg, 72% yield) as an orangy red, sticky amorphous solid.

S3.4 Two-step synthesis of mono-TIPS protected lando-lipid

To a flame dried flask charged with a stir bar and backfilled with argon was added tri-TIPS landomycinone (50.2 mg, 0.062 mmol) followed by DCM (0.62 mL) and ACN (0.2 mL), 2:1, 0.1 M. A cryostat was set to 0°C and the reaction flask was set to stir and cool. After 10 minutes, pyridine (0.32 mL, 3.73 mmol) was added dropwise over 2 minutes and cooled for 5 minutes. Lauryl chloride (0.88 mL) was added dropwise via syringe over 3 hours. The addition of the acyl chloride rapidy formed the pyridinium salt which crashes out of solution, hence the slow addition time. The reaction slurry was left to stir overnight (16 hrs). The reaction was poured over DCM/H_2O and extracted twice. The organic layer was washed with H_2O (x1), saturated sodium bicarbonate (x2), and brine (x1) then dried on sodium sulfate. The solution was rotovaped down to give a bright yellow oil that was dried on high vacuum, purified via preparatory TLC, and moved swiftly into the next reaction. The crude oil was dissolved in DCM (0.7 mL, 0.1 M) and put into

cryostat bath to cool to -5°C over 25 minutes. To the flask was added TBAF (0.35 mL at 1M in THF, 0.35 mmol). The solution began to darken until it reached a deep purple. The reaction was left to stir overnight (16 hrs). The reaction was poured over DCM/H_2O and extracted twice. The organic layer was washed with H_2O and brine then dried on sodium sulfate. The solution was rotovaped down to give a crude orange oil which was purified on preparatory TLC plate using chloroform as the solvent. The middle orange spot was collected and washed off the silica using the eluent. The pure orange oil was isolated and characterized (15.6 mg, 48% over two steps).

S3.5 Synthesis of lipated landomycinone from mono-TIPS-landomycinone

To a flame dried flask charged with a stir bar and backfilled with argon was added mono-TIPS landomycinone (36.7 mg, 0.054 mmol) followed by DCM (0.62 mL). The solution was cooled -2 over 20 minutes using a cryostat bath. To the cooled flask was added 1.6 mL of acid over 3 hours. The reaction stirred for 24 hours then was quenched with 4 ml of concentrated bicarb solution. The mixture was poured over DCM/H_2O and extracted three times. The organic layer was washed with a sat. sodium bicarbonate solution followed by a sat. brine solution. The organic layer was dried on sodium sulfate then rotovaped down and dried on high vacuum. For purification, the system used was an Automated flash column chromatography Smart Flash EPCLC W-Prep 2XY Dual Channel Automated Flash Chromatography System provided by Yamazen Corporation. Using a reverse phase small injection column, the sample was loaded in 100% chloroform and run onto a small RP column for 20 minutes. After concentrating down and drying on high vacuum, the lipated landomycinone product was isolated (7.3 mg, 26% yield) as an orange sticky oil. In addition, 20.3 mg of mono-TIPS starting material was isolated back.

S3.6: Compound characterization information

Landomycin A

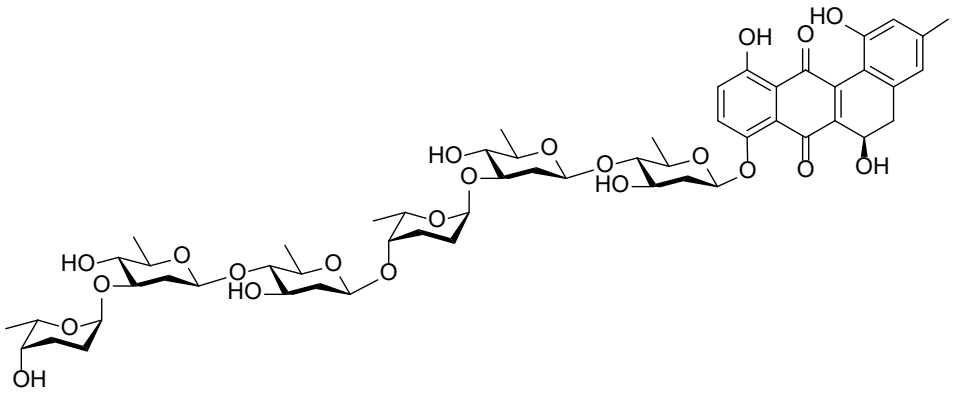

Chemical Formula: $C_{55}H_{74}O_{22}$
Exact Mass: 1086.4672
Molecular Weight: 1087.1750

^{1}H NMR (500 MHz, $CDCl_3$) δ 12.35 (s, 1H), 8.87 (s, 1H), 7.55 (d, *J* = 9.4 Hz, 1H), 7.28 (s, 1H), 6.80 (s, 1H), 6.76 (s, 1H), 5.08 (dd, *J* = 8.9, 3.0 Hz, 2H), 4.96 (s, 2H), 4.70 (s, 1H), 4.62 (s, 1H), 4.56 – 4.43 (m, 4H), 4.34 (s, 1H), 4.18 – 4.03 (m, 2H), 3.72 (m, 1H), 3.65 (s, 1H), 3.60 (dq, *J* = 13.0, 6.2 Hz, 1H), 3.56 – 3.47 (m, 3H), 3.39 (td, *J* = 8.0, 5.3 Hz, 3H), 3.29 (dt, *J* = 12.4, 6.2 Hz, 1H), 3.15 – 3.02 (m, 4H), 2.98 (t, *J* = 8.8 Hz, 1H), 2.90 (dd, *J* = 15.8, 4.5 Hz, 1H), 2.80 (d, *J* = 4.4 Hz, 1H), 2.73 (m, 1H), 2.32 (m, 4H), 2.28 – 2.19 (m, 2H), 2.14 (m, 1H), 2.07 – 1.87 (m, 5H), 1.77 (d, *J* = 11.2 Hz, 1H), 1.73 – 1.61 (m, 4H), 1.39 (dd, *J* = 8.0, 6.1 Hz, 6H), 1.27 (dd, *J* = 16.5, 6.2 Hz, 6H), 1.22 (dd, *J* = 8.6, 6.5 Hz, 6H).

^{13}C NMR (126 MHz, $CDCl_3$) δ 192.74, 182.95, 159.75, 155.14, 150.71, 146.93, 143.71, 138.76, 136.69, 132.82, 126.75, 123.71, 120.14, 119.25, 114.89, 113.26, 101.48, 100.90, 100.86, 99.69, 97.79, 97.50, 88.52, 87.87, 80.56, 80.37, 75.77, 75.26, 75.23, 72.35, 72.26, 70.86, 70.34, 69.64, 69.24, 67.72, 67.09, 62.38, 38.27, 37.62, 37.13, 37.02, 36.29, 25.48, 25.07, 24.46, 24.09, 21.19, 17.84, 17.82, 17.80, 17.01, 16.94.

ESI-MS [M+Na]: 1109.45

Tri-TIPS Landomycinone

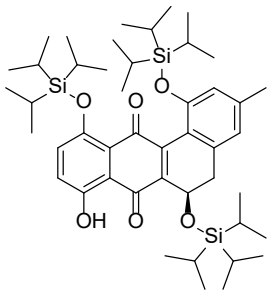

Chemical Formula: $C_{46}H_{74}O_6Si_3$
Exact Mass: 806.4793
Molecular Weight: 807.3470

^{1}H NMR (500 MHz, C_6D_6) δ 13.22 (s, 1H), 7.00 (d, *J* = 9.2 Hz, 1H), 6.92 (d, *J* = 9.2 Hz, 1H), 6.68 (s, 1H), 6.55 (s, 1H), 5.27 (t, *J* = 2.8 Hz, 1H), 2.77 (dd, *J* = 16.2, 2.3 Hz, 1H), 2.34 (dd, *J* = 16.3, 3.4 Hz, 1H), 2.08 (s, 3H), 1.34 (h, *J* = 7.4 Hz, 3H), 1.29 – 1.22 (m, 3H), 1.18 (dd, *J* = 15.7, 7.4 Hz, 19H), 1.13 (dd, *J* = 7.0, 2.1 Hz, 3H), 1.10 – 1.00 (m, 35H).

^{13}C NMR (126 MHz, C_6D_6) δ 188.67, 180.70, 156.90, 154.87, 149.05, 146.85, 141.35, 138.87, 138.21, 130.66, 127.97, 127.87, 127.68, 127.49, 124.62, 122.54, 121.01, 119.63, 118.87, 115.06, 59.87, 38.13, 29.84, 21.13, 18.10, 18.08, 18.05, 18.00, 13.34, 13.10, 12.65, 12.42, 12.18.

HRMS [M+H]: 807.4781

Tri-TBS Landomycinone

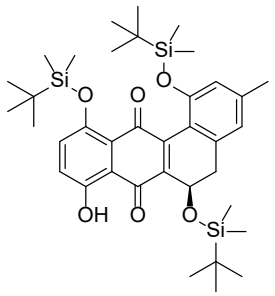

Chemical Formula: $C_{37}H_{56}O_6Si_3$
Exact Mass: 680.3385
Molecular Weight: 681.1040

^{1}H NMR (500 MHz, C_6D_6) δ 13.15 (s, 1H), 6.93 (q, *J* = 9.2 Hz, 2H), 6.56 (d, *J* = 18.7 Hz, 2H), 5.15 (dd, *J* = 3.4, 2.3 Hz, 1H), 2.66 (dd, *J* = 16.3, 2.4 Hz, 1H), 2.35 (dd, *J* = 16.2, 3.4 Hz, 1H), 2.00 (s, 3H), 1.13 (s, 9H), 0.91 (s, 9H), 0.79 (s, 9H), 0.50 (s, 3H), 0.19 (s, 3H), 0.16 (s, 3H), 0.10 (s, 6H), 0.05 (s, 3H).

^{13}C NMR (126 MHz, C_6D_6) δ 193.63, 186.42, 162.41, 159.72, 153.44, 151.96, 146.83, 143.72, 143.29, 137.13, 129.96, 128.13, 127.22, 125.64, 125.13, 119.98, 64.73, 42.97, 35.04, 31.28, 31.02, 30.71, 26.23, 23.90, 23.40, 22.97, 1.42, 0.98, 0.77, 0.59, 0.49.

HRMS [M+H]: 681.3315

Lipidated Mono-TIPS Lando

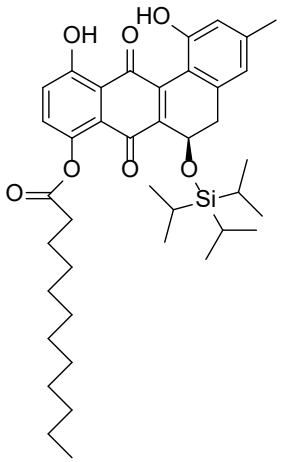

Chemical Formula: $C_{40}H_{56}O_7Si$

^{1}H NMR (500 MHz, C_6D_6) δ 11.98 (s, 1H), 8.83 (s, 1H), 6.95 (s, 1H), 6.72 (s, 2H), 6.53 (s, 1H), 5.37 (t, *J* = 2.9 Hz, 1H), 2.83 (dd, *J* = 16.0, 2.8 Hz, 1H), 2.75 (td, *J* = 7.5, 3.6 Hz, 2H), 2.40 (dd, *J* = 15.9, 3.0 Hz, 1H), 2.05 (s, 3H), 1.93 (p, *J* = 7.6 Hz, 2H), 1.44 (dt, *J* = 10.5, 6.9 Hz, 3H), 1.40 – 1.24 (m, 21H), 1.08 (dd, *J* = 5.4, 2.3 Hz, 21H), 1.02 (dd, *J* = 6.4, 3.6 Hz, 3H), 0.96 – 0.87 (m, 6H).

*Note: the proton count does not perfectly match, however, the lipid peaks overlap with grease peaks (See 2D NMR/13C)

^{13}C NMR (126 MHz, C_6D_6) δ 193.00, 180.98, 171.12, 160.73, 155.93, 144.41, 143.25, 142.85, 139.43, 137.81, 134.05, 127.97, 127.87, 127.68, 127.48, 125.66, 123.52, 121.44, 119.90, 115.26, 113.79, 60.07, 37.98, 34.25, 31.98, 29.83, 29.77, 29.74, 29.63, 29.50, 29.46, 29.33, 24.60, 22.75, 20.66, 17.90, 17.82, 13.99, 12.52.

ESI-MS [M+H]: 676.67

Lando lipid

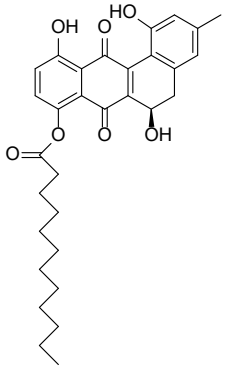

^{1}H NMR (500 MHz, C_6D_6) δ 12.01 (s, 1H), 8.91 (s, 1H), 6.94 (s, 1H), 6.79 – 6.67 (m, 2H), 6.39 (s, 1H), 4.85 (s, 1H), 2.81 – 2.67 (m, 3H), 2.43 (dd, *J* = 15.8, 4.5 Hz, 1H), 2.33 (s, 1H), 1.99 (s, 3H), 1.87 (p, *J* = 7.4 Hz, 2H), 1.54 (s, 1H), 1.31 (d, *J* = 13.2 Hz, 19H), 0.92 (t, *J* = 6.5 Hz, 4H).

*Note: the proton count does not perfectly match, however, the lipid peaks overlap with grease peaks (See 2D NMR/13C)

^{13}C NMR (126 MHz, C_6D_6) δ 192.48, 182.26, 171.26, 160.72, 155.79, 145.53, 143.35, 139.16, 137.08, 134.11, 127.98, 127.88, 127.69, 127.59, 127.49, 125.79, 123.37, 121.55, 120.11, 115.10, 113.19, 61.66, 36.21, 34.12, 31.98, 29.73, 29.62, 29.46, 29.42, 29.22, 24.60, 22.77, 20.62, 14.01.

ESI-MS [M+H]: 521.35

S3.7: NMR spectra

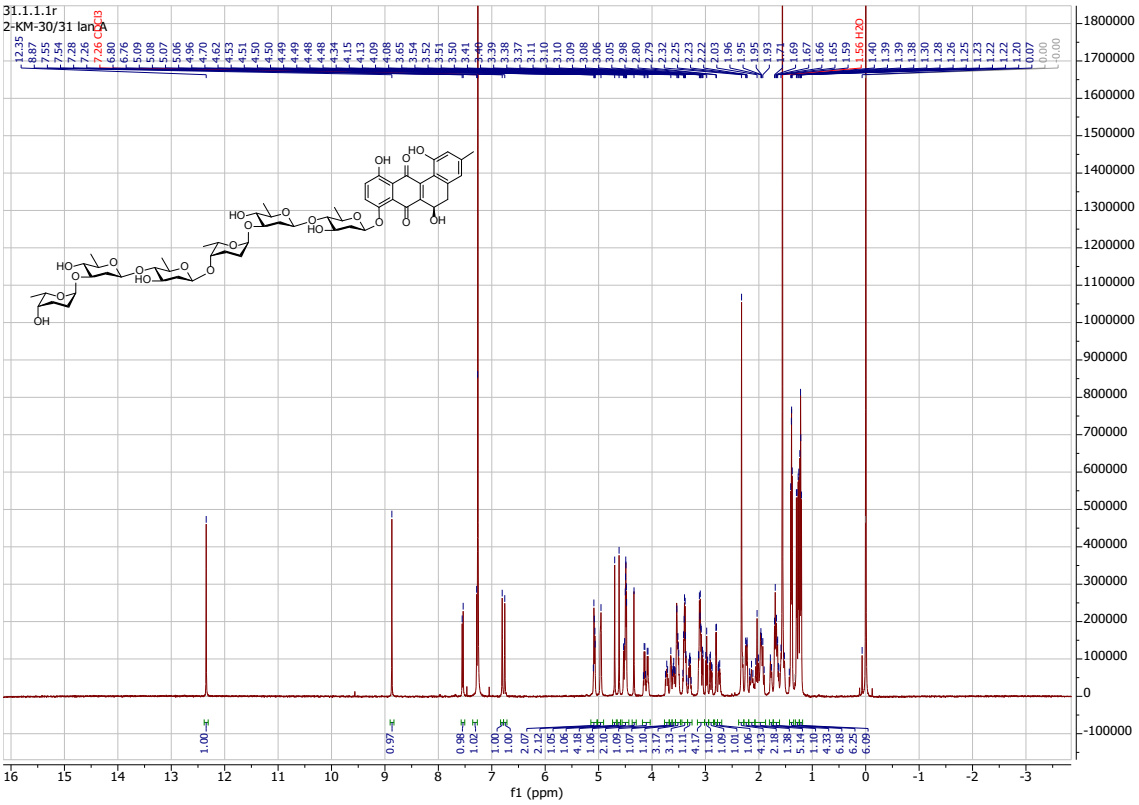

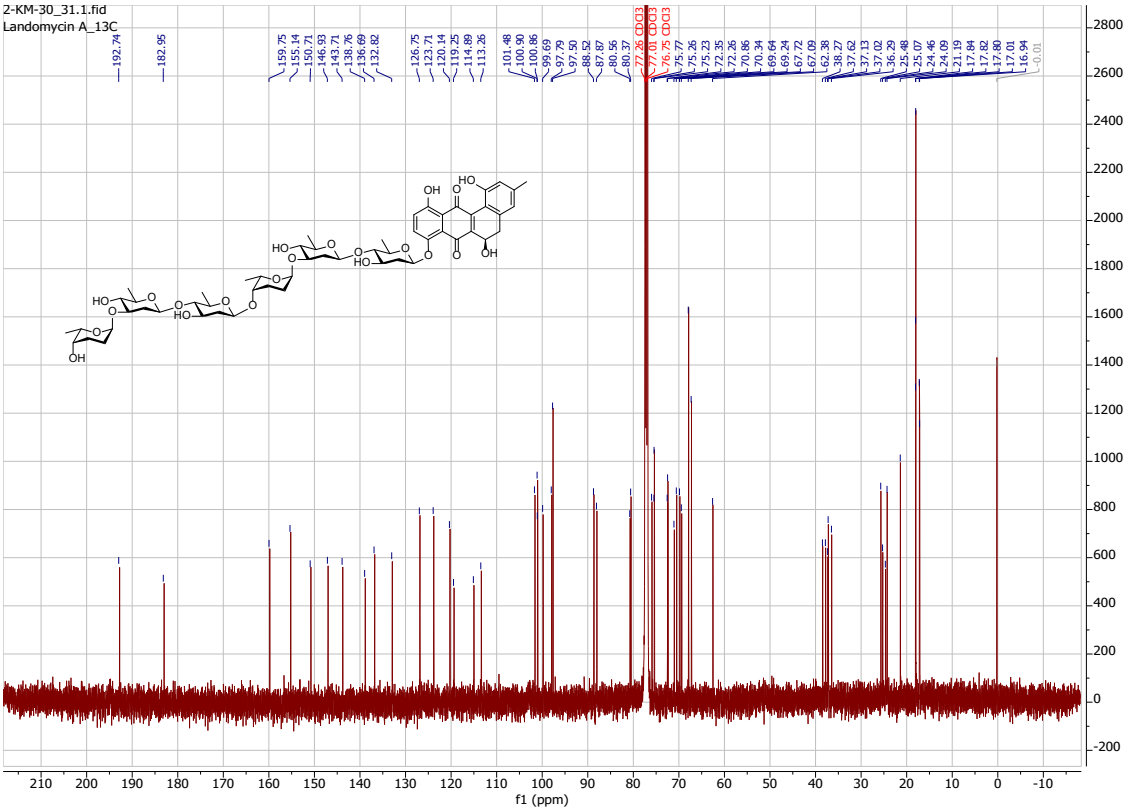
2-KM-30_31.1.fid
Landomycin A_13C
f1 (ppm)

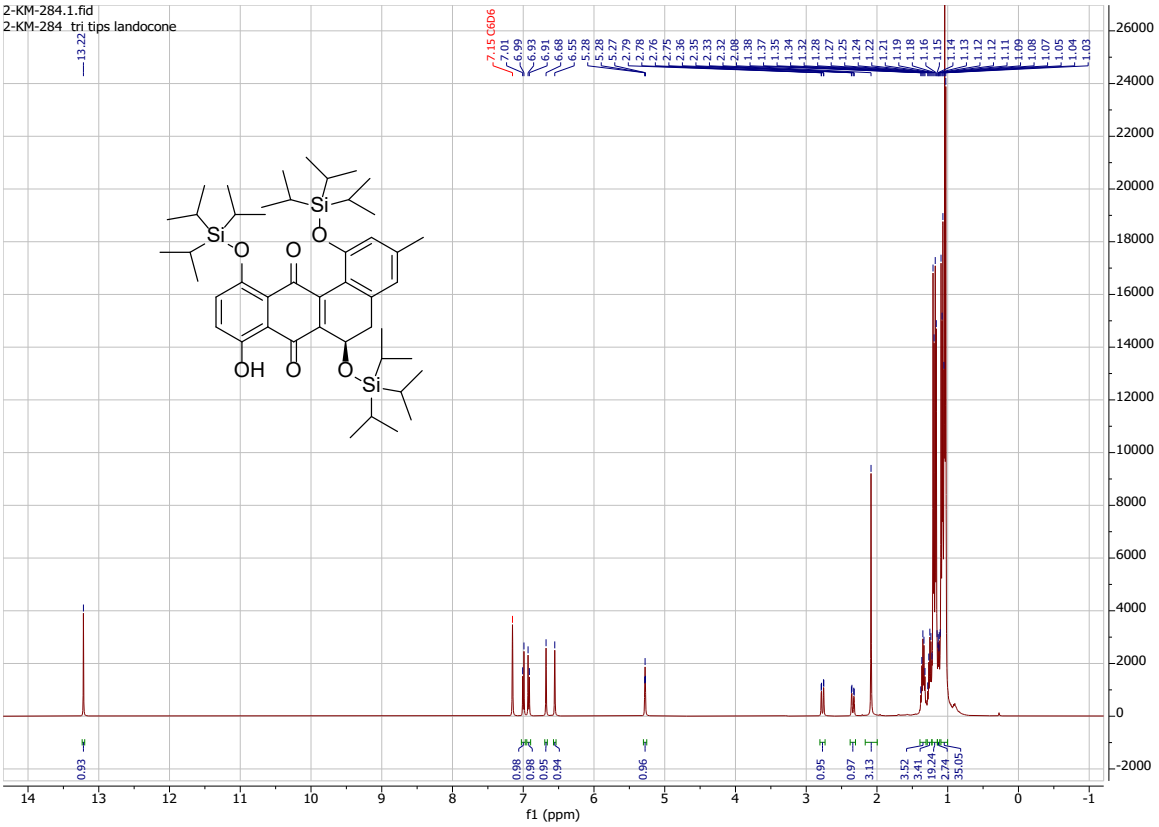
2-KM-284.1.fid
2-KM-284 tri tips landocone
f1 (ppm)

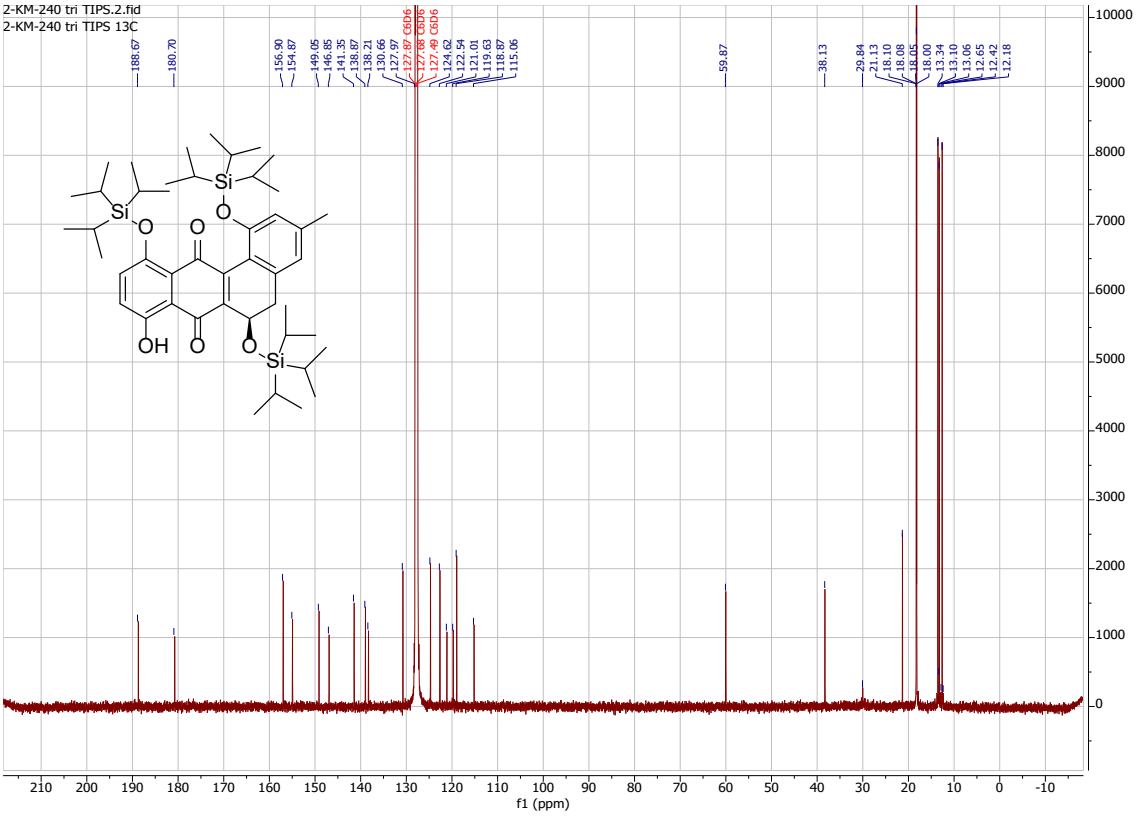
2-KM-240 tri TIPS.2.fid
2-KM-240 tri TIPS 13C
f1 (ppm)

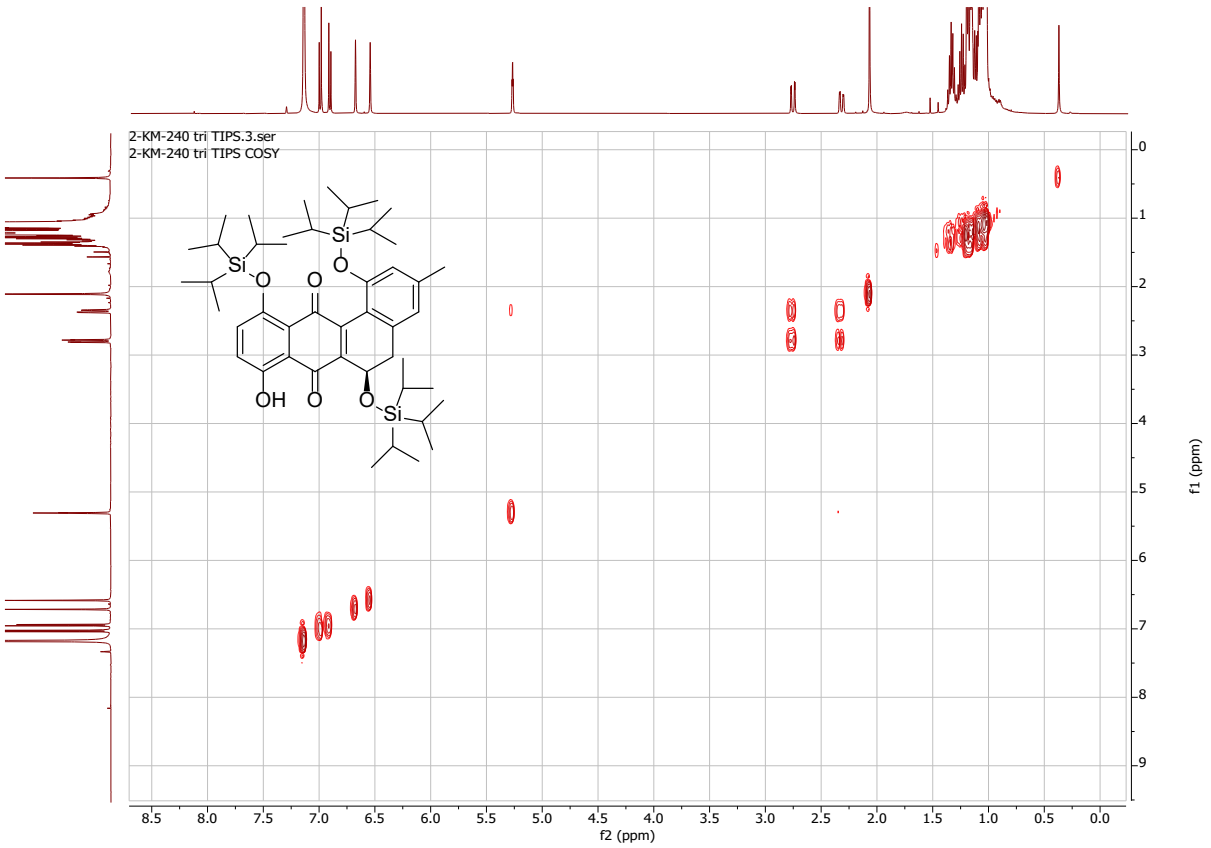
2-KM-240 tri TIPS.3.ser
2-KM-240 tri TIPS COSY
f2 (ppm)
f1 (ppm)

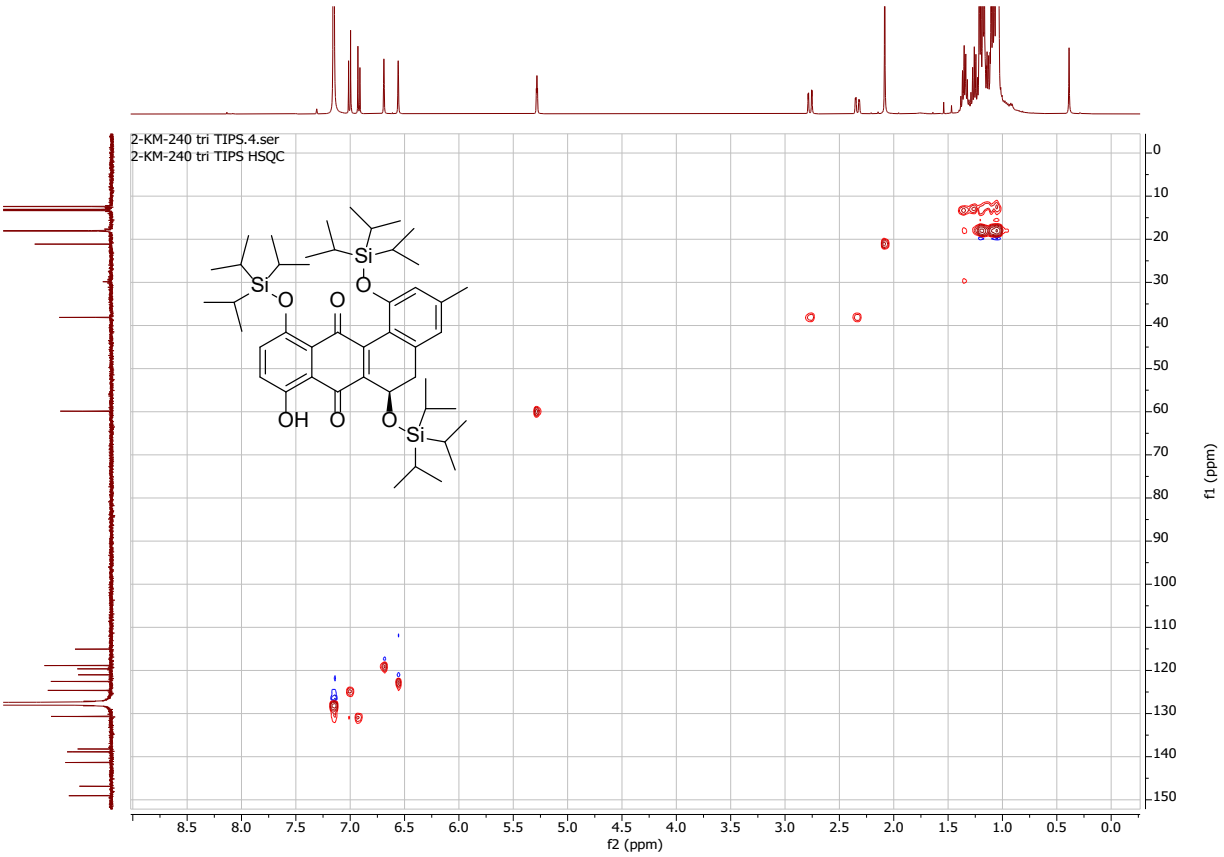
2-KM-240 tri TIPS.4.ser
2-KM-240 tri TIPS HSQC
f2 (ppm)
f1 (ppm)

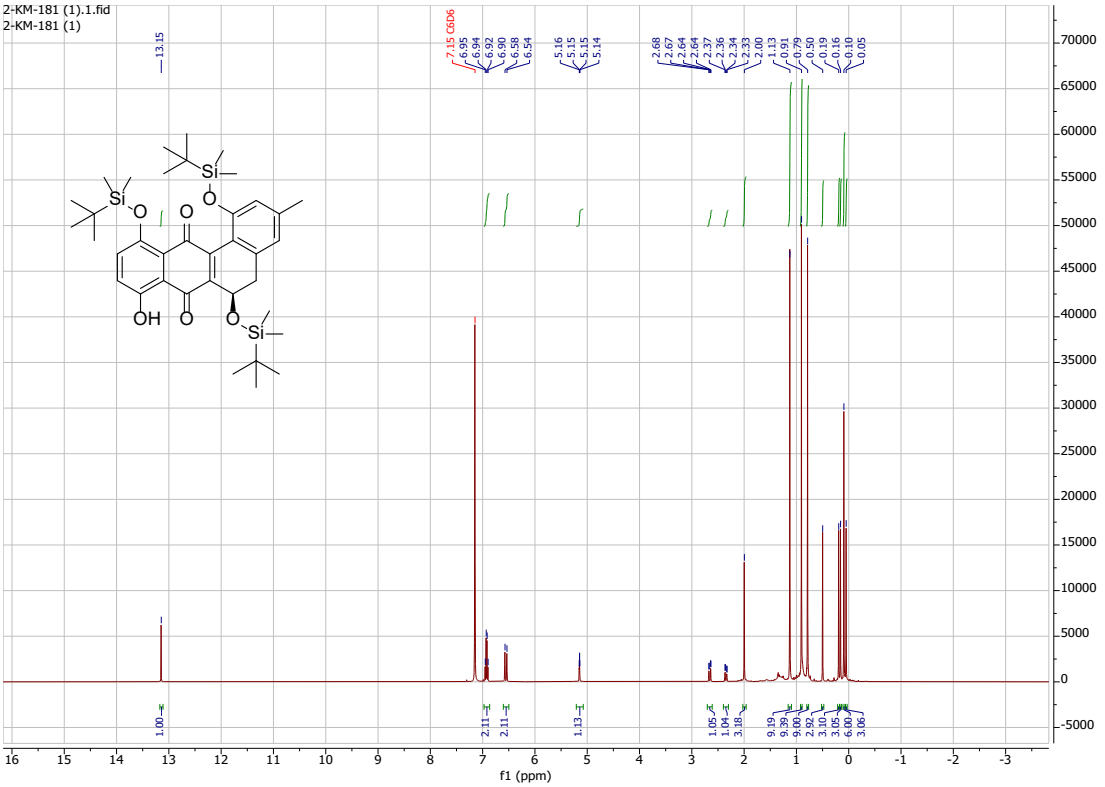
2-KM-181 (1).1.fid
2-KM-181 (1)
f1 (ppm)

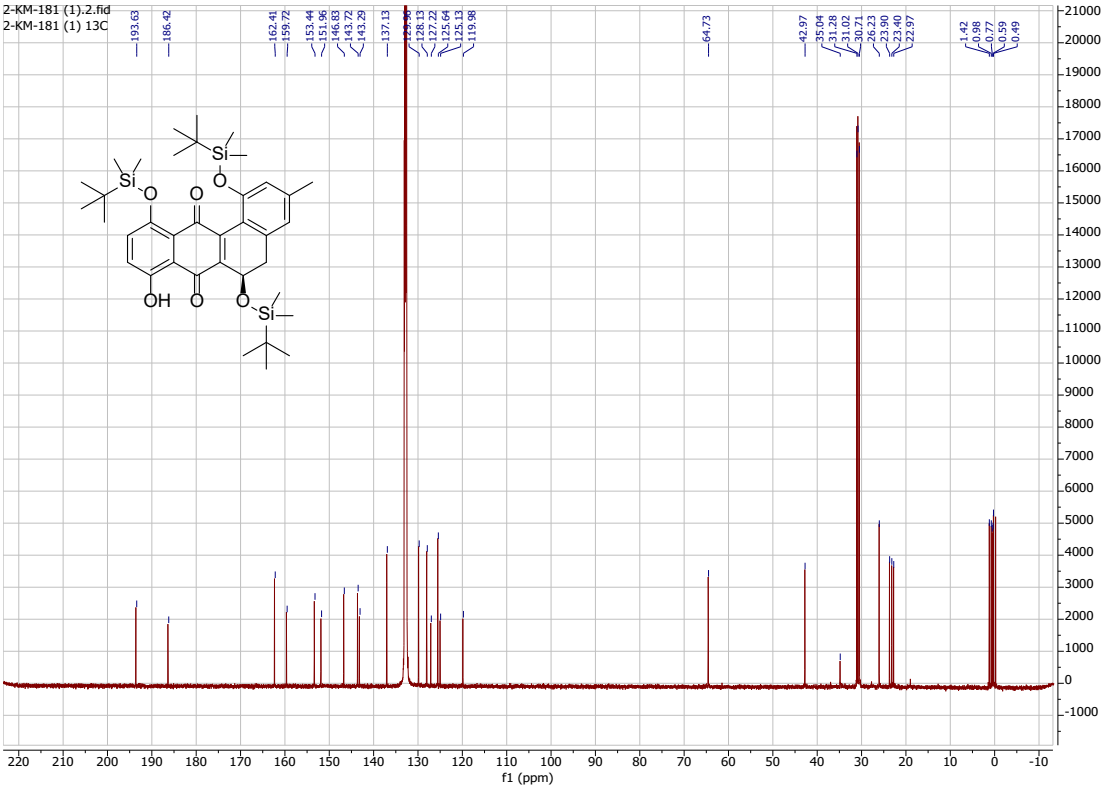
2-KM-181 (1).2.fid
2-KM-181 (1) 13C
f1 (ppm)

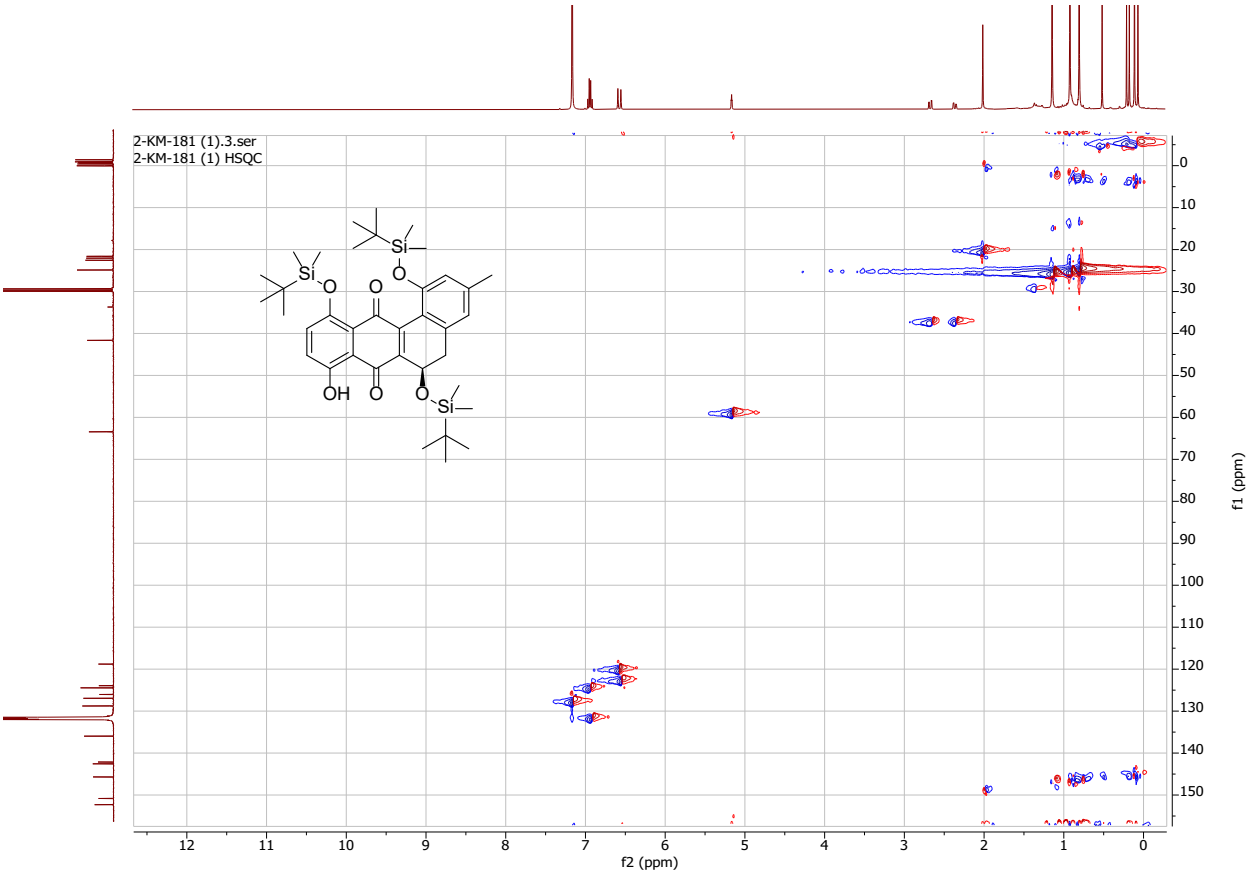
2-KM-181 (1).3.ser
2-KM-181 (1) HSQC
f2 (ppm)
f1 (ppm)

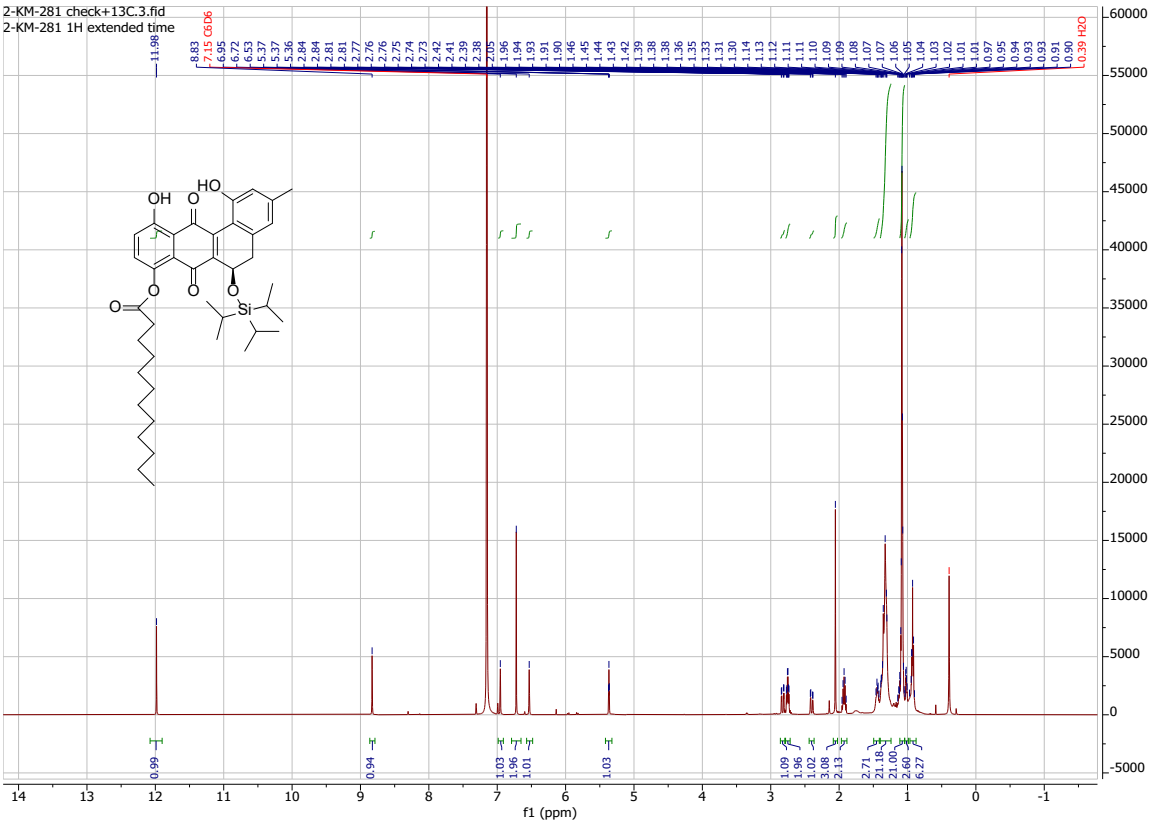
2-KM-281 check+13C.3.fid
2-KM-281 1H extended time
f1 (ppm)

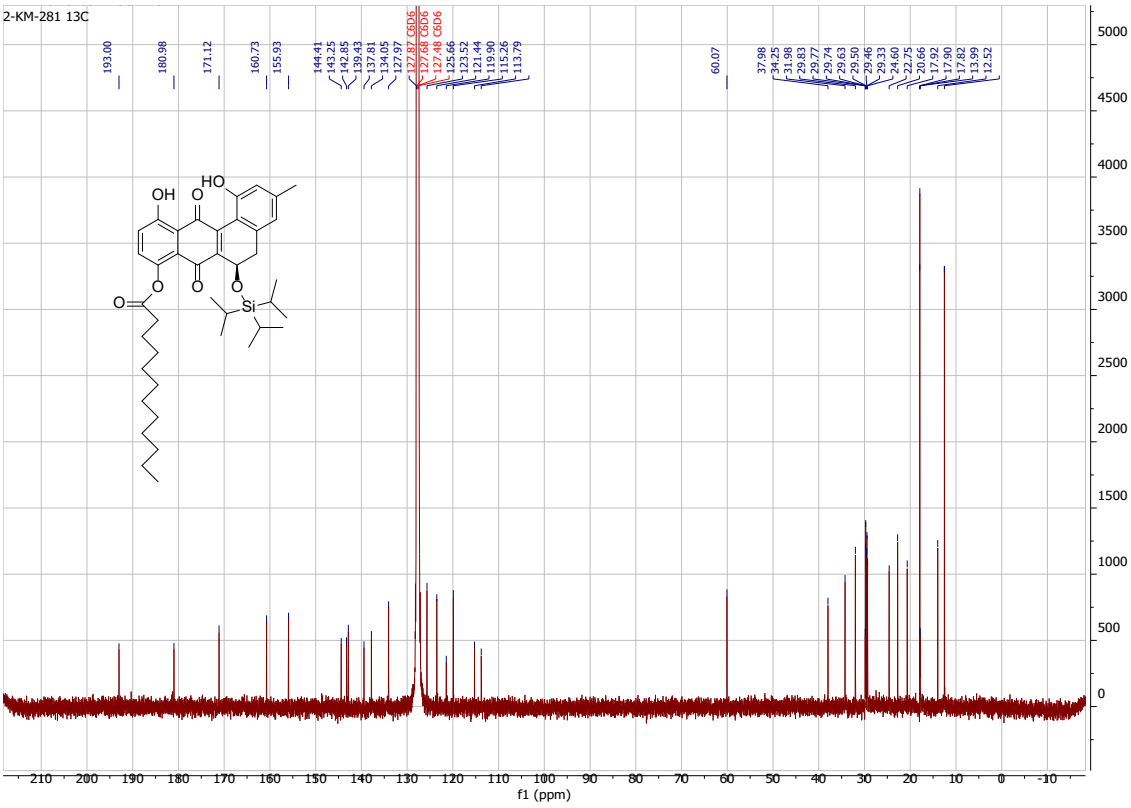
2-KM-281 13C
193.00
180.98
171.12
160.73
155.93
144.41
143.25
142.85
139.43
137.81
134.45
127.97
127.87 C6D6
127.68 C6D6
127.48 C6D6
125.66
123.52
121.44
119.90
115.26
113.79
60.07
37.98
34.25
31.98
29.83
29.77
29.74
29.63
29.50
29.46
29.33
24.60
22.75
20.66
17.92
17.90
17.82
13.99
12.52
OH
O
HO
O
O
O
O
Si
f1 (ppm)

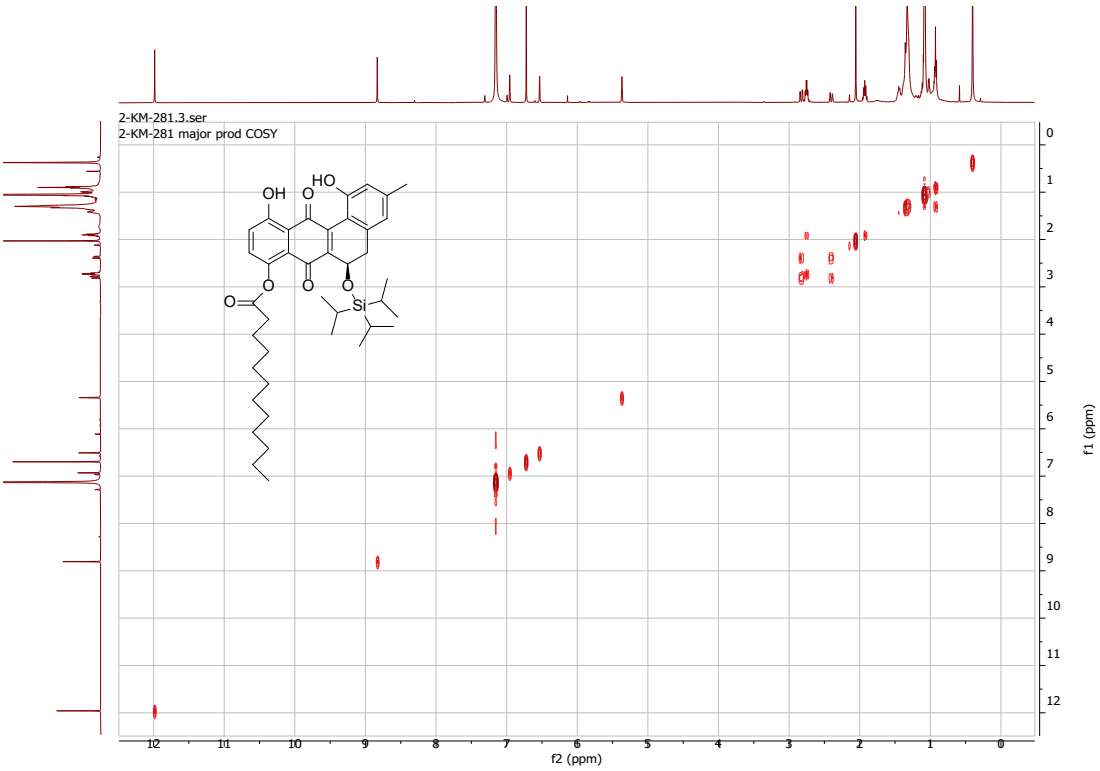
2-KM-281.3.ser
2-KM-281 major prod COSY
OH
O
HO
O
O
O
O
Si
f2 (ppm)
f1 (ppm)

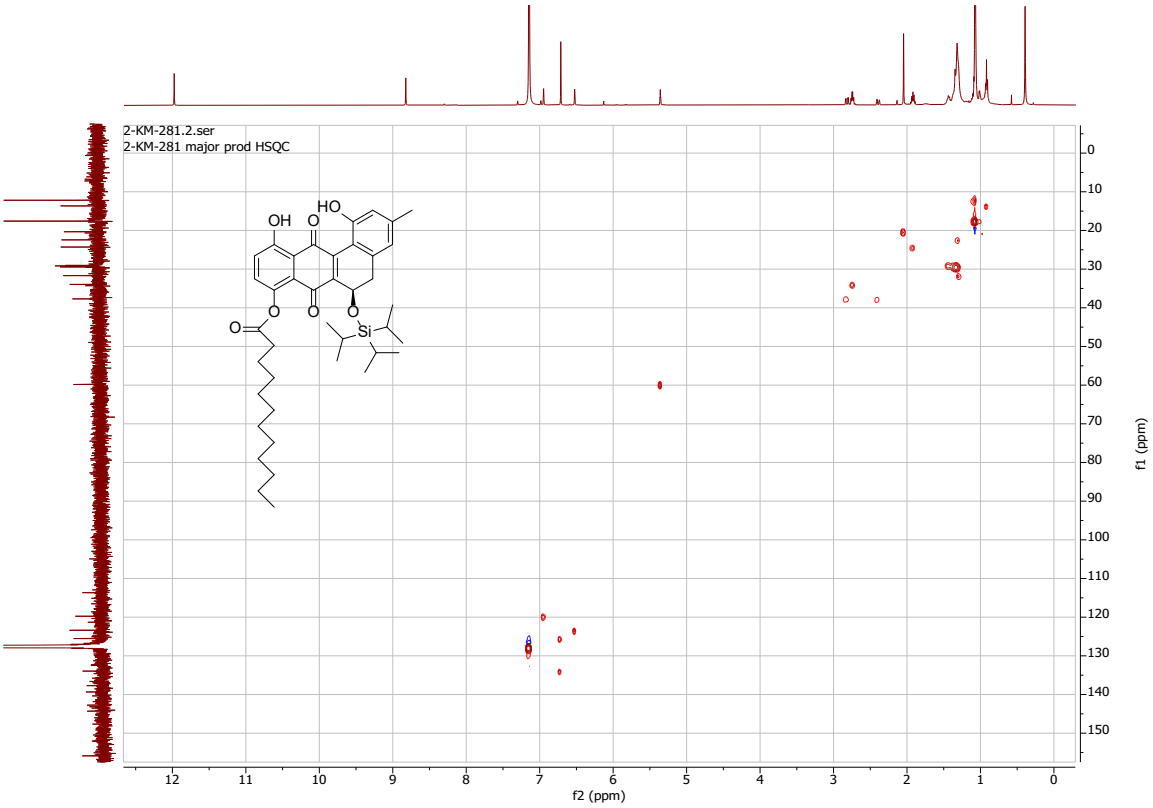
2-KM-281.2.ser
2-KM-281 major prod HSQC
OH
O
HO
O
O
O
O
Si
f2 (ppm)
f1 (ppm)

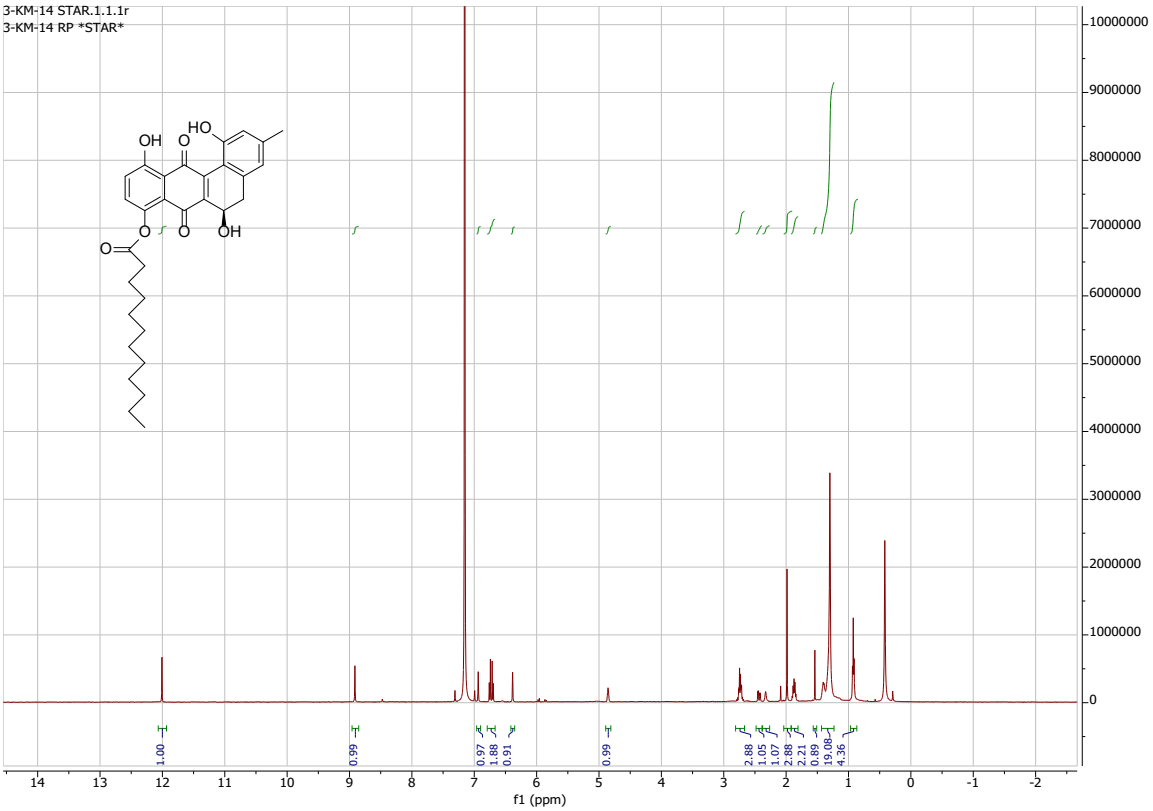
3-KM-14 STAR.1.1.1r
3-KM-14 RP *STAR*
OH
O
HO
O
O
OH
f1 (ppm)

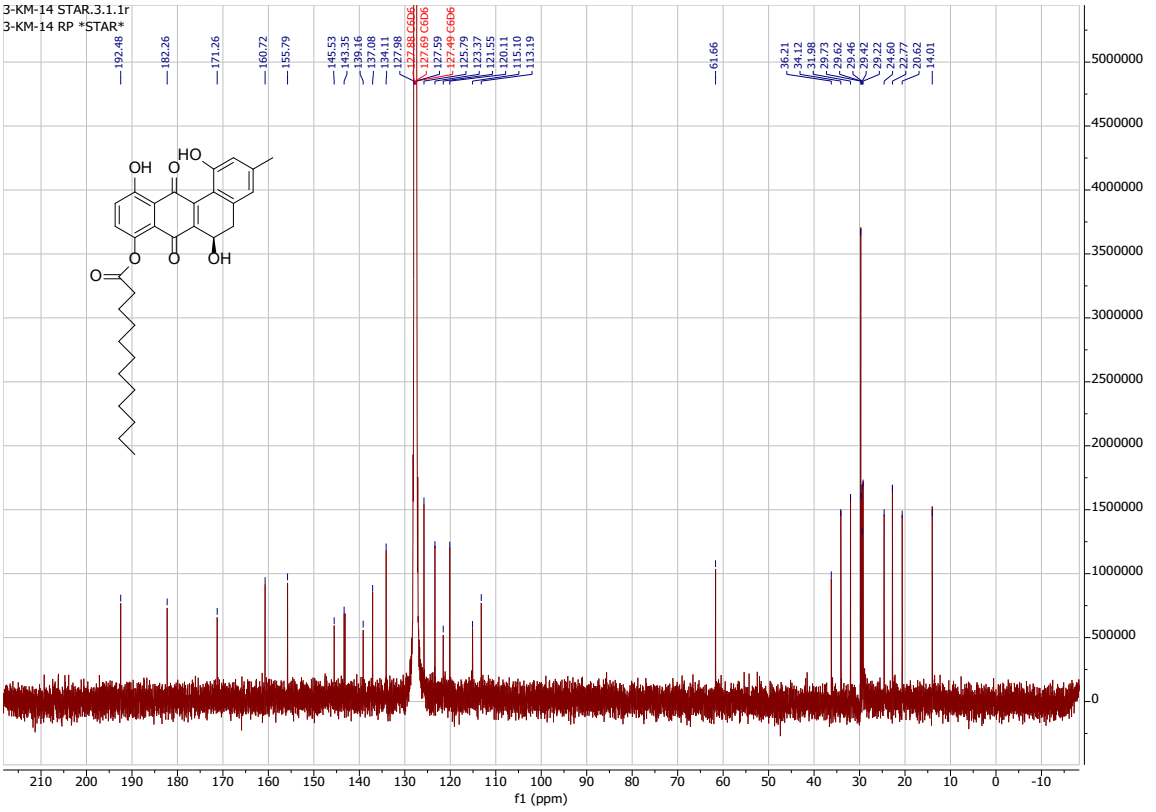
3-KM-14 STAR.3.1.1r
3-KM-14 RP *STAR*
192.48
182.26
171.26
160.72
155.79
145.53
143.35
139.16
137.08
134.11
127.98
127.88 C6D6
127.69 C6D6
127.59
127.49 C6D6
125.79
123.37
121.55
120.11
115.10
113.19
61.66
36.21
34.12
31.98
29.73
29.62
29.46
29.42
29.22
24.60
22.77
20.02
14.01
OH
O
HO
O
O
OH
O
5000000
4500000
4000000
3500000
3000000
2500000
2000000
1500000
1000000
500000
0
210 200 190 180 170 160 150 140 130 120 110 100 90 80 70 60 50 40 30 20 10 0 -10
f1 (ppm)

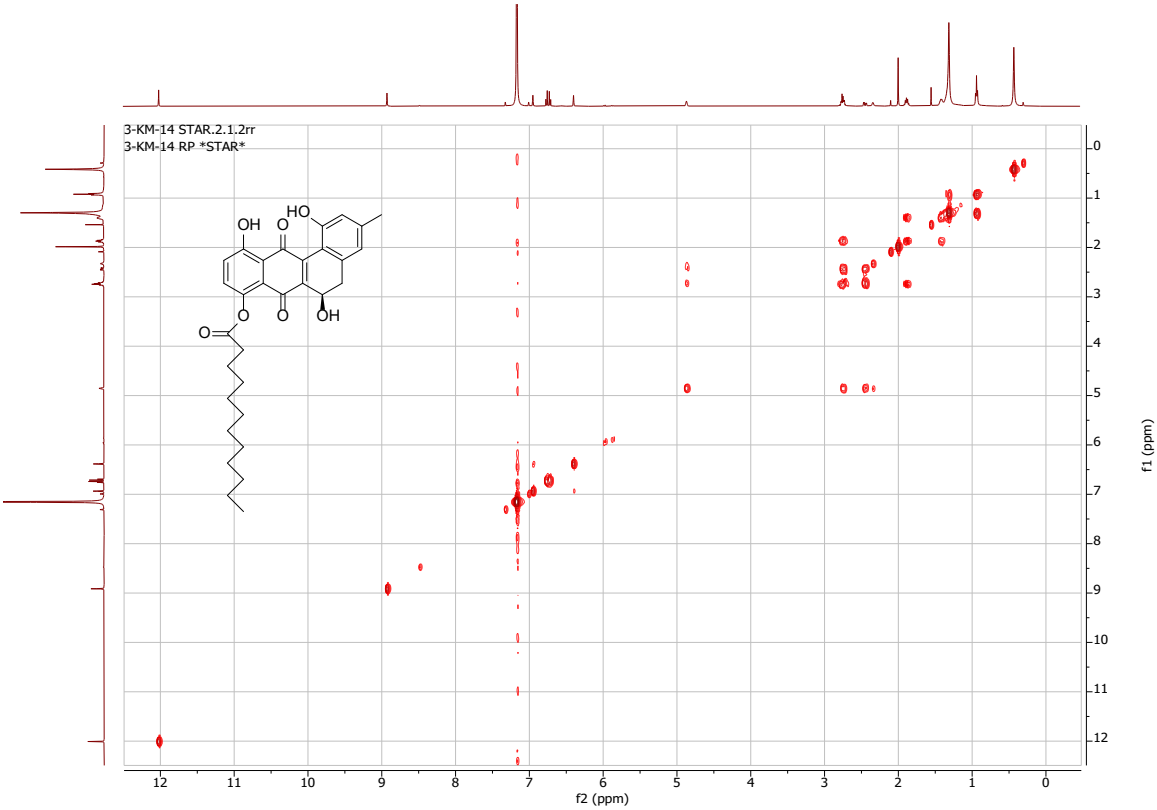
3-KM-14 STAR.2.1.2rr
3-KM-14 RP *STAR*
OH
O
HO
O
O
OH
O
0
1
2
3
4
5
6
7
8
9
10
11
12
12 11 10 9 8 7 6 5 4 3 2 1 0
f2 (ppm)
f1 (ppm)

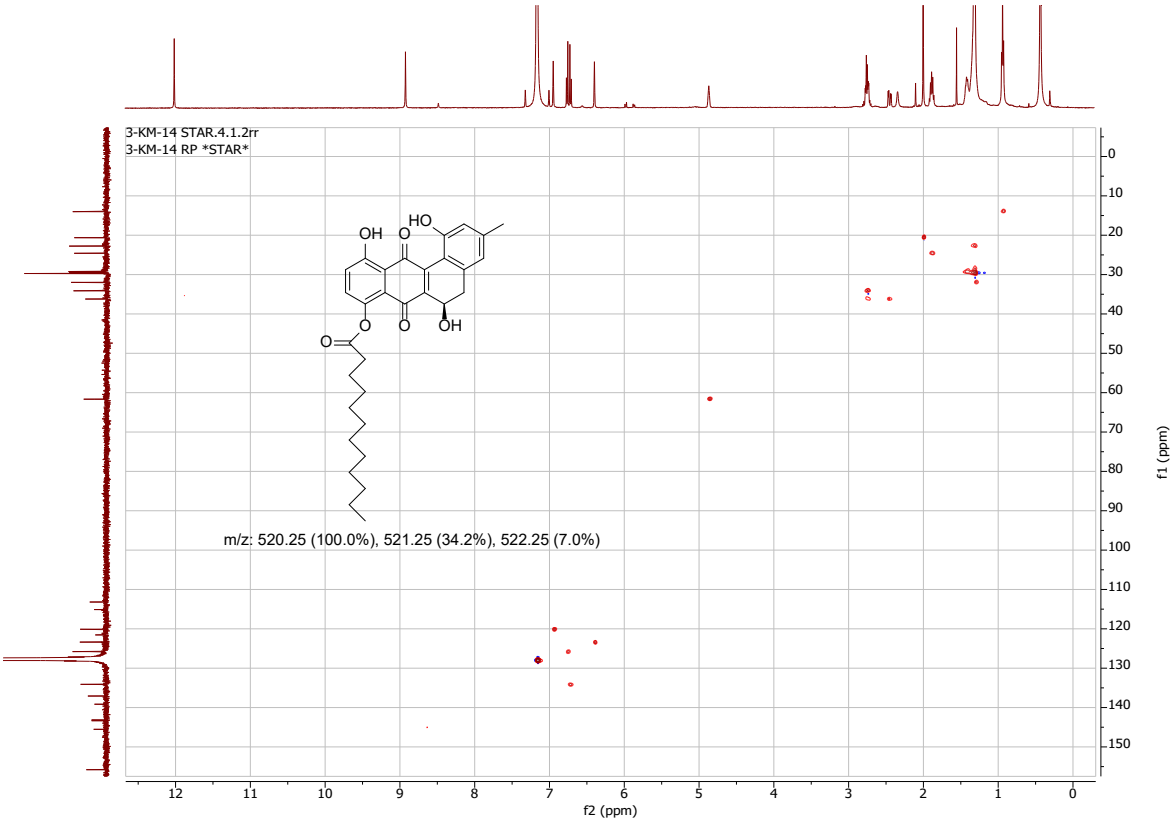
3-KM-14 STAR.4.1.2rr
3-KM-14 RP *STAR*
OH
O
HO
O
O
O
OH
m/z: 520.25 (100.0%), 521.25 (34.2%), 522.25 (7.0%)
f2 (ppm)
f1 (ppm)

Appendix III: Supporting Information for Chapter 4

S4.1: Rink Resin activation followed by amidation and deprotection

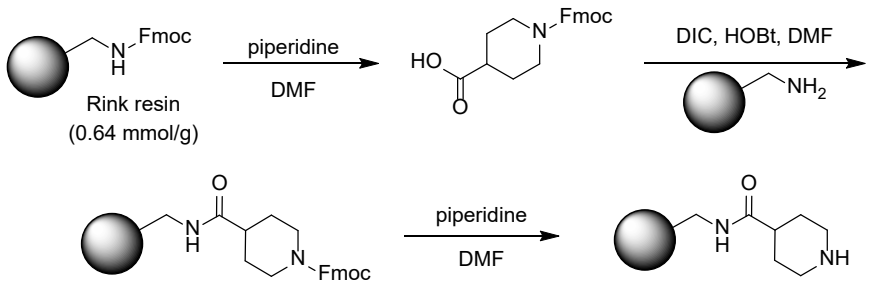

i . Rink resin (4.03 g of 0.639 mmol/g, 2.575 mmol) was suspended in a DMF solution of piperidine (25 mL of 20 %w/v, 58.72 mmol) in a 50 mL peptide reaction flask and mixed for at least 10 min. The solution was drained via a stream of N_2 and the beads were washed with clean DMF (30 mL) two times. The process was repeated once more. The beads were dried over a stream of N_2 for 5 minutes.

ii. To a 50 mL peptide reaction vessel loaded with activated resin was added 1-(9H-fluoren-9-ylmethoxycarbonyl)piperidine-4-carboxylic acid (902.2 mg, 2.567 mmol) , HOBt (Hydrate (1)) (1.18 g, 7.705 mmol) , DIC (1.20 mL, 7.664 mmol) and DMF (20 mL) under a stream of N_2 . The peptide reaction vessel was hooked into the Ferris wheel mixer and set to stir at 50 rpm overnight (18 hrs). After stirring overnight, the mixture was washed with DMF (3 x 20 mL).

iii. To the resin was added piperidine (25 mL of 20 %w/v, 58.72 mmol) and the vessel was mixed for at least 5 min. The solution was drained via a stream of N_2 and the beads were washed with clean DMF (30 mL) two times. The process was repeated once more. The beads were washed with DCM (2x15ml) to remove DMF and dried over a stream of N_2 for 5 minutes then dried on high vacuum for an hour. No further characterization was done, and the beads were stored under N_2 to be used in subsequent reactions

Source: AAPtech guide: https://www.peptide.com/custdocs/aapptec%20synthesis%20guide%202-0%20(2).pdf

S4.2: First S_NAr towards pyrimidine core

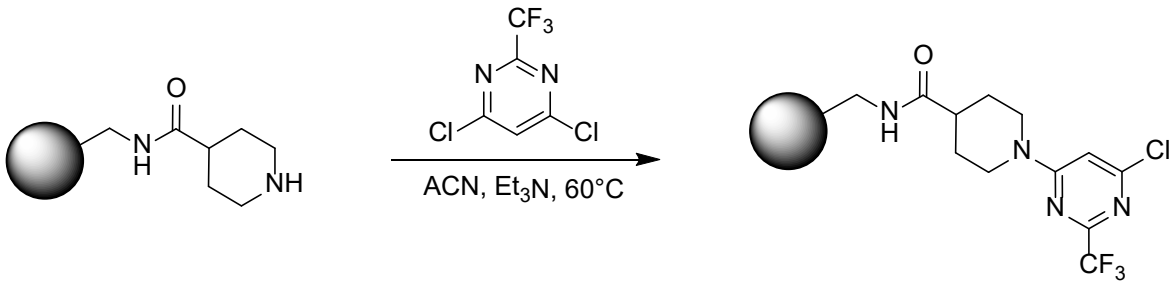

i. To the vial was added the beads (2.01g, 1.278 mmol), ACN (10 mL) followed by 4,6-dichloro-2-(trifluoromethyl)pyrimidine (1.36 mL, 9.998 mmol) a n d triethylamine (1.4 mL, 10.04 mmol) all under N_2. The Eppendorf Thermomixer was set to 65°C to sir at 450 rpm overnight. After stirring overnight, the reaction solution was drained through a filter funnel and the beads were washed with ACN (3 x 15 mL) , DCM (2 x 15 mL) . The beads were moved back to a vial and dried under vacuum .

ii. A very small scoop of beads was exposed to 1 mL of a 12% TFA/DCM solution with 2% triethyl silane for 30 min and used for UPLC analysis. The mass of the product 1-[6-chloro-2-(trifluoromethyl)pyrimidin-4-yl]piperidine-4-carboxamide ESI-MS *m/z* calc. 308.0652, was detected. No further characterization was done and the beads were used in subsequent reactions.

[M+1] Found: 309.02

Calculated: 308.07

S4.3: Second S_NAr towards pyrimidine core & cleavage

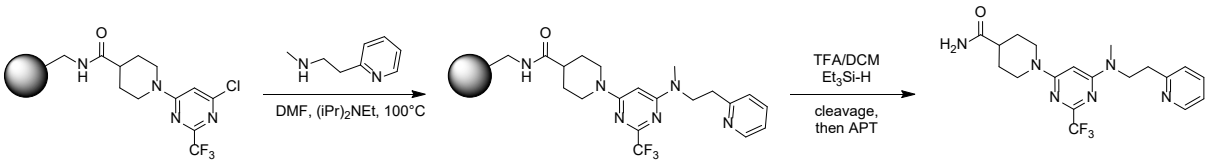

i. To a vial loaded with beads ([[1-[6-chloro-2-(trifluoromethyl)pyrimidin-4-yl]piperidine-4-carbonyl]amino] (251 mg of 0.639 mmol/g, 0.1604 mmol)) and filled with N_2 was added 2-imidazol-1-

yl-N-methyl-ethanamine (241.2 mg, 1.927 mmol) followed by DMF (2 mL) then DIPEA (340 µL, 1.952 mmol) . The Eppendorf Thermomixer was set to 80 °C to sir at 450 rpm ON. After stirring overnight, the reaction solution was drained through a filter funnel and the beads were washed with DMF (2 x 10 mL), DCM (2 x 10 mL). The beads were moved back to a vial and dried under vacuum.

ii. To the dried beads was added 5 mL of a 12% TFA/DCM solution with 2% triethyl silane stir for 2 hrs. A sample of the solution was run on the UPLC and the product was detected in decent quantity. The solution was filtered off the beads and the beads were washed with ACN (x2) DCM (2x10ml). The mixture was filtered and the solution was rotovaped down. The crude sample was sent to APT for purification.

iii. Purification by reversed-phase HPLC. Method: Waters XSelect CSH C18 OBD Prep Column; 30 x 150 mm, 5 micron. Gradient: Acetonitrile in Water with 0.1% Trifluoroacetic Acid.

[M+1] Found: 409.19

Calculated: 408.19

^{1}H NMR (300 MHz, MeOD) δ 8.87 (d, *J* = 1.5 Hz, 1H), 7.52 (t, *J* = 1.7 Hz, 1H), 7.41 (t, *J* = 1.7 Hz, 1H), 5.67 (s, 1H), 4.52 – 4.38 (m, 4H), 4.12 (dd, *J* = 6.5, 4.3 Hz, 2H), 3.06 (s, 3H), 2.97 – 2.85 (m, 2H), 2.53 (tt, *J* = 11.7, 3.9 Hz, 1H), 1.90 – 1.79 (m, 2H), 1.61 (qd, *J* = 12.3, 4.1 Hz, 2H).

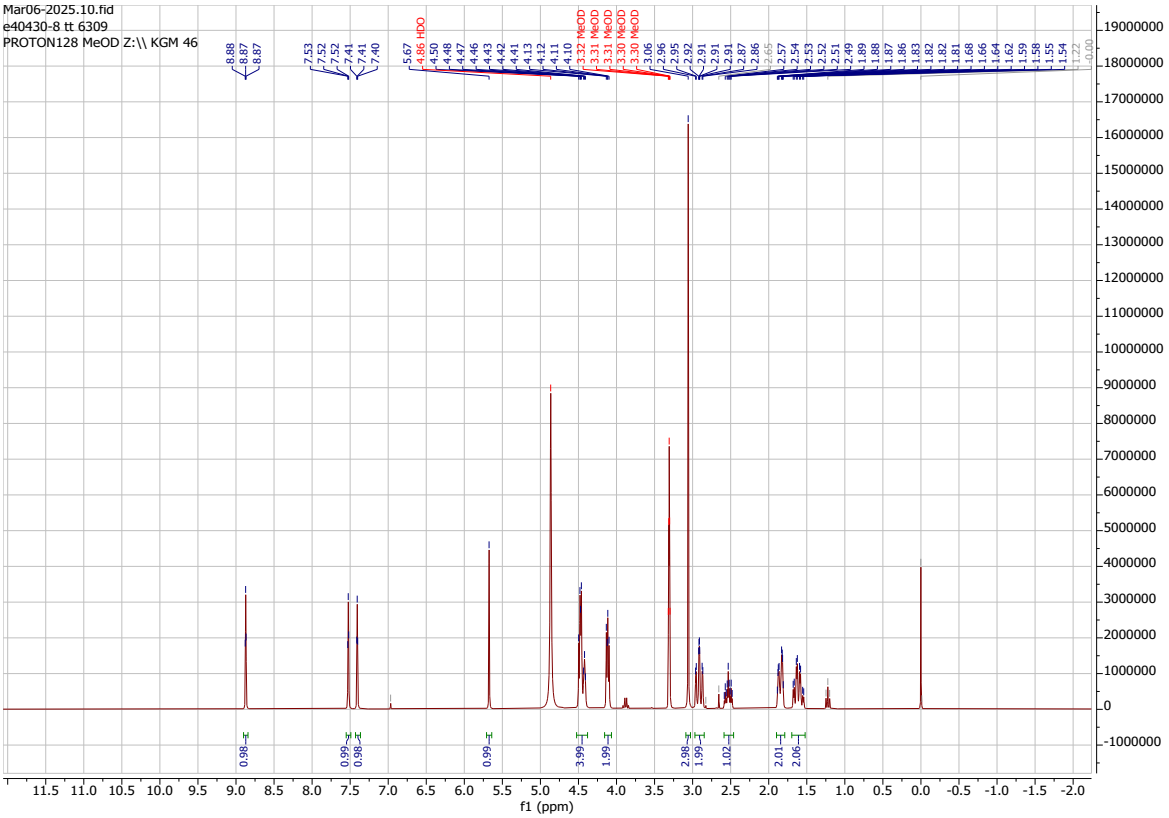
Mar06-2025.10.fid
e40430-8 tt 6309
PROTON128 MeOD Z:\\ KGM 46
f1 (ppm)

S4.4: Library Generation procedure for pyrimidine core

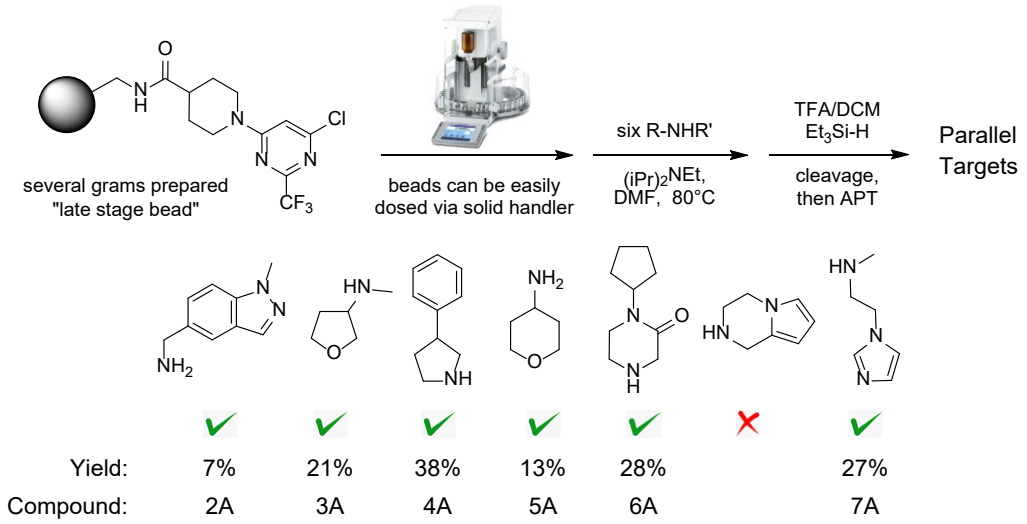

i. The QS30 weighed out the Bead with aryl halogen (170 mg of 0.64 mmol/g) into individual vials. The integrity of the beads was inspected visually and the dose head did not appear to damage the beads. Each amine was weighed out into a separate vial. Using a multichannel pipette, DMF (1.5 mL) was added to each amine vial, aspirated (x2) and transferred to the vials containing beads. Each vial was back filled with nitrogen and dosed with DIPEA (190 µL) . The Eppendorf Thermomixer was set to 100°C to sir at 450 rpm ON. After stirring overnight, the reaction mixture was transfered into 5 mL syringes equipt with a filter so the solution could be expelled without loss of the beads. The beads were washed with DMF (2 x 5 mL) and put on the shaker to stir for at least 5 min. The beads were washed with DCM (2 x 5 mL) and then put on the mixer to stir for at least 5 min. Finally, the DCM was expelled, the syringe of beads was washed with 1 mL of DCM to give clean beads.

ii. To the beads in the syringe was added 1.5 mL of 12% TFA/DCM solution with 2% triethyl silane stir f or 1.5 hrs. The solution was filtered off the beads and the beads were washed with ACN (2x5 mL) and DCM (3x5 mL). The solution was rotovaped down and the crude sample was sent to APT for purification.

iii. Purification by reversed-phase HPLC. Method: Waters XSelect CSH C18 OBD Prep Column; 30 x 150 mm, 5 microns. Gradient: Acetonitrile in Water with 0.1% Trifluoroacetic Acid. For characterization,

odd numbered wells were NMR'd to make sure the screen was indeed successful. Those documents are attached. These final compounds were not registered but just used as proof of concept for a solid phase synthesis screen.

Compound 4A:

[M+1] Found: 420.27

Calculated: 419.19

^{1}H NMR (300 MHz, $CDCl_3$) δ 7.40 – 7.33 (m, 2H), 7.30 (d, *J* = 1.3 Hz, 2H), 5.45 (d, *J* = 17.8 Hz, 1H), 5.39 (s, 1H), 4.42 (d, *J* = 13.3 Hz, 2H), 3.89 (d, *J* = 59.5 Hz, 2H), 3.53 (d, *J* = 11.8 Hz, 3H), 3.12 – 2.83 (m, 2H), 2.46 (tt, *J* = 11.2, 3.8 Hz, 2H), 2.15 (p, *J* = 9.4 Hz, 1H), 2.04 – 1.90 (m, 2H), 1.85 – 1.65 (m, 2H).

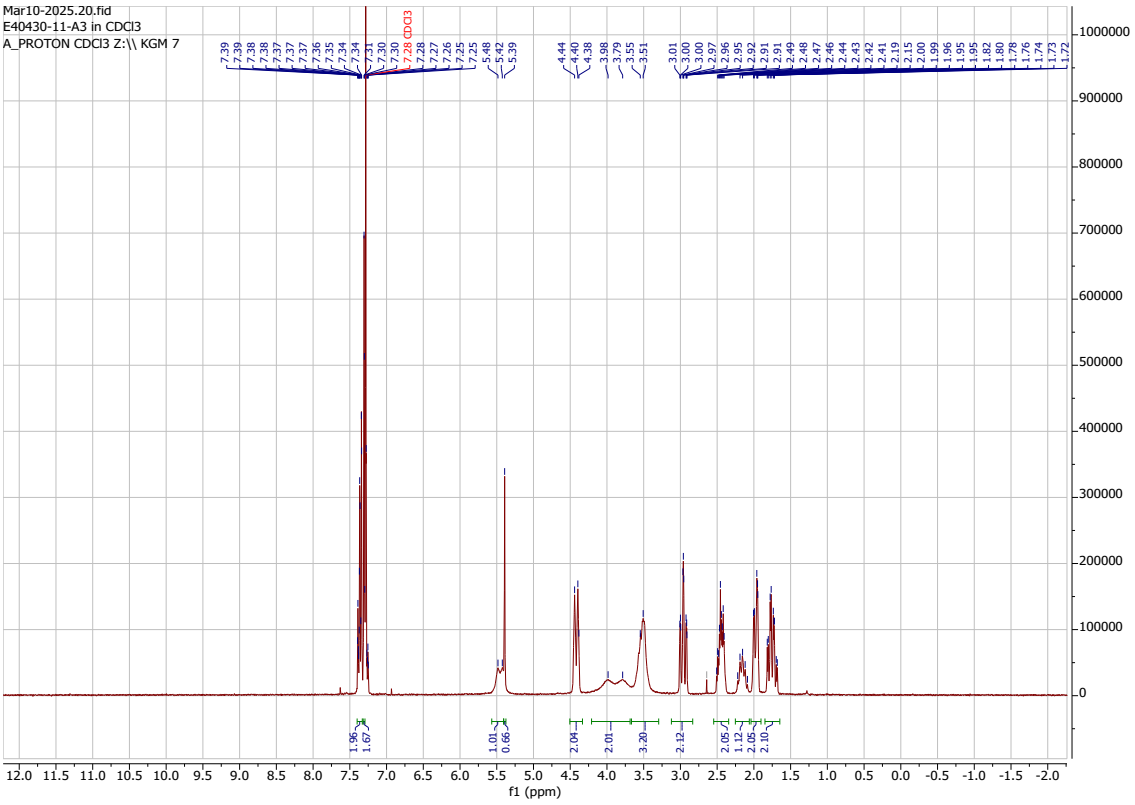

Compound 6A:

[M+1] Found: 441.31

Calculated: 440.2

^{1}H NMR (300 MHz, $CDCl_3$) δ 5.51 (d, *J* = 5.1 Hz, 2H), 5.01 (p, *J* = 8.4 Hz, 1H), 4.42 (d, *J* = 13.4 Hz, 2H), 4.09 (s, 2H), 4.04 – 3.94 (m, 2H), 3.43 – 3.34 (m, 2H), 3.00 (ddd, *J* = 13.5, 11.8, 2.9 Hz, 2H), 2.47 (tt, *J* = 11.3, 3.9 Hz, 1H), 2.02 – 1.83 (m, 4H), 1.83 – 1.60 (m, 7H), 1.58 – 1.44 (m, 2H), 1.19 (t, *J* = 7.1 Hz, 1H).

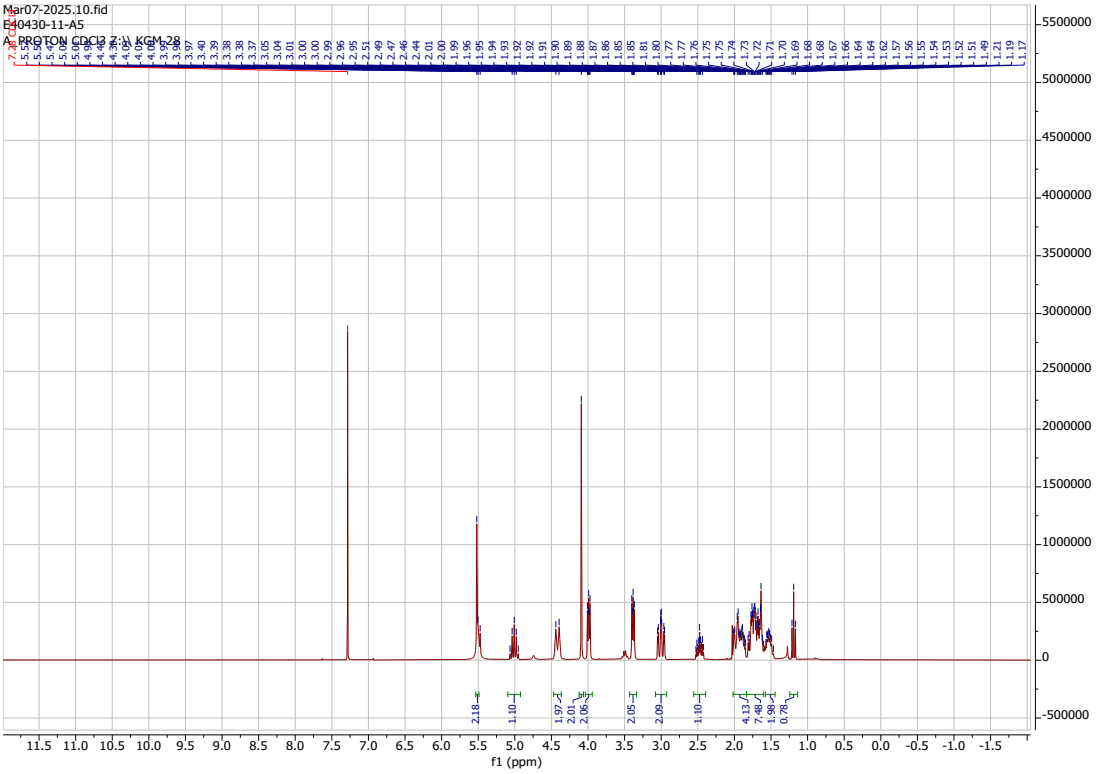

Compound 5A:

[M+1] Found: 374.31

Calculated: 373.17

Compound 2A:

[M+1] Found: 434.27

Calculated: 433.18

^{1}H NMR (300 MHz, MeOD) δ 7.95 (d, J = 0.9 Hz, 1H), 7.72 (dd, J = 1.6, 0.9 Hz, 1H), 7.56 – 7.40 (m, 2H), 5.67 (s, 1H), 4.61 (s, 2H), 4.34 (d, J = 13.5 Hz, 2H), 4.04 (s, 3H), 2.88 (td, J = 12.9, 2.8 Hz, 2H), 2.48 (tt, J = 11.6, 3.9 Hz, 1H), 1.81 (d, J = 10.9 Hz, 2H), 1.58 (qd, J = 12.4, 4.1 Hz, 2H).

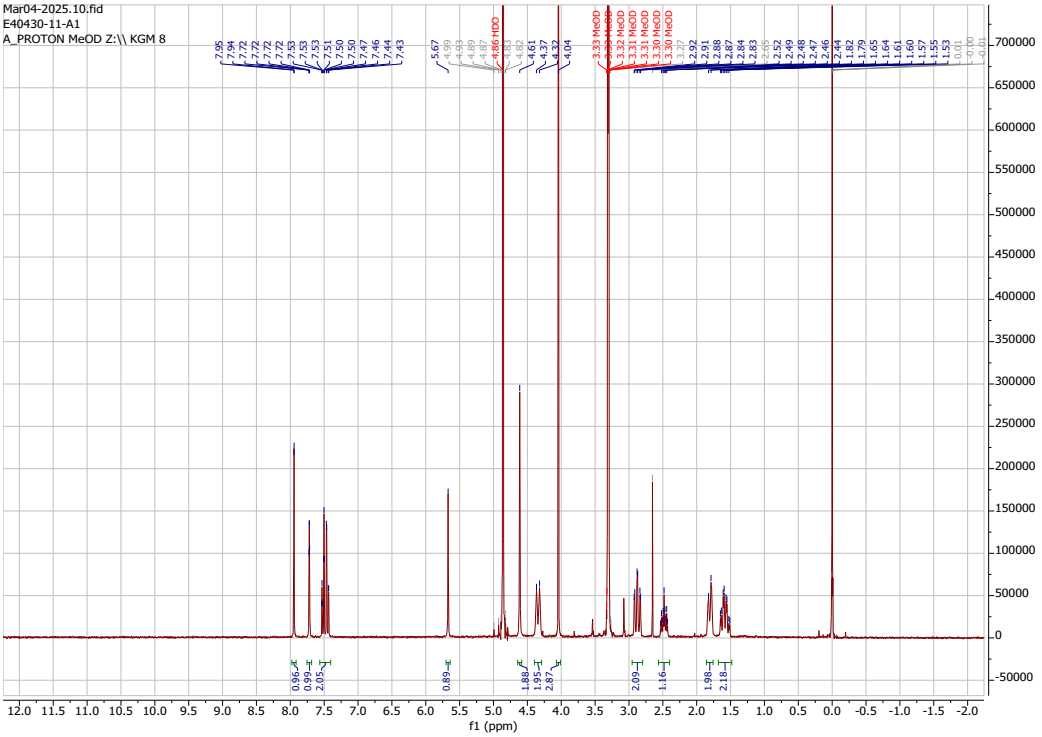

Compound 3A

[M+1] Found: 374.27

Calculated: 373.17

Compound 7A

[M+1] Found: 398.33

Calculated: 397.18

S4.6: N-Cyanation reaction towards 1,2,4-oxadiazole

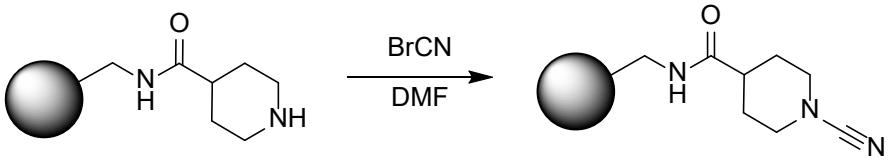

i. To a 40 mL vial was added dry beads (piperidine-4-carbonylamino) (1.05 g of 0.64 mmol/g, 0.6720 mmol). Anhydrous DMF (8.5 mL) and DIPEA (700 µL, 4.019 mmol) was added to the vial and it was set to cool to 0 °C on the stirrer for 15 minutes. Drop-wise to the cooled mixture was added cyanogen bromide (750 µL of 4.5 M, 3.375 mmol) dropwise and the reaction was allowed to stir and gradually warm to RT. The CNBr syringe was washed with 2N NaOH and put into a separate waste container. The reaction was set to stir at RT on the Eppendorf Thermomixer at 400 rpm ON.

ii. After stirring overnight, the reaction solution was drained slowly through a filter funnel into a solution of 2N sodium hydroxide with ice and put into a separate waste container. The beads were washed with DMF (3 x 20 mL), DCM (2 x 30 mL) and those washes were also added to the waste container. The beads were moved back to a vial and dried und er vacuum. No further characterization was done.

S4.7: Installation of the hydroxyl amine functionality towards the 1,2,4-oxadiazole

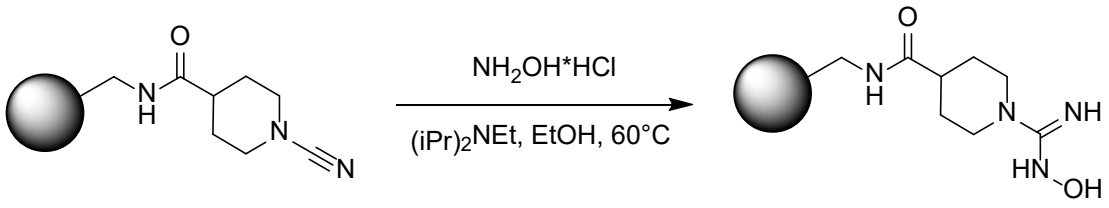

i. To a vial was added beads [(1-cyanopiperidine-4-carbonyl)amino] (500 mg of 0.639 mmol/g, 0.3195 mmol). The vial was placed on vacuum then backfilled with N_2. To the vial was added hydroxylamine (Hydrochloride salt) (117 mg, 1.684 mmol) followed by anhydrous EtOH (5 mL) and DIPEA (0.45 mL, 2.583 mmol) . The Eppendorf Thermomixer was set to 65°C to sir at 450 rpm ON. After stirring overnight, the reaction solution was drained through a filter funnel and the beads were washed with EtOH (2 x 10 mL) , DCM (2 x 20 mL). The beads were moved back to a via l and dried under vacuum.

ii. A small scoop of beads was treated with 1 mL of 12% TFA/DCM solution with 2% triethyl silane stir for 20 min. A UPLC was taken of the solution and the product mass 1-(N-hydroxycarbamimidoyl)piperidine-4-carboxamide ESI-MS *m/z* calc. 186.11168, was detected. The beads were stored in a vial to be used in subsequent reactions.

[M+1] Found: 186.11

Calculated: 187.10

S4.8: Cyclization & cleavage to form 1,2,4-oxadiazole

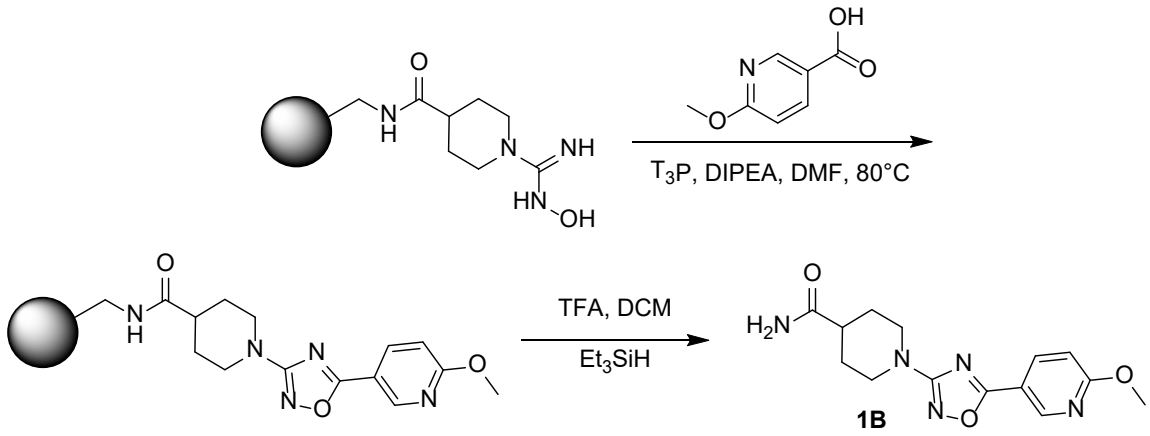

i. To a vial charged with beads [1-(hydroxycarbamoyl)piperidine-4-carbonyl]amino] (250 mg of 0.64 mmol/g, 0.1600 mmol) and backfilled with N_2 was added 6-methoxypyridine-3-carboxylic acid (approximately 122.5 mg, 0.8000 mmol) . Under a flow of $N_{2,}$ DMF (2 mL) was added followed by DIPEA (140 µL, 0.8037 mmol) and T3P (510 µL of 50 %w/v, 0.8014 mmol) . The Eppendorf Thermomixer was set to 80 °C to sir at 450 rpm ON. After stirring overnight, the mixture was washed with DMF (3 x 20 mL), DCM (2 x 20 mL), and dried under vacuum.

ii. To the dried beads was added 2.5 mL of a 12% TFA/DCM solution with 2% triethylsilane to stir for 1.5 hrs. The beads were filtered off the solution and washed with ACN (2x5 mL) and DCM (2x20 mL). The solution was concentrated, and the crude oil was sent to APT for purification.

iii. Purification by reversed-phase HPLC. Method: Waters XSelect CSH C18 OBD Prep Column; 30 x 150 mm, 5 microns. Gradient: Acetonitrile in Water with 0.2% Formic Acid. The product was successfully isolated

Compound 1B

Found: 304.30

Calc: 303.13

^{1}H NMR (300 MHz, $CDCl_3$) δ 8.90 (d, *J* = 2.4 Hz, 1H), 8.20 (dd, *J* = 8.7, 2.4 Hz, 1H), 6.86 (d, *J* = 8.7 Hz, 1H), 5.41 (d, *J* = 41.4 Hz, 2H), 4.18 (d, *J* = 13.2 Hz, 2H), 4.04 (s, 3H), 3.04 (td, *J* = 12.5, 3.0 Hz, 2H), 2.42 (ddt, *J* = 11.5, 7.5, 3.8 Hz, 1H), 2.09 – 1.95 (m, 2H), 1.86 (qd, *J* = 12.1, 4.3 Hz, 2H).

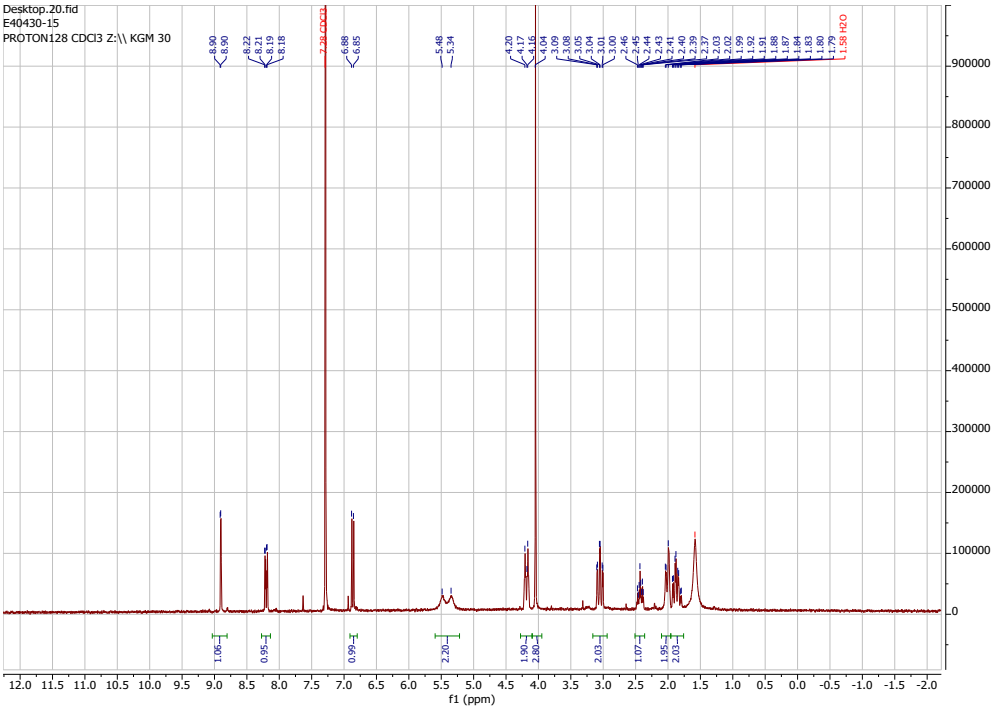

S4.9: Installation of the thiosemicarbazide on route to the 1,3.4 oxadiazole & 1,3,4-thiadiazole

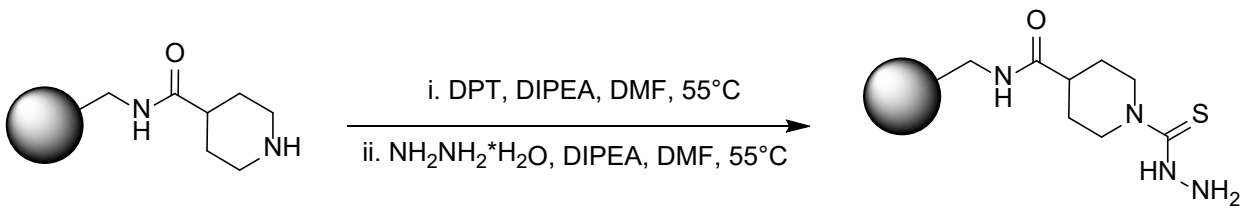

i. To a flask backfilled with N_2 was added dry beads (piperidine-4-carbonylamino) (2.0 g of 0.64 mmol/g, 1.280 mmol) a nd bis(2-pyridyloxy)methanethione (386.2 mg, 1.663 mmol) f o l l o w e d b y DMF (14 mL) . i. To a flask backfilled with N_2 was added dry beads (piperidine-4-carbonylamino) (2.0 g of 0.64 mmol/g, 1.280 mmol) and bis(2-pyridyloxy)methanethione (386.2 mg, 1.663 mmol) followed by DMF (14 mL). The beads were allowed to swell for 10 min and then DIPEA (450.0 µL, 2.583 mmol) was added to the vial. The Eppendorf Thermomixer was set to 55°C to sir at 450 rpm for 2 hrs. After the time period, the solution was drained and the beads were washed with DMF (2x20mL), then put back into a vial.

ii. To the vial was added DMF (14 mL), hydrazine (Hydrate (1)) (80 µL, 1.614 mmol) and DIPEA (450.0 µL, 2.583 mmol). The Eppendorf Thermomixer was set to 55°C to sir the mixure at 450 rpm for 3 hrs. After the 3 hr time period, the mixture was washed with DMF (3 x 20 mL), DCM (2 x 30 mL) and then dried under vacuum.

iii. A small scoop of beads was treated with 1 mL of 12% TFA/DCM solution with 2% triethyl silane stir for 20 min. A UPLC was taken of the solution and the product mass 1-(aminocarbamothioyl)piperidine-4-carboxamide ESI-MS m/z calc. 202.08884 was detected. The beads were moved into subsequent reactions.

[M+1] Found: 203.08

Calculated: 202.09

Source: *Org. Lett.* **2024**, 26, 7, 1353-1357 DOI: 10.1021/acs.orglett.3c04240

S4.10: DMTMM Acylation followed by iodine mediated desulfurative cyclization to 1,3,4 oxadiazole core

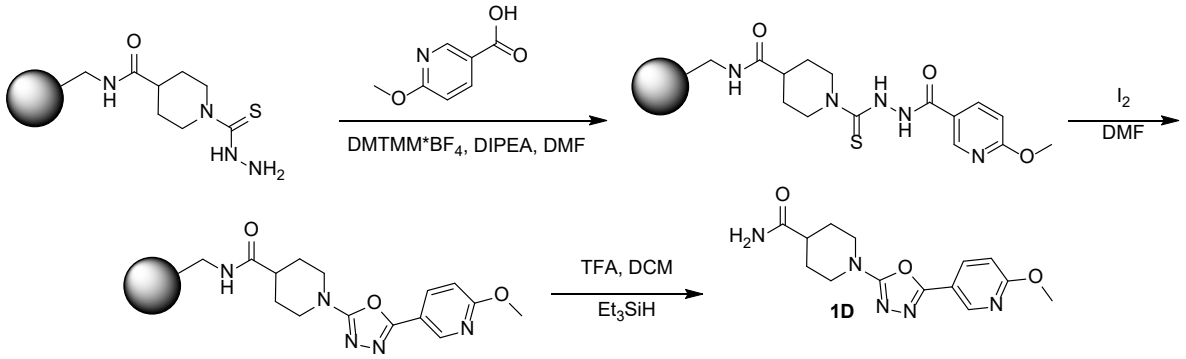

i. In a two dram vial back filled with N_2, beads [[1-(aminocarbamothioyl)piperidine-4-carbonyl]amino] (250.6 mg of 0.64 mmol/g, 0.1604 mmol) f r o m E 4 0 4 3 0 - 3 0 , 6-methoxypyridine-3-carboxylic acid (36.8 mg, 0.2403 mmol) , 4-(4,6-dimethoxy-1,3,5-triazin-2-yl)-4-methyl-morpholin-4-ium;tetrafluoroborate (211.5 mg, 0.6447 mmol) and DMF (1.2 mL) was added, followed by DIPEA (10 µL, 0.05741 mmol) . The Eppendorf Thermomixer was set to stir at 450 rpm OV. After stirring overnight, the mixture was washed with DMF (3 x 15 mL) and added to a 20 mL vial.

ii. To the 20 mL vial with beads was added Iodine (approximately 203.6 mg, 0.8020 mmol) a n d DMF (2 mL) to stir on the Eppendorf Thermomixer at 450 rpm for 40 minutes. After stirring overnight, the mixture was washed with DMF (4 x 15 mL) and DCM (2 x 15 mL) the dried under vacuum.

iii. To the dry beads was added 2 mL of a 12% TFA/ D CM solution with 2% triethyl silane to stir for 2 hrs. The mixture was filtered and washed with ACN (2x10mL) DCM (2x5mL) The solution was concentrated and the crude yellow oil was sent to APT for purification.

Source: E40430-50, *Org. Lett.* **2024**, 26, 7, 1353-1357 DOI: 10.1021/acs.orglett.3c04240

Compound 1D

[M+1] Found: 304.04

Calculated: 303.13

^{1}H NMR (300 MHz, $CDCl_3$) δ 8.68 (dd, *J* = 2.4, 0.8 Hz, 1H), 8.12 (dd, *J* = 8.7, 2.4 Hz, 1H), 6.84 (dd, *J* = 8.7, 0.7 Hz, 1H), 5.49 (d, *J* = 29.7 Hz, 2H), 4.15 (dt, *J* = 13.7, 4.1 Hz, 2H), 4.01 (s, 3H), 3.18 (ddd, *J* = 13.2, 11.6, 3.2 Hz, 2H), 2.45 (tt, *J* = 11.2, 3.8 Hz, 1H), 2.04 (dd, *J* = 13.5, 3.5 Hz, 2H), 1.98 – 1.81 (m, 2H).

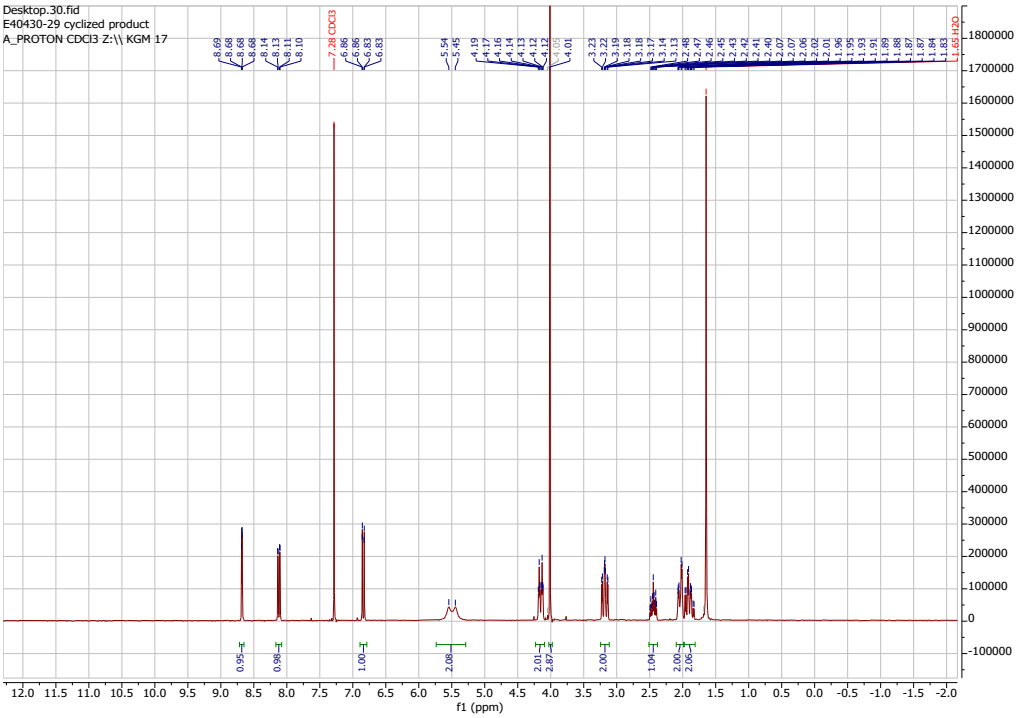

S4.11: Library format for 1,3,4-oxadiazole core

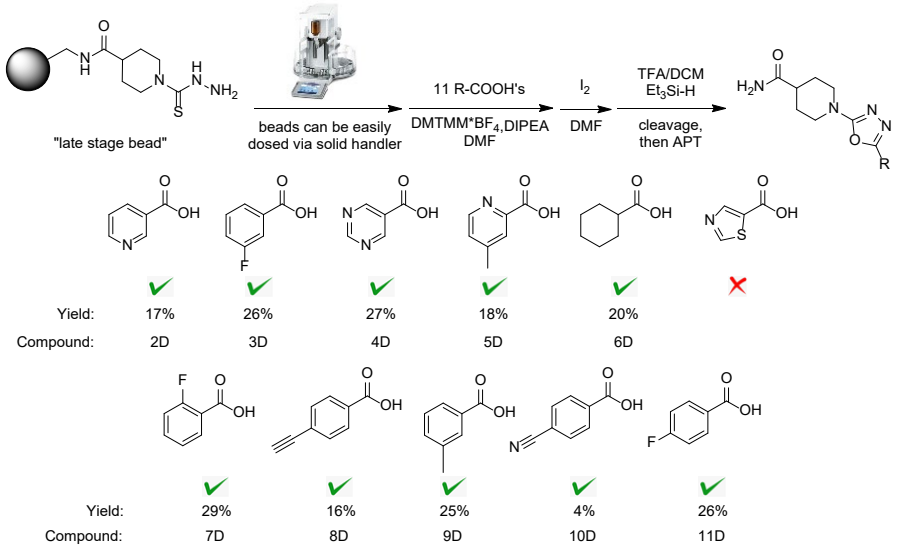

i. In a one-dram vial, Beads from E40430-52 were added via the QS-30 after WAD had dispensed the Carboxylic acids. Then, 4-(4,6-dimethoxy-1,3,5-triazin-2-yl)-4-methyl-morpholin-4-ium; tetrafluoroborate was dispensed via the QS-30. A stock solution of DIPEA and DMF (1 mL) were added to the vial. The Eppendorf Thermomixer was set to stir at 450 rpm OV. After stirring overnight, the mixture was washed with DMF (2 x 15 mL) and added to a different one-dram vial.

ii To the one-dram vials with beads were added molecular iodine in DMF to stir on the Eppendorf Thermomixer to stir at 450 rpm for 1 hr. After stirring, the mixture was washed with DMF (2 x 10 mL) and DCM (2 x 10 mL) then added those beads to a different one-dram vial.

iii. To the dry beads was added 2 mL of a 12% TFA/ DCM solution with 2% triethyl silane to stir for 1.5 hrs. The mixture was filtered and washed with both ACN and DCM two times. The solution was concentrated, and the crude yellow oil was sent to APT.

Compound 6D

[M+1] Found: 279.42

Calculated: 278.17

Compound 4D

[M+2] Found: 275.3

Calculated: 273.12

Compound 7D

[M+1] Found: 291.38

Calculated: 290.12

Compound 3D

[M+1] Found: 291.38

Calculated: 290.12

^{1}H NMR (300 MHz, DMSO) δ 7.88 – 6.74 (m, 6H), 3.99 (dt, *J* = 13.0, 3.6 Hz, 2H), 3.12 (td, *J* = 12.6, 3.0 Hz, 2H), 2.36 (tt, *J* = 11.4, 3.7 Hz, 1H), 1.82 (dd, *J* = 13.6, 3.5 Hz, 2H), 1.72 – 1.51 (m, 2H).

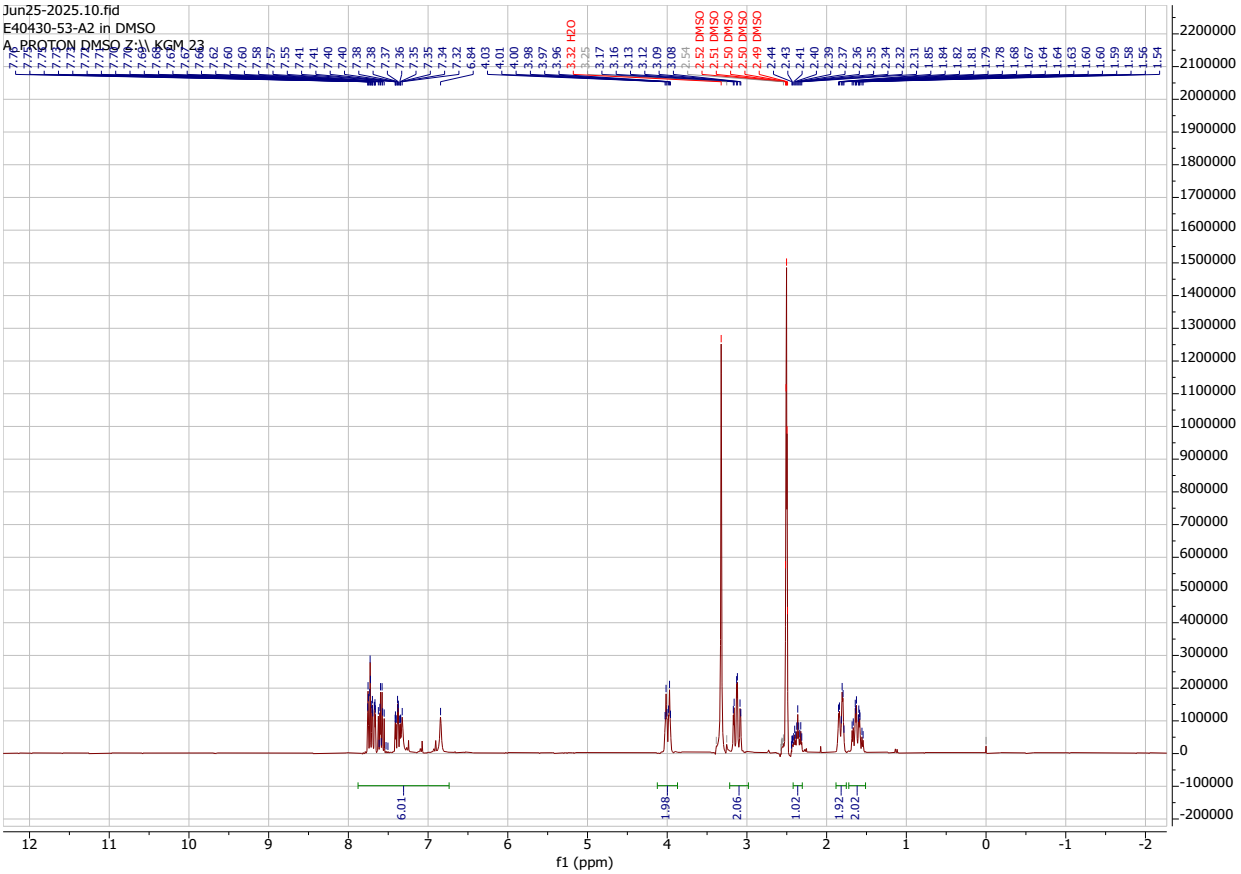

Compound 2D

[M+1] Found: 274.37

Calculated: 273.12

Compound 10D

[M+1] Found: 298.38

Calculated: 297.12

^{1}H NMR (300 MHz, DMSO) δ 8.10 – 7.90 (m, 4H), 7.32 (s, 1H), 6.84 (s, 1H), 4.00 (d, *J* = 13.0 Hz, 2H), 3.30 (s, 4H), 3.22 – 3.07 (m, 2H), 2.36 (ddt, *J* = 11.4, 7.4, 3.6 Hz, 1H), 1.83 (dd, *J* = 13.4, 3.5 Hz, 2H), 1.61 (qd, *J* = 12.2, 4.3 Hz, 2H).

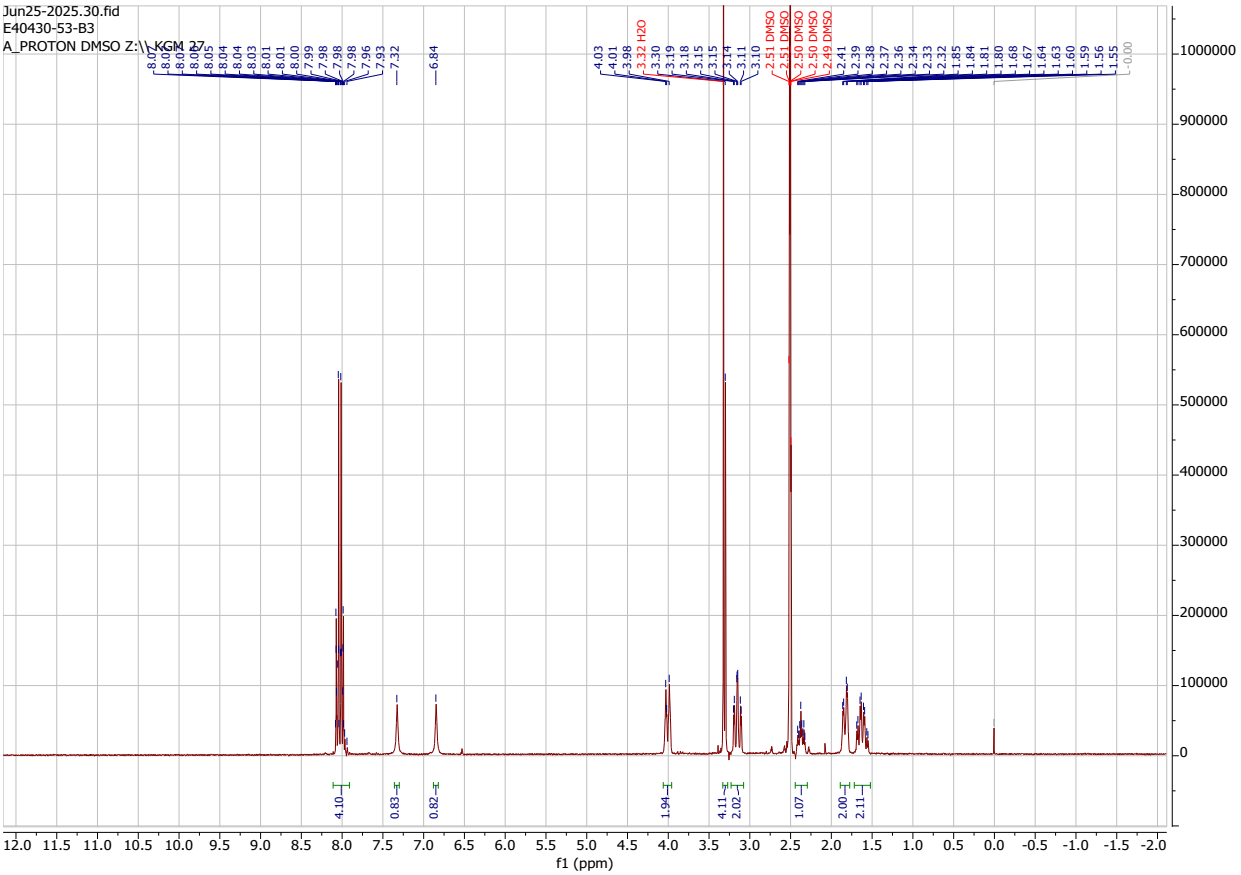

Compound 8D

[M+1] Found: 297.26

Calculated: 296.13

Compound 11D

[M+1] Found: 291.34

Calculated: 290.12

^{1}H NMR (300 MHz, DMSO) δ 8.05 – 7.81 (m, 2H), 7.42 – 6.68 (m, 4H), 3.96 (dt, *J* = 13.2, 3.7 Hz, 2H), 3.11 (td, *J* = 12.6, 3.0 Hz, 2H), 2.36 (tt, *J* = 11.4, 3.7 Hz, 1H), 1.82 (dt, *J* = 13.6, 2.2 Hz, 2H), 1.70 – 1.51 (m, 2H).

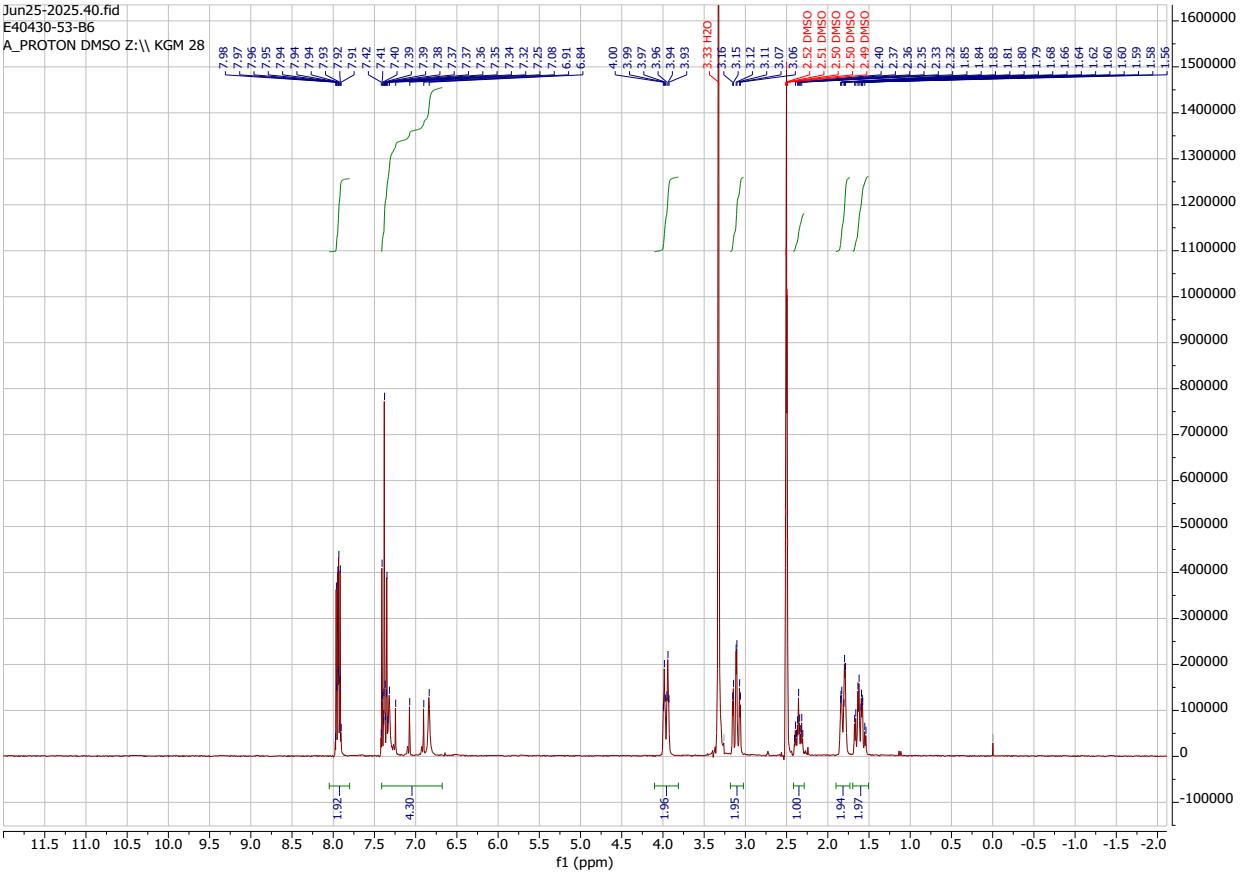

Compound 5D

[M+1] Found: 288.36

Calculated: 287.14

^{1}H NMR (300 MHz, DMSO) δ 8.53 (dd, *J* = 4.9, 0.8 Hz, 1H), 7.88 (p, *J* = 0.8 Hz, 1H), 7.40 – 7.28 (m, 2H), 6.84 (s, 1H), 3.96 (dt, *J* = 13.0, 3.7 Hz, 2H), 3.83 (s, 1H), 3.14 (td, *J* = 12.6, 3.0 Hz, 2H), 2.41 (s, 3H), 1.83 (dd, *J* = 13.6, 3.5 Hz, 2H), 1.69 – 1.54 (m, 2H).

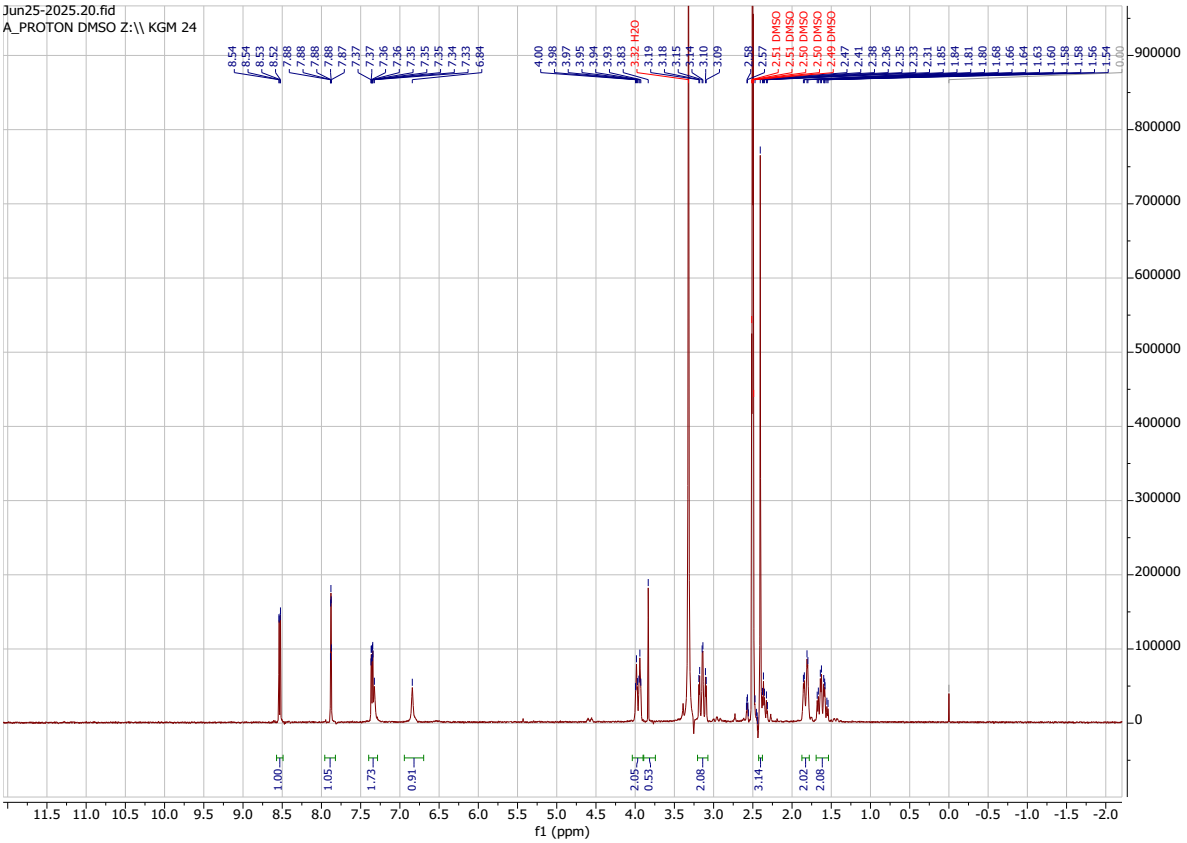

Compound 9D

[M+1] Found: 287.10

Calculated: 286.14

S4.12: Acylation and Cyclization to the 1,3,4-thiadiazole core

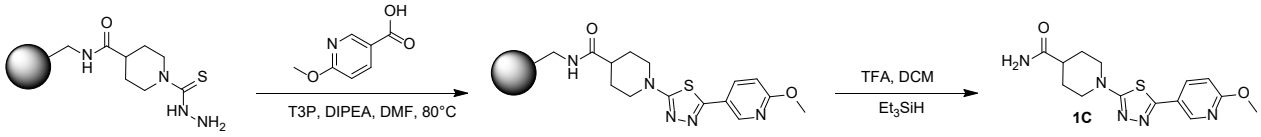

i. To a vial charged with beads [1-(aminocarbamothioyl)piperidine-4-carbonyl]amino] (256 mg of 0.64 mmol/g, 0.1638 mmol) from page E40430-27 and backfilled with N_2 was added 6-methoxypyridine-3-carboxylic acid (75.5 mg, 0.4930 mmol). Under the flow of N_2, DMF (2 mL) was added followed by DIPEA (230 µL, 1.320 mmol) and T3P (830 µL of 50 %w/v, 1.304 mmol) . The Eppendorf Thermomixer was set to 80°C to stir at 450 rpm OV. After stirring overnight, the mixture was washed with DMF (3 x 15 mL), DCM (2 x 15 mL), and dried under vacuum.

ii. To the dried beads was added 4 mL of a 12% TFA/DCM solution with 2% triethyl silane to stir for 2 hr. The beads were filtered off the solution and washed with ACN (2x10) DCM (2x1 5 m L). The solution was concentrated, and the crude oil was sent to APT for purification. Purification by reversed-phase HPLC. Method: Waters XSelect CSH C8 OBD Prep Column; 30 x 150 mm, 5 micron. Gradient : Acetonitrile in Water with 10 mM Ammonium Hydroxide) .

After purification, two main components were isolated, the intended product 1C 1-[5-(6-methoxy-3-pyridyl)-1,3,4-oxadiazol-2-yl]piperidine-4-carboxamide (4.48 mg, 9%) 1H NMR (300 MHz, CDCl3) δ 8.68 (dd, J = 2.4, 0.8 Hz, 1H), 8.12 (dd, J = 8.7, 2.4 Hz, 1H), 6.84 (dd, J = 8.7, 0.7 Hz, 1H), 5.49 (d, J = 29.7 Hz, 2H), 4.15 (dt, J = 13.7, 4.1 Hz, 2H), 4.01 (s, 3H), 3.18 (ddd, J = 13.2, 11.6, 3.2 Hz, 2H), 2.45 (tt, J = 11.2, 3.8 Hz, 1H), 2.04 (dd, J = 13.5, 3.5 Hz, 2H), 1.98 - 1.81 (m, 2H). 13C NMR (75 MHz, CDCl3) δ 175.81, 165.31, 164.02, 157.54, 144.91, 135.99, 114.64, 111.39, 77.22, 53.89, 45.86, 41.73, 27.74.

[M+1] Found: 304.02

Calculated: 303.13

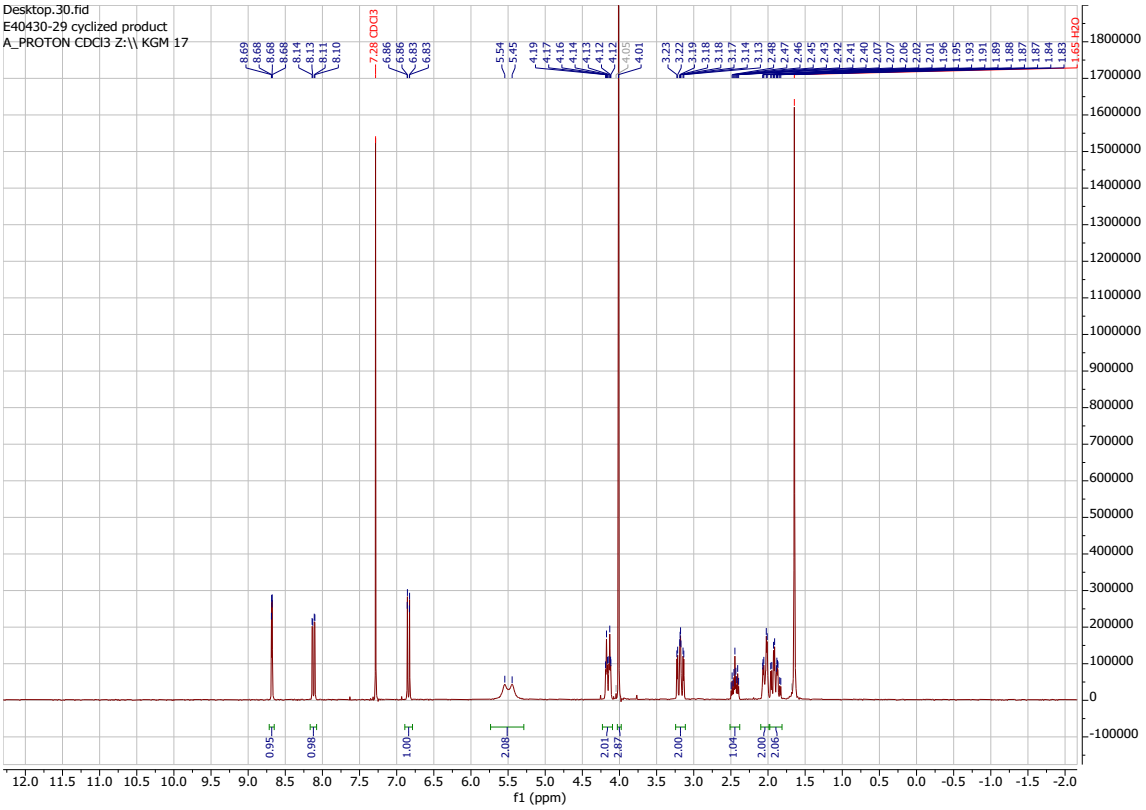
Desktop.30.fid
E40430-29 cyclized product
A_PROTON CDCl3 Z:\\ KGM 17
f1 (ppm)

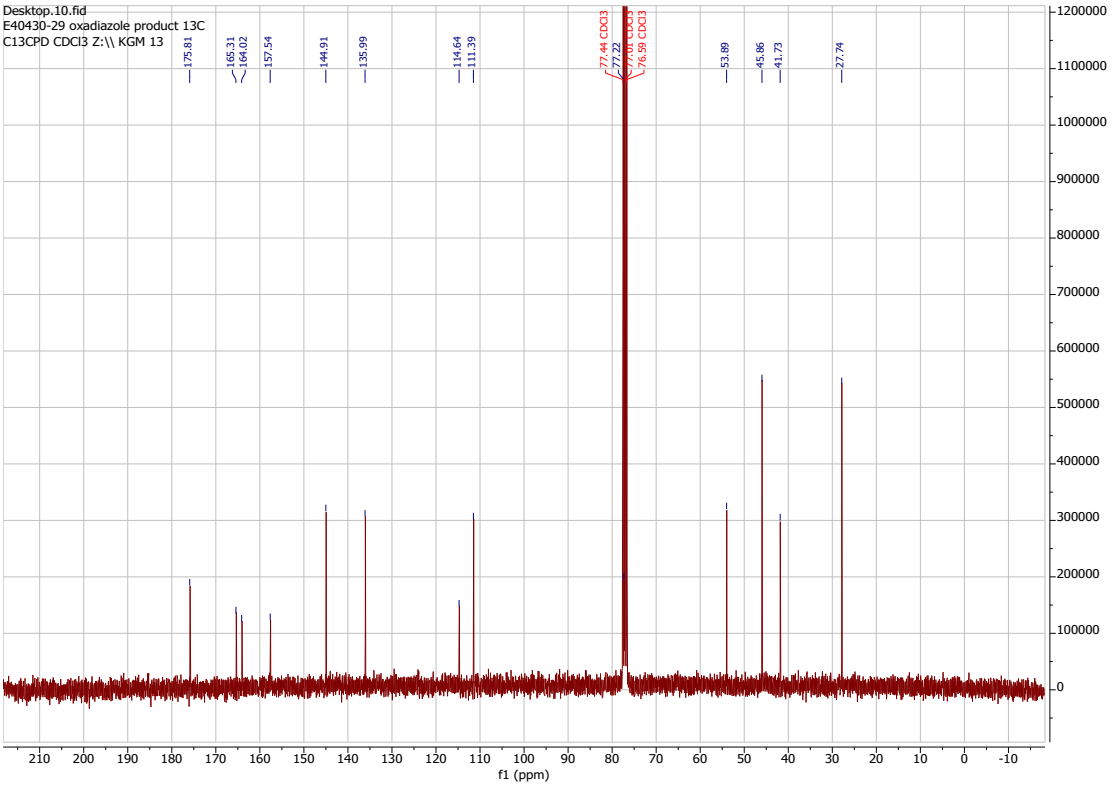
Desktop.10.fid
E40430-29 oxadiazole product 13C
C13CPD CDCl3 Z:\\ KGM 13
f1 (ppm)

Another product, 1C, a thiadiazole, differed by 16 mass units, but showed the same proton NMR 1-[5-(6-methoxy-3-pyridyl)-1,3,4-thiadiazol-2-yl]piperidine-4-carboxamide (11.86 mg, 23%) 1H NMR (300 MHz, CDCl3) δ 8.50 (dd, J = 2.4, 0.8 Hz, 1H), 8.12 (dd, J = 8.7, 2.4 Hz, 1H), 6.83 (dd, J = 8.7, 0.8 Hz, 1H), 5.45 (d, J = 37.7 Hz, 2H), 4.10 (dt, J = 13.9, 4.0 Hz, 2H), 4.00 (s, 3H), 3.27 (ddd, J = 13.1, 11.4, 3.4 Hz, 2H), 2.47 (tt, J = 11.1, 3.9 Hz, 1H), 2.10 - 1.85 (m, 4H). 13C NMR (75 MHz, CDCl3) δ 175.71, 171.34, 164.97, 155.43, 145.53, 136.57, 121.18, 111.42, 77.22, 53.82, 49.68, 41.89, 27.83.

[M+1] Found: 320.04

Calculated: 319.11

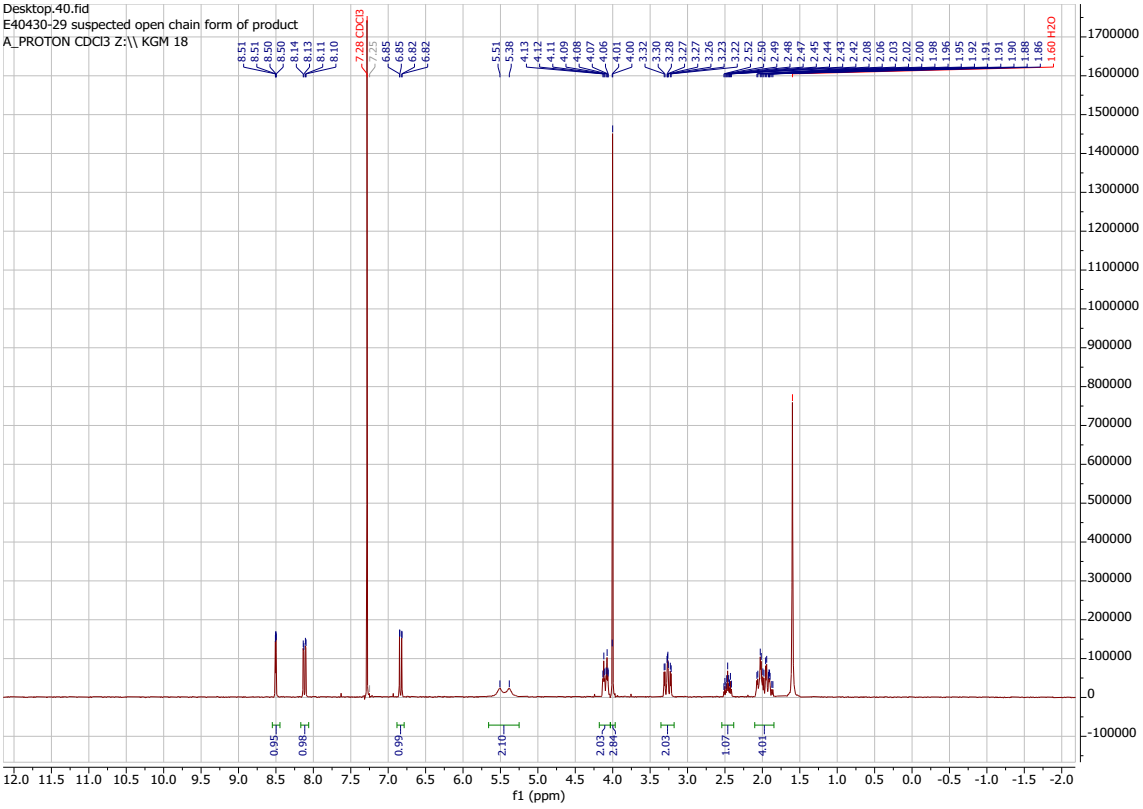

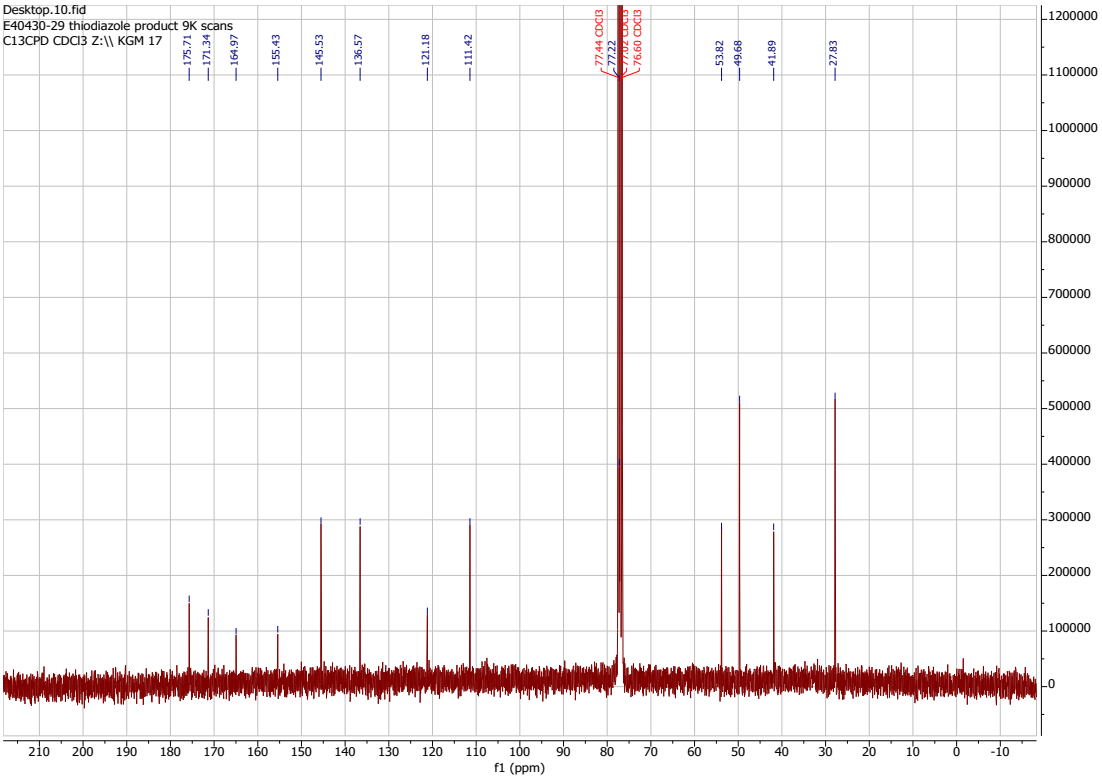

S4.13: Library for the thiadiazole

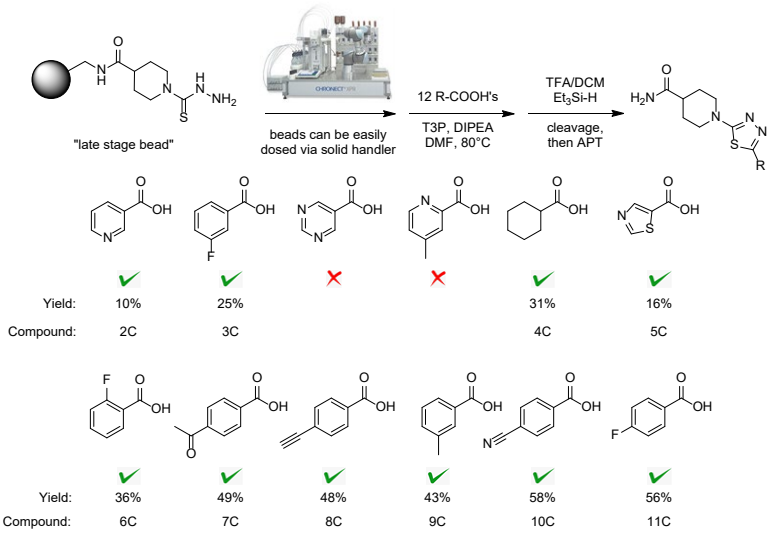

i. All carboxylic acids were dispensed as solids by WAD. To those 1 dram vials, beads (130 mg of 0.64 mmol/g) from E40430-30 were added via the Cronect solid doser. The plate was removed from the glove box. A stock solution of T3P and DIPEA was dispensed into each well in DMF (1 mL) using a

multichannel pipette and aspirated twice. The Eppendorf Thermomixer was set to 80°C to stir at 450 rpm OV. After stirring overnight, the mixture was washed with DMF (2 x 15 mL), DCM (2 x 15 mL), and dried under vacuum for at least 5 min.

ii. To the dried beads was added 2 mL of a 12% TFA/DCM solution with 2% triethyl silane. The solution was aspirated twice and set to stir for 1 hr. The beads were filtered off the solution and washed with acetone (2x10) DCM (2x15 mL). The solution was concentrated, and the crude oil was sent to APT for purification.

Purification by reversed-phase HPLC. Method: WatersXSelect CSH C8 OBD Prep Column; 30 x 150 mm, 5 micron. Gradient: Acetonitrile in Water with 10 mM Ammonium Hydroxide). The thiadiazols isolated were QC'd with UPLC. A random 4 wells were picked for NMR characterization

Compound 4C

[M+1] Found: 295.40

Calculated: 294.15

^{1}H NMR (300 MHz, DMSO) δ 7.31 (s, 1H), 6.82 (s, 1H), 3.79 (dt, *J* = 13.0, 3.7 Hz, 2H), 3.08 (td, *J* = 12.5, 3.1 Hz, 2H), 2.96 – 2.85 (m, 1H), 2.33 (tt, *J* = 11.4, 3.8 Hz, 1H), 2.02 – 1.92 (m, 2H), 1.75 (tdd, *J* = 9.9, 7.6, 4.4 Hz, 4H), 1.66 – 1.51 (m, 3H), 1.49 – 1.31 (m, 4H), 1.30 – 1.18 (m, 1H).

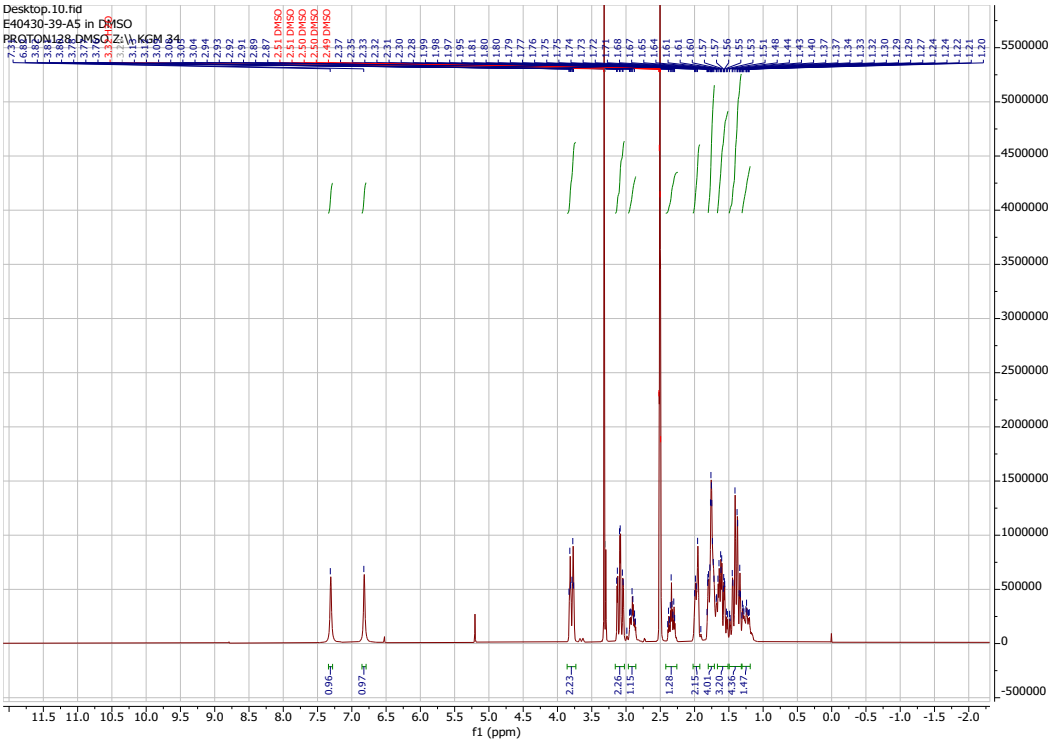

Compound 5C

[M+1] Found: 296.26

Calculated: 295.06

Compound 6C

[M+1] Found: 307.28

Calculated: 306.10

Compound 3C

[M+1] Found: 307.32

Calculated: 306.10

^{1}H NMR (300 MHz, DMSO) δ 7.66 – 7.57 (m, 2H), 7.57 – 7.47 (m, 1H), 7.37 – 7.24 (m, 2H), 6.85 (s, 1H), 3.92 (dt, *J* = 13.0, 3.7 Hz, 2H), 3.23 (td, *J* = 12.5, 3.1 Hz, 2H), 2.40 (tt, *J* = 11.3, 3.8 Hz, 1H), 1.90 – 1.77 (m, 2H), 1.74 – 1.55 (m, 2H).

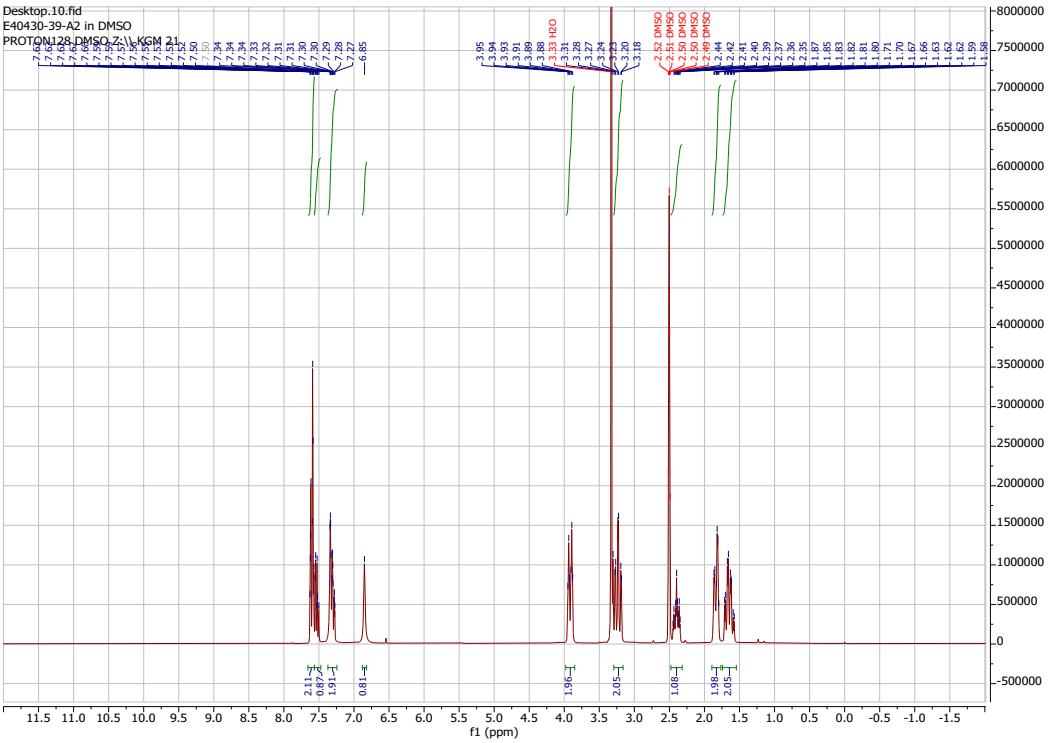

Compound 2C

[M+1] Found: 290.30

Calculated: 289.10

Compound 7C

[M+1] Found: 331.33

Calculated: 330.12

Compound 8C

[M+1] Found: 314.27

Calculated: 313.10

Compound 10C

[M+1] Found: 313.32

Calculated: 312.10

^{1}H NMR (300 MHz, DMSO) δ 7.83 – 7.73 (m, 2H), 7.63 – 7.53 (m, 2H), 7.33 (s, 1H), 6.85 (s, 1H), 4.37 (s, 1H), 3.92 (dt, *J* = 13.1, 3.6 Hz, 2H), 3.23 (td, *J* = 12.5, 3.1 Hz, 2H), 2.40 (tt, *J* = 11.3, 3.7 Hz, 1H), 1.89 – 1.77 (m, 2H), 1.74 – 1.54 (m, 2H).

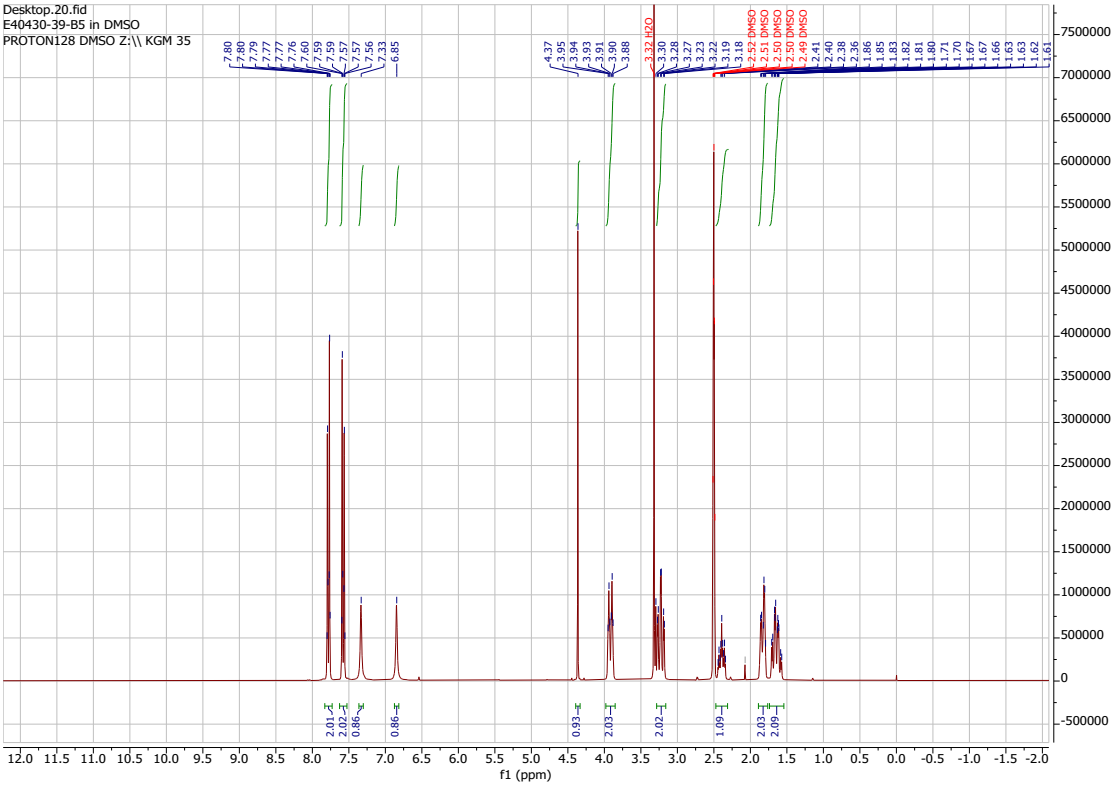

Compound 11C

[M+1] Found: 307.28

Calculated: 306.10

<u>Compound 9C</u>

[M+1] Found: 303.30

Calculated: 302.12

^{1}H NMR (300 MHz, DMSO) δ 7.65 – 7.50 (m, 2H), 7.43 – 7.25 (m, 3H), 6.85 (s, 1H), 3.91 (dt, J = 13.0, 3.6 Hz, 2H), 3.21 (td, J = 12.5, 3.1 Hz, 2H), 2.37 (s, 4H), 1.89 – 1.77 (m, 2H), 1.73 – 1.57 (m, 2H).